Integration of Design and NMPC-based Control of Processes under Uncertainty

by

Oscar Palma-Flores

A thesis
presented to the University of Waterloo
in fulfillment of the
thesis requirement for the degree of
Doctor of Philosophy
in
Chemical Engineering

Waterloo, Ontario, Canada, 2023

Examining Committee Membership

The following served on the Examining Committee for this thesis. The decision of the Examining Committee is by majority vote.

External Examiner:	Carl D. Laird Professor Department of Chemical Engineering Carnegie Mellon University
Supervisor:	Luis Alberto Ricardez-Sandoval Associate Professor Department of Chemical Engineering, University of Waterloo
Internal Member:	William Anderson Professor Emeritus Department of Chemical Engineering, University of Waterloo
	Nasser Mohieddin Abukhdeir Associate Professor Department of Chemical Engineering, University of Waterloo
Internal-External Member:	Nasser Lashgarian Azad Associate Professor Systems Design Engineering Department, University of Waterloo

Author's Declaration

I hereby declare that I am the sole author of this thesis. This is a true copy of the thesis, including any required final revisions, as accepted by my examiners.

I understand that my thesis may be made electronically available to the public.

Abstract

The implementation of a Nonlinear Model Predictive Control (NMPC) scheme for the integration of design and control demands the solution of a complex optimization formulation, in which the solution of the design problem depends on the decisions from a lower tier problem for the NMPC. This formulation with two decision levels is known as a bilevel optimization problem. The solution of a bilevel problem using traditional Linear Problem (LP), Nonlinear Problem (NLP) or Mixed-Integer Nonlinear Problem (MINLP) solvers is very difficult. Moreover, the bilevel problem becomes particularly complex if uncertainties or discrete decisions are considered. Therefore, the implementation of alternative methodologies is necessary for the solution of the bilevel problem for the integration of design and NMPC-based control. The lack of studies and practical methodologies regarding the integration of design and NMPC-based control motivates the development of novel methodologies to address the solution of the complex formulation.

A systematic methodology has been proposed in this research to address the integration of design and control involving NMPC. This method is based on the determination of the amount of back-off necessary to move the design and control variables from an optimal steady-state design to a new dynamically feasible and economic operating point. This method features the reduction of complexity of the bilevel formulation by approximating the problem in terms of power series expansion (PSE) functions, which leads to a single-level problem formulation. These function are obtained around the point that shows the worst-case variability in the process dynamics. This approximated PSE-based optimization model is easily solved with traditional NLP solvers. The method moves the decision variables for design and control in a systematic fashion that allows to accommodate the worst-case scenario in a dynamically feasible operating point. Since approximation techniques are implemented in this methodology, the feasible solutions potentially may have deviations from a local optimum solution.

A transformation methodology has been implemented to restate the bilevel problem in terms of a single-level mathematical program with complementarity constraints (MPCC). This single-level MPCC is obtained by restating the optimization problem for the NMPC in terms of its conditions for optimality. The single-level problem is still difficult to solve; however, the use of conventional NLP or MINLP solvers for the search of a solution to the MPCC problem is possible. Hence, the implementation of conventional solvers provides guarantees for optimality for the MPCC's solution. Nevertheless, an optimal solution for the MPCC-based problem may not be an optimal solution for the original bilevel problem.

The introduction of structural decisions such as the arrangement of equipment or the selection of the number of process units requires the solution of formulations involving discrete decisions. This PhD thesis proposes the implementation of a discrete-steepest descent algorithm for the integration of design and NMPC-based control under uncertainty and structural decisions following a naturally ordered sequence, i.e., structural decisions that follow the order of the natural numbers. In this approach, the corresponding mixed-integer bilevel problem (MIBLP) is transformed first into a single-level mixed-integer nonlinear program (MINLP). Then, the MINLP is decomposed into an integer master problem and a set of continuous sub-problems. The set of problems is solved systematically, enabling exploration of the neighborhoods defined by subsets of integer variables. The search direction is determined by the neighbor that produces the largest improvement in the objective function. As this method does not require the relaxation of integer variables, it can determine local solutions that may not be efficiently identified using conventional MINLP solvers.

To compare the performance of the proposed discrete-steepest descent approach, an alternative methodology based on the distributed stream-tray optimization (DSTO) method is presented. In that methodology, the integer variables are allowed to be continuous variables in a differentiable distribution function (DDF). The DDFs are derived from the discretization of Gaussian distributions. This allows the solution of a continuous formulation (i.e., a NLP) for the integration of design and NMPC-based control under uncertainty and structural decisions naturally ordered set.

Most of the applications for the integration of design and control implement direct transcription approaches for the solution of the optimization formulation, i.e., the full discretization of the optimization problem is implemented. In chemical engineering, the most widely used discretization strategy is orthogonal collocation on finite elements (OCFE). OCFE offers adequate accuracy and numerical stability if the number of collocation points and the number of finite elements are properly selected. For the discretization of integrated design and control formulations, the selection of the number of finite elements is commonly decided based on a priori simulations or process heuristics. In this PhD study, a novel methodology for the selection and refinement of the number of finite elements in the integration of design and control framework is presented. The corresponding methodology implements two criteria for the selection of finite elements, i.e., the estimation of the collocation error and the Hamiltonian function profile. The Hamiltonian function features to be continuous and constant over time for autonomous systems; nevertheless, the Hamiltonian function shows a nonconstant profile for underestimated discretization meshes. The methodology systematically adds or removes finite elements depending on the magnitude of the estimated collocation error and the fluctuations in the profile for the Hamiltonian function.

The proposed methodologies have been tested on different case studies involving different features. An existent wastewater treatment plan is considered to illustrate the implementation of back-off strategy. On the other hand, a reaction system with two continuous stirred reaction tanks (CSTRs) are considered to illustrate the implementation of the MPCC-based formulation for design and control. The D-SDA approach is tested for the integration of design, NMPC-based control, and superstructure of a binary distillation column. Lastly, a reaction system illustrates the effect of the selection and refinement of the discretization mesh in the integrated design and control framework. The results show that the implementation of NMPC controllers leads to more economically attractive process designs with improved control performance compared to applications with classical descentralized PID or Linear MPC controllers. The discrete-steepest descent approach allowed to skip sub-optimal solution regions and led to more economic designs with better control performance than the solutions obtained with the benchmark methodology using DDFs. Meanwhile, the refinement strategy for the discretization of integrated design and control formulations demonstrated that attractive solutions with improved control performance can be obtained with a reduced number of finite elements.

Acknowledgements

I would like to express my sincere gratitude to my supervisor, Prof. Luis A. Ricardez-Sandoval for his guidance, help, patience, and encouragement. Thank you for your valuable time and support during my PhD study.

I want to thank to my examining committee: Prof. Carl D. Laird, Prof., William Anderson, Prof. Nasser M. Abukhdeir, and Prof. Nasser L. Azad for their time in reading and valuable comments.

I would like to thank the financial support awarded by the Consejo Nacional de Ciencia y Tecnología CONACyT (México) and the University of Waterloo. With their assistance, my studies would not had been possible.

I want to express my gratitude with my family that encouraged me and support me every single day during this journey. I am so blessed to have so supportive parents (Dulce and Oscar), my siblings Thania, Brenda, and Brando. Also, I want to thank to my second mom Lulu and my sister Yazmin. My special thanks to my beloved Arcelia for her patience, comprehension, encouragement, and happiness (for showing me that the distance can unite us even more). This was possible thanks to all of you!

I would like to thank to my dear friends Maritza and Reyna for their help and for everything we have lived during an entire life. I met a wonderful family in Canada in my friends Dr. Daniela Lubke, Thiago Mello, Sara Kamali, Dr. Mahshad Valipour, Camila Jorente, Dr. Kavitha Menon, Han Wang, and Yanshuo Peng. This acknowledgement is extensive to my friends and colleges from the University of Waterloo. In particular, I want to thank Dr. Mina, Dr. Piyush, Dr. Suhyoung, Dr. Oswaldo, Dr. Grigoriy, Huabei, Yael, Ilse, David, Gabriel, Carlos, Simone, Meagan, Samantha, Daniel, Tannia, Yue, Kayden, Shuji, Donovan, and to all those who directly or indirect contributed to make this achievement possible.

During this journey, we all experienced a pause in our lives. This pause took two years from our lives. I hope that our future generations will never forget the sacrifices we made.

Dedication

In memory of my professional mentor and guide, Alfredo Flores, BSc (1957-2023). Your advice and teachings will always guide my path.

Table of Contents

List of Figures

List of Tables

Nomenclature

BOD Biochemical Oxygen Demand. 59

COD Chemical Oxygen Demand. 59

CQs Constraint Qualifications. 6, 19, 21, 22, 71, 74, 78, 107, 171

CSTR Continuous Stirred Tank Reactor. xi, 77, 86, 89, 92, 152, 161

D-SDA Discrete-Steepest Descent Algorithm. 7, 109, 112, 113, 134, 172–175

DAE Differential-Algebraic Equation. 3, 8, 29, 35, 37, 137

DDF Differentiable Distribution Function. 123–125, 134

DO Dynamic Optimization. 27–29

DSTO Distributed Stream-Tray Optimization. 123, 125, 126, 134, 172

ECP Extended Cutting Plane. 108

FNLPs Fixed-Nonlinear Programs. 7, 109–113, 172

GBD Generalized Benders Decomposition. 108

GDP Generalized Disjunctive Program. 108

IPLC Integer Program with Linear Constraints. 104, 109, 111–113, 134, 172

ISE Integral Squared Error. 101, 119, 127

KKT Karush-Kuhn-Tucker. 21, 73, 82, 100, 107, 134, 171

LD-BD Logic-based Discrete-Benders Decomposition. 175

LICQ Linear Independence Constraint Qualification. 21, 74

LMPC Linear Model Predictive Control. 1, 3–5, 15, 31–33, 37, 52, 53, 55, 56, 73

LPEC Linear Programs with Equilibrium Constraints. 75

MFCQ Mangasarian–Fromovitz Constraint Qualification. 21, 74

MI-MPCC Mixed-Integer Mathematical Program with Complementarity Constraints. 104, 107

MIBLP Mixed-Integer Bilevel Problem. 2, 5, 7, 26, 37, 104, 105, 134, 172

MIDO Mixed-Integer Dynamic Optimization. 31

MINLP Mixed-Integer Nonlinear Problem. 5, 7, 8, 33, 104, 108, 134, 172

MPCC Mathematical Program with Complementarity Constraints. 6, 21, 22, 37, 71–73, 77, 98, 102, 171, 175

MPEC Mathematical Programs with Equilibrium Constraints. 72, 75

NCP Nonlinear Complementarity Problem. 75

NLP Nonlinear Problem. 4, 5, 8, 41, 73, 74, 77, 102, 112, 123, 171

NMPC Nonlinear Model Predictive Control. 1–4, 6–8, 14–18, 37, 38, 40, 41, 47, 49, 52, 53, 56, 63, 73, 94, 106, 107

OCFE Orthogonal Collocation on Finite Elements. 3, 7, 8, 35–37, 76, 83, 90, 95, 122, 136, 139

ODEs Ordinary Differential Equations. 35, 76, 86

OS Operating system. 78

PDEs Partial Differential Equations. 35

PI Proportional-Integral. 32, 38, 52, 55, 56

PID Proportional-Integral-Derivative. 1, 3–5, 32, 137

PMP Pontriagyn's Minimum Principle. 27, 29, 138, 169

PSE Power Series Expansion. 6, 38, 39, 41, 42, 46–48, 53, 70

RGA Relative Gain Array. 155

RL Reinforcement Learning. 176

RMINLP Relaxed Mixed-Integer Nonlinear Problem. 112

TPBVP Two-Point Boundary Value Problem. 29, 37, 139

WCV Worst Case Variability. xi, 42, 44–46, 48

WOR Williams-Otto Reactor. 7

WWTP Waste-Water Treatment Plant. 6, 39, 49, 52, 53, 55, 59, 93, 100

A_d Tank's cross-sectional area. 51, 56, 58, 60, 79, 81, 84, 93, 94, 96

A_e Heat transfer area. 79, 86, 153

ϕ_{BF} Fischer-Burmeister function. 75

CC_a Annualized capital cost ($\$/yr$). 51, 81, 88, 90, 93, 98, 119, 154, 163

C_{A0} Initial concentration of component A. 86

C_A^{sp} Set-point for concentration of component A. 89

C_A Concentration of component A. 86

C_p^l Liquid phase heat capacity. 79, 87, 88

C_p Heat capacity. 155

Cv Valve size coefficient. 79

$\Delta\eta_p$ Step-size variation of design variables (Back-off method). 42, 47, 54, 59

$\Delta\hat{\mathbf{u}}$ Predicted change of control actions in NMPC. 16

FCP Depreciation and labor taxes. 164

$\bar{F}_p$ Purge stream. 78

$\bar{C}$ Weighting constant for the monitor function at noncollocation points. 142

$\bar{F}_w$ Cooling water stream. 86, 154

$\mathbb{H}$ Hamiltonian function. 29, 138, 143

$K_{\hat{n}}$ Distillation K-values per tray. 126

$\mathcal{L}$ Lagrangian function. 73

MG Gross return per hour. 163

Λ_i Monitor function of i^{th} finite element evaluated at noncollocation points. 142, 143, 145, 146, 148, 150

N_{FE} Total number of finite element for discretization with OCFE. 141, 145, 150

$N_\infty(\mathbf{z_E})$ ∞-*neighborhoods* formed by the external variables $\mathbf{z_E}$. 113, 114

N_{iter} Maximum number of iterations (Back-off method). 42, 49, 53, 59

N_r Number of sampled values from the objective function (Back-off method). 49, 59

N Number of trays in the distillation column. xii, 116, 117, 123

N_ς Number of uncertainty realizations. 42

OC_a Annualized operating cost ($\$/yr$). 51, 88, 93, 154

$\mathbf{\Omega}_c$ Set of decision variables in the NMPC problem. 73

PIN Total initial investment of the plant. 164

$SARE$ Cost related to sales, administration, research, and engineering expenses. 163

$S_\infty(\hat{\mathbf{z}}_\mathbf{E})$ Neighborhood containing the potential search directions in the D-SDA framework. 114, 115

UC_a Annualized utility cost ($\$/yr$). 119

UF Associated costs to utilities and process flows. 164

U_h Universal heat transfer coefficient. 79, 87, 155

VC_a Annualized variability cost ($\$/yr$). 51, 52, 68, 81, 88, 93, 94, 154, 155, 163

V_R Tank's volume (m^3). 51, 56, 58–60, 81, 84, 86, 93, 94, 96

Vj Tank's cooling/heating jacket volume. 86, 153

$\mathbf{Q_{out}}$ Weighting matrix for predicted controlled states in NMPC. 17, 40, 42, 80, 83, 84, 89–91, 94, 98, 106, 126

$\mathbf{Q_{in}}$ Weighting matrix for predicted control actions in NMPC. 17, 40, 42, 80, 83, 84, 89, 90, 94, 96, 106

Y_1 Set containing the external variables and their boundaries. 110, 111

Y_2 Set containing the logical constraints in terms of external variables. 110, 111

Y Polyhedron formed by integer logical constraints in terms of external variables. 111, 113, 115, 121

Z Polyhedron formed by integer logical constraints. 110–112

Z Polyhedron containing all the logical constraints to define a superstructure. 109

E Activation energy for the reaction. 87, 88, 155

α Relative volatility. 117, 129

β Initial neighbor in the set of external variables. 112

$\bar{M}$ Big M parameter. 48, 75, 76, 83, 149

$\bar{V}_B$ Distillation column's boil up stream. 118, 125

$\bar{F}_B$ Bottoms stream. 118

x_B Bottoms composition. 118

ϕ_{ISE} Controllability index term in the cost function. 119

k Collocation points index. 76

C_p^w Heat capacity of water. 87, 88, 155

c_s Oxygen specific saturation (mg/L). 51

c_w^{sp} Dissolved oxygen concentration set-point (mg/L). 58, 60, 94, 96, 98, 99

c_w Dissolved oxygen concentration (mg/L). 49, 55, 93, 94

$\varrho_{\hat{n}}$ Differentiable distribution function. 123

$\Delta\bar{\alpha}$ Step-size for sensitivity calculations (Finite element refinement algorithm). 143

δ_b Search space region for decision variables (Back-off method). xi, 42, 48, 52, 54, 59, 63, 65

ρ Density. 79, 87, 155

D_e Diameter. 86, 89, 116, 122, 126, 153

$\mathbf{d}_{p_{nom}}$ Disturbances at nominal conditions. 44

$\mathbf{d}_p$ Process disturbances. 16, 41, 48, 106, 137

$\bar{F}_D$ Distillate stream. 118

x_D Distillate composition. 118

$\dot{\mathbf{x}}$ Derivatives of process states. 40, 137

ϵ_H Tolerance for the approximation of the Hamiltonian function profile. 143, 148, 151

ϵ_Λ Collocation error tolerance. 142, 148, 151

ϵ_Λ Tolerance for the approximation of the Hamiltonian function profile. 143

ϵ_s Relaxation parameter for complementarity constraints. 75, 83, 90, 107, 108, 126

ε User-defined tolerance. 49, 54

$\bar{e}$ Error signal (PID controller input). 154

η_{nom} Time-independent set of decision variables at nominal condition. 44–46, 49

η Time-independent set of decision variables. 11, 28, 40, 46–48, 137

η^c Time-independent set of decision variables (lower-level problem). 40

η^c_{nom} Nominal values for time-independent decision variables (lower-level problem). 44

η^p Time-independent set of decision variables (upper-level problem). 40

η^p_{nom} Nominal values for time-independent decision variables (upper-level problem). 43, 44

F Process model function (Lower-level problem). 16, 41, 73

f Process model function. 41

f_{kd} Fraction of death biomass. 51

x_f Distillation column's feed atream composition. 119

f_k Turbine speed. 51, 55, 93

f_{ss} Process model function at steady-state. 44

$\check{g}$ Auxiliary storage parameter for inequality constraints (Back-off method). 45, 46

G Inequality constraints (Lower-level problem). 16, 20, 41, 73

g Inequality constraints. xi, 19, 41, 45, 46, 109

$g_{si,PSE}$ PSE-based inequality constraints (Back-off method). 48

$\nabla\mathcal{L}$ Gradient of the Lagrangian function. 73

g_{ss} Algebraic equality constraints at steady-state. 44

$\bar{\alpha}_i$ Length of the finite elements in OCFE. 77, 140

H Equality constraints (Lower-level problem). 16, 41, 73

h Equality constraints. 41

ΔH_{rx} Heat of reaction. 87, 88, 155

h_T^{sp} Liquid's holdup set-point. 78, 79

h_T Liquid's holdup. 86, 89, 153, 162, 163

h_{ss} Inequality constraints at steady-state. 44

h_w Height over the weir for distillation column trays. 117, 129

k' Finite elements index (lower-level problem). 77

i Finite elements index. 77, 139, 140

$\hat{i}$ External variables index. 110

r_e Iteration index (Refinement of finite elements algorithm). 143

j_u Uncertainty index. xi, 19, 40, 45, 46, 48, 96, 106, 130

k_1, k_2, k_3 Reaction constants in the Williams-Otto CSTR. 163

κ Time-weighted integral square error. 119

K_{C1} Proportional gain for PI controller. 58, 156

K_{C2} Proportional gain for PI controller. 58, 156

k_{ca} Specific cellular activity. 53, 55, 59, 95, 96

K_{D1} Derivative gain of the PID controller. 156

K_{D2} Derivative gain of the PID controller. 156

k_{dr} Biomass death rate. 53, 55, 59, 95, 96

$\hat{k}$ Integer variables index. 109

K_{I1} Integral gain of the PI controller. 156

K_{I2} Integral gain of the PI controller. 156

k_l Order of gradient in the PSE. 46

k_{od} Oxygen demand constant (hr^{-1}). 51

k_{otw} Oxygen transfer into the water constant (hr^{-1}). 51

k_{sc} Saturation constant (hr^{-1}). 51

k_t Measurement interval time. 16, 17, 117

ℓ Lagrange polynomials. 76

ϖ_{si,j_u} Penalization variables in the PSE-based formulation. 48

λ Lagrange multiplier for process model constraints. 73

$L_{\hat{n}}$ Distillation column's internal liquid flowrate profile. 118

lr_d, lr_b, lr_r Depth of the first, second and bottom layers in the decanter (m). 50

N_c Gaussian distribution mean value. 123, 125

M_C Molar hold-ups for the condenser (distillation column). 118

M_R Molar hold-ups for the reboiler (distillation column). 118

M_T Molar hold-ups in distillation column trays. 118, 119

MW Molecular weight. 87, 155

μ Lagrange multiplier for inequality constraints. 73, 74

$\bar{\mu}_w$ Specific growth rate. 53, 55, 59, 95, 96

$\hat{n}$ Index of the elements in the naturally ordered set $zs_{\hat{i}}$. 110, 117, 124

ν Lagrange multiplier for equality constraints. 73

$\omega_{i,k}$ Feasibility variable for the approximation of the Hamiltonian function profile. 148, 150

φ_{ov} Optimal value function. 22

p Index for time-independent decision variables. 47

θ_{py} Payback period. 117

$\check{\Phi}$ Auxiliary storage parameter for the objective function (Back-off method). 46

$\bar{\Phi}_{FNLP}$ Objective function for the FNLP formulation. 111

$\bar{\Phi}_{MINLP}$ Objective function for the MINLP formulation. 109

Φ Objective function (Bilevel problem). 19, 44, 46, 112

Φ_{PSE} PSE-based objective function (Back-off method). 48

$\bar{\pi}$ Slack variables. 75

Ψ Lower-level problem objective function. 20

q_2 Bottoms flowrate that leaves the decanter (m^3/h). 50

q_{in} Feed flowrate (m^3/h). 50, 53, 94

q_p Purge flowrate (m^3/h). 49, 52, 55, 67, 93

q_1 Outlet flowrate from bioreactor (m^3/h). 50

q_r Recycle flowrate (m^3/h). 52, 93

q_{out} Water treatment plant's outlet flowrate (m^3/h). 50

r_1, r_2, r_3 Reactions rates in the Williams-Otto CSTR. 163

τ Set of collocation points in OCFE. 77

r_b Iteration index (Back-off method). 42

k_{re} Reaction rate constant. 87, 88, 155

$\bar{R}$ Distillation column's reflux stream. 118, 125

$\mathbf{s}$ Potential search directions in the D-SDA. 114

si Inequality constraints index (Back-off method). 45

δ Search space parameter for the approximation-based formulation. 143, 149

σ Standard deviation. 123–125, 128, 149

$\mathbf{s_d}$ Steepest-descent search directions in the D-SDA. 114, 115

$\bar{F}_A$ Flow rate of component A. 161, 162

$\bar{F}_B$ Flow rate of component B. 161, 162

$\bar{F}_{in}$ Inlet stream. 79, 116, 117, 129, 153

$\bar{F}$ Stream. 78, 79

s_w^{sp} Organic substrate concentration set-point (mg/L). 51, 55, 58, 60, 94, 96, 98

s_{in} Inlet organic substrate concentration (mg/L). 53, 95

s_w Organic substrate concentration in the bioreactor (mg/L). 49, 51, 52, 55, 68, 93, 94, 101

τ_c Future time instants within NMPC. 16, 17, 106

θ_{tx} Tax factor. 117

t_C Control horizon in NMPC. 15, 17, 42, 81, 117

T_c Heating/cooling source's temperature. 79

T_{in} Inlet stream temperature. 79, 86, 90, 153, 154

T_{ref} Reference temperature. 87, 155

T^{sp} Temperature set-point. 78, 79

T Temperature. 78, 162, 163

$\vartheta_{i,nc}$ Feasibility variable for the estimation of the collocation error. 148, 150

τ_{I1} Time integral constant for PI controller. 58

τ_{I2} Time integral constant for PI controller. 58

t_0 Initial simulation time. 41

τ_h Tray hydraulic time constant. 118, 119

$t_{i,nc}$ Process time at i^{th} finite element and nc^{th} noncollocation point. 142

t_{op} Operation time per year. 163

t_{wc} Time at the worst-case scenario. 45, 46

t_f Final simulation time. 41

t Time. 16, 17, 29, 95, 106

t_P Prediction horizon in NMPC. 15–17, 42, 81, 106, 117

$\hat{\mathbf{u}}$ Predicted control actions in NMPC. 16

$\bar{\mathbf{u}}$ Time-varying control variables in the upper-level problem. 11, 40, 106

$\mathbf{u}^{lb}$ Lower bound on control variables. 17

ς_{nom} Set of uncertainties at nominal condition. 44

ς Set of uncertainties. 18, 19, 40, 42, 44–48, 106

w_{j_u} Probability weight of occurrence for the j_u^{th} uncertainty realization. 19, 40, 42, 55, 59, 94, 96, 106

$\mathbf{u}^{ub}$ Upper bound on control variables. 17

$\mathbf{u}$ Time-varying control variables. 137

W_{ISE} Weighting parameter to penalize the process variability. 119

x_A, x_B, x_C, x_M, x_Q, x_D Concentration for components A, B, C, M, Q, and D in the Williams-Otto CSTR. 163

x_d, x_b, x_r Biomass concentrations at first, second and bottom layers in the decanter (mg/L). 50, 94

$\hat{\mathbf{x}}$ Predicted states in NMPC. 16, 17

$\dot{\hat{\mathbf{x}}}$ Derivatives of predicted states in NMPC. 16

x_M^{sp} Concentration set-point for component E. 162

x_{in} Inlet biomass concentration (mg/L). 50, 53, 95

$\mathbf{x}^{lb}$ Lower bound on process states. 17

x_D^{sp} Concentration set-point for component P. 162

$\mathbf{x}^{sp}$ Process state set-points. 17

$x_{\hat{n}}$ Liquid phase composition profile in the distillation column. 118

$\mathbf{x}^{ub}$ Upper bound on process states. 17

$\mathbf{x}^p$ Approximated discrete solution of states $\mathbf{x}$ using OCFE. 142

$\mathbf{x}$ State of the process. 11, 17, 40, 137, 142

x_w Biomass concentrations in the bioreactor (mg/L). 50, 94

$y_{\hat{n}}$ Vapor phase composition profile in the distillation column. 118

$\mathbf{y}$ Measured states. 11, 40, 137

y_w Fraction of converted substrate to biomass. 51

$\mathbf{z_E}$ External variables. 110, 111, 113

$zs_{\hat{i}}$ Naturally ordered one-dimensional discrete set. 110

$\mathbf{z}$ Integer variables. 106, 109, 113

Chapter 1

Introduction

Traditionally, chemical processes have been designed in a sequential fashion around steady-state points taken from production design targets, followed by the design of a control scheme. This approach is referred to as a sequential process design and has been found to result often in high operating costs or even intractable process dynamics. In recent years, the academia and the industry have pointed out the need to consider dynamic and controllability aspects at the early stages of the process design. The integrated design and control approach aims to consider the interactions between operability and economic aspects simultaneously. This approach can lead to attractive designs with improved dynamic performance, and higher profits [1].

Over the past decade, a substantial number of studies have proposed a variety of approaches for the integration of design and control [2, 3, 4]. Those studies have focused mainly on the implementation of classical decentralized PID control frameworks [5]. Nevertheless, the implementation of modern control approaches using model predictive controllers has demonstrated improvements in control performance compared to applications using decentralized PID control frameworks [2, 6, 7]. A model predictive controller (MPC) solves an online optimization problem where a cost function penalizes deviations in the controlled and manipulated variables with respect to reference trajectories, i.e., set-points. To achieve this, the optimization problem is subject to a dynamic process model. If a linear process model is used, the controller is called a LMPC. On the other hand, if a nonlinear dynamic process model is enforced, the controller is referred to as a NMPC. An important feature of MPC is the possibility to include constraints in the formulation.

The interest for the implementation of LMPC strategies for simultaneous design and control has been reflected in the publication of multiple studies [4, 8, 9, 10, 2, 11]. On the other hand, when dealing with highly nonlinear processes that require a wide range of operating conditions, a LMPC may not be sufficient to adequately capture the process dynamics [12]. It thus becomes necessary to incorporate nonlinear process models for control [13]. A promising alternative for the control of highly nonlinear processes is the use of NMPC. Although it has been shown that NMPC

can improve the process performance for complex nonlinear systems, and can also manage wide operational changes in highly nonlinear processes, very few works have addressed the integration of design and NMPC-based control [14], i.e., the economic and operability benefits in the solution of an integrated design and NMPC-based control approach have not been fully explored while using NMPC. That study has focused on the solution of formulations with continuous variables. Moreover, the solution of the corresponding optimization problem for integrated design and NMPC-based control is a challenging task because the optimization problem for the NMPC is embedded within the problem for optimal process design, i.e., a formulation with two decision levels, in which the design problem requires the control actions to accommodate the process design, whereas the controller requires the information of the process to compute optimal control actions. This problem is referred to as a bilevel problem, which are very difficult to solve with conventional NLP solvers [15]. Hence, there is a lack of practical solution methodologies for integrated design and NMPC-based control formulations in the literature. Furthermore, design decisions such as the arrangement of equipment, or the determination of the number of stages/equipment are often modeled using discrete variables (i.e., integer/binary variables). These formations involving integer/binary variables for the integration of design and NMPC-based control (i.e., a MIBLP) have not been addressed yet. Thus, the implementation of NMPC for these purposes emerges as a strong research area. To fill in the gap in the literature, the focus of this thesis is to develop novel methodologies for the integration of design and NMPC-based control involving continuous and discrete variables.

In chemical engineering applications, it is not possible to have complete knowledge or understanding of a process due to uncertainties. These uncertainties can arise from various factors, such as variability in input materials or parameters, lack of precise mechanistic models, inherent process complexity, or limitations in measurement or analysis techniques. Uncertainty in process design and control can have adverse effects on the economy, quality, efficiency, and safety of the process. This may lead to unexpected outcomes or deviations from the desired dynamic process performance, particularly for highly nonlinear processes. Uncertainty is often introduced by assuming a discrete set of realizations of uncertain parameters, which can be estimated from observations based on historical data or process heuristics [1]. Managing uncertainty in process design and control involves

identifying sources of uncertainty, quantifying their impact, and implementing appropriate design and control schemes to mitigate or accommodate them. Effective management of uncertainty in process design and control can help ensure the reliability, consistency, and optimality of the process performance. Classical PID or LMPC integrated design and control applications may result in sub-optimal solutions or complicated process dynamics under such conditions; alternatively, NMPC may offer better control performance by incorporating a nonlinear process model in its formulation. Note that if the process model in the NMPC uses nominal conditions for parameters under uncertainty, it is called a nominal NMPC controller; whereas if the NMPC has access to information about the uncertain parameters, it is referred to as a robust NMPC controller. Robust model-based control has been proven to enhance control performance compared to nominal control schemes [16]. However, employing robust control approaches poses a challenge due to the fast increase of size of the NMPC formulation, leading to large-scale formulations for an integrated design and NMPC-based control framework in the presence of uncertainty. Hence, it is essential to develop a methodology for the integration of design and NMPC-based control that allows the simplification and systematic solution of formulations under uncertainty.

Optimization problems for the integration of design and control typically involve formulations with DAE models. In chemical engineering, the most widely used method for the solution of DAE models is the discretization of the differential equations using OCFE. OCFE offers adequate accuracy and numerical stability if the number of finite elements is properly selected [17]. Thus, one key aspect in the implementation of OCFE is the selection of the number of finite elements (i.e., discretization meshing), which is often decided based on a priori simulations or process heuristics [18, 19]. Also, the selection of the number of finite elements is related to the size of the optimization model. Traditionally, finite elements in an OCFE strategy are selected to be uniformly distributed (equidistribution), i.e., finite elements have the same length. To the author's knowledge, the effect of the discretization size on the solution of integrated design and control problems has not been addressed. From an integrated point of view, the process design and its dynamic behavior are closely related, i.e., variations in the process design can lead to variations in the process dynamics, and vice versa. Therefore, an accurate discretization of the integrated design and control problem may help

to avoid the computation of suboptimal solutions, e.g., processes with small time constants exhibit fast dynamic variations to external disturbances; therefore, it is necessary to implement small finite elements to capture of the process dynamics accurately. Accurate selection of the discretization meshing is expected to contribute to the computation of more economically attractive process designs with improved control performance.

1.1 Research objectives

Although NMPC offers significant features and better control performance compared to classical PID or LMPC controllers, their application for the integration of design and control under uncertainty has not been widely studied. Therefore, this research aims to develop practical and systematic methods for the integration of design and NMPC-based control for continuous and discrete applications. The current PhD study focuses on the following specific objectives:

- Propose an iterative methodology for the integration of design and NMPC-based control under uncertainty and process disturbances.
- Develop a transformation methodology for the integration of design and NMPC-based control under uncertainty and process disturbances such that the corresponding bilevel problem is transformed into a single-level formulation that can be solved using conventional NLP solvers.
- Develop a systematic methodology for the integration of design and NMPC-based control under uncertainty, process disturbances, and structural decisions in a naturally ordered discrete set (i.e., superstructures that follow the order of the natural numbers).
- Develop a methodology for the selection and refinement of the discretization finite elements for the integration of design and control.

1.2 Contributions of this research

The research conducted in this PhD thesis is expected to provide the following contributions:

- A practical decomposition back-off methodology that reduces the complexity of the original bilevel formulation by approximating the problem in terms of low-order process models. These low-order models correspond to a single-level formulation that is explicit in terms of the decision variables and can be efficiently solved with conventional NLP solvers. The proposed method can be easily adapted to different control schemes, such as LMPC or PID controllers, in addition to formulations using NMPC.

- A transformation method for the integration of design and NMPC-based control under uncertainty that avoids the use of decomposition or approximation strategies for the solution of the corresponding optimization formulation. Moreover, since the restated formulation (i.e., a single-level problem) can be solved using conventional NLP solvers, the method provides optimality guarantees for the solution of such restated problem. However, the solution for the single-level problem may not be an optimal solution for the original bilevel problem.

- A systematic strategy that transforms the MIBLP formulation into a single-level MINLP. The problem structure is exploited, such that the single-level MINLP can be expressed in terms of a reduced set of variables that represent positions over one-dimensional discrete space. This allows the reduction of the complexity of the MINLP by decomposing the problem into simpler linear and nonlinear problems that can be solved with state-of-the-art NLP solvers. Moreover, the method features the implementation of the definition of integral convexity; therefore, it allows the computation of local solutions that cannot be efficiently identified using conventional MINLP solvers, which are based on the classical definition of convexity for integer programs.

- Provide insights for the selection of finite elements for the discretization of integrated design and control formulations.

- A systematic methodology that implements physical and mathematical selection criteria for the refinement and selection of finite elements. The use of a refined discretization formulation is expected to result in improved solutions for design and control using fewer finite elements compared to implementations involving equidistributed discretization meshes.

1.3 Structure of the Thesis

A description of the structure of this thesis is presented next:

Chapter 2 presents a literature review of the subjects that are relevant for this thesis. First, the optimization formulation for the NMPC is introduced. The concept of bilevel problem is presented next, this is followed by a review of the available methodologies for the integration of design and MPC-based control. Lastly, a review of the methods for the selection and refinement of discretization meshes implemented in chemical engineering for process design is presented. The gaps in knowledge that motivate this research are discussed at the end of this chapter. The content in section 2.4 in this chapter is part of the work published in AIChE Journal [20].

Chapter 3 presents a systematic strategy for the integration of design and NMPC-based control under uncertainty. This methodology aims to determine the amount of necessary back-off to move the process design and control from an optimal steady-state design (that may be dynamically infeasible) to a new dynamically feasible process design and control. This methodology reduces the complexity of the original bilevel problem by approximating the bilevel problem in terms of PSE functions. This approximated PSE-based formulation corresponds to a single-level formulation that can be efficiently solved with traditional NLP solvers. The implementation of this method is illustrated for the integrated design and NMPC-based control of a WWTP. The challenges, features, and limitations of this methodology are highlighted and discussed in this chapter. The work presented in this chapter has been published in the IFAC World Congress Germany 2020 [21] and in Journal of Process Control [22].

Chapter 4 introduces the *classical KKT transformation* strategy to transform the bilevel problem presented in Chapter 2 into a single-level problem. Moreover, the potential reformulation strategies to restate the complementarity constraints in the MPCC to avoid violation of CQs are also presented. The implementation of this strategy is depicted for a WWTP case study. The main features and limitations of this approach are discussed in this chapter. The results of this chapter have been published in Computers & Chemical Engineering [23].

Chapter 5 presents D-SDA approach for the integration of design and NMPC-based control under uncertainty, process disturbances, and structural decisions in a naturally ordered set. The corresponding MIBLP is transformed first into a single-level MINLP using a *classical KKT transformation*. Then, the integer decisions are partitioned in sub-sets called *external variables*, such that the MINLP can be decomposed into an integer-based *master* problem and *primal* sub-problems in the form of FNLPs. The *master* and *primal* problems are solved using the D-SDA approach. The implementation of algorithmic methodology is illustrated in a case study for a binary distillation column. This work has been published in the IFAC World Congress Japan 2023 [24] and submitted for publication to AIChE Journal [25].

Chapter 6 introduces the proposed methodology for the selection and refinement of finite elements for the integration of process design and control. The widely used discretization with OCFE is implemented for this study. This chapter presents the Hamiltonian conditions for optimality and the definition of the estimated collocation error as the criteria for the selection and refinement of finite elements. The proposed methodology is tested using two case studies featuring a reaction system with two Continuous Stirred Tank Reactor (CSTRs) in series and the WOR, respectively. The results indicate that the accurate selection of the finite elements return economically attractive design with fewer elements than those obtained with naive approaches with equidistributed finite element strategies. The results of this chapter have been published in AIChE Journal [26].

Chapter 7 presents the concluding remarks achieved by the present research work. This chapter also provides recommendations for potential future work.

Chapter 2

Literature Review

The integration of design and model-based control has been an area of active research in recent years, driven by the need for more efficient and effective processes. Model-based control approaches have emerged as a promising method for improving control performance and process economy, as they allow to manage complex systems dynamics. Model predictive control (MPC) is a multivariable optimization-based control framework that has been widely used in chemical engineering. Numerous efforts involving LMPC for integrated design and control have been presented in the literature. Those studies have improved the efficiency, accuracy, and robustness of the corresponding optimization formulation. On the other hand, DAE models are the base for the optimization formulations in simultaneous design and control. Solving DAE models can be challenging doe to the presence of algebraic equations. Discretization of DAE models using OCFE is the most popular approach to convert the continuous-time model into a set of discrete-time equations that can be solved using conventional NLP or MINLP solvers. In this approach, the continuous-time dynamic model is approximated by a set of piecewise functions (commonly polynomials) leading to a set of nonlinear algebraic equations. The selection of the discretization mesh has demonstrated to have an impact in the solution of DAE models. Although the importance of this selection, the effect of the discretization accuracy has not been reported in the literature for application in integrated design and control. This chapter reviews the concepts and mathematical methods that are relevant for this work. Moreover, the knowledge gaps that serve the motivation for this PhD study are also identified in this chapter.

This chapter is organized as follows: Section 2.1 provides a background on process design and control. Section 2.2 provides an overview on nonlinear model predictive control (NMPC), followed by an overview on the concept of bilevel programming that is relevant for this study (Section 2.3). An overview of the Hamiltonian function obtained from the implementation of the Pontryagin's Minimum Principle (PMP) is provided in Section 2.4. Current applications with model-based control schemes for the integration of design and control are summarized in Section 2.5. Section

2.6 presents a overview of the current methodologies for the selection of finite elements in process design. Lastly, Section 2.7 provides a summary of this chapter.

2.1 Process design and control

The current global market's dynamic nature compels industries to strive for sustainable and near-optimal operations. Traditionally, profitability was the primary concern, but now there is a shift towards developing and operating processes that are both profitable and sustainable. Factors such as climate change, resource scarcity, and waste production have motivated the inclusion of sustainability in chemical process industries. Sustainability now encompasses economic, social, safety, and environmental aspects of company policies. Furthermore, industries need to connect their networks to customers and suppliers for efficient operations. However, various aspects of processes are traditionally handled independently, limiting their potential for improvement. Simultaneously optimizing process design and control is a core aspect of the combined problem. In the past, these two aspects were treated separately and solved sequentially, leading to poor control performance or overly conservative and expensive designs. Integrating design and control allows for transparent links between conflicting objectives and enables the identification of reliable and optimal designs while ensuring feasible operation under internal and external disruptions.

2.1.1 Classical approach for design and control of processes

A steady-state process operation refers to a condition where a process has reached a state of equilibrium, and the key process variables remain constant over time. In a steady-state operation, the process inputs, outputs, and operating conditions are maintained at a constant level, e.g., process variables such as temperature, pressure, flow rates, concentrations, and other parameters remain constant. However, processes are not operated in a steady-state mode continuously. Processes may experience transient behavior or non-steady-state conditions at certain stages. Nonetheless, the goal is often to reach a steady state as quickly as possible and maintain it for as long as required to achieve the desired process objectives.

In a classical design and control approach, chemical plants have been designed using a sequential method that involves an initial steady-state process design stage relying on economic calculations. This is then followed by the development of a control strategy, typically, based on heuristic controllability measures. Consequently, the aspects of process design and process control have traditionally been investigated as separate entities. However, this sequential approach for process design is often insufficient, as process design has the potential to strongly influence process control, i.e., an optimal steady-state design does not account for transient behavior or dynamic responses of the process. This can lead to suboptimal dynamic performance during normal operation under the effect of process disturbances. Moreover, optimal steady-state designs are often tailored to specific operating conditions and may not easily accommodate future process changes or advancements. This can limit the ability to incorporate new technologies or adapt to evolving market demands.

2.1.2 Integrated approach for process design and control of processes

Integration of design and control combines steady-state design and dynamic control considerations into a single optimization step. Process design involves decisions related to equipment sizing and determining nominal operating conditions, whereas process control involves control structure strategies that minimize variability, ensuring quality and keeping key variables within specified limits.

Simultaneous optimization of the design and control of a process often involves reconciling conflicting objectives, e.g., smaller process units may be designed based on steady-state capital cost considerations, whereas larger units are needed to handle disturbances during transient conditions. A crucial aspect in the integrated design and control framework is ensuring process flexibility, i.e., the system can meet constraints despite external disturbances or uncertainties in process parameters. The integration of design and control problem can be conceptually formulated as a mixed-integer nonlinear dynamic optimization (MIDO) formulation, e.g.,

$$\min_{\eta,\mathbf{x}(t),\mathbf{u}(t),\mathbf{y}(t)} \Phi(\eta,\mathbf{x}(t),\mathbf{u}(t),\mathbf{y}(t),\mathbf{d}_p(t),\mathbf{z},t) \tag{2.1a}$$

$$s.t.\ \ f(\eta,\varsigma,\dot{\mathbf{x}}(t),\mathbf{x}(t),\bar{\mathbf{u}}(t),\mathbf{y}(t),\mathbf{d}_p(t),\mathbf{z},t)=0, \tag{2.1b}$$

$$h(\eta,\varsigma,\mathbf{x}(t),\bar{\mathbf{u}}(t),\mathbf{y}(t),\mathbf{d}_p(t),\mathbf{z},t)=0, \tag{2.1c}$$

$$g(\eta, \varsigma, \mathbf{x}(t), \bar{\mathbf{u}}(t), \mathbf{y}(t), \mathbf{d}_p(t), \mathbf{z}, t) \leq 0, \tag{2.1d}$$

where $h : \mathbb{R}^{N_x} \times \mathbb{R}^{N_u} \times \mathbb{R}^{N_\eta} \times \times \mathbb{R}^{N_y} \times \mathbb{R}^{N_d} \times \mathbb{R}^{N_t} \rightarrow \mathbb{R}^{N_h}$ and $g : \mathbb{R}^{N_x} \times \mathbb{R}^{N_u} \times \mathbb{R}^{N_\eta} \times \mathbb{R}^{N_y} \times \mathbb{R}^{N_d} \times \mathbb{R}^{N_t} \rightarrow \mathbb{R}^{N_{si}}$ denote the equality and inequality constraints of the process, respectively; $f : \mathbb{R}^{N_x} \times \mathbb{R}^{N_u} \times \mathbb{R}^{N_\eta} \times \mathbb{R}^{N_y} \times \mathbb{R}^{N_d} \times \mathbb{R}^{N_t} \rightarrow \mathbb{R}^{N_x}$ represent the dynamic process model, i.e., Problem (2.1) is constrained by a differential-algebraic equation (DAE) model. $\mathbf{x} \in \mathbb{R}^{N_x}$ are the states of the system. $\bar{\mathbf{u}} \in \mathbb{R}^{N_u}$ represents the vector of control actions. Vector $\mathbf{y} \in \mathbb{R}^{N_y}$ represents the measured states of the system. The set of decision variables that does not depend on time ($\eta \in \mathbb{R}^{N_\eta}$) contains the process design variables and the controller tuning parameters. $\mathbf{z}$ represents integer decision variables including the choice and sequencing of process units or control structure selection. The aim of simultaneous design and control is not only to identify an optimal process design but also to maintain an acceptable level of operation in the presence of parameter uncertainty and disturbances [1].

Process control plays a crucial role in ensuring the optimal operation and performance of industrial processes. Over the years, various control strategies and schemes have been developed to address the challenges associated with process control. Among the control strategies considered in optimal design and control [27, 28], Proportional-Integral-Derivative (PID) controller has been the dominant control strategy. That control scheme is present on a large fraction of all control loops in the industry. The function for a PID is stated as follows:

$$u(t) = u^0 + K_C \bar{e}(t) + K_I \int_{t_0}^{t_f} \bar{e}(t)\ dt + K_D \frac{d\bar{e}(t)}{dt} \tag{2.2}$$

$$\bar{e}(t) = \mathbf{x}(t) - \mathbf{x}^{sp} \tag{2.3}$$

where K_C, K_I, and K_D are the controller's proportional, integral, and derivative gains, respectively. $\bar{e}(t)$ corresponds to the error signal in the PID controller. A PID controller is intuitive and simple. Moreover, cascade control frameworks can be easily handled using PID schemes. Nevertheless, PID controllers may not be based on process models; consequently, knowledge of process

dynamics (e.g., deadtime or nonlinearity of the system) may not be explicitly used to determine the control actions. Then, process control of highly nonlinear processes in a wider range of operation conditions may be very difficult [29].

Other control techniques such as the internal model control (IMC) structure involve the use of a linear process model in conjunction with the actual process. Although it can be rearranged into the conventional feedback control structure, there are several reasons for employing the IMC design procedure. Firstly, when applied to an open-loop stable process and an open-loop stable controller, the nominal closed-loop system is guaranteed to maintain stability. Additionally, the IMC design procedure facilitates the identification of inherent limitations to closed-loop performance arising from open-loop characteristics. Implementing the IMC structure offers advantages such as effective handling of manipulated variable constraints and compensation for deadtime in the control system. However, model uncertainty may not be rigorously addressed using IMC. Moreover, this controller is a multi-loop controller that does not take into account process interactions.

Advanced process control multi-variable strategies, such as model predictive control (MPC), have shown economic and performance benefits in chemical process industries and represent the state-of-the-art in process control. Integrating MPC into simultaneous design and control has been explored, considering economic objectives, controllability, and disturbance response. MPC can improve system performance by providing optimal control actions obtained from constrained optimization. It handles process variable interactions and constraints, potentially leading to better process designs compared to decentralized control strategies. However, the online optimization involved in advanced control schemes increases the complexity of the design framework. Stability and feasibility are key considerations in MPC, and their integration into design and control strategies is crucial for specifying a stable and efficient closed-loop process design. Various studies have incorporated MPC into simultaneous design and control, addressing aspects like process dimensions, system parameters, flexibility, and robustness. Some studies have also explored the integration of advanced control strategies with sustainability assessment tools. While most applications have used linear MPC, nonlinear MPC (NMPC) offers the potential for considering nonlinear dynamics and constraints. However, the non-convexity of NMPC introduces challenges in terms of problem

complexity and computational effort. Further details on NMPC are presented below in the following section.

The methodologies available in the open literature for the integration of design and control can be classified in different ways. Most of those methodologies rely on steady-state models to calculate capital costs and operating costs. Therefore, the key distinction among those methods lies in how they measure the dynamic performance of the closed-loop system, i.e., the classification can be based on how the dynamic behavior and its impact on cost are quantified. This classification consists of three approaches as follows [30, 31]:

- **Controllability index-based approach**: In this approach, the capital and operating costs are minimized based on steady-state models while incorporating specific controllability objectives. Various controllability indicators such as the relative gain array (RGA) [32], condition number [33], disturbance condition number [34], or integral error criterion have been employed to quantify dynamic performance [35]. Nevertheless, those methodologies have limitations. The economic cost associated with product variability is not explicitly considered in the process economic function. Controllability indicators are often treated as constraints or included in the cost function with ad hoc weightings, lacking a clear correlation to their actual impact on costs. Additionally, the use of steady-state or linear dynamic models in calculating controllability indices limits their applicability to a small range around a nominal steady-state. Consequently, these factors may lead to suboptimal solutions.

- **Dynamic optimization-based approach**: To address the limitations of the controllability index-based approach, a set of methodologies based on dynamic optimization has been proposed in the open literature. Instead of relying on steady-state or matrix measures, the dynamic optimization-based approach evaluates process variability through simulations using the full nonlinear dynamic model. However, the computational demands associated with nonlinear dynamic simulations often limit the analysis to a specified time horizon. Consequently, those methodologies have limitations. The computational complexity of solving nonlinear dynamic optimization problems hinders their practicality for real industrial prob-

lems. The impact of variability is not explicitly assigned an economic cost in the overall cost function, unlike capital and operating costs. The dynamic optimization-based methodologies offer advantages in handling process nonlinearity and time-dependent perturbations but face challenges related to computational complexity, e.g., the absence of clear economic cost assignment to variability, and inadequate explicit consideration of system stability.

- **Robust model-based approach**: To overcome the difficulties associated with dynamic optimization, an approach based on calculating estimated bounds on process variables is available in the open literature. Those bounds determine the system's flexibility, stability, and controllability are obtained from linear models with uncertainty instead of using the full nonlinear dynamic model. One drawback of these methodologies is that they may lead to conservative and suboptimal designs by using estimated bounds instead of actual maximal values for flexibility and controllability. Furthermore, disturbances are considered in terms of their maximal magnitude rather than their actual time profile, potentially resulting in conservative designs compared to dynamic optimization-based approaches. Nevertheless, the robust approach offers the advantage of requiring significantly less computational effort than dynamic optimization-based formulations.

Integration of design and control offers several valuable features that contribute to improved efficiency, productivity, and operational effectiveness. It enables organizations to improve operations, safety, a costs. However, it is essential to be aware of the limitations associated with process design and control, such as complexity of the formulation or uncertainties associated to the process. This PhD thesis is focused on the implementation of NMPC-based controllers; therefore, the literature review presented in the following sections is focused on the integration of design and MPC-based control.

2.2 Nonlinear Model Predictive Control

Nonlinear model predictive control (NMPC) is formulated as a horizon open-loop optimal control problem subject to a nonlinear dynamic process model and a set of operational constraints. The ba-

sic principle of operation of an NMPC-based controller is presented in Figure 2.1. NMPC generates predictions of the dynamic behavior of the system over a prediction horizon (t_P) and determines the control trajectory, over a control horizon (t_C), to maintain the process about the reference trajectory (set-point), such that a performance objective function is optimized [12]. Typically, prediction and control horizons are chosen to be finite, where $t_C \leq t_P$. The performance objective function for the NMPC aims to penalize deviations in the controlled with respect to their set-points and the changes in the manipulated variables.

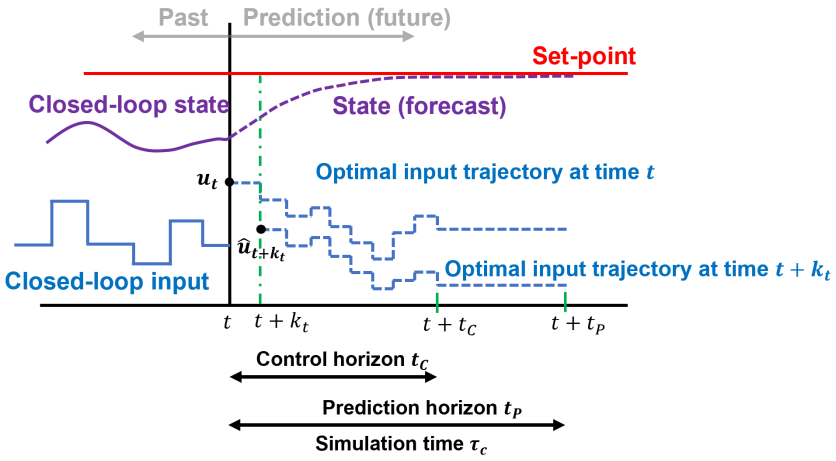

Figure 2.1: Process dynamics prediction in a nonlinear model predictive controller.

If a detailed nonlinear process model is available, the NMPC allows the accurate prediction of dynamic trajectories [36]. Accurate process models are commonly derived from first principle knowledge. On the other hand, if no first principle process model is available, it is possible to obtain a good approximation for the process model based on identification techniques; nevertheless, control strategies with LMPC are preferred under those conditions [12]. The search for a solution for the NMPC's optimization problem is time critical for on-line applications. Recent advances in computational hardware allow the solution of more complex optimization problems within a reasonable amount of time compared to past decades. The conceptual optimization problem for an NMPC-based controller can be formulated as follows:

$$\min_{\hat{\mathbf{x}}(\tau_c),\hat{\mathbf{u}}(\tau_c)} \Psi_{nmpc} = \int_t^{t+t_P} ||\hat{\mathbf{x}}(\tau_c) - \hat{\mathbf{x}}^{sp}||^2_{\mathbf{Q_{out}}}\, d\tau_c + \int_t^{t+t_C} ||\Delta\hat{\mathbf{u}}(\tau_c)||^2_{\mathbf{Q_{in}}}\, d\tau_c \tag{2.4a}$$

$$s.t.\ F(\dot{\hat{\mathbf{x}}}(\tau_c), \hat{\mathbf{x}}(\tau_c), \hat{\mathbf{u}}(\tau_c), \mathbf{d}_p, \tau_c) = 0, \tag{2.4b}$$

$$H(\hat{\mathbf{x}}(\tau_c), \hat{\mathbf{u}}(\tau_c), \mathbf{d}_p, \tau_c) = 0, \tag{2.4c}$$

$$G(\hat{\mathbf{x}}(\tau_c), \hat{\mathbf{u}}(\tau_c), \mathbf{d}_p, \tau_c) \leq 0, \tag{2.4d}$$

$$\hat{\mathbf{u}}(\tau_c) = \hat{\mathbf{u}}(t + t_C),\ \ \forall \tau_c \in [t + t_C, t + t_P) \tag{2.4e}$$

$$\hat{\mathbf{x}}(\tau_c) = \mathbf{x}(t),\ \ \forall \tau_c = t \tag{2.4f}$$

$$\hat{\mathbf{u}}(\tau_c) \in U,\ \ \forall \tau_c \in [t, t + t_C) \tag{2.4g}$$

$$\hat{\mathbf{x}}(\tau_c) \in X,\ \ \forall \tau_c \in [t, t + t_P) \tag{2.4h}$$

$$\mathfrak{X} := \left\{ \hat{\mathbf{x}} \in \mathbb{R}^{N_x} | x^{lb} \leq \hat{\mathbf{x}} \leq x^{ub} \right\},\ \ \mathfrak{U} := \left\{ \hat{\mathbf{u}} \in \mathbb{R}^{N_u} | u^{lb} \leq \hat{\mathbf{u}} \leq u^{ub} \right\} \tag{2.4i}$$

$$\mathfrak{T} := \left\{ \tau_c \in \mathbb{R}^{N_{\tau_c}} | t \leq \tau_c \leq t + t_P \right\}$$

where $H : \mathbb{R}^{N_x} \times \mathbb{R}^{N_u} \times \mathbb{R}^{N_d} \times \mathbb{R}^{N_\tau} \rightarrow \mathbb{R}^{N_h}$ and $G : \mathbb{R}^{N_x} \times \mathbb{R}^{N_u} \times \mathbb{R}^{N_d} \times \mathbb{R}^{N_\tau} \rightarrow \mathbb{R}^{N_s}$ represent the sets of equality and inequality constraints that define the feasibility region of the process, respectively. The function that describes the derivatives of states ($\dot{\hat{\mathbf{x}}}(\tau_c)$) is given by $F : \mathbb{R}^{2N_x} \times \mathbb{R}^{N_u} \times \mathbb{R}^{N_d} \times \mathbb{R}^{N_\tau} \rightarrow \mathbb{R}^{N_x}$, i.e., the dynamic process model. $\mathbf{d}_p \in \mathbb{R}^d$ represents the set of measured disturbances affecting the process; note that disturbances are assumed to remain constant along the prediction horizon (t_P). t represents to actual time of the process whereas τ_c represents the future time instants within the NMPC framework. At each time interval t, the NMPC is initialized from state measurement at time t as shown in Equation (2.4f). The NMPC uses this information, together with the process model F and constraints G and H to find a control action that can optimize the cost function (Equation (2.4a)) within the prediction horizon time t_P, i.e., $\tau_c \in [t, t + t_P)$. States are measured on intervals of time k_t. The controller implements the first control action at the simulation time $\tau_c = t + k_t$. Then, the optimal control problem is re-evaluated after the sampling time k_t, using a new set of measured states at time $t = t + k_t$. Predicted states are given by $\hat{\mathbf{x}}(\tau_c)$; $\Delta\hat{\mathbf{u}}(\tau_c)$ represents the change in the manipulated variables. In this formulation, $\hat{\mathbf{u}}(\tau_c)$ and $\hat{\mathbf{x}}(\tau_c)$ are

bounded by $\mathbf{u}^{lb}$, $\mathbf{u}^{ub}$ and $\mathbf{x}^{lb}$, $\mathbf{x}^{ub}$, respectively. Similarly, $\mathbf{Q_{out}} \in \mathbb{R}^{N_q \times N_q}$ and $\mathbf{Q_{in}} \in \mathbb{R}^{N_u \times N_u}$ are positive-defined diagonal matrices that penalizes the deviations in the predicted states $\hat{\mathbf{x}}(\tau_c)$, with respect to their desired reference (set-point) trajectories $\mathbf{x}^{sp}$, and in the control actions, respectively. In this PhD study, it is assumed that the controller has access to measurements for all states and disturbances at every sampling time t. Disturbances remain constant and equal to their measured values along the prediction and control horizons in the NMPC, i.e., predicted states ($\hat{\mathbf{x}}(\tau_c)$) are the same as measured states ($\mathbf{x}(t)$) at any time $\tau_c^0 = t$ (Equation (2.4f)). $\mathbf{Q_{out}}$, $\mathbf{Q_{in}}$, t_C, and t_P represent the tuning parameters for the NMPC. The selection of the sampling (measurement) time (k_t) is based on heuristics and depends on the dominant time constant of the process and the physical limitations of the measurement devices [37]. The features of NMPC and the effect of the tuning parameter can be found elsewhere [37, 38].

2.2.1 Robust NMPC

The formulation in Equation (2.4) assumes that the actual system (i.e., the real process) is identical to the process model in Equations (2.4b)-(2.4c), i.e., there is no model/plant mismatch or missing information for the computation of predictions in the NMPC. This scenario is seldom possible in practical applications, i.e., the actual system may deviate from the process model due to uncertainties in the system parameters, unmodeled dynamics, measurement noise, missing measurements, or unmeasured process disturbances. The inherent robustness of the nominal NMPC in Equation (2.4) corresponds to the fact that the nominal controller may manage uncertainties and disturbances without taking them directly into account [12]. However, a nominal controller does not provide any guarantee that the in actual system will satisfy feasibility constraints due to the presence of uncertainties or disturbances, i.e., a nominal NMPC may lose feasibility; hence, its guarantee of stability [16]. A *robust* NMPC framework aims to design controllers that can handle these uncertainties and disturbances by incorporating them explicitly into the NMPC formulation, or by designing feedback laws that are robust to such uncertainties [39]. The goal is to ensure that the NMPC can maintain the system's performance and stability under a wide range of uncertain conditions, which is critical for real-world applications. Careful formulation of problem (2.4) is essential to satisfy boundedness,

continuity and differentiability properties, which lead to stable and robust NMPC strategies [36]. The importance of considering model uncertainty in the analysis and design of MPC controllers has been widely studied. For LMPC, both robust stability and robust performance have been studied [40], whereas studies for NMPC have focused on robust stability rather than performance [41].

A robust NMPC explicitly accounts for uncertainties within the controller formulation. Also, it can be interpreted as a min-max formulation, in which the best control actions are computed based on the worst expected realization of the uncertainties [42]. Therefore, the control actions are feasible for all the realization in the uncertainty set (ς). Alternative robust NMPC schemes account for infinite horizon formulations in a receding horizon framework [43], or the implementation of multiobjective optimization strategies involving conflicting objectives (e.g., objectives accounting for both nominal and robust performance terms) [44].

This PhD research focuses on the study and implementation of robust NMPC based on a multi-scenario NLP formulation with state independent uncertainty realizations. The formulation for the robust NMPC (multi-scenario based controller) is as follows:

$$\min_{\hat{\mathbf{x}}(\tau_c),\hat{\mathbf{u}}(\tau_c)} \sum_{j_u=1}^{N_\varsigma} w_{j_u} \Psi_{nmpc}(\hat{\mathbf{x}}(\tau_c),\hat{\mathbf{u}}(\tau_c),\varsigma) \tag{2.5a}$$

$$s.t.\ \ F(\dot{\hat{\mathbf{x}}}(\tau_c),\hat{\mathbf{x}}(\tau_c),\hat{\mathbf{u}}(\tau_c),\varsigma,\mathbf{d}_p,\tau_c)=0, \tag{2.5b}$$

$$H(\hat{\mathbf{x}}(\tau_c),\hat{\mathbf{u}}(\tau_c),\varsigma,\mathbf{d}_p,\tau_c)=0, \tag{2.5c}$$

$$G(\hat{\mathbf{x}}(\tau_c),\hat{\mathbf{u}}(\tau_c),\varsigma,\mathbf{d}_p,\tau_c)\leq 0, \tag{2.5d}$$

$$\hat{\mathbf{u}}(\tau_c)=\hat{\mathbf{u}}(t+t_C),\ \ \forall\tau_c\in[t+t_C,t+t_P) \tag{2.5e}$$

$$\hat{\mathbf{x}}(\tau_c)=\mathbf{x}(t),\ \ \forall\tau_c=t \tag{2.5f}$$

$$\hat{\mathbf{u}}(\tau_c)\in U,\ \ \forall\tau_c\in[t,t+t_C) \tag{2.5g}$$

$$\hat{\mathbf{x}}(\tau_c)\in X,\ \ \forall\tau_c\in[t,t+t_P) \tag{2.5h}$$

$$\mathfrak{X}:=\left\{\hat{\mathbf{x}}\in\mathbb{R}^{N_x\times N_\varsigma}|x^{lb}\leq\hat{\mathbf{x}}\leq x^{ub}\right\},\ \ \mathfrak{U}:=\left\{\hat{\mathbf{u}}\in\mathbb{R}^{N_u\times N_\varsigma}|u^{lb}\leq\hat{\mathbf{u}}\leq u^{ub}\right\} \tag{2.5i}$$

$$\mathfrak{T}:=\left\{\tau_c\in\mathbb{R}^{N_{\tau_c}}|t\leq\tau_c\leq t+t_P\right\}$$

where j_u corresponds to the uncertain scenarios index and w_{j_u} stands for the weights associated to each scenario. This weighting parameter satisfies $0 \leq w_{j_u} \leq 1$ and $\sum_{j_u=1}^{N_\varsigma} w_{j_u} = 1$. Moreover, note that the process model in Equations (2.5b)-(2.5d) is also stated in function of the uncertain parameter (ς). The nominal NMPC (Equation (2.4)) exhibits inherent robustness if uncertainties do not lead to any feasibility loss, i.e., there are no violations to process constraints. If the control actions conduct to violations of process constraints, the closed-loop system may lose stability. The robust NMPC (Equation (2.5)) formulation increases the computational burden, this may be critical for on-line applications. Note that robust NMPC may yield offset for controller variables [42].

2.3 Bilevel optimization

A bilevel optimization problem corresponds to a hierarchical optimization formulation, in which a leader problem (upper-level problem) has a second optimization problem (lower-level problem) as part of its constraints [45]. Bilevel problems are *NP*-hard nonconvex formulations, often CQs are violated at every feasible point; therefore, the search for a solution to this problems is a challenging [46]. Nevertheless, bilevel problems are widely used in chemical engineering, e.g., process design and scheduling [47], water management [48], planning and scheduling [49, 50], optimization of reaction systems [51], waste-heat recovery [52], separation processes [53], etc.

2.3.1 Transformation of the bilevel problem into a single-level problem

The conceptual formulation of a bilevel optimization problem is given as follows:

$$\min_{x} \{\Phi(x, y) : g(x) \leq 0,\ (x, y) \in \mathbf{gph}\Upsilon,\ x \in X_U\} \tag{2.6}$$

where $\Phi : \mathbb{R}^{N_x} \times \mathbb{R}^{N_y} \to \mathbb{R}$ is the upper-level problem cost function, $g : \mathbb{R}^{N_x} \to \mathbb{R}^{N_s}$ is a set of inequality constraints, and $X_U \subseteq \mathbb{R}^{N_x}$ is a closed set. $\mathbf{gph}\Upsilon := \{(x, y) \in \mathbb{R}^{N_x} \times \mathbb{R}^{N_y} : y \in \Upsilon(x)\}$ corresponds to the graph of the mapping Υ, i.e.,

$$\Upsilon(x) := \{y \in Y'(x) \cap X_L : \Psi(x, y) \leq \varphi_{ov}(x)\} \tag{2.7}$$

Let the lower-level problem be defined as follows:

$$\min_{y} \{\Psi(x, y) : G(x, y) \leq 0,\ y \in X_L\} \tag{2.8}$$

where $\Psi : \mathbb{R}^{N_x} \times \mathbb{R}^{N_y} \to \mathbb{R}$ corresponds to the lower-level problem cost function, a set inequality constraints is given by $G : \mathbb{R}^{N_x} \to \mathbb{R}^{N_s}$, and $X_L \subseteq \mathbb{R}^{N_x}$ is a closed set. The bilevel problem described in Equations (2.6) and (2.8) can be described as a hierarchical game with two players. Each player make a decision according to the hierarchical order, e.g., the upper-level problem takes the first decision (x) and communicates it to the lower-level problem. Then, the lower-level problem can compute an optimal response (y) and gives it back to the upper-level problem. Therefore, the upper-level problem is able to compute a new decision [54]. Bilevel problem formulations are very difficult to solve using conventional NLP solvers. Commonly, the most practical approach to solve a bilevel formulation is by the sequential solution of the individual problem levels while updating the parameters and dependencies in each problem in an iterative fashion. Bilevel problem have been extrensively investigated by the mathematical community. The study of further properties and solution methods for bilevel problem formulations is out of the scope of this PhD study, interested readers on these subjects can review the studies by [46, 55, 45].

For engineering applications, the usual approach for the solution of the bilevel optimization problem in Equations (2.6) and (2.8) is to transform it into a single-level problem formulation. To do so, in the literature, there are at least three possible transformation strategies available [15], i.e.,

- **Primal KKT transformation**: In this transformation strategy, the lower-level problem is replaced with its necessary and sufficient optimality conditions. This strategy requires that the lower-level problem to be convex. Otherwise, the global solution of the original bilevel problem is in general not a stationary solution for the corresponding single-level problem [46]. Thus, the primal KKT transformation of problem (2.6) is as follows:

$$\min_{x,y} \{\Phi(x,y) : g(x) \leq 0,\ 0 \in \partial_y F(x,y) + NC_{Y'(x)\cap X_L}(y),\ x \in X_U\} \tag{2.9}$$

where $\partial_y F(x,y)$ is the partial derivative of the convex function $y \mapsto F(x,y)$ with respect to y, and $NC_{Y'(x)\cap X_L}(y)$ corresponds to the *normal cone* (convex analysis) to the set $Y'(x) \cap X_L$ at the point $y \in Y'(x) \cap X_L$, in which $Y'(x) := \{y : g(x,y) \leq 0\}$ and $X_L \subseteq \mathbb{R}^{N_x}$. The single-level formulation in Equation (2.9) has the feature to be fully equivalent to the bilevel optimization problem (2.6) [46]. Therefore, an optimal solution for Equation (2.9) corresponds to a solution for the original bilevel problem (Equation (2.6)).

- **Classical KKT transformation**: In this strategy, the lower-level problem in Equation (2.6) is replaced with its necessary optimality conditions (KKT conditions) [55], i.e.,

$$\begin{aligned}
&\Phi(x,y) \rightarrow min \\
&g(x,y) \leq 0 \\
&0 \in \partial_y F(x,y) + \mu^\intercal \partial_y G(x,y) \\
&\mu(x,y) \geq 0,\ G(x,y) \leq 0,\ \mu^\intercal G(x,y) = 0 \\
&x \in X_U
\end{aligned} \tag{2.10}$$

The single-level problem in Equation (2.10) corresponds to a nonsmooth mathematical program with complementarity constraints (MPCC). If the lower-level problem (Equation (2.8)) is nonconvex, then the introduction of the Lagrange multipliers (μ) in Equation (2.10) produces a single-level formulation that is no longer fully equivalent to the original bilevel problem (Equation (2.6)). MPCCs are nonconvex and highly degenerate formulations; therefore, multiple CQs are violated at every feasible point [18], e.g., LICQ [56] and MFCQ [57], which are required for a well-posed NLP. Note that implementations using MPCCs in process engineering are gaining increasing interest [18], in particular, for formulations involving nonconvex lower-level problems [58, 59]. *Classical KKT transformation* is the most often used approach

for the direct solution of bilevel problems.

- **Optimal value transformation**: The implementation of this transformation strategy requires the assumption that the lower-level problem (Equation (2.8)) admits an optimal solution for each $x \in X_U$ [55]. Hence, the objective function and constraints of the lower-level problem can be moved to the upper-level problem as follows:

$$\begin{aligned} &\Phi(x,y) \rightarrow min \\ &g(x,y) \leq 0 \\ &F(x,y) \leq \varphi_{ov}(x) \\ &G(x,y) \leq 0,\ y \in X_L \\ &x \in X_U \end{aligned} \tag{2.10}$$

  where φ_{ov} denotes the optimal value function of the lower-level problem in Equation (2.8). This function is defined in Equation (2.12). An optimal value transformation leads to non-smooth optimization problems since function φ_{ov} is not differentiable, even if the objective function and constraints in the lower-level problem are smooth. Similar to a primal KKT transformation, the optimal value transformation leads to a formulation that is fully equivalent to the original bilevel problem (Equation (2.6)) [46].

$$\varphi_{ov}(x) := \min_{y} \{\Psi(x,y) : G(x,y) \leq 0,\ y \in X_L\} \tag{2.12}$$

This PhD study focuses on the implementation of MPCCs for the transformation of the original bilevel formulation into a single level optimization formulation for the integration of design and NMPC-based control under uncertainty and process disturbances. As mentioned above, a MPCC formulation violates multiple constraint qualifications (CQs), which makes challenging the computation of a solution for these formulations. Accordingly, the use of reformulation strategies becomes necessary to avoid the violations of CQs and to facilitate the search of optimal solutions. The use

of MPCCs has been extended to chemical engineering for the integration of scheduling and control [60]; moreover, MPCCs have been a powerful tool in the solution of equilibrium operations, such as distillation [59, 61], and for the optimization of heat exchanger networks [58]. Design and control problems are specially difficult to solve due to the close dependence of the decision variables, i.e., changes in the process design has a strong effect on the process dynamics. Compared to conventional applications of MPCCs in chemical engineering that just include variables that depend on time in the formulation, a simultaneous design and control problem incorporates variables that depend on time (e.g., control laws and states profiles) together with design variables that do not depend on time (e.g., equipment sizes and operating set-points). This increases the problem's complexity since the NMPC directly depends on the process design decisions. Meanwhile, the nonconvexity of MPCCs demands an educated initialization to the problem. This is particularly challenging for applications on design and control with NMPC, since it requires to provide initialization for variables that are physically unknown a priori, e.g., initialization for *Lagrange multipliers*. A reformulated MPCC offers the feature that the problem can be solved explicitly with state-of-the-art NLP solvers, such as IPOPT; consequently, methodologies involving iterative procedures are not required. Since the MPCC can be solved as a conventional NLP, local optimality in the solution of such MPCC-based problem is guaranteed. However, an optimal solution for the MPCC-based formulation may not be an optimal solution for the original bilevel problem due to non-convexities in the lower-level problem.

2.3.2 Properties of MPCCs

If the lower-level problem in Equation (2.8) is a nonconvex formulation, its KKT conditions correspond to the necessary conditions for optimality, i.e., the corresponding KKT conditions for optimality are not sufficient to guarantee optimality in the solution for the lower-level problem. Therefore, in order to classify a solution for the MPCC (Problem (2.10)), the concept of stationarity is introduced. Certain stationary points from the MPCC problem (Problem (2.10)) such as B-*stationary* or S-*stationary* verify an optimal solution for the original bilevel problem (Problem (2.6)).

A point $\Omega^* = [x^{*,\intercal}, y^{*,\intercal}]^\intercal$ is a B-*stationary* point if it is feasible for Problem (2.10), and $s = 0$ is a solution to the following linear program [18]:

$$\min_{\mathbf{s}} \nabla\Phi(x^*, y^*)^\intercal s \tag{2.13a}$$

$$s.t.\ \ g(x^*, y^*) + \nabla g(x^*, y^*)^\intercal s \leq 0 \tag{2.13b}$$

$$\nabla\mathcal{L}(x^*, y^*) + \nabla^2\mathcal{L}(x^*, y^*)^\intercal s = 0 \tag{2.13c}$$

$$0 \leq \mu(x^*, y^*) + s_\mu \perp -(G(x^*, y^*) + s_G) \geq 0 \tag{2.13d}$$

The linear Problem (2.13) verifies that locally there is no feasible direction that improves the objective function. On the other hand, to verify *strong stationarity* consider the following sets:

$$\mathfrak{I}^{+0}(x, y) := \{si \in \{1, \ldots, N_s\} | \mu(x, y) > 0 \ and \ G(x, y) = 0\},$$

$$\mathfrak{I}^{0+}(x, y) := \{si \in \{1, \ldots, N_s\} | \mu(x, y) = 0 \ and \ -G(x, y) > 0\},$$

$$\mathfrak{I}^{00}(x, y) := \{si \in \{1, \ldots, N_s\} | \mu(x, y) = 0 \ and \ G(x, y) = 0\},$$

Weaker stationarity conditions such as *weak*, *A*-, *C*-, and *M-stationary* points can be verified. Nevertheless, these conditions are not sufficient to identify local optimality for the original bilevel problem (2.6) since they allow negative Lagrange multipliers and have feasible descent directions [18, 62], i.e.,

- ***Weak-stationary***: A point is *weak-stationary* if there exists multipliers $\lambda \in \mathbb{R}^{N_x} \times \mathbb{R}^{N_y} \times \mathbb{R}^{N_s}$ such that

  $$\nabla_\Omega \mathcal{L}_{MPCC}(\Omega^*, \lambda) = 0$$

  $$\min\left(-g(\Omega^*), \lambda^g\right) = 0,$$

  $$\forall si \in \mathfrak{I}^{+0}(\Omega^*), \lambda^\mu_{si} = 0, \ and \forall si \in \mathfrak{I}^{0+}(\Omega^*), \lambda^G_{si} = 0$$

- ***C-stationary***: A *C-stationary* point is obtained if Ω^* is *weak-stationary* and

$$\forall si \in \mathfrak{I}^{00}(\Omega^*),\ \lambda^{\mu}_{si}\lambda^{G}_{si} \geq 0$$

- ***A-stationary***: An *A-stationary* point can be identified if Ω^* is *weak-stationary* and

$$\forall si \in \mathfrak{I}^{00}(\Omega^*),\ \lambda^{\mu}_{si} \geq 0 \ or\ \lambda^{G}_{si} \geq 0$$

- ***M-stationary***: A *M-stationary* point is obtained if Ω^* is *weak-stationary* and

$$\forall si \in \mathfrak{I}^{00}(\Omega^*),\ either\ \lambda^{\mu}_{si} > 0,\ \lambda^{G}_{si} \geq 0 \ or\ \lambda^{\mu}_{si}\lambda^{G}_{si} = 0$$

- ***Strong-stationary***: A *S-stationary* point is obtained if Ω^* is *weak-stationary* and

$$\forall si \in \mathfrak{I}^{00}(\Omega^*),\ \lambda^{\mu}_{si} \geq 0,\ \lambda^{G}_{si} \geq 0$$

The assumption of *Strong-stationarity* plays a crucial role in enabling the solution of bilevel problem using NLP formulations (i.e., the implementation of MPCCs). This property ensures that a properly defined set of Lagrange multipliers can confirm the optimality of the original bilevel problem (2.6), and by appropriately reformulating the MPCC (Problem (2.10)), several equivalent and well-defined nonlinear programs can be obtained [18]. A detailed review of stationary conditions is beyond the scope of this PhD research. Further information about stationary conditions can be found elsewhere in the literature [46, 63, 64].

2.3.3 Applications involving mixed-integer bilevel problems

Design decisions such as the arrangement of equipment, or the determination of the number of stages/equipment are often modeled using integer/binary variables. A nonlinear bilevel problem involving integer decisions is referred to as a mixed-integer bilevel problem (MIBLP). Depending

on the location of the integer and continuous decision variables in the optimization formulation, the problem can be classified into four different categories [46]: i) integer upper, continuous lower; ii) purely integer problem; iii) continuous upper, integer lower; or iv) mixed-integer upper and lower.

A few algorithms can be found in the literature for the solution of MIBLPs for specific applications [65]. Edmunds and Bard [66] proposed a branch and bound algorithm for the solution of MIBLPs. Dominguez and Pistikopoulos [67] presented two algorithms using multiparametric programming techniques for the solution of integer bilevel problems. Faisca et al. [68, 69] extended the implementation of multiparametric strategies for the solution of bilevel quadratic and linear mixed-integer bilevel problems, with or without right-hand-side uncertainty. Mitsos [70] proposed an algorithm for the global optimization of nonlinear mixed-integer bilevel problems. Applications with MIBLP formulations in chemical engineering are mainly focused on the following areas: (i) supply chain management; (ii) traffic and transportation network design; (iii) energy management; (iv) safety and accident management; and (v) process system engineering. Dempe et al. [54] presented a mathematical framework for the minimization of cash-out penalties of a natural gas distribution network. They proposed to move a Boolean variable from the lower to the upper-level problem, the resulting two linear bilevel programming problems were solved using a penalty function approach. Clark [71] implemented a bilevel formulation for the steady-state optimization of a process for aniline production. Smith and Missen [72] proposed a set of bilevel problem formulations for the synthesis of chemical equilibrium processes. It can be noted that applications and solution methods for MIBLPs are more focused on a restricted class of problems. Further reviews on the methodologies for the solution of MIBLPs can be found elsewhere [73, 74, 75, 65, 76, 77]. Along this PhD thesis, the optimization problems for the integration of design and NMPC-based control correspond to mixed-integer upper and continuous lower problems. The analysis and solution of other bilevel formulations are out of the scope of this study.

2.4 Pontryagin's minimum principle and the Hamiltonian function

In the hierarchy of the decision making stages (e.g., process design, scheduling, real-time optimization, and process control) in the chemical industry, DO problems appear in process design, (dynamic) real-time optimization and process control activities [78]. In an DO problem, the goal is to find a solution for manipulated variables (e.g., optimal temperature profile) and the associated states (e.g., product concentration), such that a user-defined performance measure is optimized (e.g., throughput maximization), subject to the system dynamics and process constraints (e.g., temperature boundaries). In the context of process control, DO helps to find the operating conditions that lead to an optimal process performance while keeping the operation within the feasible operating region [79]. Finding a solution for the DO formulation by solving the necessary conditions for optimality is commonly known as the *indirect* approach. For large-scale problems, this approach becomes quite involved. As a result, methods that transform the original problem into a finite-dimensional optimization model emerged as an alternative to solve large problems more efficiently [80]. These methods belong the category referred to as the *direct* approach. A central result from the implementation of calculus of variations and the classical control theory in the context of a *indirect* approach is the celebrated Pontrygin's maximum principle developed in the mid-1950s by Pontryagin et al. [81]. The principle provides the necessary conditions for an optimal solution. For practical purposes, it is referred to as the PMP as most problems in chemical engineering are cast as minimization problems.

Although *direct* methods are becoming more popular in the solution of chemical engineering problems, the DO theory in the sense of PMP is still used due to the unique and distinctive information that can be derived from the optimality conditions. This information allows for a deep understanding of the problem and has been used to find solutions with higher accuracy than those obtained with the *direct* approach [82]. Furthermore, the necessary conditions can also be used to study the sensitivity of the optimal solution with respect to changes in the model, the inputs and the constraints [83].

The literature review presented in this section focuses on the determination of the Hamiltonian necessary conditions for optimality (i.e., an indirect solution approach) for autonomous formulations involving design (time-independent) and control (time-dependent) decisions variables. Further

formulations are out of the scope of this PhD study. Note that the content presented in this section is part of the work published in AIChE Journal [20].

DO problems involving parameters (i.e., time-independent decision variables) as part of the formulation, e.g.,the simultaneous optimal design and operation of a system, or when the final time appears as a parameter to be optimized. In order to illustrate this situation, consider the following problem with parameters and fixed final time:

$$\min_{\mathbf{x}(t),\mathbf{u}(t),\eta} \Phi\left(\mathbf{x}(t_f),\eta\right) + \int_{t_0}^{t_f} \psi\left(\mathbf{x}(t),\mathbf{u}(t),\eta,t\right) dt \tag{2.15a}$$

$$s.t. \quad f\left(\mathbf{x}(t),\dot{\mathbf{x}}(t),\mathbf{u}(t),\eta,t\right) = 0, \quad \mathbf{x}(t_0) = \mathbf{x}_0 \tag{2.15b}$$

$$h\left(\mathbf{x}(t_f),\eta\right) = 0 \tag{2.15c}$$

where η correspond to the time-independent decision variables. Process states are given by $\mathbf{x}(t)$. The objective function (2.15a) (performance measure) can take three different forms:

$$\textbf{Bolza} \quad \Phi\left(\mathbf{x}(t_f),\eta\right) + \int_{t_0}^{t_f} \psi\left(\mathbf{x}(t),\mathbf{u}(t),\eta,t\right) dt \tag{2.16}$$

$$\textbf{Lagrange} \quad \int_{t_0}^{t_f} \psi\left(\mathbf{x}(t),\mathbf{u}(t),\eta,t\right) dt \tag{2.17}$$

$$\textbf{Mayer} \quad \Phi\left(\mathbf{x}(t_f),\eta\right) \tag{2.18}$$

The three forms are equivalent in the sense that a problem with the objective function expressed in one form (e.g., Bolza) can be restated using an alternative objective function expression (e.g., Mayer) by applying an appropriate transformation, e.g., by moving the integral term in objective function as an ODE constraint in the formulation. The corresponding Hamiltonian function for the problem (2.15) is as follows:

$$\mathbb{H}\left(\mathbf{x}(t),\mathbf{u}(t),\lambda(t),\eta,t\right) = \psi\left(\mathbf{x}(t),\mathbf{u}(t),\eta,t\right) + \lambda^{\intercal}(t) f\left(\mathbf{x}(t),\dot{\mathbf{x}}(t),\mathbf{u}(t),\eta,t\right) \tag{2.19}$$

The Hamiltonian function allows to express the necessary conditions for optimality as a Hamilton's system of equations commonly used in the calculus of variations. For some problems, the constancy of the Hamiltonian is used as an indicator of optimality. To simplify the notation, the

Hamiltonian is expressed as $\mathbb{H}(t)$. The necessary conditions for optimality based on PMP are stated as follows [84]:

$$\frac{d\mathbf{x}(t)}{dt} = \frac{\partial \mathbb{H}(t)}{\partial \lambda} \tag{2.20a}$$

$$\frac{d\lambda(t)}{dt} = -\frac{\partial \mathbb{H}(t)}{\partial \mathbf{x}} \tag{2.20b}$$

$$\frac{d\gamma(t)}{dt} = -\frac{\partial \mathbb{H}(t)}{\partial \eta}, \quad \gamma(t_0) = 0 \tag{2.20c}$$

$$h\left(\mathbf{x}(t_f), \eta\right) = 0 \tag{2.20d}$$

$$\mathbf{u}(t) = arg \min_{\bar{\mathbf{w}} \in \mathfrak{U}} \mathbb{H}\left(\mathbf{x}(t), \bar{\mathbf{w}}(t), \lambda(t), \eta, t\right) \tag{2.20e}$$

$$\gamma(t_f) = \frac{\partial \Phi(t_f)}{\partial \eta} + \frac{\partial h(t_f)^\intercal}{\partial \eta} \bar{b} \tag{2.20f}$$

$$\lambda(t_f) = \frac{\partial \Phi(t_f)}{\partial \mathbf{x}} + \frac{\partial h(t_f)^\intercal}{\partial \mathbf{x}} \bar{b} \tag{2.20g}$$

where $\gamma(t) \in \mathbb{R}^{N_\gamma}$ is a vector of auxiliary functions of t. The minimization of $\mathbb{H}$ is with respect to admissible controls $\bar{\mathbf{w}}(t)$ that belong to a set $\mathfrak{U}$. Note that If the Hamiltonian function in Equation (2.19) does not depend explicitly on t, then in addition to conditions (2.20f) and (2.20g), the Hamiltonian function must satisfy to be constant over time. This condition is referred to as constancy of the *Hamiltonian* function. The set of optimality conditions (2.20) generally leads to a well-posed DAE system in the form of a TPBVP. Moreover, a key feature of PMP is that the Hamiltonian function is continuous, even if the control law is not [85].

For the solution of the conditions for optimality (2.20) using a full discretization approach (direct transcription), if sufficient discretization points are not provided, this returns a nonconstant Hamiltonian function profile [85, 86]. Therefore, this feature of the Hamiltonian function can be considered a criterion for the refinement of the number of finite elements.

Pontryagin's principle has been a powerful tool for the optimization of many chemical processes. Necessary conditions for optimality have been derived for various DO formulations. Moreover, efforts have been made to solve these conditions by applying analytical and numerical strategies. However, as chemical engineering applications become more complex and diverse, the use of PMP becomes more involved.

2.5 Integration of design & MPC-based control

The integration of design and control allows to establish a clear connection between the conflicting goals of steady-state economics and dynamic performance during the early stages of process design. An integrated design and control approach aims to identify optimal process designs and also ensure acceptable operation under parameter uncertainty and process disturbances, i.e., by accounting for uncertainties, the optimization problem can accommodate undesired scenarios and minimize process variability [1]. The specification of a sustainable process involves several key aspects, including profitability, controllability, flexibility, reliability, product quality satisfaction, safety, and environmental considerations. Process profitability refers to the ability of a process to generate a profit for a business. It is a measure of how effectively a process converts inputs (such as labor, materials, and energy) into outputs (such as goods or services) that can be sold for a profit. Controllability refers to the ability of a system to maintain desired output variables within specific bounds despite external or internal disruptions by adjusting available manipulate variables. Flexibility refers to the ability of the process to adapt to changes in demand, production requirements, or other external factors without significant disruptions or loss of efficiency. On the other hand, process reliability refers to the ability of a process to consistently produce output that meets the desired specifications and performance requirements, without unexpected failures or errors.

The use of integrated approaches to specify a sustainable process can be challenging because it involves multiple complex aspects, specially for large-scale applications. Those challenges may involve the following aspects: (i) uncertainties and disturbances, (ii) multiple (conflicting) objectives, (iii) increased problem scale, (iv) structural (discrete) decision variables, (v) local vs. global optimality, and (vi) consideration of advanced control schemes (e.g., MPC-based control schemes). The development of comprehensive solution strategies that encompasses all aspects using state-of-the-art technology is still very difficult to accomplish. Initially, available techniques for chemical process design were classified into three main categories: controllability index-based approaches, dynamic optimization, and robust-based approaches [31]. Two additional categories were added later: embedded control optimizations and black-box optimization approaches [30]. This PhD study does

not pretend to review all the methodologies and applications developed thus far for simultaneous design and control. This study is focused on the implementations for design and control using MPC-based control schemes. Further reviews regarding the integration of design and control, including its features, methodologies, and potential applications, can be found elsewhere [1, 8, 31, 87, 30, 88, 89].

Table 2.1: Prominent works that have addressed the integration of design and model-based control.

Author	**Contributions**
Brengel & Seider [10]	Implementation of a transformation strategy to obtain a single-level formulation using KT conditions for linear model formulations.
Loeblein & Perkins [90]	Implemented a back-off approach to determine a feasible steady-state design and process dynamics using a unconstrained LMPC.
Sakizlis et al. [4, 8, 91]	Incorporation of discrete decisions and the implementation of an approximation strategy to explicitly state the LMPC as part of the design model constraints.
Backer & Swartz [92]	Implementation of a KKT transformation strategy to replace the quadratic problem for LMPC in the formulation for integrated design and control.
Chawankul et al. [11]	Incorporation of variability, capital, and operability costs in a single objective function.
Ricardez-Sandoval et al. [93, 94, 95]	Robust stability and performance measures based on Lyapunov functions theory for applications under uncertainty.
Francisco et al. [96, 97, 98]	Cost functions involving investment, operating costs, and dynamical indexes in multi-model formulations.
Gutierrez et al. [99]	Implementation with interconnection structures to determine the combination of manipulated and controlled variables using centralized and decentralized LMPC controllers.
Sanchez-Sanchez & Ricardez-Sandoval [100]	Implementation of structural decisions using convex formulations for robust flexibility and asymptotic stability analyses.
Bahakim & Ricardez-Sandoval [2]	Analysis and computation of stochastic-based worst-case variability index.
Burnak & Pistikopoulos [101]	Implementation of multi-parametric programming to embed the LMPC into a MIDO formulation.
Carvalho & Alvarez [102]	Multistage solution procedure for the integration of design and infinite horizon LMPC-based control
Hoffmann et al. [14]	Implementation of economic NMPC control for process design under uncertainty.
Oyama & Durand [103]	Evaluation of the interaction between the process design and the process control using an economic nonlinear model predictive controller (eNMPC).
Tian et al. [104]	Implementation of PAROC platform for design, operational optimization, and multi-parametric LMPC for intensified reactive distillation columns

The integration of design and control has been widely studied for application with classical control schemes. Despite the advantages of MPC-based control approaches for integrated design and control, this is still an emerging research area. The main challenge in the implementation of advanced control schemes lies in the solution of an optimization problem on-line, which leads to a drastic increase in the complexity of the formulation for simultaneous design and control. Nevertheless, during the past three decades, the industry and the academia have recognized the potential of LMPC. Nowadays, LMPC represents the current state-of-the-art for process control. As mentioned previously in Chapter 1, model-based control offers the feature of handling constraints in the manipulated and controlled variables explicitly in its formulation. Moreover, model-based controllers may exhibit better control performance than conventional feedback controllers [105]. This section presents an overview of the most significant methodologies and contributions to simultaneous design and model-based control such that the current gaps in the literature can be identified. A summary of the methodologies for the integration of design and model-based control is presented in Table 2.1.

The publication of multiple studies has reflected the interest for the implementation of model-based control schemes for simultaneous design and control. The implementation of model-based controller is expected to improve the performance of the designed system compared to conventional decentralized PI or PID control strategies. One of the first studies that incorporated LMPC for simultaneous design and control was presented by Brengel and Seider [10]. They replaced the LMPC problem in the bilevel formulation using its Kuhn-Tucker conditions; a Newton homotopy solution strategy was implemented for the solution of small scale problem. They recognized that the solution of a coordinated problem is challenging due to the presence of Lagrange multipliers. Loeblein & Perkins [90] implemented a non-constrained LMPC control law to assess the variance of the constrained variables of the closed-loop system subject to stochastic disturbances. Therefore, the amount of necessary back-off from the constrains can be calculated. It aimed to determine a feasible steady-state design and process dynamics. Significant contributions to simultaneous design and MPC-based control area has been proposed by Pistikopoulos et al. [4, 8, 91, 106]. They have proposed the use of parametric-MPC to include an explicit form of the controller in the optimiza-

tion model for design and control. Sakizlis et al. [4] included the parametric explicit form of the LMPC controller as part of the process model. They implemented an outer approximation decomposition method for the simultaneous identification of the optimal process and control design with discrete decisions, i.e., a control master problem aimed to determine the controller tuning parameters, whereas a structural master problem provided the values for the discrete design decisions. Chawankul et al. [11] integrated in one objective function the costs associated to the variability, capital, and operability aspects; whereas the process design variables and the controller tuning parameters were calculated simultaneous. Robust stability and performance measures based on Lyapunov functions theory for applications in simultaneous design and LMPC-based control under uncertainty were presented by Ricardez-Sandoval et al. [93, 94, 95]. They estimated the worst case variability, process feasibility, and process stability using a structured singular value analysis. Francisco et at. [96, 97, 98] developed different methodologies for the integration of design and LMPC-based control for chemical processes. In those studies, they considered cost functions that included investment, operating costs, and dynamical indexes in multi-model formulations. Moreover, Francisco et al. [98] selected a LMPC with infinite horizon and a terminal penalty to guarantee closed-loop process stability. Results from that approach showed an improvement in control performance compared to those obtained with a classical design approach (i.e., optimal steady-state design approach). Sanchez-Sanchez & Ricardez-Sandoval [100] presented an iterative decomposition framework for integration of process flowsheet and MPC design under uncertainty; that approach considered a dynamic flexibility analysis, a robust dynamic feasibility test, a nominal stability analysis, and a robust asymptotic test for the process flowsheet selection. While in the past, those analyses were formulated as MINLPs, Sanchez-Sanchez & Ricardez-Sandoval implemented convex formulations to address such analyses. Thus, they proposed a computationally attractive methodology. Bahakim & Ricardez-Sandoval [2] introduced an stochastic-based methodology for simultaneous design and LMPC-based control under uncertainty. They determined the dynamic variability of the system using a stochastic-based worst-case variability index. On the other hand, Pistikopoulos et al. [107, 106] presented a methodology that makes use of the software platform PAROC to integrate a multi-parametric MPC (mpMPC) for process design and control

under uncertainty. In that methodology, the explicit control actions are expressed as a function of the design variables (i.e., the control is design dependent); this leads to a single design dependent mpMPC formulation. Those promising strategies contributed to reduce the computational burden associated with optimal design and control problems. Recently, Carvalho & Alvarez [102] presented a multistage solution procedure for the integration of design and infinite horizon LMPC-based control; that methodology showed an excellent performance to compute economically attractive solutions. Those previous works have pointed the features and benefits of the use of model-based controllers for optimal design and control. In further works, Oyama & Durand [103] explored the interactions between the implementation of an economic nonlinear model predictive controller (eNMPC) and the corresponding process design. They studied the impact of these interactions to the computational complexity of the controller and the process design procedure. That study suggested a set of controller design variables that can be considered as key decision variables for simultaneous process design and control problems in presence of process disturbances. Hoffmann et al. [14] implemented an unscented transform method to approximate the probability density function of inequality constrains in applications with economic NMPC under stochastic disturbances. For high probability levels, their methodology found difficulties to retrieve a feasible solution, i.e., the search for a solution for application with NMPC may represent a challenge.

In general, most of the applications addressing the integration of design and model-based control have considered LMPC frameworks. However, the dynamic behavior of highly nonlinear processes may not be effectively approximated by linear formulations. The implementation of NMPC is expected to improve the control performance and the process economics compared to application with LMPC for application in integrated design and control; moreover, note that there are no studies that have compared the LMPC and NMPC for these purposes. Integrating design and NMPC-based control remains a challenging task, as the non-convexity of the nonlinear problem adds to the size of the integrated problem, resulting in increased complexity and computational effort. To better understand the advantages and disadvantages of NMPC embedded in simultaneous design and control, a more thorough investigation is necessary, including a fair comparison of associated features and limitations, such as computational costs.

2.6 Selection of finite elements in process design

The accuracy of the discretization mesh has been intensively studied for applications in simulation and control of flow of fluids [108, 109], distillation operations [110], reaction system operations [111, 112], heat transfer [113], optimal control [86, 85, 114], among others [115, 116]. In the literature, the approaches for the selection and refinement of the discretization mesh can be divided into two classes: *relocation methods* and *grid point insertion and elimination*. In the *relocation method*, the number of discretization points is kept constant whereas they are relocated depending on the nonsmoothness of the dynamic profiles for the decision variables (i.e., dynamic profiles for controlled and manipulated variables). Liu et al. [117] implemented a mesh refining methodology that compares two different meshes to approximate a solution for optimal control problems. An adaptive finite element method based on variable knot spline interpolation was presented by Davis and Flaherty [115]. Zhao and Tsiotras [118] implemented local density functions for the refinement of the discretization mesh in the optimal control framework. They implemented different density functions based on local curvature of the graph of the intermediate solution and the first order derivative of the control variable. Assassa and Marquart [86] proposed a switching function-based methodology for the refinement of the number of finite elements. That study found that Pontryagin's minimum principle (PMP) is not sufficient as a stopping criterion on the refinement of the discretization grid, i.e., additional criteria becomes necessary for the selection and refinement of finite elements. The implementation of the PMP allows one to obtain the Hamiltonian first order necessary conditions for optimality. A key feature of PMP is that the Hamiltonian function is continuous, even if the control law is not, and constant over time for autonomous systems [85]. If sufficient discretization points are not provided for the solution of the Hamiltonian optimality conditions, this returns a non-constant Hamiltonian function profile. Therefore, this feature of the Hamiltonian function can be considered a criterion for the refinement of the number of finite elements.

Orthogonal collocation on finite elements (OCFE) is a powerful numerical technique widely used in chemical engineering to solve DAE models, ODEs, and PDEs. The OCFE method involves the use of finite element methods for discretization and orthogonal collocation to discretize the time

domain. This approach leads to a system of algebraic equations that can be efficiently solved using numerical techniques, allowing for the prediction of system behavior over time. The OCFE method has proven to be particularly useful in the simulation of complex chemical processes such as reaction kinetics, mass transfer, and heat transfer. The ability to accurately model these processes has been instrumental in the design and optimization of chemical processes, making OCFE an essential tool in the field of chemical engineering. For instance, Chen et al. [85] developed a methodology for the selection and refinement of finite elements for applications in optimal control. That methodology added/removed finite elements based on the criterion of the Hamiltonian function, whereas the size of the finite elements is refined using the criterion of the estimation of the collocation error at noncollocation points. In a *grid point insertion and elimination* strategy, the number of discretization points (e.g., the number of finite elements and collocation points in an OCFE strategy) are increased or reduced depending on the accuracy of the approximation to the functions in the optimization formulation. In most of the cases, that strategy with equidistributed finite elements provides a reasonably accurate approximation to the solution. Wright [119] found that in cases where the accuracy of the approximation is low with a collocation strategy, equidistributed finite elements may not return a unique solution to the differential equations. Russell and Christiansen [120] reviewed multiple strategies for the refinement of the discretization with collocation methods. In particular, that study pointed out the effectiveness of two methods for estimating the collocation error: extrapolation of the collocation solutions using similar meshes, and a method based on residuals. In this PhD study, OCFE is adopted as the preferred discretization technique. other discretization approaches are out of the scope of this study. The methodology and implementation of OCFE is described in Chapter 6. Further reviews on the discretization mesh refinement can be found elsewhere [116, 121].

2.7 Summary

In summary, this chapter has presented the methods, mathematical formulations, and background that are relevant for this PhD thesis. The first section presented the approaches for design and

control. The second section presented the conceptual formulation for NMPC. The consideration of uncertainty in its process model introduces robustness to the formulation. It aims to determine optimal control actions to maintain the process dynamically feasible under uncertainty. In the third section, the conceptual formulation for a bilevel problem was introduced. Potential strategies to transform the bilevel problem into a single-level problem were discussed. A classical KKT transformation strategy corresponds to the most often used for the direct solution of bilevel problems. This transformation strategy returns a single-level MPCC, which is also difficult to solve; nevertheless, there are reformulation strategies that facilitate the solution of MPCC formulations. The implementation of discrete decisions introduces an additional complexity layer to the bilevel formulation. To the author's knowledge, an implementation using NMPC for integrated design and control under uncertainty and structural decisions has not been addressed. The methods presented in the literature for the solution of MIBLPs may be case specific. A fourth section introduces the concept of Hamiltonian function and the corresponding Pontryagin's minimum principle. In the fifth section, a literature review of the development and innovations for integrated design and NMPC-based control framework was presented. Most of those studies are focused on the implementation of LMPC. The implementation of NMPC has been identified as a challenging task for the integration of design and control. In the the sixth section, an overview of the methods and applications of discretization refinement regarding process design in chemical engineering was presented. An important amount of studies has pointed out the necessity of considering the selection of the discretization mesh for the accurate approximation of DAE models. Although the importance of this selection, there is an absence of studies involving simultaneous design, control, and discretization mesh selection/refinement using OCFE. A potential criterion for the selection of the discretization mesh using OCFE is the implementation of the Hamiltonian function. This function leads to the solution of a set of necessary conditions for optimality that are described as a TPBVP. The next chapter presents a methodology that is proposed in this PhD study for the integration of design and NMPC-based control under uncertainty.

Chapter 3

Simultaneous design and nonlinear model predictive control under uncertainty: A back-off approach

As mentioned above in Chapters 1 and 2, integrated design and NMPC-based control results in a bilevel formulation. The search for a solution to this formulation may become challenging even for medium-scale applications. Moreover, the introduction of uncertainties in the process model increases the complexity and scale of the formulation. The potential benefits of using NMPC for integrated design and control has not been widely assessed in the literature; consequently, there is a lack of practical methodologies to address the solution of such complex formulation.

The back-off approach offers an attractive alternative, as it begins the search for a solution at the steady-state and systematically moves the process design towards an optimal, dynamically feasible operating point. Perkins [122] proposed the first idea of back-off. Then, Narraway and Perkins [123] refined this idea by considering linear process models, enabling the estimation of the required amount of back-off to accommodate the effect of disturbances from active constraints at the optimum steady-state. Then, the back-off approach was implemented for simultaneous design and control by Kookos and Perkins [124, 125], in which tighter upper and lower bounds on the optimal design and control were systematically generated to ensure feasibility in the process dynamics of the resulting solutions. A PSE strategy for the back-off approach was presented by Mehta and Ricardez-Sandoval [126]. This strategy was refined by Rafiei and Ricardez-Sandoval [127, 128], in which an application for the integration of design and control using decentralized PI was presented. The primary challenge of this approach is determining the necessary amount of back-off to accommodate the transient process operation [129]. Linearization of constraints [130], use of probability density functions [131], and Monte Carlo simulations [132] are among the techniques implemented for the determination of the amount of back-off.

In this PhD thesis, the proposed back-off method reduces the complexity of the original bilevel

problem by approximating the problem in terms of PSE functions. This approximation is explicitly defined for the decision variables and features the property to be a single-level problem that can be solved using conventional NLP solvers. In a systematic fashion, the proposed methodology searches for the amount of back-off to move the design and control variables from the optimal steady-state to a new dynamically feasible economic operating point that can explicitly accommodate uncertainty in the system parameters.

This chapter is organized as follows: the next section presents the formulation for simultaneous design and NMPC-based control. Section 3.2 introduces the proposed back-off methodology. The implementation of this methodology is illustrated in a case study involving a highly nonlinear wastewater treatment plant (WWTP) in Section 3.3. A summary of this chapter is presented in Section 3.5.

3.1 Simultaneous design & NMPC-based control

The dynamic process model in the NMPC framework is generally given by first principle models. These models condense the information of the process behavior and process design. Thus, an adequate process model in the NMPC enables the computation of accurate predictions with optimal control actions. When NMPC is implemented for a simultaneous design and control framework, it becomes a complex formulation since the design problem requires the information from the control actions whereas the NMPC-based controller needs to have access to process design decisions in order to compute the optimal control actions, i.e., both the design and control problems depend of each other. This leads to a called *bilevel optimization formulation* [46]. The computation of optimal solutions for a bilevel optimization problem is known to be a challenging task. In this work, for simultaneous design and NMPC-based control, the conceptual mathematical bilevel formulation is defined as follows:

$$\min_{\eta,\mathbf{x}(t),\bar{\mathbf{u}}(t),\hat{\mathbf{u}}(\tau_c),\mathbf{y}(t)} \sum_{j_u=1}^{J} w_{j_u} \Phi(\eta, \varsigma, \mathbf{x}(t), \bar{\mathbf{u}}(t), \mathbf{y}(t), \mathbf{d}_p(t), t) \tag{3.1a}$$

$$s.t.\ \ f(\eta, \varsigma, \dot{\mathbf{x}}(t), \mathbf{x}(t), \bar{\mathbf{u}}(t), \mathbf{y}(t), \mathbf{d}_p(t), t) = 0, \tag{3.1b}$$

$$h(\eta, \varsigma, \mathbf{x}(t), \bar{\mathbf{u}}(t), \mathbf{y}(t), \mathbf{d}_p(t), t) = 0, \tag{3.1c}$$

$$g(\eta, \varsigma, \mathbf{x}(t), \bar{\mathbf{u}}(t), \mathbf{y}(t), \mathbf{d}_p(t), t) \leq 0, \tag{3.1d}$$

$$\hat{\mathbf{u}}(\tau_c) = \arg\left\{ \min_{\hat{\mathbf{u}}} \Psi(\cdot) \text{ s.t. } \; F(\cdot) = 0, H(\cdot) = 0, G(\cdot) \leq 0, \hat{\mathbf{u}} \in \mathbb{R}_{+}^{N_u} \right\} \tag{3.1e}$$

$$\bar{\mathbf{u}}(t) = \hat{\mathbf{u}}(\tau_c), \quad \forall\, \tau_c = t \tag{3.1f}$$

where $h : \mathbb{R}^{N_x} \times \mathbb{R}^{N_u} \times \mathbb{R}^{N_\eta} \times \mathbb{R}^{N_\varsigma} \times \mathbb{R}^{N_y} \times \mathbb{R}^{N_d} \times \mathbb{R}^{N_t} \rightarrow \mathbb{R}^{N_h \times N_\varsigma}$ and $g : \mathbb{R}^{N_x} \times \mathbb{R}^{N_u} \times \mathbb{R}^{N_\eta} \times \mathbb{R}^{N_\varsigma} \times \mathbb{R}^{N_y} \times \mathbb{R}^{N_d} \times \mathbb{R}^{N_t} \rightarrow \mathbb{R}^{N_{si} \times N_\varsigma}$ denote the equality and inequality constraints of the process, respectively; $f : \mathbb{R}^{N_x} \times \mathbb{R}^{N_u} \times \mathbb{R}^{N_\eta} \times \mathbb{R}^{N_\varsigma} \times \mathbb{R}^{N_y} \times \mathbb{R}^{N_d} \times \mathbb{R}^{N_t} \rightarrow \mathbb{R}^{N_x \times N_\varsigma}$ represent the dynamic process model; $\mathbf{x} \in \mathbb{R}^{N_x}$ are the states of the system with derivatives indicated by $\dot{\mathbf{x}} \in \mathbb{R}^{N_x}$. $\bar{\mathbf{u}} \in \mathbb{R}^{N_u}$ represents the vector of control actions retrieved from the controller (i.e., the NMPC) as shown in Equation (3.1e). Vector $\mathbf{y} \in \mathbb{R}^{N_y}$ represents the measured states of the system. The set of decision variables that does not depend on time ($\eta \in \mathbb{R}^{N_\eta}$) contains the process design variables (η^p) (e.g., areas, volumes, flows) and the controller tuning parameters (η^c) in the NMPC framework, i.e., $\eta = [\eta^p, \eta^c]$. In this study, these tuning parameters correspond to the positive-defined diagonal matrices that penalizes the deviations in the predicted controlled variables with respect to their desired set-points, and the changes in the manipulated variables, i.e., $\mathbf{Q_{out}}$ and $\mathbf{Q_{in}}$, respectively [12]. Note that the control actions $\bar{\mathbf{u}} \in \mathbb{R}^{N_u}$ computed by Equation (3.1e) are given by the solution of the optimization problem shown in Equation (2.4).

In this study, uncertainty in the model parameters is considered. Uncertainty quantification is addressed in terms of a finite number of scenarios defined *a priori*. These scenarios of uncertainty can be defined from observations based on historical data or process heuristics [28]. The formulation shown in Problem (3.1) considers the introduction of a set of uncertainties $\varsigma \in \mathbb{R}^{N_\varsigma}$ indexed by j_u. Similarly, the probability of occurrence of the ${j_u}^{th}$ uncertainty realization is weighted by w_{j_u}. Following Problem (3.1), the process model implemented in the design problem (upper-level problem) and in the NMPC formulation (lower-level problem) has the same structure. However, the process model in the upper-level problem has access to the complete set of parameter uncertainties (ς), while

the NMPC only has access to the nominal values of the uncertain model parameters, i.e., a nominal NMPC-based controller. Consequently, functions f, g, and h (Equations (3.1b)-(3.1d), respectively) map onto the domain of uncertainties ($\mathbb{R}^{N_\varsigma}$), while the functions F, G, and H (Equations, (2.4b) -(2.4d), respectively) do not map onto this domain. To ensure dynamic feasibility in the process to external perturbation during the normal operation, a set of disturbances $\mathbf{d}_p(t)$ is included in the formulation. This set of disturbances aims determine the magnitude of the controller tuning parameters such that the NMPC can reject the expected disturbances during the normal operation. Consistently, in a real operation, the information about the future changes in the disturbances is not available. Therefore, it is assumed that the NMPC does not have access *a priori* to the set of disturbances $\mathbf{d}_p(t)$. However, the disturbances $\mathbf{d}_p$ are assumed to be part of the measurements for the NMPC, but these remain constant along the prediction horizon at every sampling time $(t + k_t)$.

As shown in Problem (3.1), the NMPC (Equation (3.1e)) has a different dimension in time with respect to the upper-level problem (i.e., the design problem in Equations (3.1a) to (3.1d)); that is, the NMPC generates predictions in a time $\tau_{nmpc} \in [t, t + t_P]$ as shown in Equation (2.4), while the upper-level problem takes place between the initial simulation time t_0 and the final time t_f (i.e., $t \in [t_0, t_f]$). The direct solution of the bilevel formulation in Equation (3.1) may become challenging even for medium-scale applications [46]. The implementation of direct approaches lead to complex highly nonlinear large-scale formulations. The proposed back-off methodology reduces the complexity of the bilevel formulation by the approximation of the original in explicit terms of PSE functions. This PSE-based model returns a single-level formulation that can be efficiently solved with conventional NLP solvers. The proposed sequential methodology is detailed next.

3.2 Back-off methodology

The back-off method seeks for the optimal design and control parameters that maintain the process in a dynamically feasible state, given a set of process disturbances. The algorithm is initialized with an optimal steady-state process design point and systematically moves away from that point to a new dynamically feasible and optimal operating point. The flowchart corresponding to the back-off

algorithm is presented in Figure 3.1. To implement this algorithm, Equation (3.1) is approximated by the use of PSE functions. These functions approximate the nonlinear model in Equation (3.1) around a WCV point. The concept of WCV-point is described later in this section. Since a PSE-based formulation has a limited region of validity, the algorithm sequentially seeks for a region in which the process design improves the process economics and dynamic feasibility. The description of each step in the algorithm is presented next.

3.2.1 Step 1: Initialization

The algorithm is initialized by defining the trajectory profiles for the disturbances $\mathbf{d}_p(t)$; the maximum number of iterations (N_{iter}) and the iteration index r_b is set to 1; the order of approximation for the PSE functions; the step-size for sensitivity calculations ($\Delta\eta_p$); the search space region for the decision variables δ_b (i.e., region of validity for the PSE functions); and an initial guess for the controller tuning parameters. Note that the parameter δ_b is a tuning parameter for this back-off methodology. This parameter is problem-specific and often defined based on heuristics or prior simulations. In this study, the matrices $\mathbf{Q_{out}}$ and $\mathbf{Q_{in}}$ are considered in the NMPC framework as the controller tuning parameter targets. Moreover, t_P and t_C in the NMPC framework are defined *a priori* using preliminary closed-loop simulations. Furthermore, a set of finite number of realizations (N_ς) for the uncertain parameters ς is defined. Each value in the set of realizations is assigned with a probability of occurrence (w_{j_u}). The values for the uncertainty realizations can be determined *a priori* using process heuristics or historical data from similar applications.

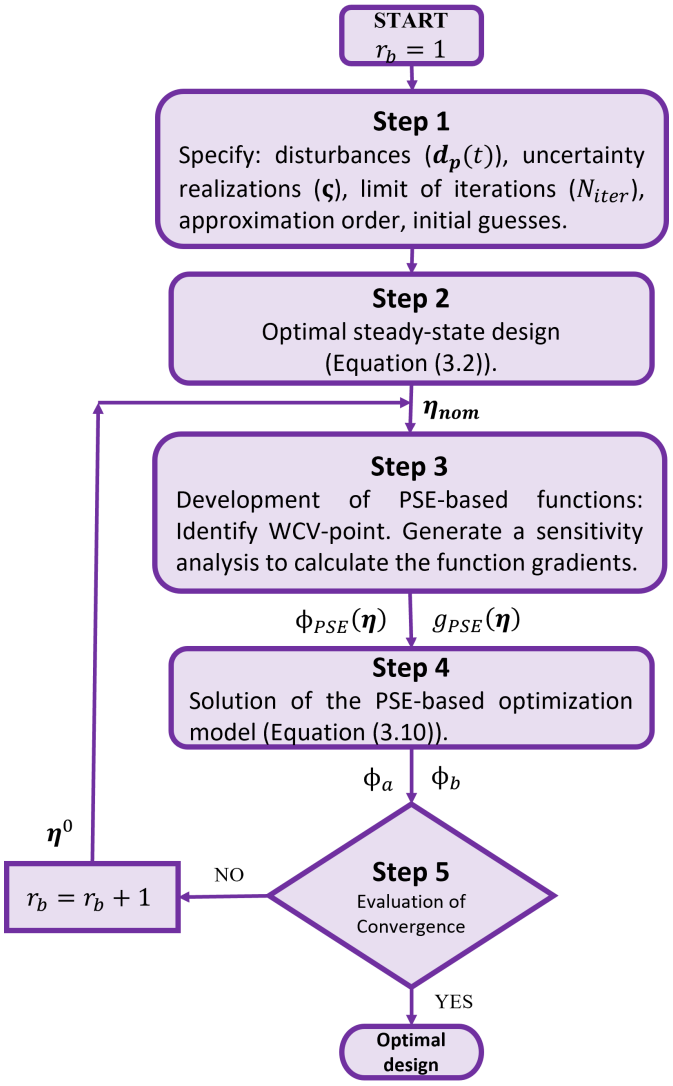

Figure 3.1: Back-off framework for integration of design and NMPC-based control.

3.2.2 Step 2: Optimal steady-state design

In Step 2, an optimal steady-state design problem is solved first to obtain a feasible starting point for the present algorithm. The solution of this problem provides the nominal values for process design variables (η^p_{nom}) for the first iteration (i.e., $r_b = 1$). This problem can be formulated as follows:

$$\min_{\eta^p_{nom}} \Phi_{ss}(\eta^p_{nom}, \mathbf{x}, \mathbf{y}, \mathbf{d}_{p_{nom}}, \varsigma_{nom}) \tag{3.2a}$$

$$\text{s.t. } f_{ss}(\eta^{p}_{nom}, \mathbf{x}, \mathbf{y}, \mathbf{d}_{p_{nom}}, \varsigma_{nom}) = 0 \tag{3.2b}$$

$$h_{ss}(\eta^{p}_{nom}, \mathbf{x}, \mathbf{y}, \mathbf{d}_{p_{nom}}, \varsigma_{nom}) = 0 \tag{3.2c}$$

$$g_{ss}(\eta^{p}_{nom}, \mathbf{x}, \mathbf{y}, \mathbf{d}_{p_{nom}}, \varsigma_{nom}) \leq 0 \tag{3.2d}$$

where $\Phi_{ss} : \mathbb{R}^{N_x} \times \mathbb{R}^{N_\gamma} \times \mathbb{R}^{N_y} \times \mathbb{R}^{N_d} \times \mathbb{R}^{N_\varsigma} \rightarrow \mathbb{R}$ represents the cost function for steady-state process design. In this problem, the cost function involves only the capital and operation costs associated to the process design. In Problem (3.2), the disturbances are assumed to be constant model parameters that are set to their corresponding nominal values ($\mathbf{d}_{p_{nom}}$). The functions f_{ss}: $\mathbb{R}^{N_x} \times \mathbb{R}^{N_\gamma} \times \mathbb{R}^{N_y} \times \mathbb{R}^{N_d} \times \mathbb{R}^{N_\varsigma} \rightarrow \mathbb{R}^{N_x}$, h_{ss}: $\mathbb{R}^{N_x} \times \mathbb{R}^{N_\gamma} \times \mathbb{R}^{N_y} \times \mathbb{R}^{N_d} \times \mathbb{R}^{N_\varsigma} \rightarrow \mathbb{R}^{N_h}$, and g_{ss}: $\mathbb{R}^{N_x} \times \mathbb{R}^{N_\gamma} \times \mathbb{R}^{N_y} \times \mathbb{R}^{N_d} \times \mathbb{R}^{N_\varsigma} \rightarrow \mathbb{R}^{N_s}$ represent the process model, the equality, and inequality constraints at steady-state, respectively. Note that uncertain parameters are set to their corresponding nominal values in Problem (3.2), (i.e., ς_{nom}). As mentioned above, the results of the solution of the optimization model (η^{p}_{nom}) are used as the starting point for the design variables in this methodology. Therefore, $\eta_{nom} = [\eta^{p}_{nom}, \eta^{c}_{nom}]$. The development of PSE-based functions is presented next.

3.2.3 Step 3: Development of PSE-based functions

PSE functions are implemented to obtain analytical expressions of the constraints in the optimization model (i.e., Equation (3.1)). Moreover, these PSE functions are defined as explicit terms of the system's uncertain parameters (ς) and the decision variables at their nominal values (ς_{nom}). Then, these PSEs-based functions are developed around the point that produces the largest variability to the process feasibility constraints under the effect of disturbances and uncertain realizations in the model parameters. This point is referred to as the worst-case variability point (WCV-point), as shown next in Figure 3.2.

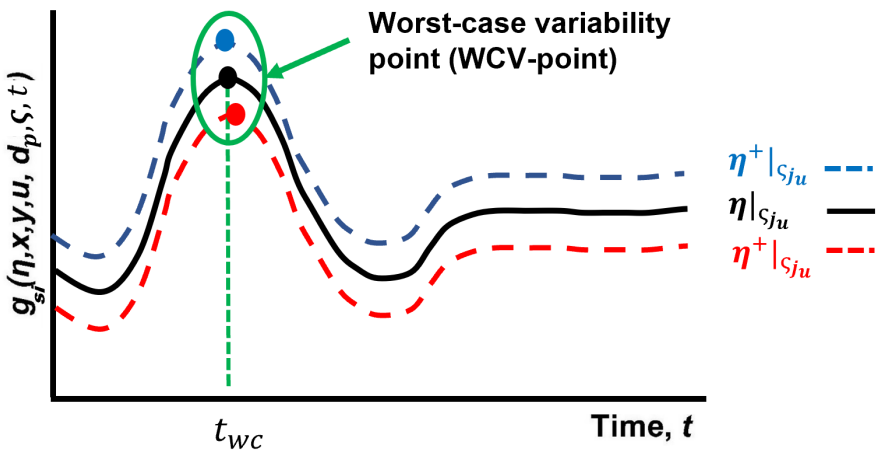

Figure 3.2: Worst case variability point (WCV-point) identified as the largest variation of the si^{th} function g, for the ${j_u}^{th}$ realization in the uncertainty set, at the time $t = t_{wc}$.

To identify the WCV-point, the closed-loop model is simulated using the nominal condition defined in step 2 (i.e., η_{nom}) for all realizations in the uncertainty vector ς under the disturbances effects defined by $\mathbf{d}_p(t)$. At the WCV-point, it is located the time at which the large variability occurs (t_{wc}) for the ς_{j_u} uncertainty realization, as shown in Figure 3.2. Thus, the formulation used for the identification of the WCV-point for each of the inequality feasibility constraints g is as follows:

$$\breve{g}^*_{si,j_u} = \max_{\mathbf{x}(t),\mathbf{y}(t)} \breve{g}_{si,j_u} \tag{3.3a}$$

$$\text{s.t. } f(\eta_{nom}, \varsigma, \dot{\mathbf{x}}(t), \mathbf{x}(t), \mathbf{y}(t), \bar{\mathbf{u}}(t), \mathbf{d}_p(t), t) = 0, \tag{3.3b}$$

$$h(\eta_{nom}, \varsigma, \mathbf{x}(t), \mathbf{y}(t), \bar{\mathbf{u}}(t), \mathbf{d}_p(t), t) = 0, \tag{3.3c}$$

$$\breve{g}_{si,j_u} = g_{si}(\eta_{nom}, \varsigma, \mathbf{x}(t), \mathbf{y}(t), \bar{\mathbf{u}}(t), \mathbf{d}_p(t), t), \quad \forall si \in \{1, \ldots, S\} \tag{3.3d}$$

$$\bar{\mathbf{u}}(\tau_c) = arg \left\{ \min_{\hat{\mathbf{u}}} \Psi(\cdot) \text{ s.t. } F(\cdot) = 0, H(\cdot) = 0, G(\cdot) \leq 0, \ \hat{\mathbf{u}} \in \mathbb{R}^{N_u} \right\} \tag{3.3e}$$

where $\breve{g}^* \in \mathbb{R}^{N_{si} \times N_\varsigma}$ is an auxiliary variable that takes the values of si^{th} functions g at the point that causes the larges variation, i.e., the WCV-point. Index si denotes to the number of inequality constraints g ($si \in \{1, \ldots, S\}$). Note that Equation (3.3) is solved j_u times for every inequality constraint si, i.e., for each realization of the uncertain parameters included in the set ς. Equation

(3.3) assumes that the decision variables remain constant at their nominal values (η_{nom}) and aim to determine the WCV-point for functions g in closed-loop under process disturbances and for every $j_u{}^{th}$ realization in the uncertainty set. Similarly, this procedure is followed for the determination of the WCV-point for the objective function Φ, i.e.,

$$\check{\Phi}^*_{j_u} = \max_{\mathbf{x}(t),\mathbf{y}(t)} \check{\Phi}_{j_u} \tag{3.4a}$$

$$\text{s.t. } f(\eta, \varsigma, \dot{\mathbf{x}}(t), \mathbf{x}(t), \mathbf{y}(t), \bar{\mathbf{u}}(t), \mathbf{d}_p(t), t) = 0, \tag{3.4b}$$

$$h(\eta, \varsigma, \mathbf{x}(t), \mathbf{y}(t), \bar{\mathbf{u}}(t), \mathbf{d}_p(t), t) = 0, \tag{3.4c}$$

$$\check{\Phi} = \Phi(\eta, \varsigma, \mathbf{x}(t), \mathbf{y}(t), \bar{\mathbf{u}}(t), \mathbf{d}_p(t), t) \tag{3.4d}$$

$$\bar{\mathbf{u}}(\tau_c) = arg \left\{ \min_{\hat{\mathbf{u}}} \Psi(\cdot) \text{ s.t. } F(\cdot) = 0, H(\cdot) = 0, G(\cdot) \leq 0, \ \hat{\mathbf{u}} \in \mathbb{R}^{N_u} \right\} \tag{3.4e}$$

where $\check{\Phi} \in \mathbb{R}^{N_\varsigma}$ is an auxiliary variable that will take the values of the cost functions Φ at the WCV-point. As in Equation (3.3), Equation (3.4) is solved j_u times until all the realizations in the set of uncertainties (ς) are tested. PSE-based approximations for the si^{th} inequality constraint g_{si} and the cost function Φ are developed around the WCV-point, i.e.,

$$g_{si,PSE}(\eta)|_{d_p(t),\varsigma_{j_u},t_{wc}} = \check{g}^*_{si,j_u}(\eta_{nom}) + \sum_{k_l=1}^{\infty} \frac{1}{k_l!} \nabla^{k_l} g_{si}(\eta)|_{t_{wc},\varsigma_{j_u}} (\eta - \eta_{nom})^{k_l}, \ \ \forall si \in \{1, \ldots, S\},$$

$$j_u \in \{1, \ldots, J\} \tag{3.5a}$$

$$\Phi_{PSE}(\eta)|_{d_p(t),\varsigma_{j_u},t_{wc}} = \check{\Phi}^*_{j_u}(\eta_{nom}) + \sum_{k_l=1}^{\infty} \frac{1}{k_l!} \nabla^{k_l} \Phi(\eta)|_{t_{wc},\varsigma_{j_u}} (\eta - \eta_{nom})^{k_l}, \ \ \forall j_u \in \{1, \ldots, J\} \tag{3.5b}$$

where $\nabla^{k_l} g_{si,j_u}(\eta)$ and $\nabla^{k_l} \Phi(\eta)$ are the $k_l{}^{th}$-order gradients for the si^{th} constraint function g and for the objective function Φ, respectively, for the j_u^{th} uncertainty realization. These gradients are calculated with respect to the decision variables (η) and evaluated at the WCV-point that was determined at time t_{wc}, as shown in Figure 3.2. Both $\check{g}^*$ and $\check{\Phi}^*$ correspond to the values of the solution of models (3.3) and (3.4), respectively. To calculate the first and second order gradients of the functions g and Φ around the WCV-point (i.e. at $t = t_{wc}$ as shown in Figure 3.2), forward (η^+) and backward (η^-) point evaluations of the functions are enforced around the WCV-point. The

values for η^+ and η^- correspond to small forward and backward step points around the nominal condition (η_{nom}). Thus, closed-loop simulations are carried out where the values for the decision variables are set to η^+ and η^-, respectively. The gradients can thus be calculated using for example finite differences, i.e.,

$$\frac{\partial g_{si}}{\partial \eta_p}|_{t_{wc},\varsigma_{ju}} = \frac{\left(\breve{g}_{si}\left(\eta_p^+\right)|_{t_{wc},\varsigma_{ju}} - \breve{g}_{si}\left(\eta_p^-\right)|_{t_{wc},\varsigma_{ju}}\right)}{\Delta\eta_p}, \ \forall p = \{1,\ldots,P\},\ si \in \{1,\ldots,S\} \tag{3.6}$$

$$\frac{\partial^2 g_{si}}{\partial \eta_p^2}|_{t_{wc},\varsigma_{ju}} = \frac{\left(\breve{g}_{si}\left(\eta_p^+\right)|_{t_{wc},\varsigma_{ju}} - 2\breve{g}_{si}\left(\eta_{p_{nom}}^+\right)|_{t_{wc},\varsigma_{ju}} + \breve{g}_{si}\left(\eta_p^-\right)|_{t_{wc},\varsigma_{ju}}\right)}{\Delta\eta_p^2}, \ \forall p = \{1,\ldots,P\},$$

$$si \in \{1,\ldots,S\} \tag{3.7}$$

$$\frac{\partial \Phi}{\partial \eta_p}|_{t_{wc},\varsigma_{ju}} = \frac{\left(\breve{\Phi}\left(\eta_p^+\right)|_{t_{wc},\varsigma_{ju}} - \breve{\Phi}\left(\eta_p^-\right)|_{t_{wc},\varsigma_{ju}}\right)}{\Delta\eta_p}, \ \forall p = \{1,\ldots,P\},\ si \in \{1,\ldots,S\} \tag{3.8}$$

$$\frac{\partial^2 \Phi}{\partial \eta_p^2}|_{t_{wc},\varsigma_{ju}} = \frac{\left(\breve{\Phi}\left(\eta_p^+\right)|_{t_{wc},\varsigma_{ju}} - 2\breve{\Phi}\left(\eta_{p_{nom}}^+\right)|_{t_{wc},\varsigma_{ju}} + \breve{\Phi}\left(\eta_p^-\right)|_{t_{wc},\varsigma_{ju}}\right)}{\Delta\eta_p^2}, \ \forall p = \{1,\ldots,P\},$$

$$si \in \{1,\ldots,S\} \tag{3.9}$$

where $\Delta\eta_p$ represents the difference between the forward step (η_p^+) and the backward step (η_p^-) for the p^{th} decision variable. Further details about sensitivity and calculation of the finite difference step can be found elsewhere [127].

Since the PSE functions are developed in closed-loop, they already take into account the NMPC performance; consequently, the sensitivity of the process constraints and objective function with respect to the optimization variables is also identified. The use of a PSE-based function approximation allows to express the optimization model in Equation (3.1) as a low-order model representation.

3.2.4 Step 4: Solution of the PSE-based optimization model

The PSE-based functions developed in Step 3 are used to rewrite the problem of design and control in explicit terms of the decision variables (η) and the system's uncertain parameters (ς). The new PSE-based optimization for integration of design and control is as follows:

$$\min_{\eta,\varpi} \Phi_{PSE}(\eta)|_{t_{wc},\varsigma_{j_u}} + \sum_{si=1}^{S}\sum_{j_u=1}^{J} \bar{M}\varpi_{si,j_u} \tag{3.10a}$$

$$\text{s.t. } g_{si,PSE}(\eta)|_{t_{wc},\varsigma_{j_u}} \leq \varpi_{si,j_u},\ \forall si = \{1,\ldots,S\},\ j_u = \{1,\ldots,J\} \tag{3.10b}$$

$$\eta_{nom}(1-\delta_b) \leq \eta \leq \eta_{nom}(1+\delta_b) \tag{3.10c}$$

$$\varpi_{si,j_u} \geq 0,\ \forall si = \{1,\ldots,S\},\ j_u = \{1,\ldots,J\} \tag{3.10d}$$

where Φ_{PSE}: $\mathbb{R}^{N_\eta} \times \mathbb{R}^{N_\varsigma} \rightarrow \mathbb{R}$ and $g_{si,PSE}$: $\mathbb{R}^{N_\eta} \times \mathbb{R}^{N_\varsigma} \rightarrow \mathbb{R}^{N_s \times N_\varsigma}$ are the PSE-based functions for the cost and the inequality constraint functions, respectively; δ_b is a prespecified parameter used to determine the search space for each decision variable in the solution of the PSE-based optimization problem stated in Equation (3.10). This parameter is considered as an indicator of the region of feasibility for the PSE-based functions. Since the PSE-based function approximation of the optimization model is only valid around the WCV-point, the correct selection of the value for parameter δ_b can determine the ratio of convergence of the algorithm. Below in this chapter, Section 3.4.3 presents a discussion about the selection of parameter δ_b when a NMPC-based framework is considered. Following Equation (3.10), ϖ_{si,j_u} is an optimization variable used to penalize violations to the si^{th} constraint equation and it ensures feasibility in the solution of the PSE-based optimization problem for all realizations j_u in the uncertainty set. With the aim to reduce constraint violations, the variables ϖ_{si,j_u} are added to the cost function as a penalty term; note that $\bar{M}$ is a sufficiently large parameter used to drive the variable ϖ_{si,j_u} to zero. Reduction of variable ϖ_{si,j_u} to zero forces the algorithm to converge to a point in which the design and control parameters are dynamically feasible under simultaneous realizations in the disturbances ($\mathbf{d}_p$) and parameter uncertainty (ς).

3.2.5 Step 5: Convergence criterion

As shown in Figure 3.1, the values obtained from the solution of the PSE-based problem (η^*) are evaluated for convergence in this step. Evaluation of convergence consists of a comparison between

mean values of the cost function for two different iteration intervals (i.e., interval $\bar{a}$ and $\bar{b}$) with N_r elements each. The convergence criterion can be expressed as follows:

$$\left| \frac{1}{N_r} \left(\sum_{\bar{a}=r_b-2N_r+1}^{r_b-N_r} \Phi_a - \sum_{\bar{b}=r_b-N_r+1}^{r_b} \Phi_b \right) \right| \leq \varepsilon \tag{3.11}$$

where Φ_a and Φ_b represent the values of the objective function $\Phi_{PSE}(\eta)$ for iterations in the intervals $\bar{a}$ and $\bar{b}$, respectively; ε is a user-defined tolerance criterion. As shown in Equation (3.11), the mean value of the cost function obtained from iterations in the interval $\bar{a}$ (i.e., $r_b - 2N_r + 1 \leq \bar{a} \leq r_b - N_r$) is compared with the mean value of the same function for the period $\bar{b}$ (i.e., $r_b - N_r + 1 \leq \bar{b} \leq r_b$). If the difference in the mean of the objective function value is less than or equal to the threshold ε, then the back-off algorithm has converged to a local optimum solution; otherwise, the values η^* are set as the new nominal values (η_{nom}) for the next iteration, i.e., $r_b = r_b + 1$, and return to Step 3. This procedure continues until a convergence criterion is met or the maximum number of iterations (N_{iter}). Note that the algorithm assumes that there are no integer decisions in the formulation [27].

3.3 Case study

To illustrate the features of the proposed back-off methodology, the integration of design and NMPC-based control of an existent WWTP is used as a case study. The WWTP process is assumed to take place in a biological reactor and a settler tank connected in series (see Figure 3.3). The settler tank has two effluents: a clean water stream and an activated sludge stream. The latter stream is recycled to the bioreactor to maintain the biological reaction activity. Since the activated sludge is constantly growing, the excess is eliminated by a purge stream (q_p). This process aims to control the substrate concentration (s_w) in the biodegradable waste stream and the dissolved oxygen concentration in the bioreactor (c_w). Since the bioreactor is an aerobic-activated reaction equipment, control on the dissolved oxygen concentrations is of special relevance for degradation of organic matter. The model of the WWTP is as follows:

$$
\begin{aligned}
\frac{dx_w}{dt} &= y_w \bar{\mu}_w \frac{s_w x_w}{k_{sc} + s_w} - k_{ca} x_w - k_{dr} \frac{x_w^2}{s_w} + \frac{x_{in} q_{in}}{V_R} + \frac{x_r q_r}{V_R} - \frac{x_w q}{V_R} \\
\frac{ds_w}{dt} &= \frac{f_{kd} k_{dr} x_w^2}{s_w} - \frac{\bar{\mu}_w s_w x_w}{(k_{sc} + s_w)} + f_{kd} k_{ca} x_w + \frac{s_{in} q_{in}}{V_R} + \frac{s_w q_r}{V_R} - \frac{x_w q_{out}}{V_R} \\
\frac{dx_d}{dt} &= \left(\frac{1}{A_d l_d} \right) \left(q_{out}(x_b - x_d) - A_d n_{nr} x_d e^{(a_{ar} x_d)} \right) \\
\frac{dx_b}{dt} &= \left(\frac{1}{A_d l_b} \right) \left(q x_w - x_b (q_{out} + q_2) + A_d n_{nr} \left(NLT \right) \right) \\
\frac{dx_r}{dt} &= \left(\frac{1}{A_d l_r} \right) \left(q_2 (x_b - x_r) + A_d n_{nr} x_b e^{(a_{ar} x_b)} \right) \\
\frac{dc_w}{dt} &= k_{otw} f_k (c_s - c_w) - k_{od} \bar{\mu}_w \frac{x_w s_w}{(k_s + s_w)} - \frac{c_w q}{V} \\
NLT &= x_d e^{(a_{ar} x_d)} - x_b e^{(a_{ar} x_b)} \\
q_r &= q_2 - q_p \\
q_1 &= q_i + q_r \\
q_{out} &= q_1 + q_2
\end{aligned}
\tag{3.12}
$$

where x_w corresponds to the biomass concentration in the bioreactor, x_{in} is the inlet biomass concentration, q_{in} stands for the feed flow rate, the plant's outlet flow rate is described by q_{out}. The biomass concentration at the different depth zones in the settler tank are described by x_d, x_b, x_r, respectively; whereas the depth of the settler tank's zones are given by lr_d, lr_b, lr_r, respectively (see Figure 3.3). Moreover, q_1 and q_2 stand for the bioreactor's outlet flow rate and settler tank's bottoms flow rate, respectively. Values for the plant's model parameters are listed on Table 3.1.

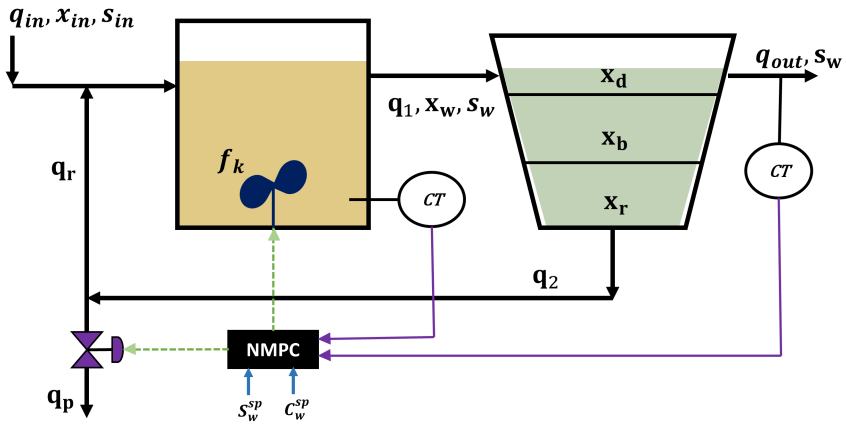

Figure 3.3: Integrated design and NMPC-based control for a wastewater treatment plant.

Table 3.1: Process model parameters: wastewater treatment plant

Parameter	Value
y_w [-]	0.5948
k_{sc} $[hr^{-1}]$	300
k_{otw} $[hr^{-1}]$	0.7
k_{od} $[hr^{-1}]$	1.0×10^{-4}
c_s $[mg/L]$	8
f_{kd} [-]	0.2
n_{nr} [-]	3.1563
a_{ar} [-]	-7.8567×10^{-4}
l_b $[m]$	1.0
l_d $[m]$	2.0
l_r $[m]$	0.5

This process aims to maintain the substrate concentration (s_w) in the bioreactor at a desired set-point (s_w^{sp}). The cost function considered in this study consists of an annualized capital cost (CC_a), an annual operating cost (OC_a), and a variability cost (VC_a). Capital cost is given by the size of the installed equipment, i.e., bioreactor's volume (V_R) and settler's cross-sectional area (A_d), i.e.,

$$CC_a = 0.16(3500V_R + 2300A_d) \tag{3.13}$$

The annual operating cost for the system (OC_a) is given by the cost of the energy consumed by effect of the manipulated variables: the speed of the aeration turbines (f_k) and the purge flow rate

(q_p) from the settler's recycle flow rate (q_r), i.e.,

$$OC_a = 870(f_k + q_p) \tag{3.14}$$

Moreover, a key objective of the process is given by the annualized variability cost (VC_a), which aims to maintain the substrate concentration (s_w) close to an specific threshold. As shown in Equation (3.15), the variability cost has a higher penalty given its environmental significance, i.e., substrate concentrations in the treated water to the effluent should remain close to 100 mg/L during operation but they cannot exceed this limit. Note that this last condition can be expressed as a constraint in the optimization problem, i.e., $s_w(t) \leq 100$.

$$VC_a = 1.0 \times 10^5 (100 - s_w)^2 \tag{3.15}$$

3.4 Results

The optimal design and NMPC-based control subject to process disturbances and model uncertainty of the WWTP presented in the previous section was solved under different scenarios. The first scenario (Section 3.4.1) compares the control performance of NMPC, LMPC, and a decentralized-PI. Scenario 2 (Section 3.4.2) describes the effect on the solution to variations in the number of uncertainty realizations. A sensitivity analysis on the impact of the parameter δ_b on the performance of the proposed back-off algorithm using a NMPC control strategy is presented in Scenario 3. Scenario 4 presents the effect of different types of disturbance profiles. For all the scenarios, the implementation was performed in GAMS V30.2.0 using CONOPT4 as the NLP solver in a platform with an Intel(R) Core(TM) i7-8700 CPU 3.20 GHz processor, 16 GB of RAM and using Windows Server 2019 Standard. The discretization of the process and NMPC optimization model was performed using orthogonal collocation on finite elements. The NMPC optimization formulation consists 20 finite elements and 3 collocation points that represents a total of 1,061 nonlinear algebraic equations with 961 variables. Each of the scenarios considered for this case study are presented next.

3.4.1 Scenario 1: Effect of the control framework

Table 3.2 shows the set of disturbances considered in this scenario. As shown in this table, the set of disturbances considers step changes in the input parameters: inlet flow rate (q_{in} [m^3/h]), inlet biomass concentration (x_{in} [mg/L]), and inlet substrate concentration (s_{in} [mg/L]). The step disturbances for this scenario are performed every 5h until a total simulation time of 35h is reached. The set of uncertainty realizations is listed in Table 3.3.

Table 3.2: Disturbance trajectory profiles (Step changes).

t [h]	x_{in} [mg/L]	s_{in} [mg/L]	q_{in} [m^3/h]
0	80	366	500
5	75	371	480
10	85	361	520
15	80	366	480
20	75	371	500
25	85	366	520
30	80	366	520

The uncertain parameters in Table 3.3 correspond to biological experimental parameters that may exhibit variations in their magnitude, i.e., specific microbial growth rate ($\bar{\mu}_w$), biomass death rate (k_{dr}), specific cellular activity (k_{ca}). Further information regarding these parameters can be found elsewhere [133]. The uncertainty realizations listed in Table 3.3 were determined under the assumption that the parameters may change within ±10% of their nominal values [127]. The maximum number of iterations (N_{iter}) in the algorithm was set to 185. The prediction and control horizons for the model-based control frameworks (i.e., LMPC and NMPC) are set to 2h. Since the bilevel formulation in Equation (3.1) may exhibit a highly nonlinear behaviour, second order PSE functions were used in the analysis to balance out accuracy in the predictions and computational costs. Rafiei & Ricardez-Sandoval [27] validated the accuracy of the PSE-based approximation for the WWTP presented in this case study. They found that the order selected for the PSE (i.e., second order) was suitable for integrated design and control applications. Note that higher order PSE approximations demand additional computational cost.

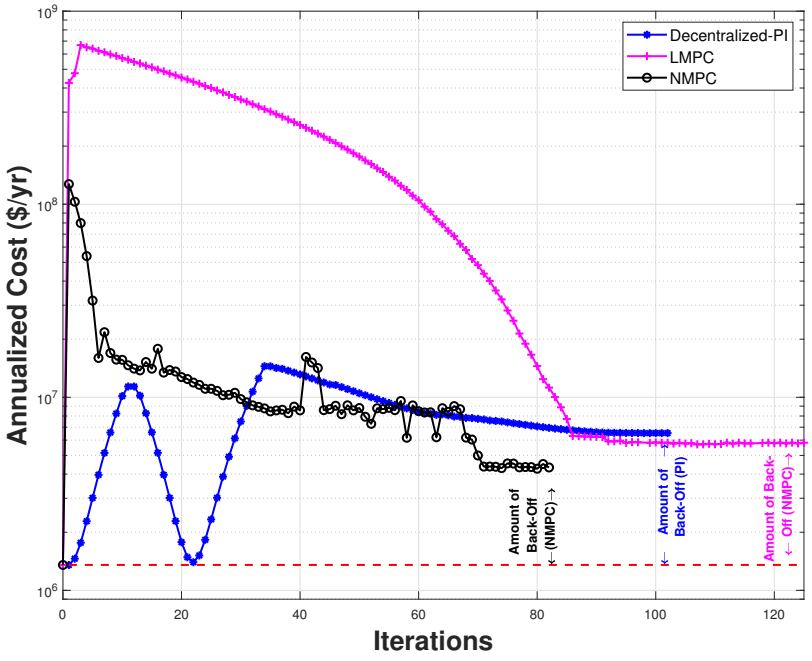

Figure 3.4: Scenario 1: Cost function convergence chart for implementations with LMPC, NMPC, and decentralized-PI.

The step size sensitivity parameter ($\Delta\eta_p$) is set to $\pm 0.005\eta_{nom}$. The tuning parameter δ_b was set to $\pm 0.05\eta_{nom}$. For the present scenario: $\eta_{NMPC} = \eta_{LMPC} = [A_d, V_R, s_w^{sp}, c_w^{sp}, Q_{s_w}, Q_{c_w}]$, and $\eta_{PI} = [A_d, V_R, s_w^{sp}, c_w^{sp}, K_{c1}, K_{c2}, \tau_{i1}, \tau_{i2}]$ represent the sets of time-independent decision variables for the implementations with NMPC-based control, LMPC-based control and PI-based control strategies, respectively. The floating point average criterion for convergence was set to $\varepsilon = 1.0 \times 10^{-2}$ with a sampling interval of $N_r = 5$, i.e., number of iterations considered for the evaluation of mean value of the cost function in Equation (3.11). The total cost of the process is expected to be in the orders of millions; thus, a small ε (i.e., $< 1.0 \times 10^{-2}$) may significantly increases the computational cost. Further reduction of this parameter (i.e., $< 1.0 \times 10^{-4}$) did not improve the results significantly, i.e., decision variables and cost function values remained the same to those obtained using $\varepsilon = 1.0 \times 10^{-2}$, whereas the CPU times increased a 28%, 23%, and 25% for the implementations using decentralized-PI, LMPC, and NMPC controllers, respectively. Hence, solutions obtained using this parameter value as the stopping criterion are accepted. In this scenario, the closed-loop sampling time for

measurement of states is set to 7.5min. The dynamic model of the WWTP was linearized using first-order Taylor series expansion. The linear version of the process model is used as the internal model in the LMPC framework. This linear process model is identified around the nominal operating conditions of the system given by the steady-state values of the process states, inputs and the manipulated variables, respectively. Note that in the present back-off algorithm, the steady-state values of the system are updated at each iteration step. Hence, the linear process models are also updated with the revised steady-state operating conditions obtained at each iteration step to ensure that the LMPC has a consistent model of the process with respect to the changes in the decision variables. For the decentralized control strategy, the control pairing between the controlled and manipulated variables was selected based on the use of a relative gain array (RGA) approach. For control purposes in the decentralized PI framework, purge flow rate (q_p) and turbine speed (f_k) are selected as manipulated variables to control the substrate concentration (s_w) and the dissolved oxygen concentration (c_w), respectively.

Table 3.3: Scenario 1: Uncertainty realizations for model parameters (WWTP).

Uncertainty realizations	**Specific growth rate** ($\bar{\mu}_w$)	**Biomass death rate** (k_{dr})	**Specific cellular activity** (k_{ca})	**Weight distribution** (w_{j_u})
1	0.18240	5×10^{-5}	1.330×10^{-4}	0.3
2	0.20064	5.5×10^{-5}	1.466×10^{-4}	0.1
3	0.16416	4.5×10^{-5}	1.199×10^{-4}	0.1
4	0.20064	4.5×10^{-5}	1.466×10^{-4}	0.1
5	0.16416	5.5×10^{-5}	1.199×10^{-4}	0.1
6	0.19152	4.7×10^{-5}	1.399×10^{-4}	0.1
7	0.17328	5.5×10^{-5}	1.266×10^{-4}	0.1
8	0.17875	5.35×10^{-5}	1.293×10^{-4}	0.1

As shown in Table 3.4, the results for Scenario 1 show that the implementation with NMPC results into an economic improvement compared with the LMPC-based framework and the PI-based control strategy, i.e., the total plant cost with an NMPC is 42% and 22% lower compared with the PI-based control framework and the LMPC-based approach, respectively. Note that the total cost in Table 3.4 involves the capital cost, operating cost, and variability cost. From the operability parameters, it is observed that the substrate set-point (s_w^{sp}) is closer to the saturation limit ($s_w \leq 100$) when a NMPC-based control is implemented, which enables a reduction in the

total plant costs. The implementations resulted in important differences in the process design, i.e., the settler's area (A_d) is almost 2 times larger when NMPC is implemented, compared with the application with decentralized-PI. On the contrary, the reactor's volume (V_R) is 30% smaller when NMPC is implemented with respect to the implementation with decentralized-PI. Table 3.4 also shows that there are differences in the process design between the solutions with LMPC and NMPC frameworks, i.e., the LMPC resulted in a 5% larger settler's area (A_d) and a 9% larger reactor's volume (V_R) compared with the results obtained for the NMPC framework. As shown in Figure 3.4, the amount of back-off required is larger for applications involving LMPC and PI controllers, i.e., the magnitude of the back-off is 30% larger with a LMPC and 2.1 times larger with a PI-based controller than that obtained with the NMPC-based formulation. In principle, the applications with PI and LMPC required a larger number of iterations to reach the convergence (i.e., 102 and 125, respectively). However, the CPU time required for the application with NMPC is 3 orders of magnitude larger than that required by the PI-based control strategy. This difference in CPU cost between the classical control approach (PI) and the model-based control frameworks (LMPC and NMPC) is mostly due to the identification of the PSE-based functions (Step 3 in Section 3.2.3). From Figure 3.4, it can be observed that the LMPC strategy reports an objective function value in the first iteration that is larger than that reported by the other two control schemes (NMPC and Decentralized-PI) at the same iteration point. Therefore, the LMPC framework begins to iterate from a point that is farther from the convergence point; thus, it requires a larger number of iterations to converge. This happens because of the use of an internal linear process model in the LMPC scheme, which caused larger constraint violations at the initial iteration steps in the algorithm. Therefore, the formulation with a LMPC required more iterations than those needed by the NMPC framework; consequently, this resulted in longer CPU times to reach converge compared with the NMPC strategy (51% larger CPU time). From Figure 3.5, it can be observed that the three control schemes tested in this study returned a feasible dynamic operation by maintaining the substrate concentration (s_w) around their corresponding set-point and under the saturation limit in the presence of process disturbances and parameter uncertainty.

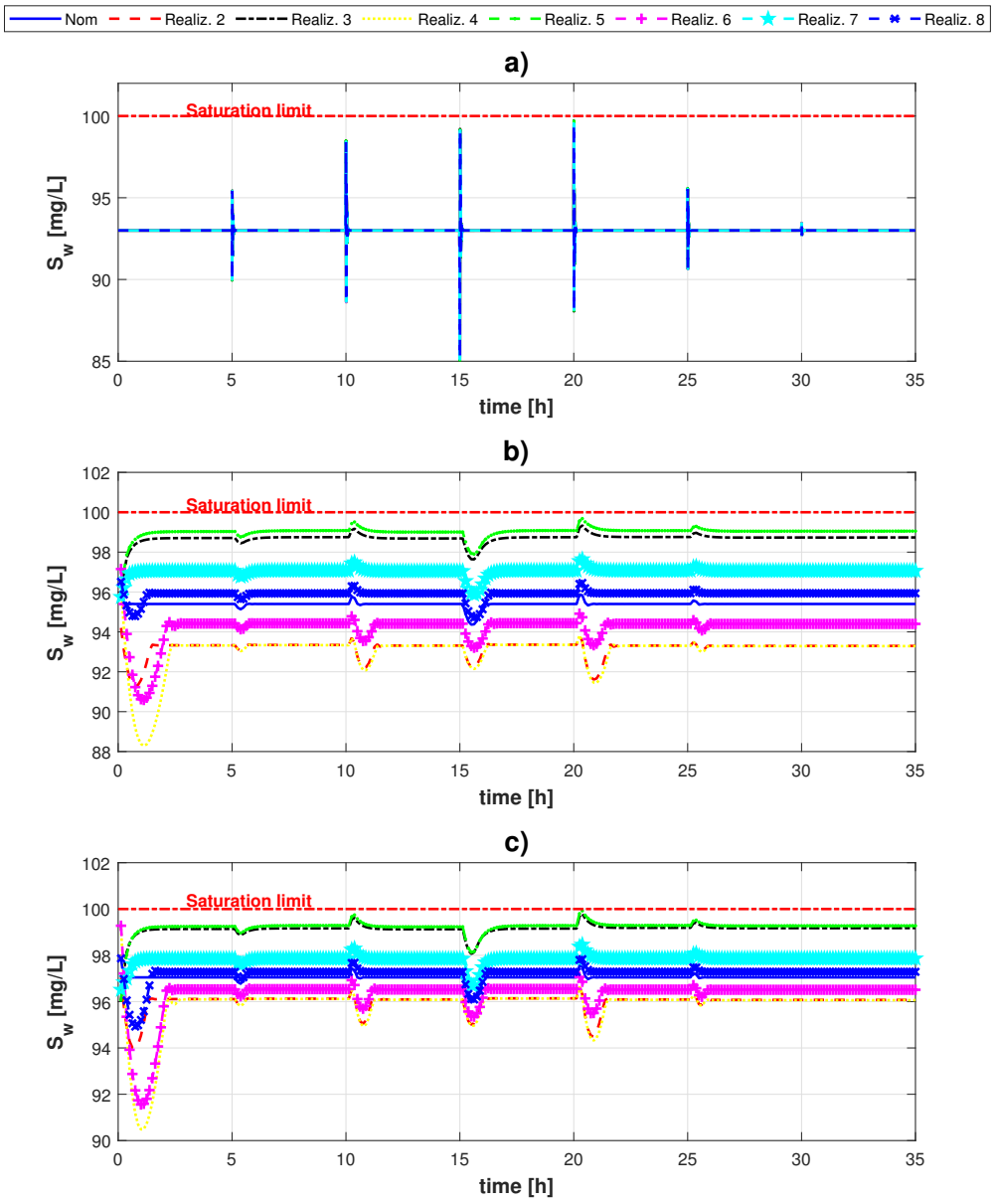

Figure 3.5: Scenario 1: Solution based closed-loop simulations for the control of the substrate (s_w) under process disturbances and parameter uncertainty; (a) decentralized PI; (b) Linear-MPC-based control; (c) NMPC-based control.

The results from this scenario show that the NMPC-based framework has multiple economic and operational benefits for process design and control; however, the CPU cost acts as a limitation

Table 3.4: Results for Scenario 1 (Effect of the control framework for WWTP)

Controller	**Decentralized PI**	**LMPC**	**NMPC**
A_d [m^2]	691.9	2070.3	1974.2
V_R [m^3]	2513.9	2002.0	1831.1
s_w^{sp} [mg/L]	93.0	95.4	97.0
c_w^{sp} [mg/L]	0.06	0.06	0.001
Q_{s_w}	–	32.18	31.71
Q_{c_w}	–	0.001	0.001
K_{C1}	0.9297	–	–
K_{C2}	0.4053	–	–
τ_{I1}	15.512	–	–
τ_{I2}	17.0925	–	–
Total cost [$/yr]	6.51×10^6	5.60×10^6	4.33×10^6
Iterations	102	125	82
Amount of Back-off	5.16×10^6	4.24×10^6	2.98×10^6
CPU time [s]	256	7.7×10^5	5.1×10^5

to perform the optimal design and NMPC-based control for larger-scale applications [134, 135, 136, 137]. To validate the quality of the solutions, the back-off method was also tested using a different initial condition with $A_d = 2830.2m^2$ and $V_R = 1573.8m^3$, whereas the optimal steady-state design was obtained at $A_d = 1774.5m^2$ and $V_R = 1241.6m^3$. In this validation test, the method converged to the same local solutions reported in Table 3.4, which is an indication of the quality of the solution obtained by the present method. The use of reduced MPC formulations, such as explicit MPC [138], might reduce the required CPU time and can be investigated in a future study. On the other hand, note that the sampling time for Scenario 1 (7.5min) may be too optimistic since the measurement of biological parameters, such as biomass and substrates, requires sophisticated techniques, e.g., biochemical oxygen demand, and therefore require longer sampling times. Thus, the next scenarios for this case study assume larger sampling times for the measurement of states in the NMPC framework.

3.4.2 Scenario 2: Effect of uncertainty

This scenario illustrates the effect of the number of uncertainty realizations considered in the formulation. In this scenario, the integration of design and control was performed under 3 different instances: (i) no uncertainty, (ii) 8 uncertainty realizations, and (iii) 13 uncertainty realizations.

Table 3.5: Scenario 2 (Back-off method): Uncertainty realizations in design parameters.

Realization #	**8 Uncertainty realizations scenario**				**13 Uncertainty realizations scenario**			
	Specific growth rate ($\bar{\mu}_w$)	**Biomass death rate** (k_{dr})	**Specific cellular activity** (k_{ca})	**Weight distribution**	**Specific growth rate** ($\bar{\mu}_w$)	**Biomass death rate** (k_{dr})	**Specific cellular activity** (k_{ca})	**Weight distribution** (w_{j_u})
1	0.1824	5×10^{-5}	1.333×10^{-4}	0.3	0.1824	5×10^{-5}	1.333×10^{-4}	0.23
2	0.1641	4.5×10^{-5}	1.199×10^{-4}	0.1	0.2006	5.5×10^{-5}	1.466×10^{-4}	0.0775
3	0.1641	5.5×10^{-5}	1.999×10^{-4}	0.1	0.1641	4.5×10^{-5}	1.199×10^{-4}	0.0775
4	0.1732	5.5×10^{-5}	1.266×10^{-4}	0.1	0.2006	4.5×10^{-5}	1.466×10^{-4}	0.0775
5	0.2188	4×10^{-5}	1.396×10^{-4}	0.1	0.1641	5.5×10^{-5}	1.199×10^{-4}	0.0775
6	0.2097	4.25×10^{-5}	1.596×10^{-4}	0.1	0.1915	4.75×10^{-5}	1.399×10^{-4}	0.0775
7	0.1459	6×10^{-5}	1.170×10^{-4}	0.1	0.1732	5.5×10^{-5}	1.266×10^{-4}	0.0775
8	0.1550	5.75×10^{-5}	1.064×10^{-4}	0.1	0.1787	5.35×10^{-5}	1.293×10^{-4}	0.0775
9					0.2188	4.0×10^{-5}	1.396×10^{-4}	0.0455
10					0.2097	4.25×10^{-5}	1.596×10^{-4}	0.0455
11					0.1459	6.0×10^{-5}	1.170×10^{-4}	0.0455
12					0.1550	5.75×10^{-5}	1.064×10^{-4}	0.0455
13					0.2042	4.40×10^{-5}	1.529×10^{-4}	0.0455

The corresponding uncertain design parameters and their realizations are shown in Table 3.5. From this table, for the case with no uncertainty, the design parameters $\bar{\mu}_w$, k_{dr}, and k_{ca} take on values from the first realization in the uncertainty sets. In this scenario, the realizations in the sets of uncertainty parameters are assumed to vary $\pm 15\%$ of their nominal values. Moreover, the sampling time considered for the present closed-loop NMPC framework is 30min. Note that this sampling time is still optimistic for a WWTP, e.g., BOD is often a 5 day measurement; also, the measurement of the COD may take a few hours to complete. However, a sampling time of 30min still demonstrates the effect of the variation in this parameter for the integration of design and NMPC-based control with respect to the results obtained in Scenario 1 (Table 3.4). In this scenario, the prediction and control horizons, the set of process disturbances, N_{iter}, $\Delta\eta_p$ are the same used as in Scenario 1. Parameter δ_b is fixed to $\pm 0.01\eta_{nom}$, and second order PSE-based function were used. For this scenario: $\eta_{NMPC} = [A_d, V_R, s_w^{sp}, c_w^{sp}, Q_{s_w}, Q_{c_w}]$ represent the set of decision variables. In addition, $\varepsilon = 0.01$ and N_r.

As shown in Table 3.6, the instance with 13 uncertainty realizations resulted in larger equipment sizes compared to the instances with no uncertainty and 8 uncertainty realizations, respectively, e.g., the reactor's volume (V_R) in the instance with 13 uncertainty realizations is 33% and 14% larger compared to the instances with no uncertainty and 8 uncertainty realizations, respectively. A similar

comparison can be made for the A_d, where the instance with 13 uncertainty realizations showed a cross-sectional area that is 38% and 81% larger compared with the instances with no uncertainty and 8 uncertainty realizations, respectively. The results for the substrate set-point (s_w^{sp}) indicate that, when no uncertainty is present, the operation of the plant is closer to the saturation limit (i.e., $s_w(t) \leq 100$). The addition of uncertainty into the analysis forces the operation to move away (i.e., back-off) to a farther set-point to remain dynamically operable. For the instances with 8 and 13 uncertainty realizations, the substrate operating set-point is almost the same ($\sim 1\%$ of difference between these instances). Note that the substrate operating set-point is slightly higher for the instance with 13 uncertainty realizations; this increase in the operating point is possible since larger equipment are specified for this instance. An increase in the equipment size also increases the time constant of the process and therefore reduces the effect of the disturbances. This also has the effect to increase the time required to reject a disturbance. As shown in Figures 3.6b and 3.6c, the design and control scheme with 8 uncertainty realizations exhibits shorter closed-loop time constants compared to the instance with 13 uncertainty realizations. This is because the former case specifies a smaller equipment sizes which enables faster disturbance rejection.

Table 3.6: Results for Scenario 2 (Back-off method)

Uncertainty realizations	**0**	**8**	**13**
A_d [m^2]	2003.4	1530.0	2774.2
V_R [m^3]	1267.3	1635.3	1903.8
s_w^{sp} [mg/L]	95.5	80.9	82.6
c_w^{sp} [mg/L]	0.0099	0.0011	0.0016
Q_{s_w}	29.3	33.48	42.25
Q_{c_w}	9.8×10^{-4}	1.0×10^{-3}	1.5×10^{-3}
Total cost [$/yr]	8.02×10^6	3.24×10^7	7.26×10^7
Iterations	70	72	62
Amount of Back-off	6.67×10^6	3.10×10^7	7.13×10^7
CPU time [s]	1.29×10^5	2.01×10^5	3.74×10^5

The addition of uncertainty realizations also resulted in higher plant costs, as shown in Table 3.6. The cost function for the instance with 13 uncertainty realizations is 85% more expensive compared to the instance with 8 uncertainty realizations. Therefore, the amount of back-off is also higher for the instance with 13 uncertainty realizations, i.e., the back-off is 2.3 times higher compared

to the instance of 8 uncertainty realizations. As shown in Table 3.6, the CPU costs increases as the number of uncertainty realizations increases; this is because the PSE identification step in the algorithm requires longer times to generate the forward and backward step simulations to calculate the corresponding gradients with respect to all decision variables for each realization considered in the uncertainty. Note that this step must be performed at every iteration step thus increasing the computational costs of the proposed algorithm.

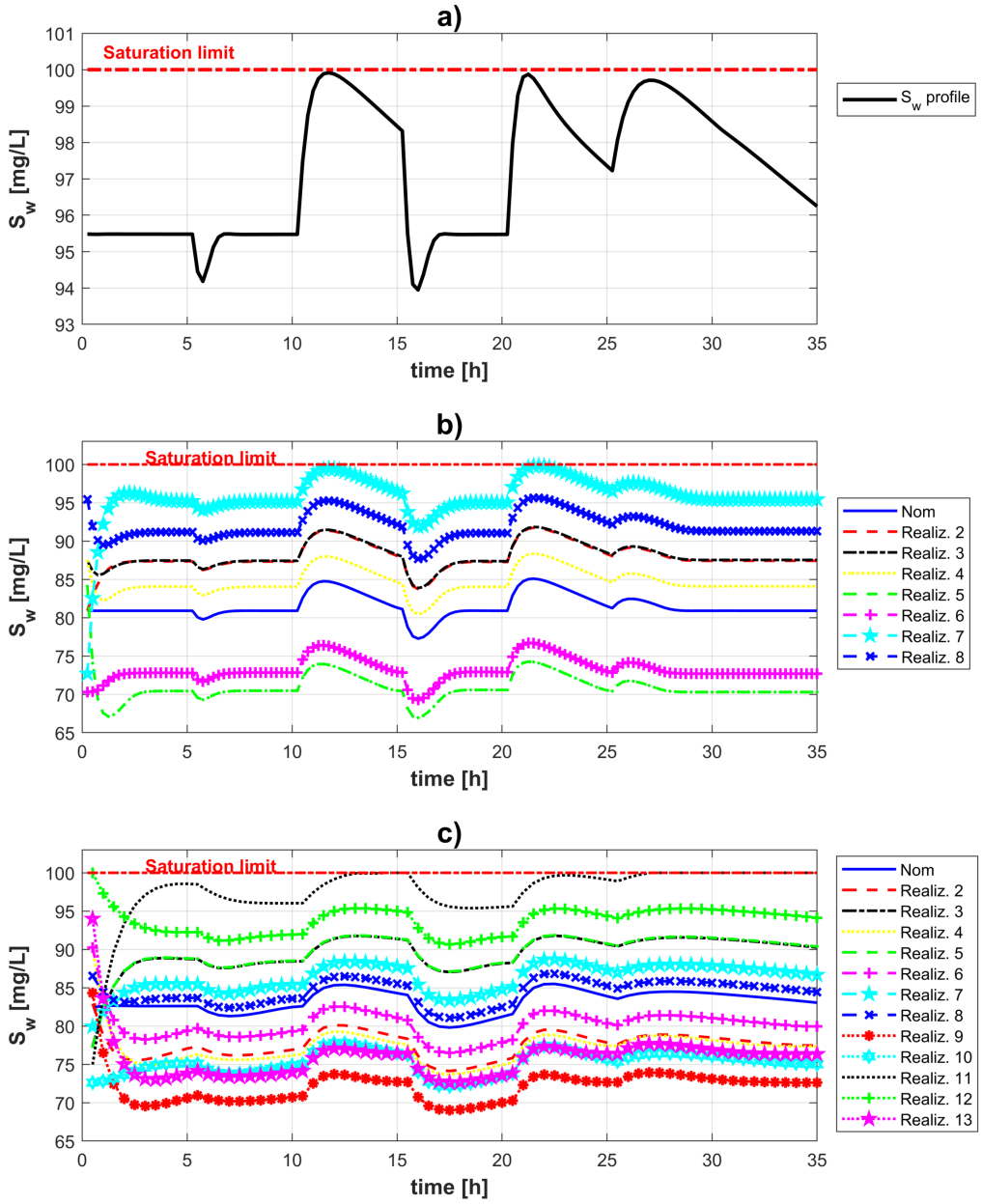

Figure 3.6: Scenario 2: Substrate closed-loop simulations under process disturbances and parameter uncertainty; (a) No uncertainty; (b) 8 uncertainty realizations; (c) 13 uncertainty realizations.

From results of Scenarios 1 and 2 listed in Tables 3.4 and 3.6, respectively, it can be observed that the set-point for s_w is closer to the saturation limit (100 mg/L) when the sampling time is set to 7.5 min, i.e., $s_w^{sp} = 97$ mg/L. On the other hand, when the sampling time is set to 30min

$s_w^{sp} = 82.6$ mg/L. Therefore, the reduction in the sampling time for the measurement of states allows the controller to detect the disturbances faster compared with the scenario with a sampling time of 30min. Note that the results for Scenario 1 were obtained under the assumption that the uncertain parameters have a variation within ±10% their nominal values whereas the results for Scenario 2 were obtained under the assumption that the uncertain parameters have a variation within ±15% their nominal values. Thus, it is not possible to perform a direct comparison of the decision variables for design (i.e., A_d and V_R). However, the effect in the operation under different sampling times for the measurement of states is shown here to reflect the impact that sampling time may have for integration of design and control problems subject to parameter uncertainty and disturbances.

3.4.3 Scenario 3: Effect of tuning parameter δ_b

In this scenario, the effect of the tuning parameter δ_b under an NMPC framework is investigated. A set of 3 different values were evaluated in this scenario, i.e., $\delta_{b1} = \pm 0.01\eta_{nom}$, $\delta_{b2} = \pm 0.03\eta_{nom}$, and $\delta_{b3} = \pm 0.05\eta_{nom}$. The set of disturbances and uncertainty realizations for this scenario are the same as in Scenario 1 (see Tables 3.2 and 3.3, respectively). The selection of values for N_{iter}, the order of approximation for the PSE-based function polynomials, $\Delta\eta$, the floating point average criterion for convergence, the process sampling time, the prediction and control horizons, the sampling time for measurement of states for the NMPC, and the set of decision variables (η_{NMPC}) remain the same as in Scenario 2.

Table 3.7 shows a comparison of the results obtained for the different values of δ_b considered in this scenario. From these results, it can be noted that for lower values of δ_b ($\delta_{b1} = \pm 0.01\eta_{nom}$), the methodology requires more iterations though the solution obtained from this instance resulted in lower costs when compared to the cases with δ_{b2} and δ_{b3}. Table 3.7 also shows that the solution with δ_{b1} exhibits a design with smaller equipment sizes, i.e., a bioreactor with slightly smaller volume (V_R) and a settler tank with a smaller area (A_d) than those obtained for the cases with δ_{b2} and δ_{b3}, respectively. Moreover, the operating point specified for the substrate concentration set-point (s_w^{sp}) is slightly closer to its saturation limit for the solution obtained with δ_{b2}, which overall improves the process economics. Despite the difference in the number of iterations required

to achieve convergence with δ_{b2} and δ_{b3} (i.e., 49 and 57 iterations, respectively), the results for the design variables remained somewhat similar, e.g., the results using δ_{b3} specifies equipment sizes for the settler's tank and reactor's volume that are 5% and 1% larger compared to those obtained using δ_{b2}, respectively. The results show that parameter δ_b has a direct effect on the convergence of the methodology and in the accuracy of the solution. Figure 3.7 illustrates the convergence of the cost function for the different values of δ_b considered in this study. As shown in this Figure 3.7, the convergence for δ_{b2} and δ_{b3} does not follow smooth trajectories, i.e., the trajectory presents peaks at certain iteration steps. This is an indication that the PSE-based optimization model was out of the region of validity for the approximation. Then, for each decision variable, the region of validity can be different and depends of the nonlinearity of the model with respect to each decision variable. Therefore, there is the possibility that the validity region with respect to each decision variable is different. A potential approach for the implementation of adaptive δ_b is the use of a trust-region methodology [27, 28]. The key idea is to optimize the maximum acceptable search region δ_b for all the decision variables around the nominal values. Although that approach eliminates the possibility that the PSE-based model converges to values out of the region of validity, it also introduces an additional layer of optimization thus increasing the computational costs. Hence, a direct implementation of such approach within the present framework would further increase the already taxing computations costs.

Table 3.7: Results for Scenario 3: Effect of the tuning parameter $delta_b$

Decision variable	$\delta_{b1} = \pm 0.01\eta_{nom}$	$\delta_{b2} = \pm 0.03\eta_{nom}$	$\delta_{b3} = \pm 0.05\eta_{nom}$
A_d [m^2]	2510.3	2923.1	3061.2
V_R [m^3]	1453.6	1477.9	1495.9
s_w^{sp} [mg/L]	88.0	89.1	88.8
c_w^{sp} [mg/L]	0.0015	0.0016	0.0015
Q_{s_w}	39.82	42.25	42.25
Q_{c_w}	8.4×10^{-4}	7.3×10^{-4}	8.9×10^{-4}
Total cost [$/yr]	4.39×10^7	4.62×10^7	4.65×10^7
Iterations	62	49	57
Amount of Back-off	4.25×10^7	4.48×10^7	4.51×10^7
CPU time [s]	1.29×10^5	2.01×10^5	3.74×10^5

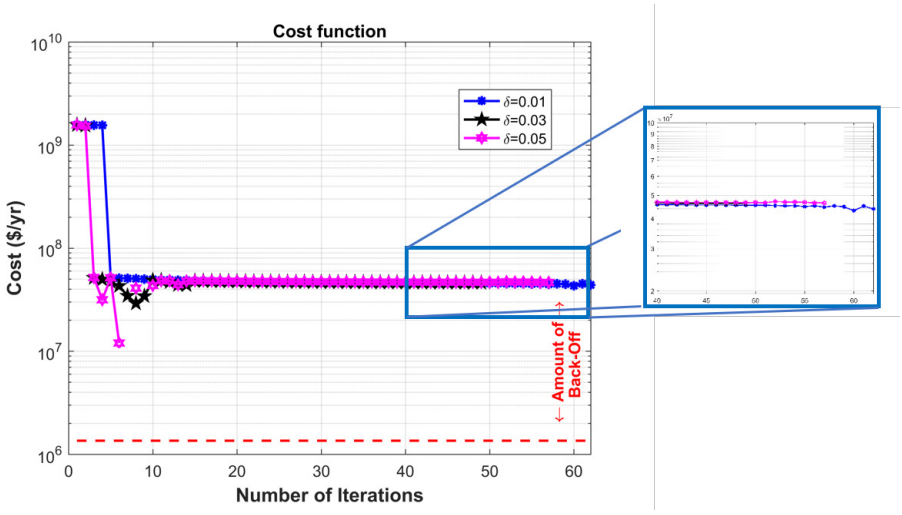

Figure 3.7: Scenario 3: Cost function convergence chart for different tuning parameter δ_b.

3.4.4 Scenario 4: Effect of disturbance dynamics

In this scenario, the effect of two different sets of disturbances for the integration of design and control is considered. This scenario is performed using step changes (Instance A) and sinusoidal changes (Instance B) as the disturbances entering the process. For the sinusoidal disturbance profile (Instance B) the amplitude and frequency follow the same magnitude and pattern as the unit steps disturbances in Table 3.2 (see Figure 3.8). In this scenario, the number of uncertainty realizations is set to 8 realizations as listed in Table 3.3. Similarly, the sampling time for measurement of states for the NMPC, the prediction and control horizons, N_{iter}, the floating point average criterion for convergence and its sampling interval (N_r), the order of approximation for the PSE-based function polynomials, $\Delta\eta$, and the set of decision variables (η_{NMPC}) remain the same as in Scenario 2. The tuning parameter δ_b is set to $\pm 0.01\eta_{nom}$.

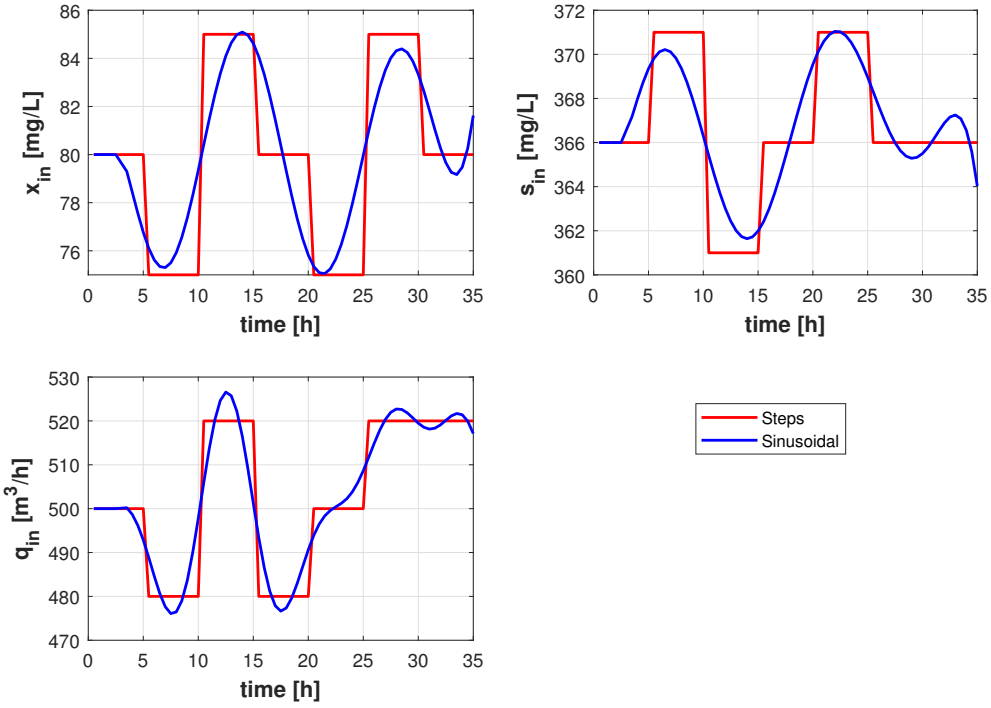

Figure 3.8: Scenario 4: Step and sinusoidal disturbance pattern

Table 3.8: Results for Scenario 4: effect of disturbance dynamics

Instance	**A**	**B**
Disturbance profile	Step	Sinusoidal
A_d [m^2]	2510.3	1974.3
V_R [m^3]	1453.6	1455.5
s_w^{sp} [mg/L]	88.0	89.2
c_w^{sp} [mg/L]	0.0015	0.0017
Q_{s_w}	39.82	42.25
Q_{c_w}	8.4×10^{-4}	6.6×10^{-4}
Total cost [$/yr]	4.39×10^7	5.72×10^7
Iterations	62	72
Amount of Back-off	4.25×10^7	5.58×10^7
CPU time [s]	1.29×10^5	1.45×10^5

As shown in Table 3.8, sinusoidal disturbances (Instance B) returned differences in the equipment design compared to those obtained from step disturbances (Instance A). The solution obtained for Instance B reported a settler's tank cross-sectional area (A_d) that is 21.3% smaller compared to

that obtained for Instance A. Also, the use of sinusoidal disturbances allows to operate under a slightly higher set-point concentration of substrate ($s_w^{sp} = 89$ mg/L) than that obtained for Instance A ($s_w^{sp} = 88$ mg/L). On the other hand, the cost for Instance A is 23% lower than that obtained for Instance B. This variation in the plant cost can be explained by comparing the control actions required to maintain the substrate (s_w) at the optimal set-point. From Figure 3.9a, it can be observed that the magnitude of the control actions in the purge flow rate (q_p) is almost 30% lower when step disturbances are implemented, compared to the control actions observed with sinusoidal disturbances (Figure 3.9b). To further investigate the robustness of the solutions obtained from Instances A and B, the sensitivity of the process design and NMPC strategies to different disturbance scenarios was considered. To perform this test, the process design and NMPC scheme obtained from Instance B was tested using step disturbances; similarly, the solution obtained from Instance A was tested using sinusoidal disturbances. Results for the test using the solution from Instance B with step disturbances are shown in Figure 3.10a. Likewise, Figure 3.10b shows the results for the test using the solution from Instance A with sinusoidal disturbances. From Figure 3.10b, it can be noted that the presence of process infeasibilities, up to 0.2% over the saturation value, i.e., the effect of step disturbances on Instance B resulted in violation of the process constraints. On the other hand, Figure 3.10b shows that the design and NMPC-based control scheme obtained from Instance A can maintain a feasible dynamic operation when sinusoidal disturbances enter the plant. This analysis shows that disturbance profiles may change the optimal design and NMPC-based control scheme. Also, the design and NMPC scheme obtained from Instance A was able to reject step and sinusoidal process disturbances. This result suggests that optimal design and NMPC schemes obtained from aggressive disturbances (e.g., step changes) can accommodate smoother disturbance profiles (e.g., ramp or sinusoidal disturbances).

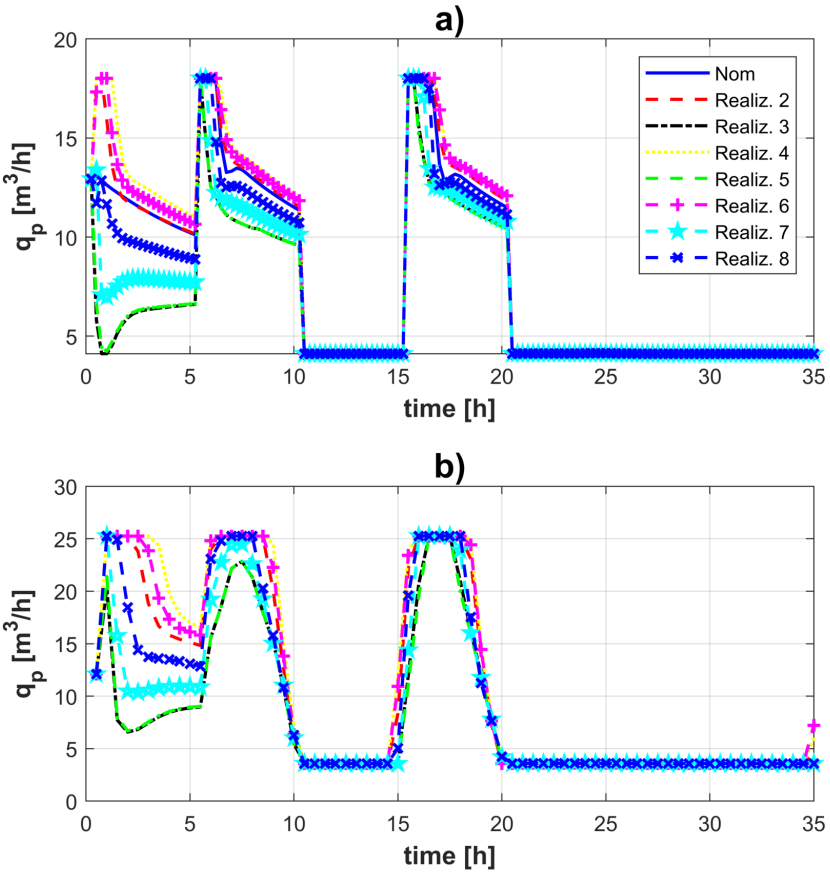

Figure 3.9: Scenario 4: Control results (a) control actions in the purge flow rate (q_p) for step disturbances; (b) control actions in the purge flow rate (q_p) for sinusoidal disturbances.

From the results presented in Scenarios 1 to 4 (i.e., Tables 3.4, 3.6-3.8), it can be noted that the NMPC's weighting parameters for the dissolved oxygen (i.e., Q_{c_w}) are at least 4 orders of magnitude lower than the weighting parameter for the substrate (i.e., Q_{s_w}). This result indicates that the current formulation is giving more importance to the control of s_w. This becomes evident when it is considered that the deviations of s_w from the saturation limit are highly penalized by the variability cost (VC_a) in the objective function. By comparing the results from Scenario 2 for Q_{s_w} without uncertainty (see Table 3.6) and the results in Scenarios 1, 3, and 4 (see Tables 3.4, 3.7, and 3.8, respectively) when step disturbances are enforced, the value of Q_{s_w} is lower when no uncertainty is considered, i.e., Q_{s_w} in Scenario 2 without uncertainty is 30% lower in magnitude with respect to

the highest weighting parameter reported for Scenarios 2 and 3 ($Q_{s_w} = 42.25$). For all the scenarios considered in this case study, it is observed that there are offsets in the controlled variables. These offsets are caused by the mismatch that the uncertainty parameter generate between the process model considered in the design problem and the internal process model in the NMPC formulation.

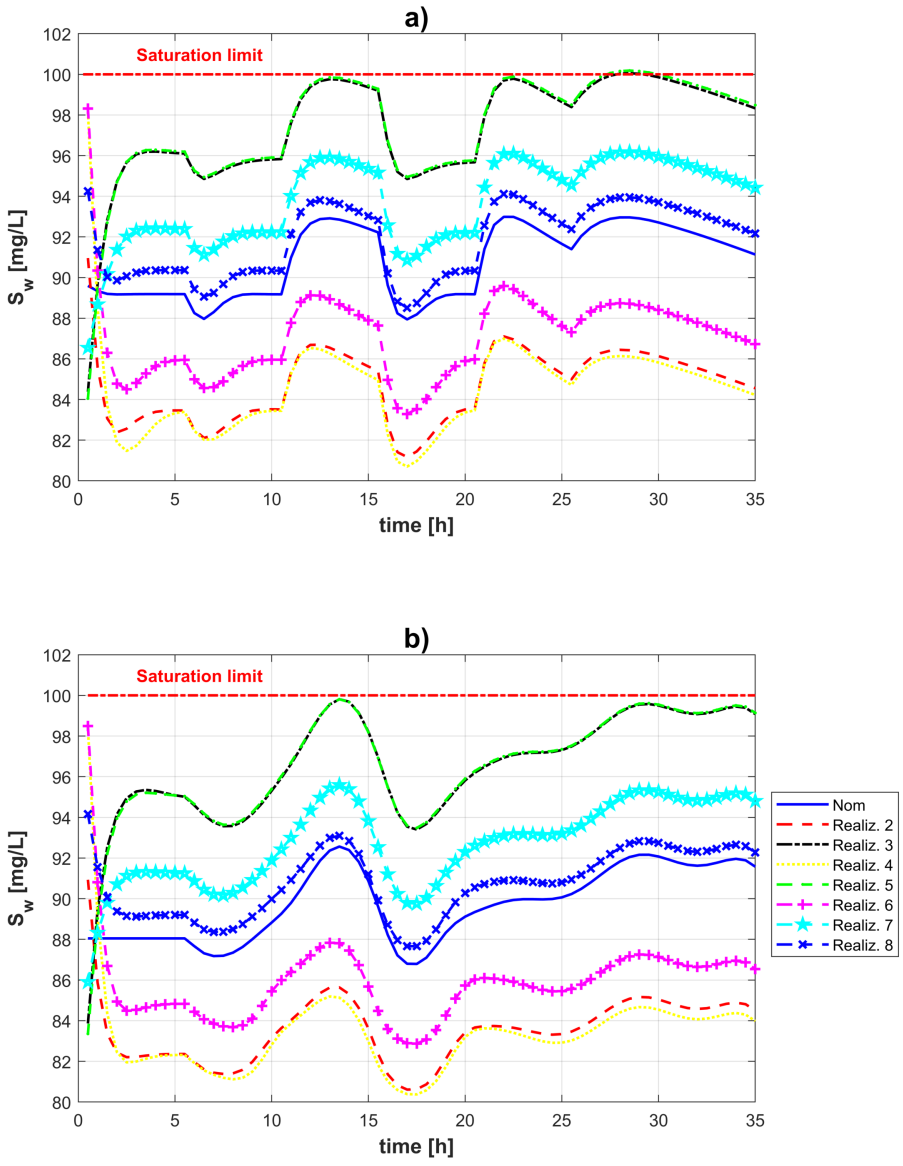

Figure 3.10: Scenario 4: Test results (a) closed-loop validation simulations for the control of substrate for the sinusoidal-based design under step disturbances; (b) closed-loop validation simulations for the control of substrate for the step-based design under sinusoidal disturbances.

3.5 Summary

This chapter presented a back-off approach for the integration of design and NMPC-based control under uncertainty and process disturbances. The methodology finds first the optimal steady-state design and then evaluates the dynamic performance of this process design in closed-loop. This allows the identification of the point that produces the largest variability to the process feasibility constraints under the effect of disturbances and uncertain realizations in the model parameters, i.e., the worst-case scenario. Model sensitivity terms are identified around this worst-case scenario to obtain an approximated explicit PSE-based optimization formulation. This formulation is explicit in terms of the optimization variables making it easily solvable using NLP solvers. The minimization of the cost function and the violations to process constraints drives the search for a solution for the integrated design and control problem.

To evaluate the performance and benefits of the proposed method, a wastewater treatment plant has been implemented. The effect of the control framework, the uncertainty realizations, disturbance profiles, and the PSE search space were assessed. The results show that the use of a NMPC-based framework leads to reduced plant costs with improved control performance compared to decentralized-PI control schemes or a LMPC strategy. The back-off method efficiently determined a solution for the bilevel problem. However, the identification of the sensitivity terms for the PSE approximation demands most of the CPU time in the proposed methodology, which may increase as more decision variables appear for larger scale formulations.

Chapter 4

Integration of design and NMPC-based control for chemical processes under uncertainty: A MPCC-based framework

The methodology presented in Chapter 3 has pointed out the benefits of using NMPC-based approaches for the integration of design and control under uncertainty. Although the back-off methodology computed economically attractive solutions with suitable control performance, the implementation of sequential approaches and approximation strategies may not guarantee optimality in the solution. As explained above in Sections 2.5 and 2.3, transformation strategies can be implemented for the transformation of bilevel problems into single-level MPCC-based formulations. Consequently, the problem may be solved using conventional NLP solvers. Nevertheless, the search for a solution for a MPCC is a challenging task, as mentioned in Section 2.3, the problem is a degenerate highly nonconvex formulation and multiple CQs are violated at every feasible point. A series of reformulation strategies for complementarity constraints have been proposed to circumvent this issue. In this chapter, the *classical KKT transformation* strategy (presented in Section 2.3.1) is implemented for the solution of the bilevel problem for integrated design and NMPC-based control under uncertainty.

This chapter is organized as follows: Section 4.1 presents the transformation strategy for the bilevel formulation, a brief overview of the quality for the solutions to MPCCs (i.e., the stationarity points) is also provided. The potential reformulation strategies for complementarity constraints in the MPCC for the integrated design and NMPC framework are shown also in this section. Section 4.2 illustrates the implementation of MPCCs in three case studies. In Section 4.3 a summary of the chapter is presented.

4.1 Transformation of Bilevel formulation

As mentioned above in Chapter 2, bilevel problems are hierarchical optimization problems that combine decisions of two decision makers, i.e., the so-called upper-level problem (leader level) and

a lower-level problem (follower level). The leader level takes the first decisions whereas the follower level reacts optimally to such decisions. The leader level problem aims to find the set of decisions, together with the follower level problem, that would optimize a cost function [139]. Bilevel problems are members of a more general class of problems called MPEC [46]. Recall from Chapter 2 that there exist at least three possible strategies to transform a bilevel problem into a MPCC: *Primal KKT transformation*, *Classical KKT transformation*, and *Optimal value transformation*. This PhD study focuses on the implementation of *Classical KKT* transformations for the reformulation of the bilevel problem that emerge in the integration of design and NMPC-based control. The implementation and further analysis of the *Primal KKT* and *Optimal value* transformations is beyond the scope of this research. Interested readers on these subjects can review the studies by Dempe et al. [46, 55, 63]. In a *Classical KKT* transformation, the lower-level problem is expressed in terms of their KKT conditions, i.e., necessary (and under certain conditions, also sufficient) conditions for optimality. These optimality conditions are included as constraints in the upper-level problem. Thus, the *classical KKT* transformation for the bilevel problem shown in Equation (3.1) into an MPCC is as follows:

$$\min_{\eta,\mathbf{x}(t),\bar{\mathbf{u}}(t),\hat{\mathbf{u}}(\tau_c),\mathbf{y}(t)} \sum_{j_u=1}^{J} w_{j_u}\Phi(\eta,\varsigma,\mathbf{x}(t),\bar{\mathbf{u}}(t),\mathbf{y}(t),\mathbf{d}_p(t),t) \tag{4.1a}$$

$$s.t.\ \ f(\eta,\varsigma,\dot{\mathbf{x}}(t),\mathbf{x}(t),\bar{\mathbf{u}}(t),\mathbf{y}(t),\mathbf{d}_p(t),t)=0,\quad \hat{\mathbf{x}}(\tau_{c_0})=\mathbf{x}(t),\ \forall\,\tau_c=t \tag{4.1b}$$

$$h(\eta,\varsigma,\mathbf{x}(t),\bar{\mathbf{u}}(t),\mathbf{y}(t),\mathbf{d}_p(t),t)=0, \tag{4.1c}$$

$$g(\eta,\varsigma,\mathbf{x}(t),\bar{\mathbf{u}}(t),\mathbf{y}(t),\mathbf{d}_p(t),t)\leq 0, \tag{4.1d}$$

$$\nabla_{\mathbf{\Omega}_c}\mathcal{L}(\eta,\hat{\mathbf{x}}(\tau_c),\hat{\mathbf{u}}(\tau_c),\lambda(\tau_c),\nu(\tau_c),\mu(\tau_c),\mathbf{d}_p,\tau_c)=0, \tag{4.1e}$$

$$F(\eta,\dot{\mathbf{x}}(\tau_c),\hat{\mathbf{x}}(\tau_c),\hat{\mathbf{u}}(\tau_c),\mathbf{d}_p,\tau_c)=0 \tag{4.1f}$$

$$H(\eta,\hat{\mathbf{x}}(\tau_c),\hat{\mathbf{u}}(\tau_c),\mathbf{d}_p,\tau_c)=0, \tag{4.1g}$$

$$G(\eta,\hat{\mathbf{x}}(\tau_c),\hat{\mathbf{u}}(\tau_c),\mathbf{d}_p,\tau_c)\leq 0, \tag{4.1h}$$

$$0\geq G(\eta,\hat{\mathbf{x}}(\tau_c),\hat{\mathbf{u}}(\tau_c),\mathbf{d}_p,\tau_c),\ \perp\ \mu(\tau_c)\geq 0, \tag{4.1i}$$

$$\bar{\mathbf{u}}(t)=\hat{\mathbf{u}}(\tau_c),\quad \forall\,\tau_c=t \tag{4.1j}$$

where $\nabla\mathcal{L}(\cdot)$ in Equation (4.1e) represents the gradient of the *Lagrangian* function, i.e., the stationarity conditions. This gradient is determined with respect to the decision variables in the NMPC problem (Equation ((2.4))), i.e., $\mathbf{\Omega}_c = [\hat{\mathbf{x}}(\tau_c), \hat{\mathbf{u}}(\tau_c)]$. The *Lagrangian* function is defined as $\mathcal{L} = \Psi(\cdot) + \lambda^\intercal F(\cdot) + \nu^\intercal H(\cdot) + \mu^\intercal G(\cdot)$. Equations (4.1g) and (4.1h) are the feasibility conditions whereas Equation (4.1i) represents the complementarity conditions to enforce that at least one of the bounds is active at the optimal solution. Variables $\lambda \in \mathbb{R}^{N_\lambda}$, $\nu \in \mathbb{R}^{N_\nu}$, and $\mu \in \mathbb{R}_+^{N_\mu}$ are the Lagrange multipliers for functions F, H, and G, respectively. Note that the complementary constraints exhibit a disjunctive behavior, which can be reformulated into equivalent expressions [18]. These alternative forms of complementarity constraints are of interest for the potential reformulations of MPCCs into NLPs.

The Problem (4.1) represents a challenging problem with NMPC for simultaneous design and control. The introduction of design variables strongly affects all the dynamic decision variables (e.g., the control profiles and trajectories of states). That is, changes in the process design impact the process dynamics, e.g., an increase or decrease in the size of the equipment modifies the time constant of the process, this may lead to unsatisfied dynamic constraints. Moreover, applications of MPCCs in process engineering, scheduling, and control of systems under uncertainty have not been widely considered. The model in Equation (4.1) explicitly incorporates uncertainty in process parameters, which have a direct effect on the process design and control decisions. Note that even applications with LMPC lead to nonconvex MPCCs. Therefore, an implementation with NMPC increases the complexity of the MPCC compared to applications with LMPC. For highly nonconvex optimization problems, a poor educated initial guess may lead to regions of feasible process designs with complicated process dynamics. This may complicate the search for an optimal solution, i.e., the optimization solver may not converge to a solution. In order to provide an educated initial guess, and reduce potential divergences in the solution process, a feasibility problem can be solved in closed-loop with the process and the NMPC for an specific process design. The NMPC was stated in terms of its KKT conditions. This allows to determine a first guess for the *Lagrange* multipliers. The solution of the feasibility problem in closed-loop was then used as the initial guess for the MPCC optimization problem.

4.1.1 Stationarity

The MPCC in Problem (4.1) is a *singular* optimization problem, i.e., it violates multiple constraint qualifications (CQs) at every feasible point. Singular problems cannot be solved directly with most of the NLP solvers [18]. Therefore, the use of reformulation strategies becomes necessary to overcome violations to CQs. In the literature there are at least three reformulation strategies for complementarity constraints. Those reformulation strategies allow to avoid violations to CQs. As a result, the MPCC is reformulated into a conventional NLP that can be solved with standard NLP solvers.

If constraint qualifications (CQs) hold for the MPCC in Equation (4.1), the KKT conditions in Equations (4.1e)-(4.1i) are necessary conditions of optimality [63]. However, the linear independence constraint qualification (LICQ), which requires the gradient of the active constraints to be linearly independent, is not satisfied for MPCCs at all feasible points. That is, at a given feasible point for the KKT conditions $(\hat{\mathbf{x}}^{\circ}, \hat{\mathbf{u}}^{\circ})$ that satisfy Equations (4.1g) and (4.1h), i.e., $H(\eta, \hat{\mathbf{x}}^{\circ}(\tau_c), \hat{\mathbf{u}}^{\circ}(\tau_c), \mathbf{d}_p, \tau_c) = 0$, $G(\eta, \hat{\mathbf{x}}^{\circ}(\tau_c), \hat{\mathbf{u}}^{\circ}(\tau_c), \mathbf{d}, \tau_c) \leq 0$, and $\mu^{\circ}(\tau_c) \geq 0$. We note that for all $G(\eta, \hat{\mathbf{x}}^{\circ}(\tau_c), \hat{\mathbf{u}}^{\circ}(\tau_c), \mathbf{d}, \tau_c) = 0$, the constraints $\mu^T(\tau_c) G(\eta, \hat{\mathbf{x}}^{\circ}(\tau_c), \hat{\mathbf{u}}^{\circ}(\tau_c), \mathbf{d}_p, \tau_c) = 0$ are satisfied; however, a similar condition holds for $\mu = 0$. This implies that the multipliers μ, if they exist, are nonunique, then the LICQ is not met [18, 62]. Moreover, a weaker condition is the MFCQ, which requires linear independence gradients for the equality constraints and the existence of a feasible search direction into the interior of the cone of inequality constraint gradients. MFCQ is a necessary and sufficient condition for boundedness of the multipliers. However, the MFCQ is also violated at all feasible points by the MPCCs. This implies that an MPCC formulation is highly degenerate and finding a solution may be a difficult task. Note that a local optimal solution of an MPCC needs not to be related to local optimal solutions of the corresponding bilevel optimization problem [46]. Then, with the aim to classify the solutions for an MPCC, it is necessary to introduce the concept of stationary points. A solution point $\Theta^* = [\eta^*, \mathbf{x}^*(t), \bar{\mathbf{u}}^*(t), \mathbf{y}^*(t)]$ and $\Omega_c^* = [\hat{\mathbf{x}}^*(\tau_c), \hat{\mathbf{u}}^*(\tau_c)]$ is *weak stationary point* if it is feasible and satisfy the necessary conditions of optimality [46, 62]. Additional weaker stationary conditions to identify *A*-, *B*-, *C*-, and *M-stationary* points contribute to the identification of potential optimal

solutions for the MPEC formulation in Equation (3.1). The verification of a B-stationary point, under certain conditions, can indicate that the MPEC-LICQ property holds [61]. A stationary point, where MPEC-LICQ holds, is an indication of bounded and unique Lagrange multipliers in the relaxed LPEC to determine B-stationarity. A stronger stationarity for a MPCC is the *strong stationarity*. *Strong stationarity* with a well-posed set of multipliers in the relaxed LPEC, for B-stationarity, verifies optimality of the MPCC formulation (Equation (4.1)).

4.1.2 Reformulation strategies for complementarity constraints

The inherent violations to CQs, at all feasible points for MPCCs, demands to reformulate the MPCC in order to avoid such violations. As mentioned above in Chapter 2, there are at least three reformulation strategies for complementarity constraints: *Regularization*, *Smoothing* and *Penalty* [140, 141, 64, 142, 143]. In a *regularized* formulation, the complementarity constraints are relaxed with a positive parameter ϵ_s. In cases where the complementarity constraints are regularized, the solution of the MPCC is obtained by the sequential solution of the regularized problem as ϵ_s approaches zero [18]. The properties and convergence features of this reformulation strategy are discussed elsewhere [141]. *Smoothing functions* (also known as NCP functions) is an alternative strategy used to replace the complementarity constraints in the MPCC formulation. This strategy is widely used for the solutions of MPCCs. The most popular smoothing function is the smoothed Fischer-Burmeister function ϕ_{BF}, i.e.,

$$\phi_{BF}(\mu, \bar{\pi}) = \mu + \bar{\pi} - \sqrt{\mu^2 + \bar{\pi}^2 + \epsilon_s} = 0 \tag{4.2}$$

where $\bar{\pi} \in \mathbb{R}^{N_s}$ is the set of positive slack variables for constraints $G(\cdot)$ (Equation (4.1h)). As in the regularization strategy, the solution of a smoothed MPCC is obtained from the sequential solution of the problem as ϵ_s approaches zero. In the literature, there is a large number of possible forms of NCP functions; a review of the different functions can be found elsewhere [144]. For the implementation of a *Penalty* strategy, the complementarities are moved from the constraints to the objective function as a penalty term. In this strategy, the challenge lies in the selection of the magnitude of the positive defined penalty parameter ($\bar{M}$). The magnitude of this parameter is not

known *a priori*. A complete review on the selection of the magnitude for the penalty parameter ($\bar{M}$), features, and convergence properties of the that reformulation strategy can be found elsewhere [141].

4.1.3 Solution strategy

For the solution of the MPCC in Equation (4.1), OCFE was considered. This discretization strategy allows to express the ODEs in the MPCC as a set of nonlinear algebraic equations. In this study, an OCFE strategy based on Lagrange polynomials (ℓ) using Radau points (k) was implemented. Radau collocation points offer the feature of continuity across element boundaries [145]. Further details on the features of OCFE can be found elsewhere [18, 146]. The discretized MPCC-based formulation presented in Equation (4.1) is as follows:

$$\min_{\eta, x_{j_u,i,k}, \bar{u}_i, y_{j_u,i,k}} \sum_{j_u=1}^{J} \sum_{i=1}^{I} \sum_{k=1}^{K} w_{j_u} \Phi_{j_u}(\eta, \varsigma_{j_u}, x_{j_u,i,k}, \bar{u}_i, y_{j_u,i,k}, d_{p_{i,k}}) \tag{4.3a}$$

$$s.t. \ \sum_{j=0}^{K} \dot{\ell}_j(\tau_k) x_{j_u,i,j} - \bar{\alpha}_i f_{j_u}(\eta, \varsigma_{j_u}, x_{j_u,i,k}, \bar{u}_i, y_{j_u,i,k}, d_{p_{i,k}}) = 0, \ \forall\, j_u = \{1, \ldots, J\},$$

$$i = \{1, \ldots, N_{FE}\},\ k = \{1, \ldots, K\} \tag{4.3b}$$

$$h_{j_u}(\eta, \varsigma_{j_u}, x_{j_u,i,k}, \bar{u}_i, y_{j_u,i,k}, d_{p_{i,k}}) = 0, \ \forall\, j_u = \{1, \ldots, J\},\ i = \{1, \ldots, N_{FE}\},\ k = \{1, \ldots, K\} \tag{4.3c}$$

$$g_{j_u}(\eta, \varsigma_{j_u}, x_{j_u,i,k}, \bar{u}_i, y_{j_u,i,k}, d_{p_{i,k}}) \leq 0, \ \forall\, j_u = \{1, \ldots, J\},\ i = \{1, \ldots, N_{FE}\},\ k = \{1, \ldots, K\} \tag{4.3d}$$

$$x_{i+1,0} = \sum_{k=0}^{K} \ell_k(1) x_{i,k}, \ \ i = \{1, \ldots, N_{FE} - 1\} \tag{4.3e}$$

$$x_f = \sum_{k=0}^{K} \ell_k(1) x_{N_{FE},k}, \ \ x_{1,0} = x(t_0) \tag{4.3f}$$

$$\nabla_{\mathbf{\Omega}_c} \mathcal{L}(\eta, \hat{x}_{i,i',k'}, \hat{u}_{i,i',k}, \lambda_{i,i',k'}, \nu_{i,i',k'}, \mu_{i,i',k'}, d_{p_i}) = 0, \ \forall\, i = \{1, \ldots, N_{FE}\},\ i' = \{1, \ldots, N'_{FE}\},$$

$$k' = \{1, \ldots, K'\} \tag{4.3g}$$

$$\sum_{j=0}^{K} \dot{\ell}_j(\tau_{k'}) x_{i,i',k'} - \bar{\alpha}_{i'} F(\eta, \hat{x}_{i,i',k'}, \hat{u}_{i,i',k'}, d_{p_i}) = 0, \ \forall\, i = \{1, \ldots, N_{FE}\},\ i' = \{1, \ldots, N'_{FE}\},$$

$$k = \{1, \ldots, K'\} \tag{4.3h}$$

$$H(\eta, \hat{x}_{i,i',k'}, \hat{u}_{i,i',k'}, d_{p_i}) = 0,\ \forall\, i = \{1, \ldots, N_{FE}\},\ i' = \{1, \ldots, N'_{FE}\},\ k' = \{1, \ldots, K'\} \tag{4.3i}$$

$$G(\eta, \hat{x}_{i,i',k'}, \hat{u}_{i,i',k'}, d_{p_i}) \leq 0,\ \forall\, i = \{1, \ldots, N_{FE}\},\ i' = \{1, \ldots, N'_{FE}\},\ k' = \{1, \ldots, K'\} \tag{4.3j}$$

$$\hat{x}_{i,i'+1,0} = \sum_{j=0}^{K} \ell_k(1)\hat{x}_{i,i',k'},\ \ i' = \{1, \ldots, N'_{FE} - 1\} \tag{4.3k}$$

$$\hat{x}_f = \sum_{j=0}^{K} \ell_k(1)\hat{x}_{i,I,k},\ \ x_{i,1,0} = x(\tau_c^0) \tag{4.3l}$$

$$0 \geq G(\eta, \hat{x}_{i,i',k'}, \hat{u}_{i,i',k'}, d_i),\ \perp\ \mu_{i,i',k'}(\tau_c) \geq 0, \tag{4.3m}$$

where $t_{i,k} = t_{i-1} + \bar{\alpha}_i \tau_k$, $\tau_0 = 0$, $0 < \tau_k \leq 1$, $k = \{1, \ldots, K\}$ are shifted Radau points (τ). Finite elements for the upper-level problem (Equations (4.3a) - (4.3f)) are indexed by i, whereas, finite elements for the lower-level problem (Equations (4.3g) - (4.3m)) are indexed by k'. N_{FE} represents the total number of finite elements in the upper-level problem whereas N'_{FE} represents the total number finite elements in the lower-level problem. $\bar{\alpha}_i$ is the length of the finite elements i and k'. Lagrange polynomials are defined as $\ell_k(\tau) = \prod_{j=0,\neq k}^{K} \frac{(\tau - \tau_j)}{(\tau_k - \tau_j)}$ and $\dot{\ell}_k(\tau) = \frac{d\ell_k(\tau)}{d\tau}$. The NLP formulation in Problem (4.3) provides an accurate approximation to the MPCC in Equation (4.1).

4.2 Case studies

This section presents three case studies to illustrate the implementation of MPCCs for the integration of design and NMPC-based control. The first case study addresses the optimal design and liquid level and temperature control of a storage tank. The second case study addresses the optimal design and control of a two continuous stirred tank reactors (CSTRs) system. This case study aims to maintain the outlet concentration of reactant around the desired set-point. In the third case study, an existent wastewater treatment plant is presented. This plant is subject to process disturbances in the inlet stream and uncertainty in the process parameters that describe the kinetics of the biological reactions. The first case study aims to demonstrate the implementation of the *classical KKT transformation* strategy for integration of design and NMPC-based control. In the first

case study (Section 4.2.1), the corresponding bilevel problem is presented first, followed by MPCC-based formulation. Three reformulation strategies for complementarity constraints were considered for the solution of the MPCC-based formulation, as presented in section 4.1.2. Those reformulation strategies for complementarity constraints aim to avoid violations to CQs in the solution of the optimization problem. The second case study illustrates the use of MPCCs for a medium scale design and NMPC-based control problem. In the third case study, the use of MPCCs is illustrated for the integration of design and control of a highly nonlinear process under uncertainty. Moreover, the proposed integrated approach was compared with the traditional sequential design and control approach for the case studies 2 and 3. In all case studies, the results are discussed and point out the features and weakness of the solution strategy. All numerical implementations were performed in GAMS 37.1 and IPOPT was used as the NLP solver. OS and hardware specifications are as follows: 64-bit Windows Server 2019, Intel(R) Core(TM) i7-8700 CPU, 3.20GHz, and 16GB RAM.

4.2.1 Storage tank

The first case study proposes the integration of design and NMPC-based control of a heated storage tank (Figure 4.1). Controlled variables in this process are the liquid's temperature (T) and the tank's outlet stream ($\bar{F}$). Since there is no pump installed at the output flow rate, the storage tank must maintain a certain liquid holdup set-point ($h_T^{sp} = 5m$) to guarantee a certain discharge pressure, while the temperature T must be kept at $313.3K$ (Temperature set-point (T^{sp})). Moreover, due to special requirements, the tank has an extra outlet stream (i.e., a *purge* ($\bar{F}_p$)). The magnitude of the purge stream is assumed to follow a square function of the liquid holdup (i.e., $\bar{F}_p = Cv\sqrt{h_T(t)}$). The dynamic model of this storage tank is given by the mass and energy balances and is as follows:

$$\frac{dh_T(t)}{dt} = \frac{\bar{F}_{in}(t) - \bar{F}(t) - \bar{F}_p(t)}{\rho A_d}, \tag{4.4a}$$

$$\frac{dT(t)}{dt} = \bar{F}_{in}(t)\frac{(T_{in}(t) - T(t))}{\rho A_d h_T} + \frac{U_h A_e (T_c(t) - T(t))}{\rho A_d h_T C_p^l}, \tag{4.4b}$$

$$h_T(t_0) = h_T^{sp}, \;\; T(t_0) = T^{sp} \tag{4.4c}$$

where Cv is the purge valve size coefficient, ρ is the liquid's density, A_d is the tank's cross sectional area, U_h is the universal heat transfer coefficient, the heat transfer area is given by A_e, and C_p^l is the liquid's heat capacity. h_T^{sp} and T^{sp} correspond to the liquid's holdup and temperature set-points, respectively. The values for the model parameters presented in Equation (4.4) are shown in Table 4.1. To ensure the robustness in the solution, Table 4.2 presents a set of step disturbances in the flow rate and temperature of the inlet stream (i.e., $\bar{F}_{in}$ and T_{in}, respectively). These disturbances are enforced in intervals of 20 minutes upto a total simulation time of 110 minutes.

Table 4.1: Values for the model parameters (Storage tank case study)

Parameter	**Value**
$\rho\ [kg/m^3]$	900
$U_h A_e\ [J/(min\,K)]$	5.0×10^4
$T^{sp}\ [K]$	313.3
$h_T^{sp}\ [m]$	5.0
$C_p^l\ [J/(kg\,K)]$	239

Table 4.2: Disturbance trajectory profiles (Step Changes) for the storage tank case study

t $[min]$	T_{in} $[K]$	$\bar{F}_{in}$ $[kg/min]$
0	293	100
5	298	85
25	285	120
45	293	150
65	305	95
85	293	100

An NMPC is implemented in this first case study. It is assumed that the liquid's level and temperature are controlled through the manipulation of the temperature on a heating coil (T_c) and the outlet stream flow rate ($\bar{F}$), as shown in Figure 4.1. Moreover, it is assumed that the NMPC has a perfect process model and that the NMPC has access to the measurements for all the states and disturbances. The optimization problem for the NMPC is as follows:

$$\min_{\bar{F}(\tau),\hat{T}_c(\tau),\hat{h}(\tau),\hat{T}(\tau)} Q_h \int_t^{t+t_P} (\hat{h}(\tau_c) - h^{sp})^2\, d\tau_c + Q_T \int_t^{t+t_P} (\hat{T}(\tau_c) - T^{sp})^2\, d\tau_c + Q_{\bar{F}} \int_t^{t+t_C} \Delta\hat{F}^2(\tau_c)\, d\tau_c + Q_{T_c} \int_t^{t+t_C} \Delta\hat{T}_c^2(\tau_c)\, d\tau_c \quad (4.5a)$$

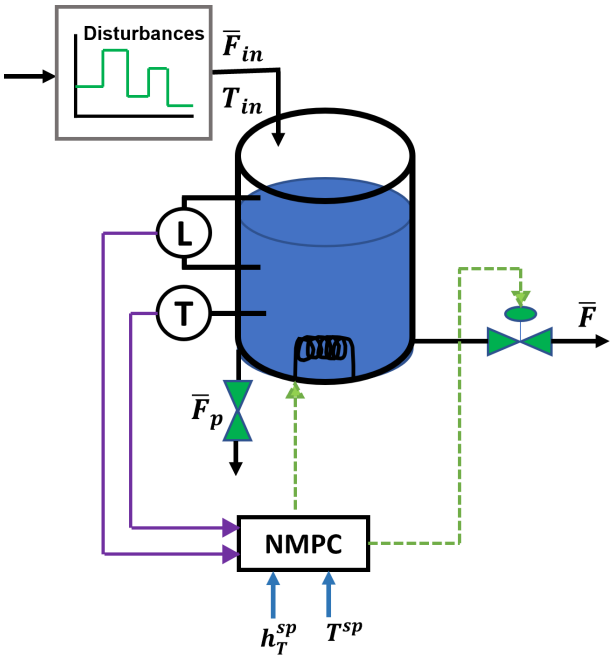

Figure 4.1: Integrated design and control of a liquid storage tank.

$$s.t.\ \frac{d\hat{h}_T(\tau_c)}{d\tau_c} = \frac{\bar{F}_{in}(\tau_c) - \hat{F}(\tau_c) - \bar{F}_p(\tau_c)}{\rho A_d}, \tag{4.5b}$$

$$\frac{d\hat{T}(\tau_c)}{d\tau_c} = \bar{F}_{in}(\tau_c)\frac{(T_{in}(\tau_c) - \hat{T}(\tau_c))}{\rho A_d h_T} + \frac{U_h A_e(\hat{T}_c(\tau_c) - \hat{T}(\tau_c))}{\rho A_d h_T C_p^l}, \tag{4.5c}$$

$$h_T(\tau_{c_0}) = h_T(t),\ \ T(\tau_{c_0}) = T(t), \tag{4.5d}$$

$$\bar{F}^{lb} \leq \hat{F}(\tau_c) \leq \bar{F}^{ub},\ \ T_c^{lb} \leq \hat{T}_c(\tau_c) \leq T_c^{ub} \tag{4.5e}$$

where Q_h and Q_T are the weighting tuning parameters ($\mathbf{Q_{out}} = [Q_h, Q_T]$) to penalize deviations on the controlled variables ($\hat{h}_T(\tau_c)$ and $\hat{T}(\tau_c)$, respectively) with respect to the set-points ($h_T^{sp} = 5m$ and $T^{sp} = 313.3K$, respectively). $Q_{\bar{F}}$ and Q_{T_c} are the weighting tuning parameters ($\mathbf{Q_{in}} = [Q_{\bar{F}}, Q_{T_c}]$) to penalize changes in the manipulated variables and represent optimization variables in the present formulation (i.e., $\hat{F}(\tau_c)$ and $\hat{T}_c(\tau_c)$, respectively). The dynamic model of the process in Equations (4.5b) and (4.5c) corresponds to the model in Equations (4.4a) and (4.4b). The initial values for the controlled variables are given by the measurements for the liquid level and

temperature (i.e., h_T and T) at time t (Equation 4.5d). Equation 4.5e enforces bounds on the manipulated variables. The lower bounds are given by $\bar{F}^{lb}$ and T_c^{lb} whereas the upper bounds are given by $\bar{F}^{ub}$ and T_c^{ub}. In this case study, t_P and t_C in the NMPC are both set to 5 minutes. This horizon was selected by performing closed-loop simulations under process disturbances with a fixed tank design. The closed-loop simulations aimed to maintain the controlled variables on the desired set-points. The sampling period for the measurement of states was set to 1 minute.

For the integration of design and control, the cost function considered in this case study consists of the addition of an annualized capital cost (CC_a) and a variability cost (VC_a). Capital cost is defined as a function of the tank's volume (V_R), i.e.,

$$CC_a = 10V_R^{1.085} \tag{4.6}$$

Similarly, VC_a is described by the penalization of the deviations in time of the liquid's temperature and the liquid's holdup with respect to their corresponding set-points, i.e.,

$$VC_a = 100 \int_{t_0}^{t_f} (T(t) - T^{sp})^2 \, dt + 1000 \int_{t_0}^{t_f} (h_T(t) - h_T^{sp})^2 \, dt \tag{4.7}$$

The bilevel problem is formulated with the objective function in terms of Equations (4.6) and (4.7) subject to the dynamic process model (Equation (4.4)) and the optimization problem for the NMPC (Equation (4.5)), i.e.,

$$\min_{A_d, V_R, T(t), h_T(t), \bar{F}(t), T_c(t), \mathbf{Q_{in}}, \mathbf{Q_{out}}} CC_a + VC_a \tag{4.8}$$

$s.t.$ Dynamic process model (Equation (4.4)),

Process constraints,

Optimization problem for NMPC (Equation (4.5)).

From Equation (4.8), it can be observed that the decision variables selected for this problem are the tank's cross sectional (A_d) and volume (V_R), the time-dependent state profiles ($h_T(t)$ and $T(t)$) and the control actions ($\bar{F}(t)$ and $T_c(t)$), and the weights Q_h, Q_T, $Q_{\bar{F}}$, and Q_{T_c} in the

NMPC formulation. Process constraints consider bounds on decision variables, these are included in Equation (4.8) to ensure that the final design and control scheme remain within the acceptable feasible region. Implementation of the *classic KKT transformation* strategy leads to the formulation of the corresponding MPCC for this problem:

$$\min_{A_d,V_R,T(t),h_T(t),\bar{F}(t),T_c(t),\mathbf{Q_{in}},\mathbf{Q_{out}}} CC_a + VC_a \tag{4.9a}$$

$$s.t.\ \frac{dh_T(t)}{dt} = \frac{\bar{F}_{in}(t) - \bar{F}(t) - \bar{F}_p(t)}{\rho A_d}, \tag{4.9b}$$

$$\frac{dT(t)}{dt} = \bar{F}_{in}(t)\frac{(T_{in}(t) - T(t))}{\rho A_d h_T} + \frac{U_h A_e (T_c(t) - T(t))}{\rho A_d h_T C_p^l}, \tag{4.9c}$$

$$h_T(t_0) = h_T^{sp},\ \ T(t_0) = T^{sp},\ \ \bar{F}(t) = \bar{F}(\tau_c + k_t),\ \ T_c(t) = T_c(\tau_c + k_t) \tag{4.9d}$$

$$\nabla_{\mathbf{\Omega}_c}\mathcal{L}(A_d, V_R, \hat{T}(\tau_c), \hat{h}_T(\tau_c), \hat{F}(\tau_c), \hat{T}_c(\tau_c), \lambda_1(\tau_c), \lambda_2(\tau_c), \mu_F^L(\tau_c), \mu_F^U(\tau_c), \mu_{T_c}^L(\tau_c), \mu_{T_c}^U(\tau_c)) = 0 \tag{4.9e}$$

$$\frac{d\hat{h}_T(\tau_c)}{d\tau_c} = \frac{\hat{F}_{in}(\tau_c) - \hat{F}(\tau_c) - \hat{F}_p(\tau_c)}{\rho A_d},\ \ \frac{d\hat{T}(\tau_c)}{d\tau_c} = \hat{F}_{in}(\tau_c)\frac{(T_{in}(\tau_c) - \hat{T}(\tau_c))}{\rho A_d h_T} + \frac{U_h A_e (\hat{T}_c(\tau_c) - \hat{T}(\tau_c))}{\rho A_d h_T C_p^l}, \tag{4.9f}$$

$$0 \geq \bar{F}^{lb} - \hat{F}(\tau_c) \perp \mu_F^L \leq 0,\ \ 0 \geq \hat{F}(\tau_c) - \bar{F}^{ub} \perp \mu_F^U \leq 0, \tag{4.9g}$$

$$0 \geq T_c^{lb} - \hat{T}_c(\tau_c) \perp \mu_{T_c}^L \leq 0,\ \ 0 \geq \hat{T}_c(\tau_c) - T_c^{ub} \perp \mu_{T_c}^U \leq 0, \tag{4.9h}$$

where $\lambda_1(\tau_c) \in \mathbb{R}^{N_\lambda}$, $\lambda_2(\tau_c) \in \mathbb{R}^{N_\lambda}$, $\mu_F^L(\tau_c) \in \mathbb{R}^{N_\mu}$, $\mu_F^U(\tau_c) \in \mathbb{R}^{N_\mu}$, $\mu_{T_c}^L(\tau_c) \in \mathbb{R}^{N_\mu}$, and $\mu_{T_c}^U(\tau_c) \in \mathbb{R}^{N_\mu}$ are the *Lagrange* multipliers for the NMPC's optimization problem. Equations (4.9a)-(4.9d) correspond to the objective function and the process model, i.e., the design problem whereas Equations (4.9e)-(4.9h) are the KKT conditions for the NMPC in Equation (4.5), i.e., the control problem. In the KKT conditions, Equation (4.9e) describes the stationarity conditions, Equation (4.9f) are the feasibility constraints, and Equations (4.9g) and (4.9h) are the complementarity constraints. The gradient of the *Lagrangian* function for the NMPC problem (Equation (4.9e)) is defined with respect to the set of decision variables in Equation (4.5), i.e., $\mathbf{\Omega}_c = [\hat{F}(\tau_c), \hat{T}_c(\tau_c), \hat{h}_T(\tau_c), \hat{T}(\tau_c)]$. The formulation of the MPCC was solved using a different reformulation strategy for the complementarity constraints, i.e., *regularization* (Scenario 1), *smoothing*

(Scenario 2), and *penalty* (Scenario 3). In the *regularization* strategy, the regularized-MPCC was solved in two NLP stages while the magnitude of the relaxation parameter ϵ_s was reduced. The regularized-MPCC was solved with $\epsilon_s = 1 \times 10^{-2}$ and the solution was then used to re-initialize that same problem but with the relaxation parameter reduced to $\epsilon_s = 0$. The penalty parameter $\bar{M}$ in the *penalty* strategy was selected to be $\bar{M} = 1 \times 10^{6}$. In all scenarios, the model was discretized using OCFE. For the upper-level problem, 110 finite elements were implemented. The lower-level problem was discretized with 5 finite elements. In both problems, 3 Radau collocation points were used. Closed-loop simulations showed that this mesh size (discretization) can accurately approximate the model functions. The corresponding number of variables and equations of the MPCCs for each scenario are shown in Table 4.3.

Table 4.3: Results for the temperature-level tank case study.

Scenario	**1**	**2**	**3**
Strategy	Regularization	Smoothing	Penalty
A_d $[m^2]$	7.1	7.1	7.1
V_R $[m^3]$	45.9	45.9	45.9
Q_h	1.55×10^{6}	2.604	8.48×10^{4}
Q_T	1.08×10^{4}	9×10^{-3}	2.93×10^{5}
$Q_{\bar{F}}$	1.06	1.04×10^{-5}	1.08×10^{5}
Q_{T_c}	5.02	1.53×10^{-6}	1.54×10^{5}
Model equations	36,417	36,417	23,773
Model variables	36,424	36,424	36,424
Total cost [$/yr]	124.9	125.1	125.3
CPU time [s]	692.4	1003.5	189.3
Solution	B-stationary	weak-stationary	weak-stationary

As shown in Table 4.3, the design of the tank is the same in all the scenarios, i.e., tank's volume V_R and cross-sectional area A_d. However, the controller tuning parameters (i.e., matrices $\mathbf{Q_{out}}$ and $\mathbf{Q_{in}}$) exhibit significant differences between the solutions obtained from each reformulation strategy. In Scenario 2 (smoothing), the tuning parameters have differences of at least 4 orders of magnitude with respect to results obtained with the regularization and penalty strategies (i.e., Scenarios 1 and 3, respectively). When comparing Scenarios 1 and 3, the tuning parameters $\mathbf{Q_{out}}$ have a difference of only one order of magnitude. Moreover, in Scenario 3, it can be noted that the tuning parameters $\mathbf{Q_{in}}$ are 5 orders of magnitude larger than those obtained in Scenario 1 (*regularization* strategy).

Closed-loop simulations were performed on each scenario to validate the resulting design and control scheme. As shown in Figure 4.2a), the dynamic profile for temperature takes slightly longer times to return to the set point for the smoothing strategy (i.e., Scenario 2). This difference in the control performance is explained by the differences of the orders of magnitude in the controller tuning parameters; the controller has lower penalizations for deviations in the control trajectories. The results in Figure 4.2 also show that the smoothing strategy (Scenario 2) exhibited the largest closed-loop settling time. Figure 4.2b) shows slightly less aggressive control actions on T_c for Scenario 2 compared with Scenarios 1 and 3. This also agrees with the observations in the temperature profile in Scenario 2. The results for the tuning parameters $\mathbf{Q_{out}}$ and $\mathbf{Q_{in}}$, in particular for this case study, revealed that the sensitivity of the model to these decision variables is not significant. This is confirmed with the results from IPOPT; the solver reported shadow prices for these decision variables around 1×10^{-11}, i.e., a unit increase in the decision variable has an effect of 1×10^{-11} on the cost of the objective function. Therefore, the process economics in the formulation is dominated by the design variables (V_R and A_d). Hence, the design variables in all scenarios converged to the same results. Note that the optimal solutions to the MPCC satisfy process operation targets and constraints at a minimum cost.

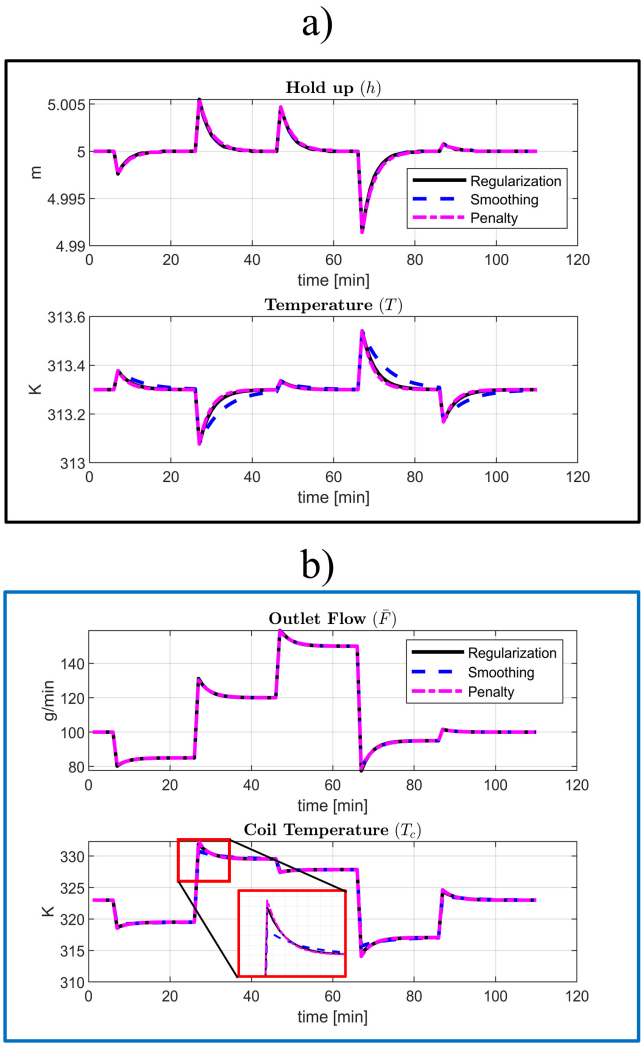

Figure 4.2: Validation simulations under process disturbances for the storage tank case study, with the different reformulation strategies: *regularization* (Scenario 1), *smoothing* (Scenario 2), and *penalty* (Scenario 3); a) Dynamic profiles for controlled variables (i.e., h_T and T); b) Dynamic profiles for manipulated variables (i.e., $\bar{F}$ and T_c).

In this case study, the implementation of three reformulation strategies reported in the literature was presented [46, 18]. The implementation of each one of these strategies mainly depends on the user's experience, the characteristics of the problem and the complementarities, model's size and complexity. For instance, a regularization strategy has a wide popularity because it is easy to implement. On the other hand, the most widely used strategy to solve MPCCs is smoothing functions since they allow to break the nonlinearity that arises by the product of decision variables. Moreover,

the penalty strategy is preferred when barrier optimization solvers are implemented (like KNITRO or IPOPT). Additional details describing the features and challenges on the implementation of different reformulation strategies can be found in the literature [46, 64, 141, 142, 143].

4.2.2 Two CSTRs in series

The second case study is based on a system presented by Luyben [147]. This case study presents a simple reaction system with 2 CSTRs in series as shown in Figure 4.3. An irreversible liquid phase exothermic reaction $\mathcal{A} \rightarrow \mathcal{B}$ is taking place on each reactor. The reactors have cooling jackets to remove the heat of the reaction. The feed flow rate to the system ($\bar{F}$ $[lbmol/min]$) has a concentration C_{A0} and a temperature T_{in} $[^{\circ}F]$. The reactant leaving the first reactor has a concentration C_{A1}, while the corresponding concentration at the outlet stream of the second reactor is given by C_{A2}. The original problem presented by Luyben [147] requires that both reactors have the same size, i.e., these are symmetric units. Reactor's volume is given by V_R (since both reactors are the same size, the reactor's volume is assumed to be the same), whereas the temperatures of the reaction media in each reactor are T_1 and T_2, respectively. The design decisions are given by the diameter (D_e $[ft]$) and height (h_T $[ft]$) of the CSTRs. The aspect ratio (h_T/D_e) is set to 2. Moreover, the cooling jacket volume (Vj) and heat-transfer area (A_e) are functions of h_T and D_e, i.e., $Vj = f_{Vj}(h_T, D_e)$ and $A_e = f_{Ae}(h_T, D_e)$. Fresh water streams are introduced to the jackets as cooling media ($\bar{F}_{w1}$ and $\bar{F}_{w1}$, respectively) with an initial temperature T_c^0 $[^{\circ}F]$. Therefore, the temperatures for the cooling jackets are T_{c1} and T_{c2}, respectively. This process aims to reach a specified concentration of A in the product stream $C_{A2} = 0.05$ $[lbmol_A/ft^3]$. The dynamic model of this process considers mass and energy balances (6 ODEs) and a set of equality constraints (4 algebraic equations). The NMPC considered for this case study uses the plant model, i.e., there is no mismatch between the actual process model and the dynamic model used by the controller. In this case study, it is assumed that the controlled variables are the concentrations in the CSTRs (i.e., C_{A1} and C_{A2}), while, the manipulated variables are the flow rates of the cooling water on each reactor (i.e., $\bar{F}_{w1}$ and $\bar{F}_{w2}$). For this case study, the process model is shown in Equation (4.10), Table 4.4 shows the values for model parameters, and the MPCC-based formulation are

included in the Appendix A. Additionally, to demonstrate the benefits of the integrated design and control approach, in this case study, a sequential design and control study is also performed. In this sequential approach, the reaction system is designed at steady-state. Then, the controller is tuned in closed-loop subject to changes in the disturbances [37].

Table 4.4: Values for the model parameters (CSTRs case study)

Parameter	**Value**
C_p^l $[BTU/(ft^3\,R)]$	37.5
ΔH_{rx} $[BTU/lbmole]$	-15,000
E $[BTU/lbmole]$	30,000
k_{re} $[hr^{-1}]$	4.08×10^{10}
ρ $[lb/ft^3]$	50
MW $[lb/lbmole]$	50
C_p^w $[BTU/(ft^3\,R)]$	62.38
U_h $[BTU/(hr\,ft^2\,R)]$	150
T_{ref} $[R]$	600
T_1^L, T_2^L $[R]$	542.8
T_1^U, T_2^U $[R]$	670.0
T_{c1}^L, T_{c2}^L $[R]$	532.0
T_{c1}^U, T_{c2}^U $[R]$	668.0
$\bar{F}_{w1}^U$ $[ft^3/hr]$	600.7
$\bar{F}_{w2}^U$ $[ft^3/hr]$	100.8
$\Delta\bar{F}_w$ $[ft^3/hr]$	40.0

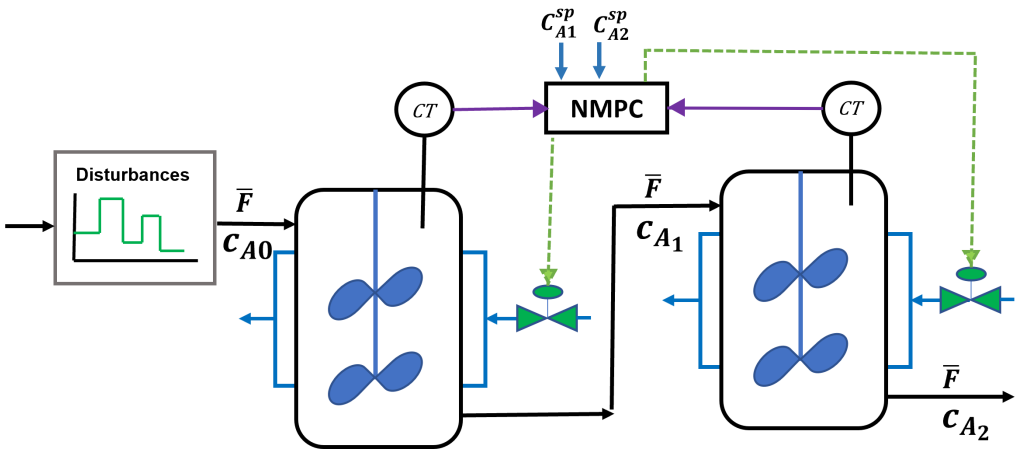

Figure 4.3: Integrated design and NMPC-based control of a reaction system with 2 CSTRs in series.

$$\frac{dC_{A1}}{dt} = \frac{\bar{F}}{V_R}(C_{A0} - C_{A1}) - ra_1, \;\; C_{A1}(t_0) = C_{A1}(0) \tag{4.10a}$$

$$\frac{dT_1}{dt} = \frac{\bar{F}}{V_R}(T_{in} - T_1) + \frac{(-\Delta H_{rx})ra_1}{C_p^l} - \frac{U_h A_e(T_1 - T_{c_1})}{V_R C_p^l}, \;\; T_1(t_0) = T_1(0) \tag{4.10b}$$

$$\frac{dT_{c1}}{dt} = \frac{\bar{F}_{w1}}{Vj}(T_c^0 - T_{c_1}) + \frac{U_h A_e(T_1 - T_{c_1})}{VjC_p^w}, \;\; T_{c1}(t_0) = T_{c1}(0) \tag{4.10c}$$

$$\frac{dC_{A2}}{dt} = \frac{\bar{F}}{V_R}(C_{A1} - C_{A2}) - ra_2, \;\; C_{A2}(t_0) = C_{A2}(0) \tag{4.10d}$$

$$\frac{dT_2}{dt} = \frac{\bar{F}}{V_R}(T_1 - T_2) + \frac{(-\Delta H_{rx})ra_2}{C_p^l} - \frac{U_h A_e(T_2 - T_{c_2})}{V_R C_p^l}, \;\; T_2(t_0) = T_2(0) \tag{4.10e}$$

$$\frac{dT_{c2}}{dt} = \frac{\bar{F}_{w2}}{Vj}(T_c^0 - T_{c_2}) + \frac{U_h A_e(T_2 - T_{c_2})}{VjC_p^w}, \;\; T_{c2}(t_0) = T_{c2}(0) \tag{4.10f}$$

$$ra_1 = k_{re} e^{\frac{-E}{RT_1}} C_{A1} \tag{4.10g}$$

$$ra_2 = k_{re} e^{\frac{-E}{RT_2}} C_{A2} \tag{4.10h}$$

where C_p^l is the liquid's phase heat capacity, the heat of reaction is given by ΔH_{rx}, E stands for the activation energy for the reaction, k_{re} is the reaction rate constant, C_p^w corresponds to the heat capacity of water. For the integration of design and control, a cost function consists of the addition of an annualized capital cost (CC_a), an operating cost (OC_a), and a variability cost (VC_a). The CC_a is related to the size of the required equipment. Hence, the pressure vessel costs functions reported by Douglas [148] are implemented, i.e.,

$$CC_a = 3834(D_e^{1.066} + h_T^{0.802}) \tag{4.11}$$

The OC_a depends on the cost of the conditioning, pumping, and availability of the cooling water, i.e.,

$$OC_a = 37 \int_{t_0}^{t_f} \bar{F}_{w1}(t) + \bar{F}_{w2}(t) \; dt \tag{4.12}$$

With regards to the VC_a function, the deviations of C_{A2} with respect to the set-point are penalized, i.e.,

$$VC_a = 1.0 \times 10^6 \int_{t_0}^{t_f} (C_{A2}(t) - C_{A2}^{sp})^2 \, dt \tag{4.13}$$

where $C_A^{sp}{}_2$ corresponds to the set-point of C_{A2}. The bilevel problem is formulated with the objective function subject to the dynamic process model and the optimization model for the NMPC-based controller as follows:

$$\min_{D_e, h_T, \mathbf{x}(t), \mathbf{u}(t), C_{A1}^{sp}, \mathbf{Q_{out}}} \Phi = CC_a + OC_a + VC_a \tag{4.14}$$

$s.t.$ Dynamic process model,

Process constraints,

Optimization problem for NMPC,

Operation boundaries.

where the matrix $\mathbf{Q_{out}}$ corresponds to the tuning parameters for the NMPC-based formulation in Equation (2.4a). From the objective function in Equation (4.14), it can be observed that the decision variables include D_e and h_T, the concentration set-point for reactant A in the first CSTR (C_{A1}^{sp}), and the trajectories of the states (i.e., $\mathbf{x}(t) = [C_{A1}(t), T_1(t), T_{c1}(t), C_{A2}(t), T_2(t), T_{c2}(t)]$). The control decisions correspond to the trajectories for the manipulated variables ($\bar{\mathbf{u}}(t) = [\bar{F}_{w1}(t), \bar{F}_{w2}(t)]$). Table 4.5 shows the set of process disturbances considered in this case study, these correspond to step changes in the parameters C_{A0} and T_{in} in the inlet flow rate. The disturbances are enforced in intervals of 25 hours upto a total simulation time of 75 hours. Prediction and control horizons in the NMPC are both set to 5 hours. As in the first case study, control and prediction horizons were selected using closed-loop simulations under process disturbances with a fixed design for the CSTRs. To simplify the analysis, the weighting parameters $\mathbf{Q_{in}}$ (Equation (2.4a)) to penalize changes in the manipulated variables ($\bar{F}_{w1}$ and $\bar{F}_{w2}$) were fixed to 0.16 and 0.38. Closed-loop simulations were implemented for the selection of the magnitude for the weighting parameters $\mathbf{Q_{in}}$. Note that the changes in the manipulated variables raised to the square are in the orders of 1×10^2, whereas the integral square error for the controlled variables is in the order of 1×10^{-6}. These changes are quantified in the objective function for the NMPC, therefore, to make significant the effect of the

Table 4.5: Disturbance trajectory profiles (Step Changes) for the 2 CSTRs case study.

t $[h]$	C_{A0} $[mol_A]$	T_{in} $[^\circ F]$
0	1.0	600
5	0.95	585
30	0.98	615
55	1.0	600

changes in the controlled variables, the magnitude of matrix $\mathbf{Q_{out}}$ is expected to be large and the magnitude of matrix $\mathbf{Q_{in}}$ should be set to relatively small values. More details about the selection of NMPC tuning parameters can be found elsewhere [37]. The MPCC-based problem was reformulated with a *regularization* strategy. This strategy required three sequential solutions of the formulation as the parameter ϵ_s was reduced in magnitude, i.e., a first solution to the regularized-MPCC was obtained with $\epsilon_s = 1 \times 10^{-2}$, the solution was taken as the initial guess to re-solve the problem but the relaxation parameter was reduced to $\epsilon_s = 1 \times 10^{-6}$, this procedure was repeated with $\epsilon_s = 1 \times 10^{-8}$. *Smoothing* and *Penalty* strategies were also implemented, however, no convergence to a solution in a reasonable CPU limit of time ($1.0 \times 10^6\, s$) was obtained with these strategies. Furthermore, OCFE was implemented for the discretization of the model. The optimization model was discretized with 300 finite elements for the upper-level problem and 20 finite elements for the lower-level problem with 3 Radau collocation points in both problems. As in the first case study, closed-loop simulations showed that this mesh size can accurately approximate the model functions. The *regularized*-MPCC has 629,717 nonlinear equations and 950,861 variables. For the sequential design and control study, the optimization problem consists of the minimization of the CC_a subject to the process model at steady-state. In this optimization problem, no disturbances are enforced, i.e., C_{A0} and T_{in} were fixed at their nominal values (i.e., $1.0\, lbmol_A/ft^3$ and $600^\circ F$, respectively). In the sequential approach, design and control variables are the same as in the integrated method. Note that the controller tuning parameters $\mathbf{Q_{out}}$ for the sequential steady-state design were adjusted based on closed-loop simulations of the process subject to the disturbance specifications presented in Table 4.5.

As shown in Table 4.6, the controller weighting parameter $\mathbf{Q_{out}}$ is in the orders of thousands

Table 4.6: Results for the reaction system with two CSTRs case study.

Optimization variable	**Integrated approach (MPCC)**	**Sequential approach**
D_e $[ft]$	8.7	7.6
h_T $[ft]$	17.5	15.2
C_{A1}^{sp}	0.35	0.223
$Q_{C_{A1}}$	8.8×10^4	1.0×10^5
$Q_{C_{A2}}$	6.8×10^4	1.0×10^4
Capital cost [$/yr]	3.86×10^5	2.95×10^5
Total cost [$/yr]	1.29×10^6	5.89×10^6
CPU time [s]	3.55×10^5	0.113
Solution	weak-stationary	-

for the integrated design and control approach. This is due to the small deviations observed in the controlled variables with respect to the set points, i.e., squared deviations are in the orders of 1×10^{-6}. Therefore, the values for the weighting parameters $\mathbf{Q_{out}}$ are expected to be large. Figure 4.4 shows the dynamic profiles for the controlled and manipulated variables in closed-loop simulation under the process disturbances used in this case study (Table 4.5) for the integrated approach. Note that the system is able to reject the disturbances and to keep the process on target. From results in Table 4.6 and Figure 4.4 for the integrated approach, it is observed that the largest conversion of reactant A is carried out in the first reactor; therefore, the requirements of cooling water are higher (i.e., $> 500 ft^3/h$) compared to the water services required for the second reactor (i.e., $< 85 ft^3/h$). Furthermore, Figure 4.4 also shows that the largest effects of the disturbances are observed on C_{A1} in the first reactor. Therefore, a larger weight is assigned to $Q_{C_{A1}}$ (i.e., $Q_{C_{A1}} > Q_{C_{A2}}$) to force the controller to implement more aggressive control actions in the first CSTR. By comparing the results in case study 2 (Table 4.6), with those obtained for case study 1 (Table 4.3), it can be observed that there is an increase of two orders of magnitude in the CPU time for case study 2. Note that the model in case study 2 is approximately 17 times larger than the model in case study 1, i.e., the model in Equation (4.14) (case study 2) has 629,717 nonlinear equations whereas the model in Equation (4.8) has 36,417 nonlinear equations. Therefore, the CPU time increased proportionally with the increase of the size in the optimization model. As it is shown below for the third case study, this proportional increase in the computational cost may not always hold. The results show that the

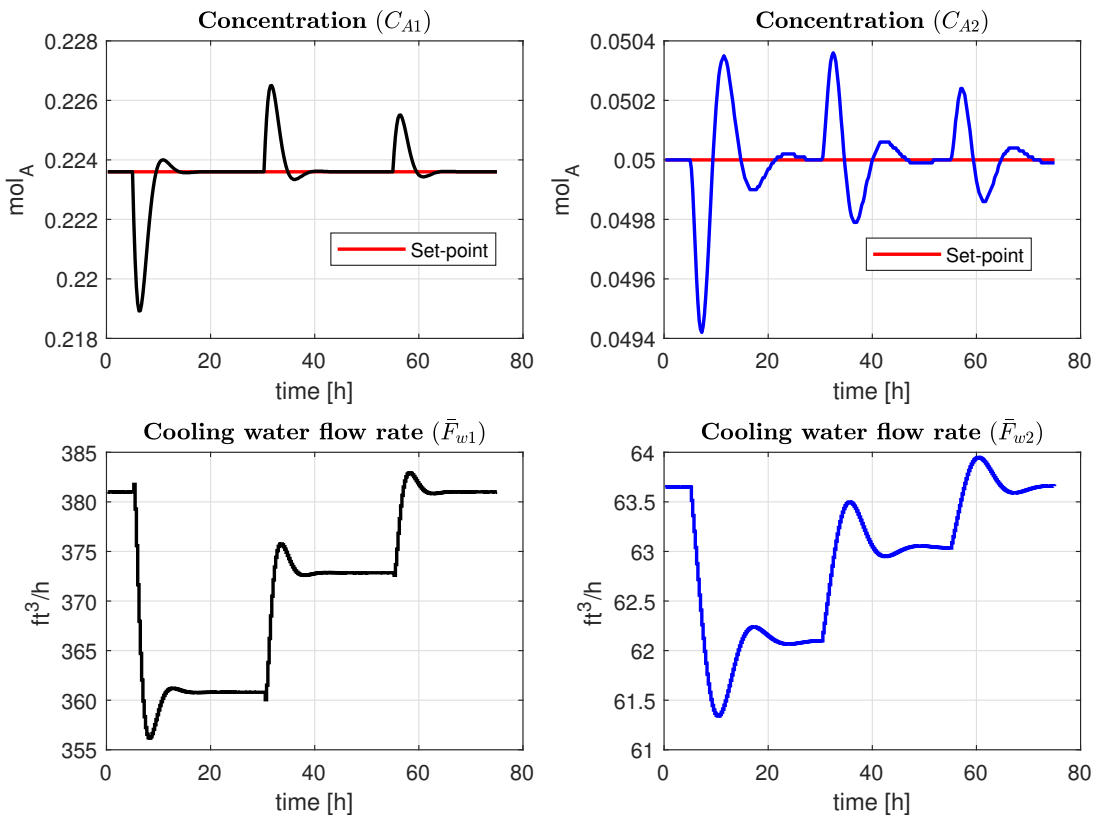

Figure 4.4: Validation simulations under process disturbances for the reaction system with two CSTRs case study. Dynamic profiles for the controlled variables (i.e., C_{A1} and C_{A2}) and manipulated variables (i.e., $\bar{F}_{w1}$ and $\bar{F}_{w2}$).

reaction system minimizes costs and complies with the process requirements for the conversion of component $\mathcal{A}$ while the controller is able to reject the process disturbances. As shown in Table 4.6, the sequential approach returned a 15% smaller equipment compared with the integrated approach; hence, the capital cost is 23% smaller for the former. However, the quantification of the operability and variability costs shows that the total cost obtained from the sequential approach is 5 times larger than those obtained from the integrated approach. This is mostly because the sequential design and control approach returned processes with complex dynamics (open-loop unstable system) that is quite challenging to control. Note that the results obtained for the sequential approach are in agreement with the observations and analysis presented by Luyben [147].

4.2.3 Wastewater treatment plant

The next case study considers the integration of design and NMPC-based control of a WWTP under uncertainty and process disturbances. This process is based on the case study presented in Chapter 3 (Section 3.3). The process takes place in a biological reactor and a settler tank (clarifier) connected in series (Figure 3.3). The settler tank has two effluents: a clean water stream and an activated sludge stream. The latter stream is recycled to the bioreactor to maintain the biological reaction activity. Since the activated sludge is constantly growing, the excess is eliminated by a purge stream (q_p). This process aims to control the substrate concentration (s_w) in the biodegradable waste stream and the dissolved oxygen concentration in the bioreactor (c_w). Since the bioreactor is an aerobic-activated reaction equipment, control on the dissolved oxygen concentrations is of special relevance for degradation of organic matter. Therefore, this process must maintain the substrate concentration (s_w) in the bioreactor at a desired set-point. As in CSTRs case study, the benefits of the integration of design and NMPC-based control of the WWTP are demonstrated through the comparison with a sequential design and control study. In this sequential approach, the WWTP is designed in steady-state under uncertainty. Then, the controller is tuned in closed-loop, based on the dynamic response of the process to disturbances.

The cost function considered in this study consists of the sum of an annualized capital cost (CC_a), operating cost (OC_a), and a variability cost (VC_a). The annualized capital cost is given by the size of the installed equipment, i.e., bioreactors volume (V_R) and settler's cross-sectional area (A_d). The expression for CC_a is as follows:

$$CC_a = 0.16(3500V_R + 2300A_d) \tag{4.15}$$

The operating cost for the system (OC_a) is given by the cost of the energy consumed by effect of the manipulated variables: the speed of the aeration turbines (f_k) and the purge stream (q_p) from the settler's recycle stream (q_r), i.e.,

$$OC_a = 870 \int_{t_0}^{t_f} f_k(t)\ dt + 1131 \int_{t_0}^{t_f} q_p(t)\ dt \tag{4.16}$$

The annualized variability cost (VC_a) aims to maintain the substrate concentration (s_w) close to an specific saturation value. This term in the objective function is highly penalized due to its environmental significance, i.e., the substrate concentrations in the treated water at the outlet stream must remain close to the saturation limit (100 mg/L) during the normal operation but this cannot be exceed. The expression for the VC_a is as follows:

$$VC_a = 1000 \int_{t_0}^{t_f} (100 - s_w(t))^2 \, dt \tag{4.17}$$

Based on the above, the cost function subject to the dynamic process model and the optimization problem for the NMPC-based controller leads to the following bilevel problem for the integration of design and control of the WWTP under uncertainty:

$$\min_{A_d, V_R, \mathbf{x}(t), f_k(t), q_p(t), s_w^{sp}, c_w^{sp}, \mathbf{Q_{in}}, \mathbf{Q_{out}}} \Phi = \sum_{j_u=1}^{J} w_{j_u} \left(CC_a + OC_a + VC_a\right) \tag{4.18}$$

$s.t.$ Dynamic process model, $\forall\ j_u = \{1, \ldots, J\}$

Process constraints,

Optimization problem for NMPC.

Operation boundaries.

where w_{j_u} is the weighting parameter for the probability of occurrence of the j_u^{th} realization of uncertainty. In this case study, the decision variables include parameters for the controller, e.g., the operating set-points for the substrate and dissolved oxygen (i.e., s_w^{sp} and c_w^{sp}, respectively), the matrices $\mathbf{Q_{out}}$ and $\mathbf{Q_{in}}$ for the NMPC, and the control action trajectories (i.e., $q_p(t)$ and $f_k(t)$). Moreover, the decisions related to the design are given by A_d, V_R as well as the dynamic trajectories for the plant states ($\mathbf{x}(t) = [x_w, s_w, x_d, x_b, x_r, c_w]$). Additional to the control targets s_w and c_w, the plant states include the biomass concentrations in the bioreactor (x_w) and in the different layers of the settler's tank (i.e., x_d, x_b, x_r, respectively). The dynamic model for this process is given by 6 ODEs, 3 equality constraints, and 5 inequality constraints. The model for the process is shown in Equation (3.12), where as the formulation for the MPCC are included in Appendix B. Table 4.7 shows the set of disturbances considered for this case study. These disturbances consider step changes in the input parameters for the inlet flow rate (q_{in} $[m^3/h]$), the inlet biomass concentration

(x_{in} $[mg/L]$), and the inlet substrate concentration (s_{in} $[mg/L]$). These step disturbances are performed every 5 hours until a total simulation time of 35 hours is reached. Moreover, Table 4.8 shows the set of uncertainty realizations considered for the present case study. The parameters under uncertainty correspond to biological experimental parameters that may exhibit variations in their values, i.e., specific microbial growth rate ($\bar{\mu}_w$), biomass death rate (k_{dr}), and the specific cellular activity (k_{ca}). It is assumed that the values of the parameters under uncertainty may vary within $\pm 10\%$ of their nominal values [127]. Note that the upper-level problem has access to all the realizations in the uncertain parameter set. As explained in Section 3.1, the process model in the NMPC uses the nominal values (Scenario 1) for the parameters under uncertainty (i.e., $j_u = 1$ in Table 4.8). Note that the NMPC requires the measurement or estimation for all the states at time t to compute a prediction for the control actions. The presence of uncertainties in the upper level problem generates a mismatch with the dynamic model in the NMPC. Thus, to determine the effect of uncertainty on the process design and controller performance, 3 different scenarios for this case study are proposed: Scenario 1 considers that the controller receives the measurement for all the plant states, which is assumed to operate under the nominal realization of the uncertain parameters. Scenario 2 considers that the controller receives the measurement for all the plant states, which is assumed to operate under the second realization in the uncertain parameters (i.e., $j_u = 2$ in Table 4.8). Scenario 3 assumes that the plant operates under the third realization of uncertainty (i.e., $j_u = 3$ in Table 4.8). The prediction and control horizons in the NMPC are set both to 4 hours. The MPCC-based formulation for the integration of design and NMPC-based control of the WWTP was solved with a *penalty* reformulation strategy for the complementarity constraints, the penalty parameter was set to $\bar{M} = 1 \times 10^{11}$. *Smoothing* and *Regularization* strategies were also implemented; however, no convergence to a solution in a reasonable CPU limit of time ($1.0 \times 10^6\, s$) was obtained with these strategies. OCFE is implemented for the discretization of the model (70 finite elements for the upper-level problem and 8 finite elements for the lower-level problem with 3 Radau collocation points for both problem levels). Accordingly, the *penalty*-MPCC considers 71,731 equations with 106,572 variables.

As shown in Table 4.9, slight differences in the design parameters for each scenario were obtained,

Table 4.7: Disturbance trajectory profiles (Step Changes) for the WWTP case study.

t $[h]$	x_{in} $[K]$	s_{in} $[kg/min]$	q_{in} $[m^3/h]$
0	80	366	500
5	75	371	480
10	85	361	520
15	80	366	480
20	75	371	500
25	85	366	520
30	80	366	520

Table 4.8: Uncertainty realizations in design parameters for the WWTP case study.

Uncertainty realizations (j_u)	**Specific growth rate** $(\bar{\mu}_w)$	**Biomass death rate** (k_{dr})	**Specific cellular activity** (k_{ca})	**Weight distribution** (w_{j_u})
1	0.1824	5.0×10^{-5}	1.333×10^{-4}	0.50
2	0.2006	5.5×10^{-5}	1.466×10^{-4}	0.25
3	0.1732	5.5×10^{-5}	1.266×10^{-4}	0.25

i.e., the settler's area (A_d) is 8% and 4% smaller for Scenarios 2 and 3, respectively, compared with the solution obtained for Scenario 1. Likewise, the reactor's volume (V_R) is 16% and 5% larger for Scenarios 2 and 3, respectively, compared with the solution obtained for scenario 1. From an operational point of view, Scenario 3 allowed an operation at a higher set-point for s_w^{sp}, i.e., 92.9 [ppm] whereas Scenario 2 resulted in a higher set-point for c_w^{sp}, i.e., 3.0 [ppm]. Moreover, it can be noted that the controller weighting parameters Q_{s_w} and Q_{c_w} are approximately the same in all the scenarios. However, the weight Q_{c_w} in Scenario 1 is 5 orders of magnitude smaller compared to those obtained for Scenarios 2 and 3. Additionally, it is observed that the values for the controller parameters $\mathbf{Q_{in}}$ are negligible in magnitude for all scenarios, this indicates that the changes in the manipulated variables are not penalized in the NMPC strategy. Note that the MPCC-based problem is highly non-convex, the differences in the controller tuning parameters may be a consequence of the implementation of local NLP solvers, i.e., the solver may converge to different local solutions. Additionally, the differences in the set-points for the substrate (s_w^{sp}) and dissolved oxygen (c_w^{sp}) may demand different controller tuning parameters. Also, since in each scenario the controller receives the measurement of process states produced by different realizations in the uncertain parameters,

Table 4.9: Results for the WWTP case study.

Optimization variable	**Scenario 1** (Nominal) ($j_u = 1$ in Table 4.8)	**Scenario 2** ($j_u = 2$ in Table 4.8)	**Scenario 3** ($j_u = 3$ in Table 4.8)	**Augmented model** (Analysis on the effect of the discretization)
A_d $[m^2]$	2716.3	2577.7	2569.9	2720.0
V_R $[m^3]$	1705.8	1986.5	1787.9	1720.8
s_w^{sp}	90.7	87.2	92.9	90.5
c_w^{sp}	1.13	3.0	1.09	1.6
Q_{s_w}	22.58	23.58	22.60	22.91
Q_{c_w}	1×10^{-4}	22.25	13.38	0.01
Q_{q_p}	0.0	0.88	0.01	0.01
Q_{f_k}	0.0	0.0	0.0	0.44
Capital cost [$/yr]	1.95×10^6	2.02×10^6	1.95×10^6	1.96×10^6
Total cost [$/yr]	7.15×10^6	9.49×10^6	7.22×10^6	7.16×10^6
CPU time [s]	2,019	19,036	8,339	71,606
Solution	Weak-stationary	Weak-stationary	Weak-stationary	Weak-stationary

differences in the magnitude of the controller tuning parameters are expected (Table 4.9).

A closed-loop simulation under process disturbances and uncertainty for all the scenarios are presented in Figure 4.5. In this closed-loop simulation, the simulation time was extended to allow the process to reach steady-state. From Figure 4.5a), it is noted that for Scenario 1, where plant operates using nominal realizations in the uncertain parameters, the system tends to operate around the set-point. This was expected since there is no mismatch between the dynamic model for the actual process and the NMPC for this scenario. On the other hand, from Figures 4.5b) and 4.5c), it can be observed that the process reaches a steady-state condition but none of the dynamic trajectories are able to operate around their corresponding set-points, i.e., there is an offset between the process operation and the actual desired set-point. Although Scenario 3 specified a higher operation set-point for substrate (s_w^{sp}), the offsets in the operation with respect to the set-point produces dynamic profiles for substrate s_w around the same operation region in all scenarios, i.e., steady-state concentrations of s_w above $80\,ppm$ and below $97\,ppm$. Even when the parameters under uncertainty present variations within 10% with respect to their nominal values, it was found that the plant operation under different realizations of uncertainty resulted in process designs with up to 16% of variations in the equipment sizes with respect to the nominal scenario. To further

investigate the differences between the solutions in the scenarios for this case study, the solution for Scenario 1 was tested assuming that the plant operates under the second realization in the uncertain parameters (i.e., $j_u = 2$ in Table 4.8). As shown in Figure 4.6, an offset with respect to the set-point in the profile for s_w is observed. However, note that the plant remained dynamically feasible in the presence of this operational condition. These results indicate that the implementation of *robust*-NMPC frameworks may reduce the presence of offsets in the plant operation. Additionally, for the sequential design and control study, the optimization problem consists of the minimization of the CC_a subject to the process model at steady-state under uncertainty. The set of uncertain parameters is shown in Table 4.8. In this sequential design approach, design and control decision variables remain the same as in the integrated approach. Moreover, no disturbances are enforced at the design stage. The controller tuning parameters $\mathbf{Q_{out}}$ for the steady-state design were then adjusted based on the closed-loop response under the disturbance specifications presented in Table 4.7.

As expected, the sequential approach resulted in smaller equipment sizes (a 30% smaller reactor and settler tank). This represents a 34% smaller capital cost for the sequential approach with respect to the integrated approach. However, the process is dynamically infeasible due to constraint violations (see Figure 4.7).

To compare the solutions in this case study, the Back-off approach presented in Chapter 3 is also implemented in this case study. As mentioned above in Chapter 3, the Back-off methodology approximates the bilevel formulation using power series expansions (PSE) to reformulate the problem into a single level optimization formulation that is explicit for the decision variables. Then, the model is iteratively solved until an economically attractive process design and an operating point that is dynamically feasible under process disturbances and parameter uncertainty is found. The results for Scenario 1 with the back-off approach resulted in significant differences in the solution compared to that obtained by the MPCC framework, i.e., $A_d = 2630.0m^2$ and $V_R = 1431.0m^3$; this represent a settler's area 7.5% smaller and a reactor's volume 14.5% smaller compared to the results obtained from the proposed MPCC framework. However, the operating set-points for substrate (s_w^{sp}) and dissolved oxygen (c_w^{sp}) are lower in the implementation of the back-off approach, i.e.,

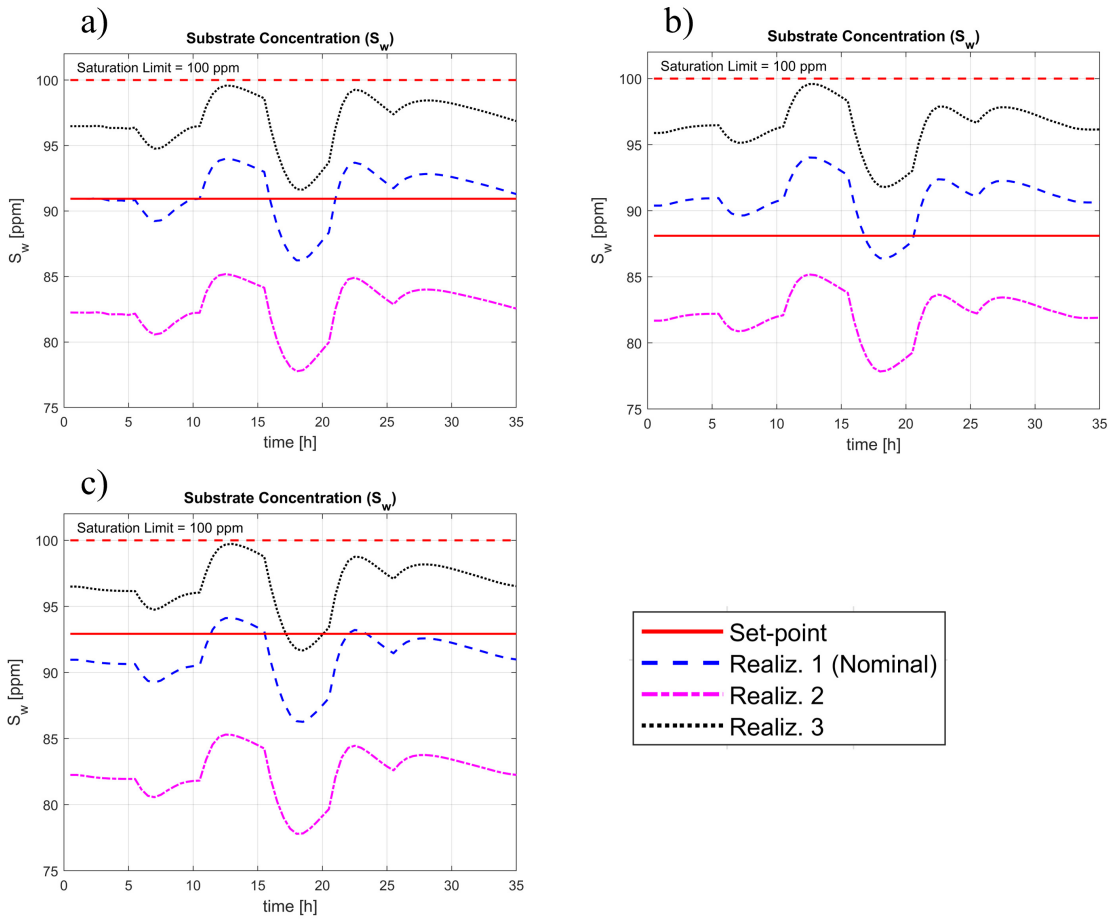

Figure 4.5: Substrate closed-loop simulations under process disturbances and parameter uncertainty; a) Measurement in the nominal uncertainty realization; b) Measurement in the second uncertainty realization; c) Measurement in the third uncertainty realization.

$s_w^{sp} = 89.8\,ppm$ and $c_w^{sp} = 1.7 \times 10^{-3}\,ppm$; this represents differences of 3% and 99.9%, respectively, compared with the results with the MPCC framework. Note that the composition for c_w^{sp} is small in magnitude from both solutions; this tends to inflate the differences when comparing these values. Moreover, the results for the controller weighting parameters are in the same order of magnitude for both approaches (Back-off and MPCC). The total cost for both approaches has notable differences, i.e., total cost (Back-off) is $8.29 \times 10^6\,\$/yr$; this represents an increase of 13% compared with the solution obtained with the MPCC approach. On the other hand, the CPU time for the back-off methodology was of $7.2 \times 10^4\,s$. As shown in Table 4.9, the MPCC strategy reduces the CPU time by one order of magnitude compared with the implementation with the back-off approach (2,019

s). Nevertheless, finding a solution with the MPCC-based formulation is not an easy task. It was found that the initial guess plays a crucial role in the solution of the optimization model using MPCC. An inaccurate initialization of the *Lagrange* multipliers for the controller's KKT conditions makes overly challenging the optimization solver to converge to a solution. Hence, a first guess for the *Lagrange multipliers* was computed using closed-loop simulations with a fixed process design that was selected using heuristics (e.g., optimal steady-state design). In those simulations, the NMPC optimization formulation is substituted with its KKT conditions for optimality. Then, the values for the *Lagrange* multipliers were used to initialize the MPCC for the simultaneous design and NMPC-based control of the WWTP under process disturbances with no uncertainty in design parameters. This MPCC formulation with no uncertainty required a CPU time of $5.03 \times 10^4\, s$ to compute an optimal solution. The complete set of values for the solution of the MPCC without uncertainty was used to initialize the problem under uncertainty. This allowed to the optimization solver to converge to optimal solutions with a reduction of orders of magnitude in the CPU time.

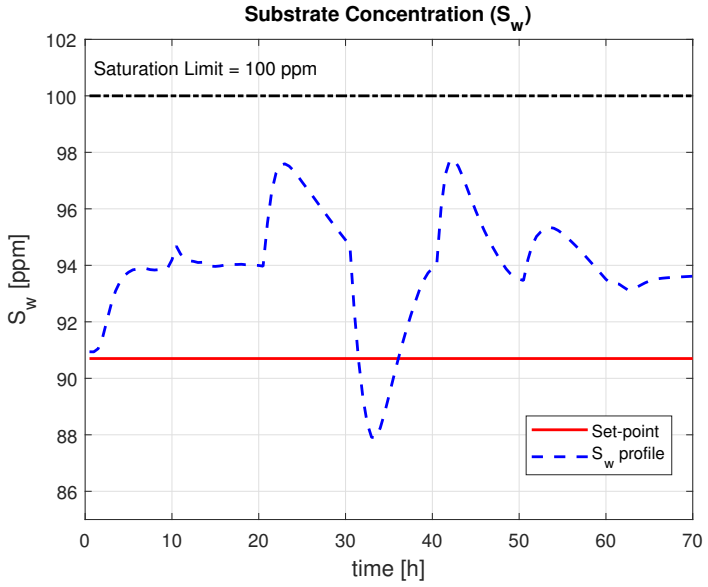

Figure 4.6: Validation closed-loop simulation for the WWTP assuming that the plant operates under the second realization in the uncertain parameters.

Additionally, for the first scenario presented in this case study, it was proposed to evaluate the effect on the selection of the mesh size for discretization of the MPCC problem in Equation (4.1). As explained above, the results for case study 3 in Table 4.9 were computed for a discretization

with 70 finite elements for the upper-level problem and 8 finite elements for the lower-level problem with 3 Radau collocation points for both problem levels. It is proposed to evaluate the effect of the discretization on the solution of the optimization problem. To consider this effect, the number of finite elements for Scenario 1 was increased to 140 for the upper-level problem and 16 for the lower-level problem with 3 Radau collocation points for both problem levels. The resulting optimization formulation (Augmented model) includes 143,462 equations with 213,140 variables, which is double the size of the formulation considered for Scenario 1.

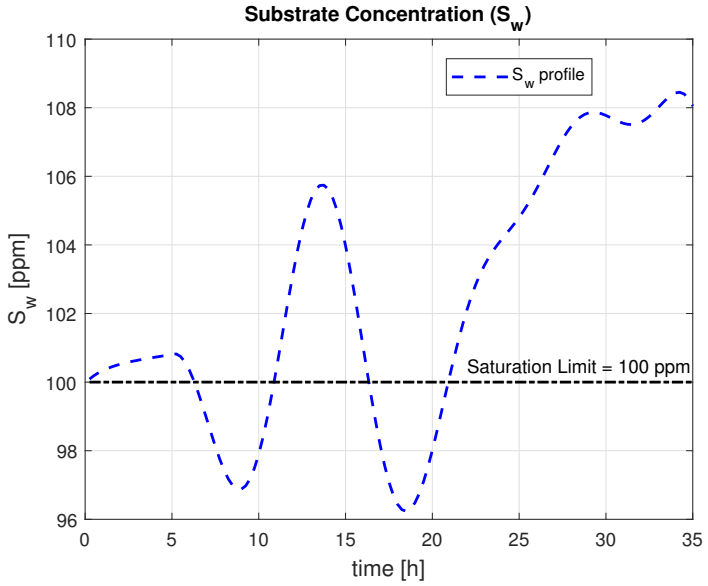

Figure 4.7: Closed-loop simulation for the optimal steady-state design (WWTP case study).

As shown in Table 4.9, the differences in the design variables are small between the results for Scenario 1 and those obtained from the augmented model, i.e., design variables from the latter have an average of 0.22% difference with respect to the solution from the former. The differences in the process dynamics were calculated through the evaluation of the ISE for the substrate (s_w). The ISE obtained from both Scenario 1 and the augmented model are similar (229.8 for Scenario 1 and 206.7 for the augmented model). Table 4.9 also shows that increasing the number of finite elements has a large impact on the CPU time, i.e., the CPU time reported for the augmented model is one order of magnitude larger to that reported for the Scenario 1. For more complex systems, the selection on the number of finite elements for the discretization of the optimization model may lead to larger

differences in the process design and the economics of the system. The selection of the discretization depends on the nature of the problem, e.g., for stiff problems the size of the discretization mesh is key to capture events that occur at different time scales thus requiring a combination of large and small finite elements. Typically, it is recommended to perform a previous numerical analysis to determine a good discretization of the model. This analysis can be performed via simulation with fixed process designs and evaluation of the dynamic response of the system under different discretization meshes.

4.3 Summary

This chapter presented a direct method for the solution of the bilevel formulation for the integration of design and NMPC-based control under uncertainty. This method assumes the transformation of the bilevel formulation into a single-level problem referred to as a mathematical program with complementarity constraints (MPCC). In this transformation strategy, the lower-level problem is substituted by its first order necessary conditions for optimality, which are a set nonlinear algebraic equations. Then, this set of algebraic equations are added to the upper-level problem as part of the constraints. The implementation of complementarity constraints introduces an inherent nonconvexity and linear dependence of constraints. To overcome this issue, it is necessary the use of reformulation strategies to rewrite the complementarity constraints in equivalent forms, which allows the solution of the MPCC using conventional NLP solvers.

The first case study showed the features and benefits of three different reformulation strategies for the complementarity constraints in the solution of the MPCC formulation. Moreover, the effect of uncertainty in design parameters was illustrated for a case study with a highly nonlinear process. Although the solutions for the MPCCs may not represent a solution to the original bilevel formulation, the solutions for the formulations with MPCCs resulted in economically attractive process design and NMPC-based control schemes. On the other hand, when a proper initialization is available, the formulation with MPCCs showed an improvement of orders of magnitude in the CPU times compared with the back-off approach presented in Chapter 3. The formulations addressed in this

chapter and Chapter 3 involve only continuous variables. However, discrete decisions such as the arrangement of equipment or the determination of the number of stages/equipment are often modeled using integer/binary variables. The solution of those formulations may require the implementation of different strategies to address the discontinuities resulting from the integer decisions.

Chapter 5

Integrated Design and NMPC-based Control under Uncertainty and Structural Decisions: A Discrete-Steepest Descent Algorithm Approach

The methodologies presented in Chapters 3 and 4 are focused on the solution of integrated design and NMPC-based control formulations involving continuous decision variables, i.e., no discrete variables were considered. Nevertheless, process design decisions in chemical engineering such as the arrangement of equipment, or the determination of the number of stages/equipment are often modeled using integer/binary variables. A nonlinear bilevel problem involving integer decisions is referred to as a MIBLP. As mentioned in Chapter 2, MIBLPs can be classified in different categories depending on the location of the integer and continuous decision variables. In this PhD thesis, it is assumed that the discrete decisions are associated to the upper-level problem (design problem); therefore, the NMPC is assumed as a continuous optimization problem.

This chapter presents a methodology that aims to determine the optimal location of processing units or streams over a naturally ordered discrete set, e.g., number of trays in a distillation column or the number of reaction units in series. Since the NMPC is assumed a continuous formulation, the MIBLP for simultaneous design and control can be restated in terms of its KKT conditions for optimality (i.e., a classical KKT transformation strategy). As in Chapter 4, complementarity constraints in the corresponding MI-MPCC can be reformulated to obtain a single-level MINLP.

The proposed methodology introduces the concept of *external variables*, in which the set of binary variables describing the process superstructure are partitioned in sub-sets of integer variables. This partition of discrete variables allows the decomposition of the single-level MINLP into a *master* IPLC and a set of *primal* sub-problems. This decomposition approach allows the solution of the single-level MINLP in an iterative fashion through the exploration of neighborhoods described by the *external variables*. The proposed methodology implements a steepest-descent search direction to explore the discrete search space. The algorithmic framework implements a stopping criterion

based on the concept of *integral convexity*. Therefore, local feasible solutions can be found efficiently compared to commercial MINLP solver. The convergence of the algorithm is guaranteed [149].

The current chapter is organized as follows: Section 5.1 introduces the MIBLP formulation for the integration of design and NMPC-based control under uncertainty and structural decisions over naturally ordered discrete set; in Section 5.2 the MIBLP is transformed into a conventional MINLP; the concept of *external variables* and the decomposition of the single-level MINLP are presented in Section 5.3; Section 5.4 presents the D-SDA methodology; meanwhile, an illustrative case study is included in Section 5.5; finally, Section 5.5 provides a chapter summary.

5.1 Mixed-integer bilevel problem formulation

The conceptual mathematical formulation for the MIBLP for the integration of design and NMPC-based control under uncertainty and structural decisions is stated as follows:

$$\min_{\eta,\mathbf{x}(t),\bar{\mathbf{u}}(t),\mathbf{z}} \sum_{j_u=1}^{J} w_{j_u} \Phi(\eta, \varsigma, \mathbf{x}(t), \bar{\mathbf{u}}(t), \mathbf{d}_p(t), \mathbf{z}, t) \tag{5.1a}$$

$$s.t.\ \ f(\eta, \varsigma, \dot{\mathbf{x}}(t), \mathbf{x}(t), \bar{\mathbf{u}}(t), \mathbf{d}_p(t), \mathbf{z}, t) = 0, \tag{5.1b}$$

$$h(\eta, \varsigma, \mathbf{x}(t), \bar{\mathbf{u}}(t), \mathbf{d}_p(t), \mathbf{z}, t) = 0, \tag{5.1c}$$

$$g(\eta, \varsigma, \mathbf{x}(t), \bar{\mathbf{u}}(t), \mathbf{d}_p(t), \mathbf{z}, t) \leq 0, \tag{5.1d}$$

$$\hat{\mathbf{u}}(\tau_c) = \arg\left\{ \min_{\hat{\mathbf{u}}(\tau_c)} \Psi(\cdot) \,\text{s.t.}\, F(\cdot) = 0, H(\cdot) = 0, G(\cdot) \geq 0, \hat{\mathbf{u}} \in \mathbb{R}^{N_u} \right\} \tag{5.1e}$$

$$\bar{\mathbf{u}}(t) = \hat{\mathbf{u}}(\tau_c), \quad \forall\, \tau_c = t \tag{5.1f}$$

where $h : \mathbb{R}^{N_x} \times \mathbb{R}^{N_u} \times \mathbb{R}^{N_\eta} \times \mathbb{R}^{N_\varsigma} \times \mathbb{R}^{N_d} \times \mathbb{Z}^{N_z} \times \mathbb{R}^{N_t} \to \mathbb{R}^{N_h \times N_\varsigma}$ represents the set of inequality constraints that define the feasibility region of the design problem; $f : \mathbb{R}^{2N_x} \times \mathbb{R}^{N_u} \times \mathbb{R}^{N_\eta} \times \mathbb{R}^{N_\varsigma} \times \mathbb{R}^{N_d} \times \mathbb{Z}^{N_z} \times \mathbb{R}^{N_t} \to \mathbb{R}^{N_x \times N_\varsigma}$ represents the dynamic process model; $\mathbf{x}(t) \in \mathbb{R}^{N_x}$ are the states of the system with time derivatives indicated by $\dot{\mathbf{x}}(t) \in \mathbb{R}^{N_x}$. $\bar{\mathbf{u}}(t) \in \mathbb{R}^{N_u}$ represents the vector of control actions retrieved from the controller (i.e., the NMPC in Equation (2.4)). The set of decision variables that does not depend on time ($\eta \in \mathbb{R}^{N_\eta}$) contains the process design variables (e.g., areas,

volumes, flows) and the controller tuning parameters in the NMPC framework. In this study, these tuning parameters correspond to the positive-defined diagonal matrices that penalizes the deviations in the predicted controlled variables with respect to their desired set-points, and the changes in the manipulated variables, i.e., $\mathbf{Q_{out}}$ and $\mathbf{Q_{in}}$, respectively [12]. The set of binary variables is given by $\mathbf{z} \in \mathbb{Z}^{N_z}$. Moreover, the vector $\varsigma \in \mathbb{R}^{N_\varsigma}$ represents the uncertain parameters included in the optimization model. Note that the control actions $\bar{\mathbf{u}} \in \mathbb{R}^{N_u}$ computed by Equation (5.1e) are given by the solution of the optimization problem for the NMPC. In Equation (5.1), t represents the actual time of the process whereas τ_c is the future time instants within the NMPC framework. At each time interval $t + k_t$ (sampling time) in the upper-level problem, the NMPC computes a prediction of the dynamic behavior of the process within a prediction horizon time t_P, i.e., $\tau_c \in [t, t + t_P)$. Then, the controller implements the first control action at the simulation time $\tau_c = t + k_t$. To ensure dynamic feasibility in the process to external perturbation during the normal operation, for the formulation in Equation (5.1) a set of disturbances $\mathbf{d}_p(t)$ is included. This set of disturbances aims determine the magnitude of the controller tuning parameters such that the NMPC can reject the expected disturbances during the normal operation. Consistently, in a real operation, the information about the future changes in the disturbances is not available. Therefore, it is assumed that the NMPC does not have access *a priori* to the set of disturbances $\mathbf{d}_p(t)$. However, it is assumed that the disturbances $\mathbf{d}_p$ are part of the measurements for the NMPC, but these remain constant along the prediction horizon at every sampling time $(t + k_t)$. The uncertainty is quantified through a finite number of scenarios defined *a priori*. These uncertain scenarios are defined from observations based on historical data or process heuristics [150]. Thus, the bilevel formulation considers the introduction of j_u^{th} uncertainty realizations; the probability of occurrence of each realization j_u is weighted in the objective function by w_{j_u}. In Equation (5.1e), $F : \mathbb{R}^{2N_x} \times \mathbb{R}^{N_u} \times \mathbb{R}^{N_d} \times \mathbb{R}^{N_\tau} \to \mathbb{R}^{N_x}$ corresponds to the dynamic process model in the NMPC; whereas the inequality constraints are given by the function $G : \mathbb{R}^{N_x} \times \mathbb{R}^{N_u} \times \mathbb{R}^{N_d} \times \mathbb{R}^{N_\tau} \to \mathbb{R}^{N_s}$. Note that the process model in the design problem (upper-level problem) and the process model in the NMPC (lower-level problem) have the same structure. Nevertheless, the controller does not have access to the complete set of parameters under uncertainty (ς). Alternatively, uncertain parameters may appear also in the lower-level problem. If

the controller (lower-level problem) does not have full access to the parameters under uncertainty, it is referred to as a nominal NMPC controller. Conversely, if the controller has full access to the parameters under uncertainty, it is referred to as a robust NMPC controller [12]. Accounting for the uncertain parameters in the upper-level problem allows to accommodate uncertainties in the process design to guarantee dynamic feasibility in the solution. In the optimization formulation (Equation (5.1)), the introduction of uncertainty realizations increases the size of the optimization model; consequently, the computational burden for the search of a solution also increases.

From Equations (5.1a) and (5.1e), note that the binary variables are part of the decision variables only in the upper-level problem. Although NMPC requires information from the upper-level problem, the binary variables are considered as parameters for the lower-level problem, i.e., the NMPC does not consider binary (structural) decisions in its formulation. Therefore, the NMPC is a nonlinear program (NLP). This is particularly useful because it is possible to obtain the necessary conditions for optimality for the NMPC problem.

5.2 Classical KKT Transformation

To transform the MIBLP stated in Equation (5.1) into a single-level MINLP, a *Classical KKT transformation* is implemented. This transformation strategy requires that the optimization problem for the NMPC (lower-level problem) to be a continuous formulation, i.e., a NLP. Therefore, the lower-level problem can be expressed in terms of its KKT conditions. The set of algebraic equations corresponding to the KKT conditions for the NMPC are included as constraints in the upper-level problem. This leads to a Mixed-Integer Mathematical Program with Complementarity Constraints (MI-MPCC). MI-MPCC is a singular problem, i.e., multiple constraint qualifications (CQs) are violated at every feasible point [18]. To overcome this issue, a *regularization* strategy was implemented, in which the complementarity constraints are relaxed with a positive parameter ϵ_s. Note that there are other reformulation strategies reported in the literature, e.g., the implementation of smoothing functions or the use of penalty terms in the objective function. The analysis of the features and convergence properties of those reformulation strategies is out of the scope of this

PhD research for formulations involving discrete decisions but interested readers can review those techniques elsewhere [141, 144]. Thus, the resulting regularized MINLP for the integration of design and NMPC-based control under uncertainty and structural decisions can be stated as follows:

$$\bar{\Phi}_{MINLP} = \min_{\eta,\mathbf{x}(t),\bar{\mathbf{u}}(t),\mathbf{z}} \sum_{j_u=1}^{J} w_{j_u} \Phi(\eta, \varsigma, \mathbf{x}(t), \bar{\mathbf{u}}(\tau), \mathbf{d}_p(t), \mathbf{z}, t) \tag{5.2a}$$

$$s.t.\ \ f(\eta, \varsigma, \dot{\mathbf{x}}(t), \mathbf{x}(t), \bar{\mathbf{u}}(t), \mathbf{d}_p(t), \mathbf{z}, t) = 0, \quad \mathbf{x}(t_0) = \mathbf{x}_0, \tag{5.2b}$$

$$h(\eta, \varsigma, \mathbf{x}(t), \bar{\mathbf{u}}(t), \mathbf{d}_p(t), \mathbf{z}, t) = 0, \tag{5.2c}$$

$$g(\eta, \varsigma, \mathbf{x}(t), \bar{\mathbf{u}}(t), \mathbf{d}_p(t), \mathbf{z}, t) \leq 0, \tag{5.2d}$$

$$\nabla_{\mathbf{\Omega}} \mathcal{L}(\eta, \hat{\mathbf{x}}(\tau_c), \hat{\mathbf{u}}(\tau_c), \lambda(\tau_c), \nu(\tau_c), \mu(\tau_c), \mathbf{d}_p, \mathbf{z}, \tau_c) = 0, \tag{5.2e}$$

$$F(\eta, \dot{\hat{\mathbf{x}}}(\tau_c), \hat{\mathbf{x}}(\tau_c), \hat{\mathbf{u}}(\tau_c), \mathbf{d}_p, \mathbf{z}, \tau_c) = 0, \quad \hat{\mathbf{x}}(\tau_{c_0}) = \mathbf{x}(t),\ \forall \tau_c = t \tag{5.2f}$$

$$G(\eta, \hat{\mathbf{x}}(\tau_c), \hat{\mathbf{u}}(\tau_c), \mathbf{d}_p, \mathbf{z}, \tau_c) \geq 0, \quad \mu(\tau_c) \geq 0 \tag{5.2g}$$

$$\mu^{\intercal}(\tau_c) G(\eta, \hat{\mathbf{x}}(\tau_c), \hat{\mathbf{u}}(\tau_c), \mathbf{d}_p, \mathbf{z}, \tau_c) \leq \epsilon, \tag{5.2h}$$

$$\bar{\mathbf{u}}(t) = \hat{\mathbf{u}}(\tau_c), \quad \forall \tau_c = t \tag{5.2i}$$

where ϵ_s is a positive relaxation parameter. $\nabla_{\mathbf{\Omega}_c} \mathcal{L} : \mathbb{R}^{N_{\hat{x}}} \times \mathbb{R}^{N_{\hat{u}}} \times \mathbb{R}^{N_\eta} \times \mathbb{R}^{N_\lambda} \times \mathbb{R}^{N_\nu} \times \mathbb{R}_+^{N_\mu} \times \mathbb{R}^{N_d} \times \mathbb{Z}^{N_z} \times \mathbb{R}^{N_\tau} \rightarrow \mathbb{R}^{N_{\hat{x}} \times N_{\hat{u}} \times N_{\hat{y}}}$ is the gradient of the *Lagrangian* function, i.e., the stationarity conditions. This gradient is determined with respect to the decision variables in the NMPC problem, i.e., states and control actions ($\mathbf{\Omega}_c = [\hat{\mathbf{x}}(\tau_c), \hat{\mathbf{u}}(\tau_c)]$). $\lambda(t) \in \mathbb{R}^{N_\lambda}, \nu(t) \in \mathbb{R}^{N_\nu}$, and $\mu(t) \in \mathbb{R}_+^{N_\mu}$ in Equations (5.2e) and (5.2h) are the Lagrange multipliers associated to constraints in the optimization formulation for the NMPC, respectively.

The solution strategy for the formulation in the Problem (5.2) is critical due to the complexity of the MINLP. Traditional local deterministic strategies such as GBD or ECP highly depend on the initialization [151, 152, 153]. On the other hand, global MINLP solvers are computationally expensive and beyond the scope of this PhD study. Those algorithms work best with the reformulation of the MINLP in Equation (5.2) as a GDP. In a GDP formulation, disjunctions and logic propositions are used to consider discrete decisions. The presence of integer variables complicates the search for a

solution to problem (5.2) because of the nonlinear relations in the integer domain and the nonlinear expressions in the integer-continuous domain. Therefore, a general-purpose MINLP solver may not be able to find a solution. In this study, a specialized algorithm proposed by Linan et al. [149] is implemented, i.e., a Discrete-Steepest Descent Algorithm (D-SDA). This algorithm exploits the problem structure such that the optimization problem can be expressed in terms of a set of variables that represent positions over one-dimensional discrete space (*external variables*).

A local search is possible in the neighborhood described by these *external variables*. To do so, the original MINLP (Equation (5.2)) is decomposed into a *master* IPLC and *primal* sub-problems with discrete variables fixed at integer values, i.e., FNLPs. This decomposition strategy is presented next.

5.3 Decomposition of the MINLP framework

This section introduces the mathematical framework for the decomposition of the MINLP in Equation (5.2) into a *master* IPLC and *primal* FNLPs. In the original MINLP, the integer decisions ($\mathbf{z}$) determine the optimal placement of units or streams. The set of integer variables can be partitioned into sub-groups referred to as *external variables*. Since the constraints represented with function g (Equation (5.2d)) contains a finite number of linear inequalities to define the locations of streams or units, i.e., logical constraints, a set of purely integer logical constraints can be represented by a polyhedron $Z \subseteq \mathbb{Z}^{N_z}$ as follows:

$$Z = \left\{ \mathbf{z} \in \mathbb{Z}^{N_z} : \sum_{\hat{k}=1}^{N_z} a_{\hat{l},\hat{k}} z_{\hat{k}} \leq b_{\hat{k}} \ \forall \hat{l} \in \mathfrak{L} \right\} \tag{5.3}$$

where $\mathbf{z} \in \mathbb{Z}^{N_z}$ are integer variables with index $\hat{k}$, if the integer variables of the MINLP in Equation (5.2) are fixed at a value $\mathbf{z} = \hat{\mathbf{z}}$, the problem becomes a FNLP, i.e., the formulation only includes continuous optimization variables. The purpose of fixing the integer variables in Equation (5.2) is to represent the MINLP as a set of nonlinear problems: $\bar{\Phi}_{MINLP} = \min\{\bar{\Phi}_{FNLP}(\hat{\mathbf{z}}) : \hat{\mathbf{z}} \in \mathbb{Z}^{N_z}\}$. Therefore, a solution for the MINLP (Equation (5.2)) may be found by solving a finite series of

FNLPs ($\forall\ \hat{\mathbf{z}} \in \mathbb{Z}^{N_z}$) and comparing their solutions, e.g., through a *complete enumeration* strategy. On the other hand, an enumeration strategy is only tractable with low-dimensional problems if the MINLP is properly bounded.

In this study, the location of streams/units is defined by a set of binary variables. Thus, it is assumed that the discrete variables in Equation (5.2) are binary variables (i.e., $\mathbf{z} \in \{0,1\}^{N_z}$) that represent the position of streams/units in the optimal superstructure. These binary variables can be partitioned into N_E groups; one group for each external variable ($\mathbf{z_E} \in \mathbb{Z}^{N_E}$), i.e., $\mathbf{z_E} = [\mathbf{z_{E,1}}, \mathbf{z_{E,2}}, \ldots, \mathbf{z_{E,}}_{N_z}]$. For the *external variables*, each vector $\mathbf{z_{E,}}_{\hat{i}} = [z_{E,\hat{i},1}, z_{E,\hat{i},2}, \ldots, z_{E,\hat{i},N_{zs_{\hat{i}}}}]$, $\forall\, \hat{i} \in \mathfrak{E} = \{1, 2, \ldots, N_E\}$ contains the binary variables that define the optimal location of a single stream/unit of type $\hat{i} \in \mathfrak{E}$ over a naturally ordered one-dimensional discrete set $zs_{\hat{i}} = \{1, 2, \ldots, N_{zs,i}\}$, $\forall\, \hat{i} \in \mathfrak{E}$. Also, $\hat{n}$ is defined as the index of the elements in the naturally ordered set $zs_{\hat{i}}$. Moreover, the constraint $\sum_{\hat{n} \in zs_{\hat{i}}} z_{\hat{n},\hat{i}} = 1\ \forall\, \hat{i} \in \mathfrak{E}$ must hold to apply a decomposition of Equation (5.2) in terms of the *external variables* ($\mathbf{z_E}$). This constraint ensures that each stream or unit in the superstructure is associated only to one physical position. Each binary variable must be expressed as a piecewise function as follows:

$$z_{\hat{n},\hat{i}} = \begin{cases} 1, & z_{E,\hat{i}} = \hat{n},\ \ \forall \hat{n} \in zs_{\hat{i}},\ \forall \hat{i} \in \mathfrak{E} \\ 0, & otherwise \end{cases} \tag{5.4}$$

$$Y_1 = \left\{ \mathbf{z_E} \in \mathbb{Z}^{N_E} : 1 \leq \mathbf{z_E} \leq N_{zs,\hat{i}},\ \forall \hat{i} \in \mathfrak{E} \right\} \tag{5.5}$$

$$Y_2 = \left\{ \mathbf{z_E} \in \mathbb{Z}^{N_E} : \sum_{\hat{i}=1}^{N_E} a_{\hat{m},\hat{i}} z_{E,\hat{i}} \leq b_{\hat{m}},\ \forall \hat{m} \in \mathfrak{M} \right\} \tag{5.6}$$

$$\mathbf{z_E} \in Y = Y_1 \cap Y_2 \tag{5.7}$$

where Equations (5.4)-(5.7) allow expressing each binary variable in terms of the N_E external variables, which allows the constructions of a convex polyhedron (Equation (5.5)) for the search range of the *external variables*. The set Y_1 contains the external variables and their boundaries; whereas the set Y_2 contains the equivalent form of the logical constraints in Z that can be represented linearly in the *external variables'* domain (Equation (5.6)). The convex polyhedron of the

external variables Y (Equation (5.7)) is the intersection between the optimal delimitation (Y_2) and the required delimitation (Y_1). In this study, it is assumed that all the constraints in Z can be represented linearly in the optional convex polyhedron Y_2, i.e., all logical constraints are represented in the *external variables'* domain. The implementation of the reformulation with external variables is illustrated in below in Section 5.5. The single-level MINLP for simultaneous design and control (Equation (5.2)) can be decomposed into a *master* IPLC and *primal* FNLPs sub-problems using *external variables*. The corresponding *master* IPLC is as follows:

$$\bar{\Phi}_{MINLP} = \min_{\hat{\mathbf{z}}_\mathbf{E}} \bar{\Phi}_{FNLP}(\hat{\mathbf{z}}_\mathbf{E}) \tag{5.8}$$
$$\hat{\mathbf{z}}_\mathbf{E} \in Y$$

where the objective function $\bar{\Phi}_{FNLP}(\hat{\mathbf{z}}_\mathbf{E})$ is given by the solution of the *primal* FNLPs sub-problems. These *primal* sub-problems are obtained by stating Equation (5.2) in terms of the *external variables* ($\mathbf{z}_\mathbf{E}$), i.e.,

$$\bar{\Phi}_{FNLP}(\hat{\mathbf{z}}_\mathbf{E}) = \min_{\eta,\mathbf{x}(t),\bar{\mathbf{u}}(t)} \sum_{j_u=1}^{J} w_{j_u} \Phi(\eta, \varsigma, \mathbf{x}(t), \bar{\mathbf{u}}(t), \mathbf{d}_p(t), \hat{\mathbf{z}}_\mathbf{E}, t) \tag{5.9a}$$
$$s.t.\ \ f(\eta, \varsigma, \dot{\mathbf{x}}(t), \mathbf{x}(t), \bar{\mathbf{u}}(t), \mathbf{d}_p(t), \hat{\mathbf{z}}_\mathbf{E}, t) = 0, \quad \mathbf{x}(t_0) = \mathbf{x}_0, \tag{5.9b}$$
$$h(\eta, \varsigma, \mathbf{x}(t), \bar{\mathbf{u}}(t), \mathbf{d}_p(t), \hat{\mathbf{z}}_\mathbf{E}, t) = 0, \tag{5.9c}$$
$$g(\eta, \varsigma, \mathbf{x}(t), \bar{\mathbf{u}}(t), \mathbf{d}_p(t), \hat{\mathbf{z}}_\mathbf{E}, t) \leq 0, \tag{5.9d}$$
$$\nabla_{\mathbf{\Omega}_c} \mathcal{L}(\eta, \hat{\mathbf{x}}(\tau_c), \hat{\mathbf{u}}(\tau_c), \lambda(\tau_c), \nu(\tau_c), \mu(\tau_c), \mathbf{d}_p, \hat{\mathbf{z}}_\mathbf{E}, \tau_c) = 0, \tag{5.9e}$$
$$F(\eta, \dot{\hat{\mathbf{x}}}(\tau_c), \hat{\mathbf{x}}(\tau_c), \hat{\mathbf{u}}(\tau_c), \mathbf{d}_p, \hat{\mathbf{z}}_\mathbf{E}, \tau_c) = 0, \quad \hat{\mathbf{x}}(\tau_{c_0}) = \mathbf{x}(t),\ \forall\, \tau_c = t \tag{5.9f}$$
$$H(\eta, \hat{\mathbf{x}}(\tau_c), \hat{\mathbf{u}}(\tau_c), \mathbf{d}_p, \hat{\mathbf{z}}_\mathbf{E}, \tau_c) = 0, \tag{5.9g}$$
$$\mu^\intercal(\tau_c) G(\eta, \hat{\mathbf{x}}(\tau_c), \hat{\mathbf{u}}(\tau_c), \mathbf{d}_p, \hat{\mathbf{z}}_\mathbf{E}, \tau_c) \leq \epsilon, \tag{5.9h}$$
$$\bar{\mathbf{u}}(\tau_c) = \hat{\mathbf{u}}(\tau_c), \quad \forall\, \tau_c = t \tag{5.9i}$$

The *primal* FNLPs in Equation (5.9) can be solved with state-of-the-art NLP solvers. The *master* problem (Equation (5.8)) oversees the logical requirements by verifying that $\hat{\mathbf{z}}_\mathbf{E} \in Y$. The

decomposition of the MINLP in Equation (5.2) aims to use the binary variables as parameters in the *primal* sub-problems. In the *primal* FNLPs, any expression that can be calculated as a function of the binary variables is expressed in terms of the *external variables* ($\hat{\mathbf{z}}_{\mathbf{E}}$). The *primal* FNLPs can be solved with conventional NLP solvers, e.g., IPOPT [154]. On the other hand, the *master* IPLC problem is aimed to be solved with a Discrete-Steepest Descent Algorithm (D-SDA) [155]. This algorithm is based on the discrete convex analysis theory. The usual definition of convexity in integer programming states that an integer program is convex if a convex problem is obtained when relaxing the integer requirement [151]. Instead, the field of discrete convex analysis uses its own definition, i.e., *integral convexity*. This result is useful, because an integer problem may be *integrally convex*, even if the RMINLP is non-convex according to the traditional definition of convexity [149]. Therefore, if a discrete convex analysis based method (such as the D-SDA) is used to solve a problem, different local solutions with improved costs and control performance can be found compared to applications with traditional MINLP solvers [149]. The theory proposed by Murota [155] states that the condition of *integral convexity* can be verified with the value of the objective function exclusively at integer points. The review of the theory of *integral convexity* is beyond the scope of this research. Interested readers on this subject can review the study presented in [155].

A simplification that arises when solving the *master* IPLC (Equation (5.8)) is that the domain of the objective function Φ (Equation (5.2a)) can be further reduced to a subset $A \subseteq \mathbb{Z}^{N_z}$ by using the convention $\Phi(\mathbf{z}) = +\infty$, $\forall \mathbf{z} \notin Z$, e.g., if Z is a polytope (i.e., Z is bounded as defined in [156]), the subset $A \subseteq \mathbb{Z}^{N_z}$ corresponds to the collection of points that surround Z. The surroundings of Z are referred to as a *disjoint envelope*, which is defined according to the number of integer neighbors of a point $\beta \in \mathbb{Z}^{N_z}$ inside Z (i.e., boundary points in Z) defined as follows:

$$B(\beta) = \{\mathbf{z}_{\mathbf{E}} \in Z : \|\beta - \mathbf{z}_{\mathbf{E}}\|_\infty \leq 1\}\,,\ \beta \in \mathbb{Z}^{N_z} \tag{5.10}$$

$$A = \left\{\beta \in \mathbb{Z}^{N_z} \setminus Z : |B(\beta)| \geq 1\right\} \tag{5.11}$$

where Equation (5.10) defines the set of integer neighbors (inside Z) of a point β, whereas the definition of the *disjoint envelope* of Z is given by Equation (5.11). These definitions are useful

to determine the size of the partitions of the binary variables ($\mathbf{z}$) into *external variables* $\mathbf{z_E}$. In this work, we assume that ($\mathbf{z_E}$) can form neighborhoods $N_\infty(\mathbf{z_E}) = \{\mathbf{z_E} + \chi_{Z_1} - \chi_{Z_2},\ \forall Z_1, Z_2 \subseteq \{1,\ldots,N_E\}\}$ denoted as ∞-*neighborhoods*. In this definition of $N_\infty(\mathbf{z_E})$, $\chi_{Z_1} = [\chi_{Z_1,1},\ldots,\chi_{Z_1,N_E}]$ is the indicator or characteristic vector of the subset Z_1 of $\{1,\ldots,N_E\}$. Applying this theory to the *master* IPLC, it is possible to develop a systematic algorithm for the search of a local solution for the original MINLP. Further details about the features, methodologies, and theorems that support the mathematical framework discussed in this section can be found elsewhere [149].

5.4 Discrete-Steepest Descent Algorithm

In this section, the Discrete-Steepest Descent Algorithm (D-SDA) is described for the solution of the *master* IPLC and the *primal* FNLPs, i.e., the strategy proposed in this work to address the integration of design and NMPC-based control under uncertainty for naturally ordered structures. The local search strategy implemented in this work is presented in Algorithm 1. This algorithm uses the D-SDA guidelines proposed in [157], in which the *master* problem executes a local search in the neighborhood described by the external variables. This local search consists of the solution of the *primal* FNLPs in the neighborhood described by the external variables. The solutions of the FNLPs in the neighborhood are evaluated and used to determine a search direction, if that exists. The search direction corresponds to the one that provides the steepest descent in the objective function. A brief description of this logic-based optimization algorithm presented in Algorithm 1 is provided next.

- **Stage 1 (Initialization):** The algorithm is initialized with a feasible initial solution for the discrete and continuous variables, i.e., a feasible initial design and control ($\hat{\mathbf{z}}_{\mathbf{E},\mathbf{init}}$, $\eta_{\mathbf{init}}$, $\mathbf{x_{init}}(t)$, $\bar{\mathbf{u}}_{\mathbf{init}}(\tau_c)$).

- **Stage 2 (Feasibility):** The feasibility of the initial superstructure is verified according to the logical constraints in the set Y, i.e., if the initial superstructure does not satisfy the logical constraints in Y, the algorithm stops and determines that the problem is infeasible. The topic

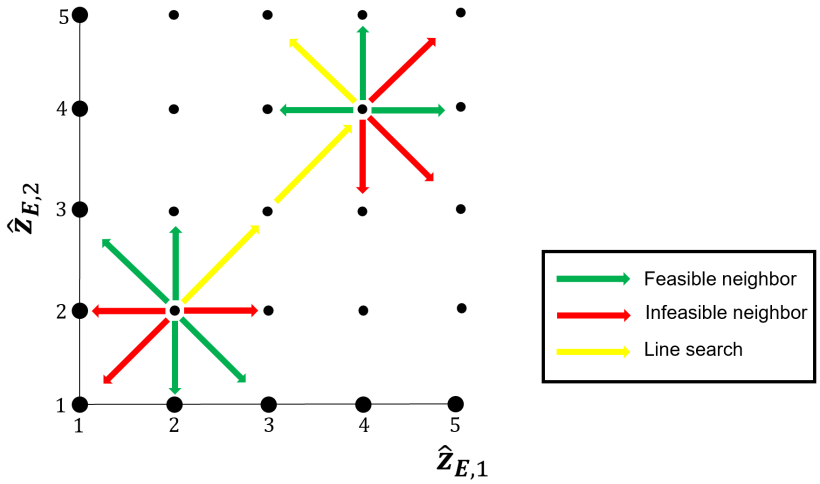

Figure 5.1: Local searches in the ∞-neighborhoods (N_∞) described by the *external variables* ($\hat{\mathbf{z}}_\mathbf{E}$) and line search in Algorithm 1.

of the initialization of the superstructure is out of the scope of this work. Interested readers on this subject can review the study presented by Turkay and Grossmann [158].

- **Stage 3 (∞-Neighborhoods):** In this stage, the search sets $N_\infty(\mathbf{z_E})$ and $S_\infty(\hat{\mathbf{z}}_\mathbf{E})$ are created. The set $N_\infty(\mathbf{z_E})$ contains the points that are compared with $\hat{\mathbf{z}}_\mathbf{E}$ at **Stage 4** to verify local optimality. This verification for optimality over $N_\infty(\mathbf{z_E})$ assumes the solution of $3^{N_E}-1$ FNLPs. Note that the computational burden increases exponentially as N_E increases.

- **Stage 4 (Local search):** The solutions of the FNLPs in the neighborhood $N_\infty(\hat{\mathbf{z}}_\mathbf{E})$ are calculated and compared to determine if there exists a superstructure that improves the solution with respect to the initial point. If the initial solution of a FNLP at $\hat{\mathbf{z}}_\mathbf{E}$ (i.e., $\bar{\Phi}_{FNLP}(\hat{\mathbf{z}}_\mathbf{E})$) is lower than the solutions of the FNLPs in the $N_\infty(\hat{\mathbf{z}}_\mathbf{E})$ (i.e., $\bar{\Phi}_{FNLP}(\beta)$), then a solution at $\hat{\mathbf{z}}_\mathbf{E}$ was found, i.e., if $\bar{\Phi}_{FNLP}(\hat{\mathbf{z}}_\mathbf{E}) \leq \bar{\Phi}_{FNLP}(\beta)$, $\forall \beta \in N_\infty(\hat{\mathbf{z}}_\mathbf{E})$ is satisfied, a local solution is found; otherwise, the set S_∞ contains the potential directions $\mathbf{s}$ for the steepest-descent direction ($\mathbf{s_d}$). In this local search, infeasible solutions of the FNLPs in in the neighborhood $N_\infty(\hat{\mathbf{z}}_\mathbf{E})$ are not considered for the determination of potential search directions. Note that the initialization for the continuous variables of the FNLPs during the local search (i.e., $\bar{\Phi}_{FNLP}(\beta)$, $\forall \beta \in N_\infty(\hat{\mathbf{z}}_\mathbf{E})$) corresponds to the values for the continuous variables from the initial solution in the neighborhood at $\bar{\Phi}_{FNLP}(\hat{\mathbf{z}}_\mathbf{E})$. This allows the suitable initialization of

the primal and dual variables in the FNLPs during the neighborhood exploration.

- **Stage 5 (Steepest descent):** The steepest-descent direction $\mathbf{s_d}$ is selected from the set $S_\infty(\hat{\mathbf{z}}_\mathbf{E})$ such that the vector $\hat{\mathbf{z}}_\mathbf{E} + \mathbf{s_d}$ is in the domain of Y and provides the greatest improvement for the objective function, i.e., $\bar{\Phi}_{FNLP}(\hat{\mathbf{z}}_\mathbf{E} + \mathbf{s_d}) \leq \bar{\Phi}_{FNLP}(\beta)$, $\forall \beta \in N_\infty(\hat{\mathbf{z}}_\mathbf{E})$. Once the steepest-descent direction $\mathbf{s_d}$ was selected, the algorithm stores this vector (i.e., $\bar{\mathbf{s}}_\mathbf{d} \leftarrow \mathbf{s_d}$) such that a line search can be executed in this search direction.

- **Stage 6 (Line search):** In this stage, the algorithm solves only the FNLPs in the search direction given by the vector $\bar{\mathbf{s}}_\mathbf{d}$, i.e., $\bar{\Phi}_{FNLP}(\hat{\mathbf{z}}_\mathbf{E} + \bar{\mathbf{s}}_\mathbf{d})$. A complete neighborhood search in $N_\infty(\hat{\mathbf{z}}_\mathbf{E} + \bar{\mathbf{s}}_\mathbf{d})$ is not executed; nevertheless, if $\hat{\mathbf{z}}_\mathbf{E} + \bar{\mathbf{s}}_\mathbf{d} \notin Y$ or $\bar{\Phi}_{FNLP}(\hat{\mathbf{z}}_\mathbf{E} + \bar{\mathbf{s}}_\mathbf{d}) \geq \bar{\Phi}_{FNLP}(\hat{\mathbf{z}}_\mathbf{E})$, the algorithm goes back to Stage 3 to execute a new neighborhood search in order to determine a new steepest-descent direction (see Figure 5.1). A local variable $\bar{\Phi}_P$ is introduced in Stages 5 and 6 to avoid calculating $\bar{\Phi}_{FNLP}$ twice for the same input. This procedure is repeated until the convergence criterion specified in Stage 4 is satisfied.

This algorithm efficiently explores the feasible region of discrete variables using partitions of the integer variables (*external variables*). This aims to avoid multiple binary variables for a single discrete decision. Consequently, the D-SDA allows the implementation of an alternative stopping criterion that is not available in any of the existing MINLP or logic-based local solvers [149]. Furthermore, decision variables in the *master* IPLC are only integer, this allows two important features of the D-SDA: (i) additional reformulations for the logical constraints or relaxation of the integer variables in the *master* problem are not required; and (ii) all discrete decisions found by the *master* IPLC are integer solutions. On the other hand, the proposed algorithmic framework does not support generalized formulations, in which the binary variables do not follow a particular structured order. In this study, local solutions are accepted; hence, the implementation of local solvers (e.g., IPOPT [154]) for the solution of the *primal* FNLPs is preferred because unbounded KKT multipliers can be handled in the NMPC problem. Further details on the implementation, features, and mathematical proofs of the D-SDA for the optimization of superstructures can be found elsewhere [149, 159].

Algorithm 1 Pseudocode for the Discrete-Steepest Descent Algorithm (D-SDA).

Input: $\hat{\mathbf{z}}_{\mathbf{E},\mathbf{init}}$, $\eta_{\mathbf{init}}$, $\mathbf{x}_{\mathbf{init}}(t)$, $\bar{\mathbf{u}}_{\mathbf{init}}(t)$
Output: $\mathbf{z}^*$, η^*, $\mathbf{x}^*(t)$, $\bar{\mathbf{u}}^*(t)$
Stage 1. Initialization: Initialize the *external* and continuous variables: $\hat{\mathbf{z}}_{\mathbf{E}} \leftarrow \hat{\mathbf{z}}_{\mathbf{E},\mathbf{init}}$; η, $\mathbf{x}(t)$, $\bar{\mathbf{u}}(t) \leftarrow \eta_{\mathbf{init}}$, $\mathbf{x}_{\mathbf{init}}(t)$, $\bar{\mathbf{u}}_{\mathbf{init}}(t)$
Stage 2. Feasibility:
if $\hat{\mathbf{z}}_{\mathbf{E}} \notin dom_{\mathbb{Z}} \Psi_{FNLP} \subseteq Y$ **then return** stop: The problem is infeasible
else
Continue to **Stage 3**.
end if
Stage 3. ∞**-Neighborhoods:** Create the sets $N_\infty(\hat{\mathbf{z}}_{\mathbf{E}}) = \{\beta \in Y : \|\beta - \hat{\mathbf{z}}_{\mathbf{E}}\|_\infty\}$ and $S_\infty(\hat{\mathbf{z}}_{\mathbf{E}}) = \{\mathbf{s} : \beta - \hat{\mathbf{z}}_{\mathbf{E}} = \mathbf{s}, \forall \beta \in N_\infty(\hat{\mathbf{z}}_{\mathbf{E}})\}$.
Stage 4. Local Search: Calculate $\Phi_{FNLP}(\beta)$, $\forall \beta \in N_\infty(\hat{\mathbf{z}}_{\mathbf{E}})$.
if $\Phi_{FNLP}(\hat{\mathbf{z}}_{\mathbf{E}}) \leq \Phi_{FNLP}(\beta)$, $\forall \beta \in N_\infty(\hat{\mathbf{z}}_{\mathbf{E}})$, **then return** stop: $\hat{\mathbf{z}}_{\mathbf{E}} = \hat{\mathbf{z}}^*_{\mathbf{E}}$ is a local minimizer of the problem. $\mathbf{z}^* \leftarrow \hat{\mathbf{z}}^*_{\mathbf{E}}$
else
Continue to **Stage 5**.
end if
Stage 5. Steepest Descent: Select a vector $\mathbf{s_d}$ from $S_\infty(\hat{\mathbf{z}}_{\mathbf{E}})$ such that $\hat{\mathbf{z}}_{\mathbf{E}} + \mathbf{s_d} \in dom_{\mathbb{Z}} \Phi_{FNLP}$ and $\Phi_{FNLP}(\hat{\mathbf{z}}_{\mathbf{E}} + \mathbf{s_d}) \leq \Phi_{FNLP}(\beta)$, $\forall \beta \in N_\infty(\hat{\mathbf{z}}_{\mathbf{E}})$. Let $\Phi_P \leftarrow \Phi_{FNLP}(\hat{\mathbf{z}}_{\mathbf{E}})$, $\hat{\mathbf{z}}_{\mathbf{E}} \leftarrow \hat{\mathbf{z}}_{\mathbf{E}} + \mathbf{s_d}$, $\Phi_{FNLP}(\hat{\mathbf{z}}_{\mathbf{E}} - \mathbf{s_d}) \leftarrow \Phi_P$, and $\bar{\mathbf{s}}_{\mathbf{d}} \leftarrow \mathbf{s_d}$.
Stage 6. Line Search: Calculate $\Phi_{FNLP}(\hat{\mathbf{z}}_{\mathbf{E}} + \bar{\mathbf{s}}_{\mathbf{d}})$
if $\hat{\mathbf{z}}_{\mathbf{E}} + \bar{\mathbf{s}}_{\mathbf{d}} \notin Y$ or $\Phi_{FNLP}(\hat{\mathbf{z}}_{\mathbf{E}} + \bar{\mathbf{s}}_{\mathbf{d}}) \geq \Phi_{FNLP}(\hat{\mathbf{z}}_{\mathbf{E}})$, **then return** Let $\hat{\mathbf{z}}_{\mathbf{E}} \leftarrow \hat{\mathbf{z}}_{\mathbf{E}}$ and go to **Stage 3**.
else
Let $\Phi_P \leftarrow \Phi_{FNLP}(\hat{\mathbf{z}}_{\mathbf{E}})$, $\hat{\mathbf{z}}_{\mathbf{E}} \leftarrow \hat{\mathbf{z}}_{\mathbf{E}} + \bar{\mathbf{s}}_{\mathbf{d}}$, $\Phi_{FNLP}(\hat{\mathbf{z}}_{\mathbf{E}} - \bar{\mathbf{s}}_{\mathbf{d}}) \leftarrow \Phi_P$, repeat **Stage 6**.
end if

5.5 Case Study: Binary distillation column

To illustrate the features of the proposed D-SDA approach, the integration of design and NMPC-based control of a binary distillation column under uncertainty is considered. This case study is based on the system presented by Schweiger and Floudas [160]. The goal is to determine the column design that separates a saturated liquid feed into bottoms and distillate products with a purity above 90% in the distillate (i.e., $x_D \geq 0.9$) in a total simulation time of 80min (Minimum reflux is not allowed in order to avoid a distillation column design with infinite number of trays). This study aims to determine the number of trays (N), location of the feed stream ($\bar{F}_{in}$), and the diameter of the column (D_e). The superstructure for the distillation column is shown in Figure 5.2.

It is assumed equimolar overflow, constant relative volatility (α), partial reboiler, total condenser, adiabatic operation, no pressure drop, and thermodynamic equilibrium at each stage. The trays in the distillation column are indexed by $\hat{n}$. Structural decisions are modeled by the binary variables $z^f_{\hat{n}} \in \{0,1\}$, $\forall \hat{n} \in INT$ and $z^r_{\hat{n}} \in \{0,1\}$, $\forall \hat{n} \in INT$ (i.e., the existence of feed and reflux streams, respectively, at the $\hat{n}^{th}$ tray). $INT \subseteq \mathbb{N}$ represents the set of trays in the superstructure. Thus, the location of the reflux stream determines the total number of trays (N). The dynamic process model for the binary distillation column is shown in Equation (5.12), while the model parameters are displayed in Table 5.1.

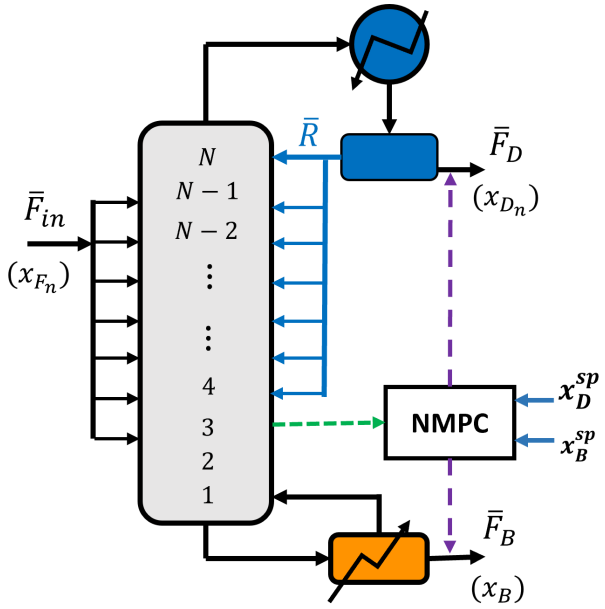

Figure 5.2: Superstructure for the Binary Distillation Column case study. The integer decisions aim to determine the optimum feed tray and the total number of trays (N).

Table 5.1: Model parameter for the binary distillation column case study.

Parameter	**Value**
h_w $[m]$	0.0254
θ_{py} $[yr]$	4.0
α	2.5
θ_{tx}	0.4
$\bar{F}_{in}$ $[kmol/min]$	1.00
t_C $[min]$	30
t_P $[min]$	30
k_t $[min]$	5

$$M_R \frac{dx_B}{dt} = L_1(x_1 - x_B) + V(x_B - y_B) \tag{5.12a}$$

$$M_T \frac{dx_{\hat{n}}}{dt} = L_{\hat{n}+1}(x_{\hat{n}+1} - x_{\hat{n}}) + V(y_{\hat{n}-1} - y_{\hat{n}}) + z^f_{\hat{n}} \bar{F}_{in}(x_f - x_n) + z^r_{\hat{n}} \bar{R}(x_D - x_{\hat{n}}) \tag{5.12b}$$

$$M_C \frac{dx_D}{dt} = V(y_{N_{max}} - x_D) \tag{5.12c}$$

$$\tau_h \frac{d\bar{F}_B}{dt} = L_1 - \bar{V}_B - \bar{F}_B \tag{5.12d}$$

$$\tau_h \frac{dL_{\hat{n}}}{dt} = L_{\hat{n}+1} - L_{\hat{n}} + z^f_{\hat{n}} \bar{F}_{in} + z^r_{\hat{n}} \bar{R} \tag{5.12e}$$

$$\tau_h \frac{d\bar{F}_D}{dt} = \bar{V}_B - \bar{R} - \bar{F}_D \tag{5.12f}$$

$$y_{\hat{n}} = \frac{\alpha x_{\hat{n}}}{1 + x_{\hat{n}}(\alpha - 1)} \tag{5.12g}$$

$$M_T = 7.538115 \left(\left(\left(\frac{0.0014134}{D_e} \right)^{2/3} \right) + h_w \right) D_e^2 \tag{5.12h}$$

$$\frac{d\kappa}{dt} = t(x_D - x_D^{sp})^2 + t(x_B - x_B^{sp})^2 \tag{5.12i}$$

$$M_C = 100 M_T, \quad M_R = 100 M_T \tag{5.12j}$$

$$\tau_h = 0.05271 D_e^{4/3} \tag{5.12k}$$

$$D_c \geq 0.6719 \sqrt{V_{ss}} \tag{5.12l}$$

$$x_f = 0.45 + \frac{0.9}{1 + e^{-80(t-5)}} \tag{5.12m}$$

For the tray hydraulics, it is implemented the *Francis* weir formulation in Equation (5.12h) to calculate the molar hold-ups (M_T). The tray time constants (τ_h) are stated in function of the column's diameter (Equation (5.12k)). The reboiler and condenser liquid hold-ups are in function of the tray hold-ups (Equation (5.12h)), i.e., M_R and M_C, respectively.

As shown in Figure 5.2, the controlled variables correspond to the liquid compositions at distillate ($x_D(t)$) and bottoms ($x_B(t)$), whereas the manipulated variables are the reflux ($\bar{R}(t)$) and boil up ($\bar{V}_B(t)$) streams. Also, the set of dynamic variables involve the liquid composition ($x_{\hat{n}}(t)$), liquid flowrates from each tray ($L_{\hat{n}}(t)$), bottoms and distillate flowrates ($\bar{F}_D(t)$ and $\bar{F}_B(t)$, respectively), and vapor composition ($y_{\hat{n}}(t)$). Additional continuous time invariant decision variables involve the

tray liquid hold up (M_T), the tray hydraulic time constant (τ_h), the operation set-points for distillate and bottoms (x_D^{sp} and x_B^{sp}, respectively), and the NMPC controller tuning parameters. The tuning parameters in the objective function for the NMPC correspond to the weighting parameters Q_{x_D} and Q_{x_B} that penalize the deviations in the predicted controlled variables with respect to their desired set-points, i.e., $Q_{x_D}\left(\hat{x_D}(\tau_c) - x_D^{sp}\right)^2$ and $Q_{x_B}\left(\hat{x_B}(\tau_c) - x_B^{sp}\right)^2$, respectively. Also, the optimal selection of the weighting parameters $Q_{\bar{R}}$ and $Q_{\bar{V}}$ that penalize the changes in the predicted manipulated variables is considered, i.e., $Q_{\bar{R}}\left(\Delta\hat{R}(\tau_c)\right)^2$ and $Q_{\bar{V}}\left(\Delta\hat{V}_B(\tau_c)\right)^2$, respectively. To enforce process dynamics, it is considered a step disturbance in the feed stream composition (x_f), i.e.,

$$x_f = 0.45 + \frac{0.09}{1 + e^{-80(t-5)}} \tag{5.13}$$

For the NMPC, prediction and control horizons are both set to 30min. These horizons were selected using closed-loop simulations subject to the disturbance in Equation (5.13). As explained in Section 5.1, it is assumed that the binary variables are only related to the upper-level problem, i.e., the NMPC is a continuous formulation. Therefore, it is possible to obtain the first order conditions for optimality for the NMPC (lower-level problem).

In this case study, the objective function aims to minimize the annualized capital cost (CC_a) that depends on the equipment design (i.e., $CC_a = f_c(D_e, N)$), an utility cost (UC_a) that depends on the boil up stream (i.e., $UC_a = f_u(\bar{V}_B)$), and the weighted controllability index (ϕ_{ISE}) given by the ISE, i.e.,

$$\Phi = \underbrace{\theta_{tx}(19390V_{ss})}_{UC_a} + \underbrace{\frac{12.3(615 + 324D_e^2 + 486(6 + 0.76N)D_e) + 61.25N(0.7 + 1.5D_e^2)}{\theta_{py}}}_{CC_a} + W_{ISE}\underbrace{\kappa(t_f)}_{\phi_{ISE}} \tag{5.14}$$

where W_{ISE} is a weighting parameter that aims to penalize the process variability. In this case study, W_{ISE} is set to 1×10^4. The controllability term ($\kappa(t_f)$) is given by the integration of the time-weighted ISE of the distillate and bottoms compositions:

$$\frac{d\kappa}{dt} = t(x_D - x_D^{sp})^2 + t(x_B - x_B^{sp})^2 \tag{5.15}$$

The set of logical constraints to describe the superstructure in Figure 5.2 are as follows:

$$N = \sum_{\hat{n}=1}^{N_{max}} \hat{n} z_{\hat{n}}^r \tag{5.16a}$$

$$\sum_{\hat{n}=1}^{N_{max}} z_{\hat{n}}^f = 1 \tag{5.16b}$$

$$\sum_{\hat{n}=1}^{N_{max}} z_{\hat{n}}^r = 1 \tag{5.16c}$$

$$\sum_{\hat{n}=1}^{N_{max}} \hat{n} z_{\hat{n}}^f \geq 4 \tag{5.16d}$$

$$\sum_{\hat{n}=1}^{N_{max}} \hat{n} z_{\hat{n}}^r \geq 10 \tag{5.16e}$$

$$\sum_{\hat{n}=1}^{N_{max}} \hat{n} z_{\hat{n}}^r - \hat{n} z_{\hat{n}}^f \geq 4 \tag{5.16f}$$

where the number of trays in the distillation column is obtained from Equation (5.16a). Equation (5.16b) ensures the existence of only one feed stream. Equation (5.16c) avoids the existence of multiple reflux stream. Equation (5.16d) ensures that the feed stream enters on tray 4 or above, while Equation (5.16e) allows the reflux stream to enter on tray 10 or above. Equation (5.16f) allows the existence of at least four trays between the feed and reflux streams. As mentioned above, the discrete decisions correspond to the location of the feed streams ($z_{\hat{n}}^f$) and the total number of trays ($z_{\hat{n}}^r$), i.e., the location of the reflux stream. The associated binary variables $z_{\hat{n}}^f$ and $z_{\hat{n}}^r$ can be represented as functions of 2 *external variables*, i.e., z_E^f and z_E^r, respectively. In this case study, the reformulation of binary variables in terms of external variables is as follows:

$$z_n^f = \begin{cases} 1, & z_E^f = \hat{n} \ \ \forall \hat{n} \in INT \\ 0, & otherwise \end{cases} \tag{5.17}$$

$$z_n^r = \begin{cases} 1, & z_E^r = \hat{n} \ \ \forall \hat{n} \in INT \\ 0, & otherwise \end{cases} \tag{5.18}$$

$$Y_1 = \left\{ \begin{array}{ll} \mathbf{z_E} \in \mathbb{Z}^2 : & 1 \leq z_E^f \leq N_{max} \\ & 1 \leq z_E^r \leq N_{max} \end{array} \right\} \tag{5.19}$$

$$Y_2 = \left\{ \begin{array}{ll} \mathbf{z_E} \in \mathbb{Z}^2 : & N - \hat{n} z_E^r = 0, \quad \forall \hat{n} \in INT \\ & \hat{n} z_E^f - 4 \geq 0 \quad \forall \hat{n} \in INT \\ & \hat{n} z_E^r - 10 \geq 0 \quad \forall \hat{n} \in INT \\ & \hat{n} z_E^r - \hat{n} z_E^f - 4 \geq 0 \quad \forall \hat{n} \in INT \end{array} \right\} \tag{5.20}$$

$$Y = Y_1 \cap Y_2 = \left\{ \begin{array}{ll} \mathbf{z_E} \in \mathbb{Z}^{N_E} : & N - \hat{n} z_E^r = 0, \quad \forall \hat{n} \in INT \\ & \hat{n} z_E^f - 4 \geq 0 \quad \forall \hat{n} \in INT \\ & \hat{n} z_E^r - 10 \geq 0 \quad \forall \hat{n} \in INT \\ & \hat{n} z_E^r - \hat{n} z_E^f - 4 \geq 0 \quad \forall \hat{n} \in INT \\ & 1 - z_E^f \leq 0 \quad \forall \hat{n} \in INT \\ & z_E^f - N \leq 0 \\ & 1 - z_E^r \leq 0 \\ & z_E^r - N \leq 0 \end{array} \right\} \tag{5.21}$$

where Y contains the set of constraints for the *master* problem. This case study was solved under different scenarios. The first scenario (Section 5.5.1) evaluates the performances of the D-SDA using different initial points for the structural decisions for the distillation column under no uncertainty. Scenario 2 (Section 5.5.2) presents the distributed stream-tray optimization method (DSTO) and evaluates its performance given the initial points stated in Scenario 1 for the distillation column under no uncertainty. The effect on the solution subject to model uncertainty using the D-SDA approach is presented in Scenario 3 (Section 5.5.3). Furthermore, in Scenario 4 (Scenario 5.5.4), the DSTO method for the solution of the problem under uncertainty is implemented. For all the scenarios, the implementation was performed in GAMS V40.4.0 in a platform with an Intel®Core™

17-8700 CPU 3.20 GHz processor, 16GB of RAM using Windows Server 2019 Standard. IPOPT 3.14.3 was implemented as the main NLP solver using linear solver MA86 and a desired convergence tolerance set to 1.0×10^{-7}, all other solver options are as default. OCFE is implemented for the discretization of the single-level optimization problem in Equation (5.2), i.e., 16 finite elements for the upper-level problem with 5 Radau collocation points, and 6 finite elements with 3 Radau collocation points for the lower-level problem are implemented for all scenarios. Two different levels of discretization are needed because the design problem (upper-level problem) is solved over a longer simulation time compared to the NMPC controller (lower-level problem), i.e., the upper-level problem is simulated over an 80min horizon, whereas the NMPC has a prediction horizon of 30min. Note that the lower-level problem dominates the size of the optimization formulation; therefore, a selection of fewer collocation points in the lower-level problem also reduces the computational burden. Also, note that this may produce a process model mismatch between the model in the different problem levels. Closed-loop simulations showed that this discretization can accurately approximate model functions on each problem level. The maximum number of equilibrium trays (N_{max}) is set to 30.

5.5.1 Scenario 1: D-SDA with no uncertainty

To evaluate the performance of the D-SDA for the search of a local solution for the binary distillation column in this case study, three different initialization for the structural decisions are proposed: (i) 15 total trays and the feed stream located at the 5^{th} tray (Instance 1); (ii) 16 total trays with the feed stream located at the 8^{th} tray (Instance 2); (iii) 25 total trays and the feed stream located at the 5^{th} tray (Instance 3). As shown in Table 5.2 (Scenario 1: D-SDA), slight differences in the superstructure were obtained for the distillation column. Instance 3 returned smaller column's diameter (D_e) compared to Instances 1 and 2, i.e., D_e for Instance 3 is 0.12% and 1.6% smaller compared to the result for Instances 1 and 2, respectively. From an operational point of view, the three instances determined a mole fraction set-point for the distillate around 0.98. Moreover, it is noted that the controller weighting parameters Q_{x_D} have significant differences. The magnitude of Q_{x_D} for Instance 1 is 50% smaller compared to Instance 2, whereas Q_{x_D} for Instance 3 is one order

of magnitude smaller compared to the results for Instance 2. Regarding the process economics, the solution for Instance 3 returned the lowest total cost, i.e., 3.590×10^4 [$\$/yr$]. Although, Instance 2 led to a 2.5% lower capital cost compared to the results for Instance 3, the utility cost for Instance 2 is 7.4% higher than those obtained for Instance 3. Hence, this explains the difference in the total cost of Instance 3 with respect to Instances 1 and 2. Furthermore, from the results for Instances 1 and 3, it is observed that the discrete decisions for the distillation column returned the same results; nevertheless, the results for the continuous variables (e.g., controller tuning parameters, column's diameter, etc.) have differences between those instances. Since the FNLPs for this case study are nonconvex, the same values in the discrete decisions may not converge to unique solutions for the continuous variables. The solutions obtained for the FNLPs depend on the initial points. As mentioned above, during the neighborhood search and line search, the FNLPs are initialized using previous feasible solutions. Hence, the solutions for the structural decisions for Instances 1 and 3 are near the solution obtained for Instance 2 (i.e., the superstructure for Instance 2 is an immediate neighbor to the superstructure found for Instances 1 and 3). This implies that even if the combination of values for the discrete decisions is the same as for Instance 2 (i.e., 15 trays and a feed stream at the 8th tray), the algorithm may not find an improvement in the objective function for Instances 1 and 3. This is because the initialization for the continuous variables at that neighbor may be different in each case.

5.5.2 Scenario 2: DSTO with no uncertainty

To compare the solutions obtained with the proposed framework, it is implemented an alternative methodology based on the DSTO method presented in [161]. In that methodology, the stream locations for feed and reflux are allowed to be continuous variables in a DDF. That methodology assumes the solution of a continuous formulation that can be solved with conventional NLP solvers. In this case study, the DDF is derived from a discretization of a Gaussian distribution with mean value N_c and standard deviation σ. Moreover, for the DSTO method, the number of trays (N) is defined as the integer value of N_c (i.e., $N = int[N_c]$) and a real variable $a = N_c - N$. Therefore, the DDFs ($\varrho_{\hat{n}}$) are defined as follows:

Table 5.2: Results for the binary distillation column case study for Scenarios 1 and 2.

Optimization variable	**Scenario 1: D-SDA**			**Scenario 2: DSTO**		
	Instance 1	Instance 2	Instance 3	Instance A	Instance B	Instance C
Trays (N)	16	15	16	15	16	19
Feed tray	9	8	9	9	9	10
D_e $[m]$	0.784	0.796	0.783	0.793	0.776	0.747
x_D^{sp}	0.978	0.98	0.978	0.978	0.978	0.978
x_B^{sp}	0.02	0.02	0.02	0.02	0.02	0.02
Q_{x_D}	28.1	57.7	5.49	1.76	1.25	0.89
Q_{X_B}	0.5	0.5	0.5	0.5	0.5	0.5
$Q_{\bar{R}}$	0	4.3	0	6.0×10^{-4}	0	0
$Q_{\bar{V}}$	0	9.9	0	0	0	0
Initial Feed tray	5	8	5	5	8	5
Initial Reflux tray	15	16	25	15	16	25
Equations		141,743			146,444	
Variables		141,596			146,326	
ISE	0.031	0.0038	0.039	0.036	0.044	0.014
Capital cost $[\$/yr]$	2.537×10^4	2.473×10^4	2.536×10^4	2.465×10^4	2.514×10^4	2.705×10^4
Utility cost $[\$/yr]$	1.055×10^4	1.132×10^4	1.054×10^4	1.080×10^4	1.035×10^4	9.582×10^3
Total cost $[\$/yr]$	3.593×10^4	3.605×10^4	3.590×10^4	3.545×10^4	3.549×10^4	3.664×10^4
CPU $[s]$	1.200×10^5	1.003×10^4	5.263×10^5	1.175×10^5	1.194×10^5	1.102×10^5
Neighborhoods	4	2	4	-	-	-
Iterations	-	-	-	4	4	6

$$\varrho_{\hat{n}} = \frac{e^{-\left(\frac{\hat{n}-N_c}{\sigma}\right)^2}}{\sum_{\hat{n}'=1}^{N} e^{-\left(\frac{\hat{n}'-N_c}{\sigma}\right)^2}} \; \hat{n} \in \{1, \ldots, N_{max}\} \; \hat{n}' \in \{1, \ldots, N_{max}\} \tag{5.22}$$

where the DDF features the following properties: (i) The values of the DDF are positive everywhere, i.e., $\varrho_{\hat{n}} \geq 0$, $\hat{n} \in \{1, \ldots, N_{max}\}$. (ii) Summation of the DDF over the index of trays ($\hat{n}$) is equal to unity, i.e., $\sum_{\hat{n}} \varrho_{\hat{n}} = 1$. (iii) The distribution is symmetric to N if $a = 0$, i.e., $N_c = N$. If $a = 0.5$, then $N_c = N + 0.5$ and the values of the DDF are symmetric to $N + 0.5$. (iv) Asymmetric distribution if $a \neq 0$ and $a \neq 0.5$. (v) The skewness in the asymmetric property depends on the values of a. If $0 < a < 0.5$, skewness is positive; whereas if $0.5 < a < 1$, skewness is negative. (vi) If $N_c = 1$ or $N_c = N_{max}$, the DDF is skewed to one direction only. (vii) The distribution function can be concentrated to a single tray in the column as long as the value of σ is small enough such that $\varrho_{\hat{K}} = 1$ and $\varrho_{\hat{n}} = 0 \; \forall \; \hat{n} \neq \hat{K}$, $\hat{n} \in \{1, \ldots, N_{max}\}$. For this, standard deviation is set to $\sigma \geq 0.35$ [161]. Although a solution strategy with a decreasing sequence of values for σ may yield a better results. Further description and details about the features of DDF and the selection of σ can be found

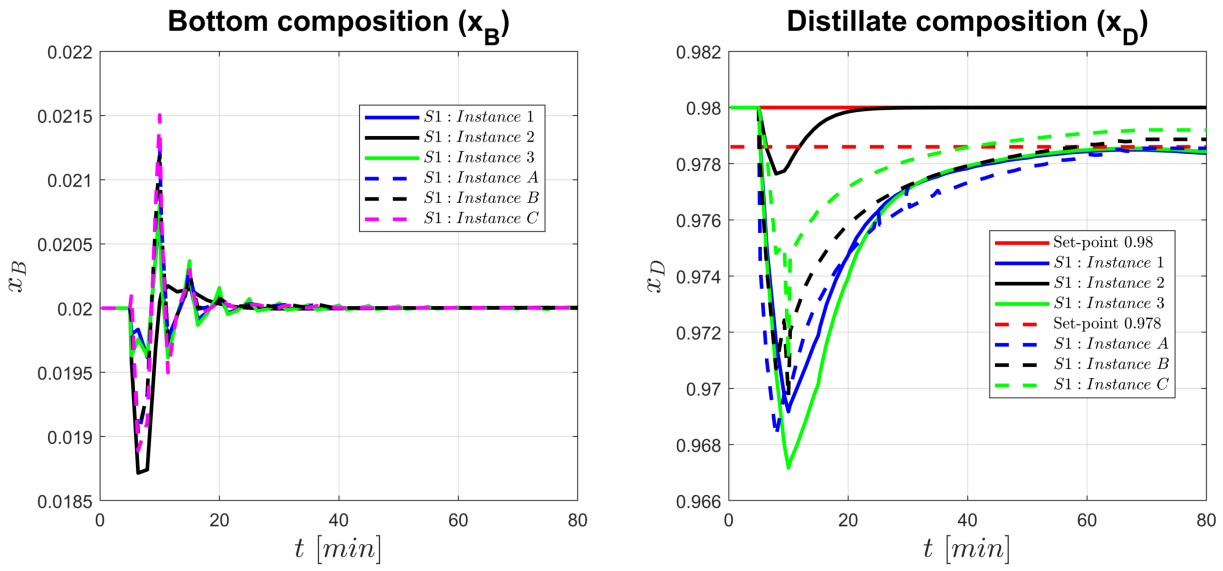

Figure 5.3: Concentration profiles of distillate and bottom for Scenarios 1 (Instances 1 to 3) and 2 (Instances A to C) for the binary distillation column case study.

elsewhere [161]. In this work, the solution of the continuous formulation for simultaneous design and NMPC-based control is addressed by solving a series of NLP's with a decreasing sequence of σ, starting each iteration from the previous solution. The implementation of the DSTO also requires the specification of the feed and reflux streams in terms of DDFs as follows:

$$\bar{R}_{\hat{n}} = \bar{R}\varrho^{\bar{r}}_{\hat{n}} \quad \text{and } \bar{V}_{B_n} = \bar{V}_B\varrho^{\bar{v}}_{\hat{n}} \; \forall \; \hat{n} \in \{1, \ldots, N_{max}\} \tag{5.23}$$

where $\varrho^{\bar{r}}_{\hat{n}}$ and $\varrho^{\bar{v}}_{\hat{n}}$ are the values for the DDFs (Equation (5.22)) for the reflux and boil up streams, respectively. $\bar{R}_{\hat{n}}$ and $\bar{V}_{B_{\hat{n}}}$ are the reflux and boil up streams entering into the $\hat{n}^{th}$ tray, respectively, i.e., on each tray enters a fraction of the flow rates of streams $\bar{R}$ and $\bar{V}_B$ equivalent to the values of the DDFs ($\varrho^{\bar{r}}_{\hat{n}}$ and $\varrho^{\bar{v}}_{\hat{n}}$). In the cases when $N_c << N_{max}$, the trays between N_c and N_{max} may be dry because no liquid is flowing through them. To address this issue, the methodology introduces new complementarity conditions that allows to model the phase equilibrium as follows:

$$y_{\hat{n}} - \zeta_{\hat{n}} K_{\hat{n}}(T_{\hat{n}}, x_{\hat{n}}) x_{\hat{n}} = 0 \; \forall \; \hat{n} \in \{1, \ldots, N_{max}\} \tag{5.24}$$

$$1 - \zeta_{\hat{n}} = s^{\hat{n}}_L - s^{\hat{n}}_V \; \forall \; \hat{n} \in \{1, \ldots, N_{max}\} \tag{5.25}$$

$$L_{\hat{n}} \geq 0, \;\; s_L^{\hat{n}} \geq 0, \;\; \forall \; \hat{n} \in \{1, \ldots, N_{max}\} \tag{5.26a}$$

$$V_{\hat{n}} \geq 0, \;\; s_V^{\hat{n}} \geq 0, \;\; \forall \; \hat{n} \in \{1, \ldots, N_{max}\} \tag{5.26b}$$

$$L_{\hat{n}} s_L^{\hat{n}} \leq \epsilon_s \; \forall \; \hat{n} \in \{1, \ldots, N_{max}\} \tag{5.26c}$$

$$V_{\hat{n}} s_V^{\hat{n}} \leq \epsilon_s \; \forall \; \hat{n} \in \{1, \ldots, N_{max}\} \tag{5.26d}$$

where $s_L^{\hat{n}}$ is a positive defined slack variable corresponding to the complementarity constraint in Equation (5.26); Distillation K-values are given by $K_{\hat{n}}$; $y_{\hat{n}}$ and $x_{\hat{n}}$ are the mole fractions in the vapor and liquid phase, respectively, on the $\hat{n}^{th}$ tray; $L_{\hat{n}}$ and $V_{\hat{n}}$ corresponds to the flowrate of liquid and vapor flowing in the $\hat{n}^{th}$ tray, respectively; whereas $\zeta_{\hat{n}}$ is a correction factor that is necessary to ensure feasibility in the equilibrium for dry trays. If $\zeta_{\hat{n}} < 1$, then $s_L^{\hat{n}} > 0$ and $L_{\hat{n}} = 0$. If $\zeta_{\hat{n}} > 1$, then $s_V^{\hat{n}} > 0$ and $V_{\hat{n}} = 0$. The complementarity constraints are approximated in Equation (5.26) using a regularization strategy. In this case study, the relaxation parameter for complementarity constraints ϵ_s is set to 1.0×10^{-6}. For the integration of design and control of the binary distillation column, Equations (5.22) to (5.26) are added to the upper-level problem (Equation (5.1d)) as part of the constraints.

To evaluate the effectiveness of the DSTO method for the search of a local solution for the binary distillation column case study with no uncertainty, the same initialization superstructures as in Scenario 1 is implemented, i.e., (i) 15 trays and a feed stream located at the 5^{th} tray (Instance A); (ii) 16 trays and a feed stream located at the 8^{th} tray (Instance B); (iii) 25 trays and a feed stream located at the 5^{th} tray (Instance C). The results for the continuous formulation using the DSTO method (Scenario 2) are shown in Table 5.2. From the results, it can be noted that Instance C returned smaller column's diameter with respect to Instances A and B, i.e., D_e for Instance C is 6% and 3% smaller compared to Instances A and B, respectively. Moreover, it is observed that the controller tuning parameters $\mathbf{Q_{out}}$ are in the same order of magnitude with slight differences. From an economic point of view, the solution for Instance A shows a lower total cost compared to Instances B and C, i.e., total cost for Instance A is 0.11% and 3.2% smaller with respect to the

results for Instances B and C, respectively.

As shown in Table 5.2, the D-SDA approach returned solutions around the 16 trays in the distillation columns, whereas the DSTO method led to varied solutions, i.e., distillation column designs with 15 to 19 trays. Moreover, Instances 1-3 (Scenario 1) averaged 0.787m for the distillation column's diameter (D_e) with a standard deviation of 0.007m. In comparison, Instances A-C (Scenario 2) averaged 0.772m for D_e with a standard deviation of 0.023m. In other words, variations in the column's designs are one order of magnitude smaller in the solutions with the D-SDA compared to the DSTO method. With regards to the process economics, it is noted that Instance A (Scenario 2) returned the lowest total cost (i.e., 3.545×10^4). On the contrary, the controllability aspect indicates that the solution for Instance 2 (Scenario 1) led to a better control performance, i.e., Instance 2 returned the lowest ISE. This is visually demonstrated in Figure 5.3. From this figure, it is observed smaller variations and a faster response in the control profiles in the solution for Instance 2 compared to the other instances. Additionally, from Table 5.2, it can be appreciated that Instance B returned the smallest utility cost (i.e., 1.035×10^4) in detriment of the ISE (i.e., the worst control performance). Additionally, in this case study, the implementation of commercial local solvers (i.e., an Outer Approximation (OA) solver (DICOPT) and a Branch & Bound (B&B) solver (SBB)) for the solution of the corresponding MINLP (Problem (5.2)) did not return a solution within a reasonable amount of time (i.e., $1.0 \times 10^6 s$).

As to comparison of the CPU times (Table 5.2), it can be noticed that Instance 2 (Scenario 1) required the shortest CPU time to converge, i.e., $1.003 \times 10^4 s$. Note that the CPU time for the rest of instances is in the same order of magnitude, while Instance 3 demanded the largest CPU time 5.263×10^5. This is almost five times larger the CPU time required by Instances A-C. For the implementation of the D-SDA (Scenario 1), only 1% of the CPU time was spent on the solution of *master* IPLC problems. Note that the D-SDA solves 8 *primal* FNLPs during the neighborhood search. As a result, the neighborhood search (Stage 3 in the algorithm) demanded 77.6% of the CPU time. The rest of the CPU time was mainly dedicated to the line search and initialization of the algorithm. On the other hand, the DSTO method demanded on average 71% of the CPU time for the location of an initial point. The rest of the CPU time was spent in the solution of the NLPs

using a decreasing sequence of values for σ.

Additionally, we implemented alternative NLP solvers such as CONOPT and KNITRO for both methodologies (i.e., D-SDA and DSTO) for Scenarios 1 and 2, i.e., i) D-SDA/CONOPT; ii) D-SDA/KNITRO; iii) DSTO/CONOPT; iv) DSTO/KNITRO. In this scenario, the superstructure was initialized using 16 total trays with the feed stream located at the 8th tray. The maximum number of equilibrium trays (N_{max}) was set to 30. The rest of the parameters for the NMPC controller and the discretization scheme remained the same as in the case study. The configuration for the solvers is presented in Table 5.3.

Table 5.3: Configuration for the solvers CONOPT and KNITRO

Settings	**CONOPT**	**Settings**	**KNITRO**
`lim_variable`	1.0×10^{13}	`linsolver`	MA86
`Tol_Feas_Max`	1.0×10^{-5}	`ftol_iters`	150
`Tol_Feas_Min`	4.0×10^{-7}	`infeastol_iters`	200
`Tol_Opt_LinF`	1.0×10^{-7}	`bar_linsys_storage`	1
		`hessopt`	LBFGS
		`algorithm`	2

As shown in Table 5.4, the D-SDA using KNITRO converged to the same values for the structural decision variable as that obtained for Instance 2 (Scenario 1). However, the column's diameter for Instance 2 is slightly smaller (i.e., 1%) compared to the results using KNITRO. The largest differences between the results for Instance 2 (Scenario 1) and the implementation of the D-SDA with KNITRO are in the controller tuning parameters, i.e., the D-SDA/KNITRO returned tuning parameters that are 2 orders of magnitude larger compared to those obtained for Instance 2. In contrast, the controller performance for Instance 2 returned an ISE that is one order of magnitude smaller compared to the D-SDA/KNITRO. In terms of computational demands, the D-SDA/KNITRO required CPU times that are 8 times larger than those needed by Instance 2. Moreover, the DSTO/CONOPT converged to the same values for the discrete decision variables as that obtained for Instance C (Scenario 2). The largest differences between the results for Instance C and the DSTO/CONOPT are observed for the controller tuning parameters, i.e., Q_{x_D} and $Q_{\bar{R}}$ obtained from DTSO/CONOPT are two and four orders of magnitude larger, respectively, when compared to Instance C. This leads to a slight difference in the Utility costs, where the process is

0.18% more economic in terms of the utility cost for Instance C compared to the DSTO/CONOPT. Furthermore, the DSTO/CONOPT required twice the CPU time compared to the computational demands needed by IPOPT for Instance C.

Table 5.4: Results for the binary distillation column case study using alternative NLP solvers.

Optimization variable	**D-SDA (KNITRO)**	**DSTO (CONOPT)**
Trays (N)	15	19
Feed tray	8	10
D_e $[m]$	0.804	0.747
x_D^{sp}	0.98	0.98
x_B^{sp}	0.02	0.02
Q_{x_D}	0.5	12.8
Q_{X_B}	708.5	0.5
$Q_{\bar{R}}$	108.4	8203
$Q_{\bar{V}}$	2054	0.0
Equations	236,932	256,221
Variables	235,846	255,118
ISE	0.067	0.014
Capital cost $[\$/yr]$	2.499×10^4	2.708×10^4
Utility cost $[\$/yr]$	1.111×10^4	9.600×10^3
Total cost $[\$/yr]$	3.611×10^4	3.668×10^4
CPU $[s]$	8.457×10^4	2.408×10^5
Neighborhoods	2	-
Iterations	-	4

The implementation of other NLP solvers led to similar results to those obtained for Scenarios 1 and 2 (Table 5.2). However, there are significant variations in the CPU times depending on the selection of the NLP solver (Table 5.4). Also, note that the solutions shown in Table 5.4 correspond to instances ii) D-SDA/KNITRO and iii) DSTO/CONOPT, whereas the implementations for i) D-SDA/CONOPT and vi) DSTO/KNITRO did not converge to feasible solutions. Further comparison and selection of NLP solvers can be found elsewhere [18].

5.5.3 Scenario 3: D-SDA under uncertainty

In this scenario, a set of uncertainty realizations in three model parameters is introduced for the distillation column case study. The formulation under uncertainty is solved using the D-SDA approach. Table 5.5 shows the set of uncertainty realizations considered in the present case study. The parameters under uncertainty correspond to the feed stream flowrate ($\bar{F}_{in}$), the relative volatility (α), and the height over the weir on the trays (h_w). It is assumed that the values for the parameters

under uncertainty may vary within ±15% of their nominal values. Note that the nominal values for the uncertain parameters correspond to the first realization listed in Table 5.5 (i.e., $j_u = 1$). The upper-level problem (design problem) has access to all the realizations in the uncertain parameter set, whereas the NMPC (lower-level problem) has only access to the nominal values (realization $j_u = 1$), i.e., a nominal NMPC controller is implemented. The presence of uncertainties in the upper-level problem generates a mismatch with the internal dynamic model used by the NMPC framework. The rest of the model parameters remain the same as in Scenario 1 (see Table 5.1). Note that the presence of uncertainties in the bilevel formulation does not modify the number of logical constraints, i.e., the formulation of the *master* IPLC problem in the D-SDA is not affected by the presence of the uncertainties in Table 5.5. Nevertheless, these uncertainties are accounted for in the *primal* FNLPs. Therefore, the objective function for the *primal* FNLPs considers the probability of occurrence of each realization j_u in the set of uncertainties, i.e.,

$$\Phi_{j_u} = \underbrace{\theta_{tx}\left(19, 390 V_{ss}\right)}_{UC_a} + \underbrace{\frac{12.3(615 + 324D_e^2 + 486(6 + 0.76N)D_e) + 245N(0.7 + 1.5D_e^2)}{\theta_{py}}}_{CC_a} + W_{ISE}\underbrace{\kappa_{j_u}(t_f)}_{\phi_{ISE}} \quad (5.27)$$

where the controllability term ($\kappa(\varsigma, t_f)$) is in function of the uncertainty realizations. $\kappa_{j_u}(t_f)$ is given by the integration of the time-weighted ISE of the distillate and bottoms compositions, i.e., $\frac{d\kappa_{j_u}}{dt}$. The superstructure for the distillation column is initialized with 25 trays and the feed stream at the 5^{th} tray.

Results for Scenario 3 are shown in Table 5.6. From these results, it can be noted that a larger column's diameter (D_e) is obtained in Scenario 3 compared to the results in Scenario 1 (Table 5.2), i.e., D_e in Scenario 3 is 78% larger compared to the averaged diameter in Scenario 1. Moreover, it is observed that Scenario 3 returned a design with fewer trays (14 trays) compared to Scenarios 1 and 2 (Table 5.2). The economic aspects show an increase of 76% in the total cost for Scenario 3 with respect to Instances 1-3 in Scenario 1. This is explained by the increase in the capital cost observed in Scenario 3 with respect to the solutions in Scenario 1, i.e., Scenario 3 returned a 95% larger

Table 5.5: Uncertainty realizations in the model parameters for the binary distillation column case study.

Uncertainty realizations (j_u)	**Feed stream** $(\bar{F}_{in})$ $[kmol/min]$	**Relative volatility** (α)	**Height over the weir** (h_w) $[m]$	**Weight distribution** (w_{j_u})
1	1.00	2.500	0.025400	0.60
2	1.10	2.375	0.022860	0.10
3	0.90	2.625	0.027940	0.10
4	1.13	2.450	0.026416	0.05
5	0.87	2.550	0.024384	0.05
6	1.05	2.575	0.027178	0.04
7	0.95	2.425	0.023622	0.04
8	0.92	2.600	0.026670	0.02

capital cost compared to Instances 1-3 in Scenario 1. The increase in the capital cost observed for Scenario 3 is attributed to the increase in the column's diameter with respect to the solutions in Scenarios 1 and 2. On the other hand, utility cost in Scenario 3 showed an increase of 30% with respect to Scenario 1. From a controllability point of view, Scenario 3 averaged an integral squared error ($\bar{\text{ISE}}$) two orders of magnitude larger than the results for Scenario 1. These differences in the ISE values can be attributed to the presence of uncertainty in the process model parameters.

Table 5.6: Results for Scenarios 3 and 4: binary distillation column under uncertainty.

Optimization variable	**Scenario 3: D-SDA**	**Scenario 4: DSTO**
Trays (N)	14	21
Feed tray	9	9
D_e $[m]$	1.407	2.26
x_D^{sp}	0.98	0.99
x_B^{sp}	0.01	0.01
Q_{x_D}	0.5	2.11
Q_{X_B}	0.5	0.5
$Q_{\bar{R}}$	0.0007	0.004
$Q_{\bar{V}}$	0	0.0004
Equations	236,932	256,221
Variables	235,846	255,118
$\bar{\text{ISE}}$	1.853	17.962
Capital cost $[\$/yr]$	4.924×10^4	9.198×10^4
Utility cost $[\$/yr]$	1.412×10^4	1.240×10^4
Total cost $[\$/yr]$	6.336×10^4	1.043×10^5
CPU $[s]$	7.204×10^5	7.193×10^5
Neighborhoods	5	-
Iterations	-	3

5.5.4 Scenario 4: DSTO under uncertainty

In Scenario 4, the DSTO method is implemented for the integration of design and NMPC-based control of the binary distillation column (Figure 5.2) under uncertainty. In this scenario, the set of uncertainty realizations shown in Table 5.5 that correspond to the same realizations implemented in Scenario 3 are introduced. The upper-level problem has access to the complete set of uncertainty realizations, whereas the NMPC (lower-level problem) uses the nominal values for the parameters under uncertainty (i.e., realization $j_u = 1$). The rest of the model parameters, objective function, and discretization remain the same as in Scenario 3. The initial superstructure for the distillation column remains the same as in Scenario 3, i.e., 25 trays and the feed stream at the 5^{th} tray. The results for this Scenario are shown in Table 5.6. From these results, it can be observed an increase in the size of the distillation column with respect to the results in Scenario 2 (Table 5.2), i.e., Scenario 4 returned a column design with 21 trays and a column's diameter (D_e) of $2.26m$, whereas Instance C (Scenario 2) returned a design with 19 trays and $D_e = 0.747m$. The economic results for Scenario 4 show an increase of one order of magnitude in the total cost with respect to the results in Scenario 2 (Table 5.2). Also, it is noted an increase of three orders of magnitude in the $I\bar{S}E$ for Scenario 4 with respect to the results in Scenarios 1 and 2.

Additionally, a comparison of the results in Scenarios 3 and 4 shows that the D-SDA converged to a smaller distillation column design, i.e., D_e is 37% smaller for the solution in Scenario 3 compared to the solution in Scenario 4; moreover, a design with fewer trays was computed using the D-SDA (Scenario 3) compared to the DSTO method (Scenario 4). Consequently, the total cost is higher in Scenario 4 with respect to Scenario 3, i.e., Scenario 4 returned a 64% higher total cost compared to Scenario 3. From a controllability point of view, the D-SDA returned a solution with an averaged ISE that is one order of magnitude smaller to the solution obtained with the DSTO method (Figure 5.4). Furthermore, note that the CPU times for Scenarios 3 and 4 are in the same orders of magnitude (Table 5.6), i.e., the CPU time in Scenario 3 is only 0.15% larger than the CPU time reported for Scenario 4.

The implementation of the D-SDA requires the solution of several FNLPs for the exploration

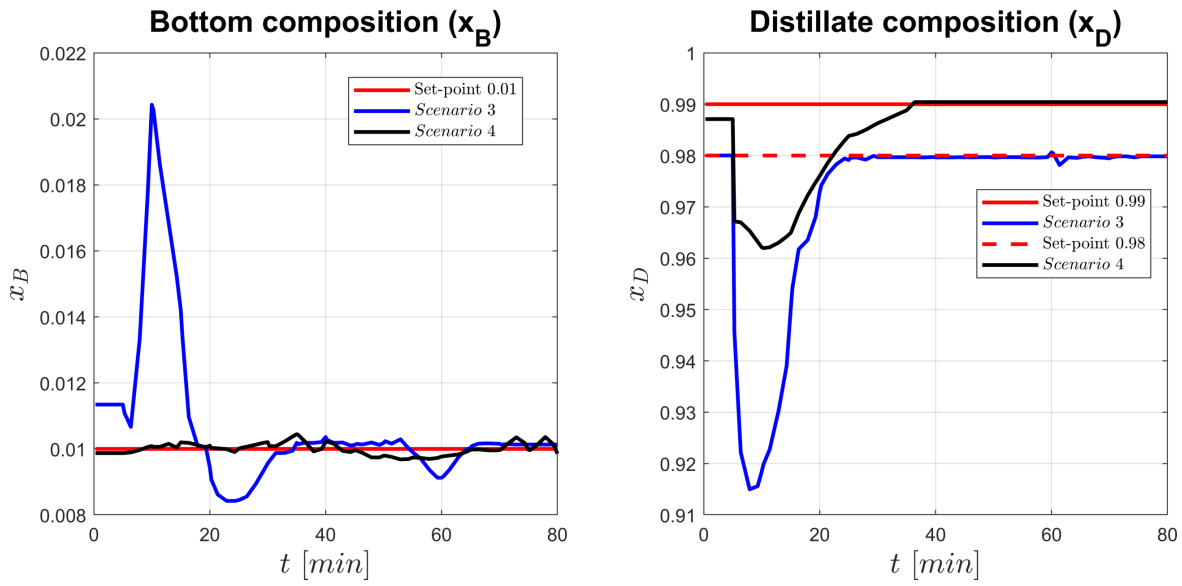

Figure 5.4: Concentration profiles of distillate and bottom for Scenarios 3 and 4 for the binary distillation column case study.

of the neighborhoods defined by the *external variables*. On the other hand, the DSTO method demands the solution of a highly nonconvex NLPs, i.e., the introduction of Gaussian functions in the DSTO method increases the nonconvexity of the optimization formulation. On the contrary, the FNLPs in the D-SDA approach are simpler formulations compared to the NLP in the DSTO method because all the logical constraints are not included in the FNLPs but in the *master* IPLC. Therefore, the DSTO method converged to local solutions that were closer to the initial point, whereas the D-SDA is able to circumvent this issue. Also, it was found that the presence of logical constraints, complementarity constraints, and Gaussian functions in the formulation for the DSTO method made the search harder for a solution of the corresponding NLP, i.e., the search for a solution to the NLP in the DSTO method demanded the proper selection of boundaries in most of the decision variables; otherwise, the NLP would produce convergence to low-quality local optima or overall lack of convergence. Note that the NLP solver and its configuration for tolerances was the same for both methods (i.e., D-SDA and DSTO) for all the scenarios. This was done to make a fair comparison between the proposed D-SDA and the DSTO algorithms.

5.6 Summary

The formulation for integrated design and NMPC-based control under uncertainty and structural decisions demands the solution of a MIBLP. In this chapter, a D-SDA approach to address the simultaneous design and NMPC-based control of process under uncertainty and naturally ordered structural decisions is proposed. The key idea is to implement an algorithm-based methodology to determine the optimal location of processing units or streams over a naturally ordered discrete set. In this methodology, the MIBLP is transformed into a single-level MINLP by the implementation of a KKT transformation strategy. The binary variables associated to the superstructure can be expressed as a function of reduced variable sets called *external variables*. This allows the decomposition of the single-level MINLP into a master (IPLC) and a set of primal sub-problems. The master problem is constructed from the *external variables* and solved with a D-SDA approach, whereas the primal sub-problems are conventional nonlinear problems (NLPs) obtained by fixing the binary variables according to the solution obtained from the master problem, i.e., the D-SDA executes a local search, in which the master problem explores the neighborhoods described by the external variables. This aims to determine a search direction that provides the steepest descent in the objective function. The proposed algorithmic framework does not follow the usual definition of convexity for integer programs, but it is based on the definition of integral convexity. Consequently, a steepest-descent direction strategy can be implemented to explore the discrete search space. Thus, the proposed D-SDA computes local solutions that cannot be efficiently identified using conventional MINLP solvers. Note that the decomposition strategy reduces the complexity of the formulation because all logical constraints are solved in the master problem; consequently, the primal sub-problems are simpler NLPs compared to the original MINLP. To compare the performance of the proposed D-SDA approach, an alternative well established methodology based on the DSTO method was implemented. In that methodology, the integer decisions in the single-level MINLP are allowed to be continuous variables in a DDF. Therefore, the resulting continuous formulation can be solved with conventional NLP solvers.

The D-SDA and DSTO methods were illustrated in a case study for the integration and NMPC-

based control under uncertainty and structural decisions for a binary distillation column. Results from the case study showed that the DSTO method converged to local solutions that were closer to the initialization point. On the other hand, the D-SDA allowed to skip sub-optimal solution regions because the framework does not demand the relaxation of the discrete variables.

Chapter 6

Selection and refinement of finite elements for the integration of design and control: A Hamiltonian function approach

The literature has pointed out that process dynamic performance is strongly coupled with process design decisions [103, 162]. In the integration of design and control framework, dynamic decision variables (e.g., controlled variables, manipulated variables, states, etc.) and static decision variables (e.g., equipment size, controller tuning parameters, etc.) are closely related.

This chapter describes a methodology for the selection and refinement of the discretization mesh for integrated design and control in formulations involving continuous variables, i.e., nonlinear programming (NLP) formulations. The discretization of the optimization problem is performed with OCFE. The proposed methodology improves the algorithm-based method introduced by Chen et al. [85] through the implementation of static and dynamic decision variables in the optimization formulation for integrated design and control, i.e., changes in the process design that modify the process dynamics are accounted. The proposed methodology features the relocation of finite elements and the systematic addition/elimination of finite elements. The Hamiltonian function and the estimation of the collocation error at noncollocation points are implemented as the criteria for the selection and refinement of the finite elements. Note that the implementation of further strategies for the selection and refinement of the finite elements for the discretization of the optimization formulation is out of the scope of this study. To the author's knowledge, studies addressing the accurate selection of finite elements using OCFE in the context of integration of design and control framework are not available.

The present chapter is organized as follows: Section 6.1 introduces the Mayer formulation of the problem for the integration of design and control. The algorithm for the refinement and selection of finite elements is detailed in Section 6.2. Section 6.3 illustrates the implementation of the proposed methodology in two case studies. A chapter summary is presented at the end in Section 6.4.

6.1 Problem for the integration of design and control

In this chapter, the optimization formulation for the integration of design and control is stated in terms of a DAE formulation as follows:

$$\min_{\eta,\mathbf{x}(t),\mathbf{u}(t),\mathbf{y}(t)} \Phi_d(\eta) + \psi_c(\eta, \mathbf{x}(t_f), \mathbf{u}(t_f), \mathbf{y}(t_f), \mathbf{d}_p(t_f), t_f) \tag{6.1a}$$

$$s.t.\ \ f(\eta, \dot{\mathbf{x}}(t), \mathbf{x}(t), \mathbf{u}(t), \mathbf{y}(t), \mathbf{d}_p(t)) = 0, \quad \mathbf{x}(t_0) = \mathbf{x}_0 \tag{6.1b}$$

$$\Phi_c(\eta, \dot{\psi}_c(t), \psi_c(t), \dot{\mathbf{x}}(t), \mathbf{x}(t), \mathbf{u}(t), \mathbf{y}(t), \mathbf{d}_p(t)) = 0, \quad \psi_c(t_0) = 0 \tag{6.1c}$$

$$h(\eta, \mathbf{x}(t), \mathbf{u}(t), \mathbf{y}(t), \mathbf{d}_p(t)) = 0, \tag{6.1d}$$

$$g(\eta, \mathbf{x}(t), \mathbf{u}(t), \mathbf{y}(t), \mathbf{d}_p(t)) \leq 0, \tag{6.1e}$$

$$\mathbf{u}^{lb} \leq \mathbf{u}(t) \leq \mathbf{u}^{ub},\ \mathbf{x}^{lb} \leq \mathbf{x}(t) \leq \mathbf{x}^{ub},\ t \in [t_0, t_f] \tag{6.1f}$$

where $h : \mathbb{R}^{N_x} \times \mathbb{R}^{N_u} \times \mathbb{R}^{N_\eta} \times \mathbb{R}^{N_y} \times \mathbb{R}^{N_d} \to \mathbb{R}^{N_h}$ and $g : \mathbb{R}^{N_x} \times \mathbb{R}^{N_u} \times \mathbb{R}^{N_\eta} \times \mathbb{R}^{N_y} \times \mathbb{R}^{N_d} \to \mathbb{R}^{N_s}$ represent the sets of equality and inequality constraints that define the feasibility region of the design problem, respectively; $f : \mathbb{R}^{2N_x} \times \mathbb{R}^{N_u} \times \mathbb{R}^{N_\eta} \times \mathbb{R}^{N_y} \times \mathbb{R}^{N_d} \to \mathbb{R}^{N_f}$ represents the dynamic process model; $\mathbf{x}(t) \in \mathbb{R}^{N_x}$ are the states of the system with derivatives indicated by $\dot{\mathbf{x}}(t)$. $\mathbf{u}(t) \in \mathbb{R}^{N_u}$ represents the vector of control actions. Vector $\mathbf{y}(t) \in \mathbb{R}^{N_y}$ is the vector of algebraic variables. The set of decision variables that do not depend on time ($\eta \in \mathbb{R}^{N_\eta}$) contains the process design variables (e.g., cross-sectional areas and equipment capacities) and the controller tuning parameters (e.g., proportional gains, integration reset constants and derivative time constants for a PID control). A set of deterministic disturbances $\mathbf{d}_p(t) \in \mathbb{R}^{N_d}$ is also included in the formulation. In the objective function, the first term $\Phi_d(\eta) \in \mathbb{R}^1_+$ represents an economic term that only depends on static decision variables, e.g., capital cost; whereas the second term $\psi_c : \mathbb{R}^{N_x} \times \mathbb{R}^{N_u} \times \mathbb{R}^{N_\eta} \times \mathbb{R}^{N_y} \times \mathbb{R}^{N_d} \to \mathbb{R}^1$ accounts for transient costs in the process operation, e.g., operating cost. The formulation in Equation (6.1) is stated as a "Mayer problem". The optimization formulation in Equation (6.1) can be stated in some other equivalent forms, e.g., Lagrange or Bolza formulations [20]. To transform Equation (6.1) into a Bolza formulation, differential Equation (6.1c) is moved to the objective function as an integral term replacing function ψ_c; whereas a Lagrange formulation requires only an

integral term in the objective function, i.e., no scalar terms such as function $\Phi_d(\eta)$ is present in the objective function. In this work, a Mayer formulation is adopted for simplicity; this allows a straightforward specification of the corresponding Hamiltonian function for the optimization problem (6.1). The implementation of other formulation is out of the scope of this study. Interested readers are encouraged to review [20] regarding the implementation of PMP in chemical engineering. The optimization problem (6.1) can be discretized with OCFE and solved with conventional NLP solvers. Traditionally, the number of finite elements is fixed and equidistributed (equally sized finite elements). Nevertheless, the accuracy in the selection of the number of finite elements is not taken into account while solving this problem. In the context of integration of design and control, there are no studies addressing an adequate selection of the discretization mesh for problem (6.1). As mentioned above, the implementation of PMP through the calculation of the Hamiltonina function may serve as a criterion for the selection of the finite elements. The Hamiltonian function is continuous and constant over time for autonomous systems; conversely, underestimation of the dicretization points may lead to non-constant profiles for the Hamiltonian function. This feature can determine the accuracy of the discretization for problem (6.1). The evaluation of the Hamiltonian function demands the solution of the first order necessary conditions for optimality. For the optimization model in Equation (6.1), Hamiltonian first order necessary conditions for optimality are stated in terms of a DAE problem. From the Mayer problem (6.1), the corresponding Hamiltonian function can be stated as follows:

$$\begin{aligned}\mathbb{H}(t) = \lambda_c \Phi_c(\eta, \dot{\psi}_c(t), \psi_c(t), \mathbf{x}(t), \mathbf{u}(t), \mathbf{y}(t), \mathbf{d}_p(t)) + \lambda(t)^\intercal f(\eta, \mathbf{x}(t), \mathbf{u}(t), \mathbf{y}(t), \mathbf{d}_p(t)) \\ + \nu(t)^\intercal h(\eta, \mathbf{x}(t), \mathbf{u}(t), \mathbf{y}(t), \mathbf{d}_p(t)) + \mu(t)^\intercal g(\eta, \mathbf{x}(t), \mathbf{u}(t), \mathbf{y}(t), \mathbf{d}_p(t)) + \gamma_u^L(t)^\intercal(\mathbf{u}^{lb} - \mathbf{u}(t)) \\ + \gamma_u^U(t)^\intercal(\mathbf{u}(t) - \mathbf{u}^{ub}) + \gamma_x^L(t)^\intercal(\mathbf{x}^{lb} - \mathbf{x}(t)) + \gamma_x^U(t)^\intercal(\mathbf{x}(t) - \mathbf{x}^{ub}) \quad (6.2)\end{aligned}$$

where $\lambda(t) \in \mathbb{R}^{N_\lambda}$, $\lambda_c(t) \in \mathbb{R}^{N_{\lambda_c}}$, $\nu(t) \in \mathbb{R}^{N_\nu}$, $\mu(t) \in \mathbb{R}_+^{N_\mu}$, $\gamma_u^L(t) \in \mathbb{R}_+^{N_{\gamma_u}}$, $\gamma_u^U(t) \in \mathbb{R}_+^{N_{\gamma_u}}$, $\gamma_x^{lb}(t) \in \mathbb{R}_+^{N_{\gamma_x}}$ and $\gamma_x^{ub}(t) \in \mathbb{R}_+^{N_{\gamma_x}}$ are adjoint variables that serve as multipliers on the constraints for the optimization formulation. From the Hamiltonian function $\mathbb{H}$: $\mathbb{R}^{2N_x} \times \mathbb{R}^{N_u} \times \mathbb{R}^{N_\eta} \times \mathbb{R}^{N_y} \times \mathbb{R}^{N_d} \times \mathbb{R}^{N_\lambda} \times \mathbb{R}^{N_{\lambda_c}} \times \mathbb{R}^{N_\nu} \times \mathbb{R}_+^{N_\mu} \times \mathbb{R}_+^{N_{\gamma_u}} \times \mathbb{R}_+^{N_{\gamma_x}} \to \mathbb{R}^{N_H}$ in Equation (6.2) the necessary conditions

for optimality for the problem (6.1) are as follows:

$$\frac{d\lambda(t)}{dt} = -\frac{\partial \mathbb{H}(t)}{\partial x}, \ \frac{d\lambda_{\mathbf{c}}(t)}{dt} = -\frac{\partial \mathbb{H}(t)}{\partial \psi} \tag{6.3a}$$

$$\frac{d\mathbf{x}(t)}{dt} = \frac{\partial \mathbb{H}(t)}{\partial \lambda} = f(\eta, \mathbf{x}(t), \mathbf{u}(t), \mathbf{y}(t), \mathbf{d}_p(t)), \quad x(t_0) = x_0 \tag{6.3b}$$

$$\frac{d\psi_c(t)}{dt} = \frac{\partial \mathbb{H}(t)}{\partial \lambda_c} = \Phi_c(\eta, \psi_c(t), \mathbf{x}(t), \mathbf{u}(t), \mathbf{y}(t), \mathbf{d}_p(t)), \quad \psi_c(t_0) = \psi_{c_0} \tag{6.3c}$$

$$\frac{\partial \mathbb{H}(t)}{\partial \nu} = h(\eta, \mathbf{x}(t), \mathbf{u}(t), \mathbf{y}(t), \mathbf{d}_p(t)) = 0, \tag{6.3d}$$

$$\frac{d\gamma(t)}{dt} = -\frac{\partial \mathbb{H}(t)}{\partial \eta}, \quad \gamma(t_0) = 0 \tag{6.3e}$$

$$\frac{\partial \mathbb{H}(t)}{\partial \mathbf{u}} = 0, \ \frac{\partial \mathbb{H}(t)}{\partial y} = 0 \tag{6.3f}$$

$$\lambda(t_f) = \frac{\partial \Phi(t_f)}{\partial \mathbf{x}} + \frac{\partial h(t_f)^{\intercal}}{\partial \mathbf{x}} \bar{b}, \ \ \gamma(t_f) = -\frac{\partial \Phi(t_f)}{\partial \eta} + \frac{\partial h(t_f)^{\intercal}}{\partial \eta}, \quad \lambda_{\mathbf{c}}(t_f) = 1 \tag{6.3g}$$

$$0 \leq \gamma_u^L(t) \perp (\mathbf{u}(t) - \mathbf{u}^{lb}) \geq 0, \ \ 0 \leq \gamma_u^U(t) \perp (\mathbf{u}^{ub} - \mathbf{u}(t)) \geq 0 \tag{6.3h}$$

$$0 \leq \gamma_x^L(t) \perp (\mathbf{x}(t) - \mathbf{x}^{lb}) \geq 0, \ \ 0 \leq \gamma_x^U(t) \perp (\mathbf{x}^{ub} - \mathbf{x}(t)) \geq 0 \tag{6.3i}$$

where $\gamma(t) \in \mathbb{R}^{N_\gamma}$ is a vector of auxiliary functions to account for the effect of the static decision variables on the optimality conditions. The formulation in Equation (6.3) represents the solution of a TPBVP. From the solution of the TPBVP, states, control laws, static variables, and adjoint variables are determined, which can then be used to evaluate the Hamiltonian function (6.2). The differential equations in the optimization formulation (6.1) can be transformed into a set of algebraic equations by the implementation of discretization techniques. This is described next.

6.1.1 Dicretized model: Orthogonal collocation on finite elements

In OCFE, the approximation with polynomials satisfies the differential equations exactly at specific collocation points. In this study, OCFE strategy based on Lagrange polynomials using Radau collocation points is implemented. Note that the refinement strategy considered in this research for the finite elements does not depend on the selection of the trial function and polynomial roots in the OCFE; therefore, other polynomials and roots may be chosen. The OCFE approach requires $K + 1$ interpolation points to approximate the states ($\mathbf{x}(t) \in \mathbb{R}^{N_x}$) in a given finite element i.

The approximation of the system states (Equations (6.3b) and (6.3c)) using Lagrange interpolation polynomials is as follows:

$$x_k(t) = \sum_{k=0}^{K} \ell_k(\tau) x_{i,k}, \;\; \ell_k(\tau) = \prod_{j=0,\neq k}^{K} \frac{(\tau - \tau_j)}{(\tau_k - \tau_j)}, \;\; t \in [t_{i-1}, t_i], \;\; \tau \in [0,1] \tag{6.4}$$

where $t = t_{i-1} + \bar{\alpha}_i \tau$, $\tau_0 = 0$, $0 < \tau_k \leq 1$, $k = \{1, \ldots, K\}$ are shifted Radau points and $\bar{\alpha}_i$ is the length of the i^{th} finite element. OCFE with Radau points has the property that $x(t_{i,k}) = x_{i,k}$, where $t_{i,k} = t_{i-1} + \tau_k \bar{\alpha}_i$. The length of each finite element i is given by $\bar{\alpha}_i$. Moreover, Radau collocation points feature a better numerical stability compared with other frameworks such as Gauss collocation points [163]. Nevertheless, Gauss collocation points can achieve a higher algebraic precision ($O(\bar{\alpha}_i^{K+2})$). *Lagrange* polynomials offer the feature to produce physically meaningful quantities (e.g., temperatures, concentrations, etc.). Note that other polynomials such as power series polynomials or B-splines do not offer these features [114]. The corresponding discretized formulation with OCFE for the optimization problem shown in (6.5) is as follows:

$$\min_{\eta, x_{i,k}, \bar{u}_{i,k}, y_{i,k}} \Phi_d(\eta) + \psi_c(\eta, x_{N_{FE},K}, u_{N_{FE},K}, y_{N_{FE},K}, d_{p_{N_{FE},K}}) \tag{6.5a}$$

$$s.t. \sum_{j=0}^{K} \dot{\ell}_j(\tau_k) x_{i,j} - \bar{\alpha}_i f(\eta, x_{i,k}, u_{i,k}, y_{i,k}, d_{p_{i,k}}) = 0, \;\; \forall\, k = \{1, \ldots, K\}, \; i = \{1, \ldots, N_{FE}\} \tag{6.5b}$$

$$\sum_{j=0}^{K} \dot{\ell}_j(\tau_k) \psi_{c_{i,j}} - \bar{\alpha}_i \Phi_c(\eta, x_{i,k}, u_{i,k}, y_{i,k}, d_{p_{i,k}}) = 0, \;\; \forall\, k = \{1, \ldots, K\}, \; i = \{1, \ldots, N_{FE}\} \tag{6.5c}$$

$$h(\eta, x_{i,k}, u_{i,k}, y_{i,k}, d_{p_{i,k}}) = 0, \;\; \forall\, k = \{1, \ldots, K\}, \; i = \{1, \ldots, N_{FE}\} \tag{6.5d}$$

$$g(\eta, x_{i,k}, u_{i,k}, y_{i,k}, d_{p_{i,k}}) \leq 0, \;\; \forall\, k = \{1, \ldots, K\}, \; i = \{1, \ldots, N_{FE}\} \tag{6.5e}$$

$$x_{i+1,0} = \sum_{j=0}^{K} \ell_j(1) x_{i,j}, \;\; i = \{1, \ldots, N_{FE} - 1\} \tag{6.5f}$$

$$x_f = \sum_{j=0}^{K} \ell_k(1) x_{N_{FE},j}, \;\; x_{1,0} = x(t_0) \tag{6.5g}$$

$$\mathbf{u}^{lb} \leq u_{i,k} \leq \mathbf{u}^{ub}, \;\; \mathbf{x}^{lb} \leq x_{i,j} \leq \mathbf{x}^{ub}, \;\; \forall\, k = \{1, \ldots, K\}, \; i = \{1, \ldots, N_{FE}\} \tag{6.5h}$$

where $\dot{\ell}_k(\tau)$ is the derivative of the *Lagrange* polynomials (i.e., $\dot{\ell}_k(\tau) = \frac{d\ell_k(\tau)}{d\tau}$), finite elements and collocation points are indexed by i and k, respectively. Note that index j is an alias of index k. If the finite elements are sufficiently small in length, the discretized formulation in Equation

(6.5) provides an accurate approximation to the optimization problem in Equation (6.1) [145]. The size of the optimization problem depends on the selection of the number collocation points (K) and the number of finite elements (N_{FE}). Thus, conventional NLP solvers can be implemented for the solution of the discretized problem (6.5). Similarly, the Hamiltonian function and the optimality conditions in Equations (6.3) and (6.2) can be discretized using OCFE, respectively. A complete review of the development, features, and numerical properties of OCFE can be found elsewhere [145, 17, 164].

6.1.2 Estimation of the collocation error

Optimization formulations that are discretized with equidistributed finite elements (i.e., same size finite elements $\bar{\alpha}_1 = \bar{\alpha}_1 = \ldots = \bar{\alpha}_I$) are generally easier to solve [18]. Nevertheless, by allowing the finite elements to "move" (i.e., finite elements are allowed to change in size), the finite elements can concentrate in those regions where states profiles experience large variations in the states gradients. This may provide a more accurate approximation to the differential equations in the optimization problem (6.1) with fewer finite elements. Note that the formulation in Equation (6.1) considers continuous process design and control decisions. The implementation of discrete controllers (control actions defined by sampling intervals) may affect the distribution of the discretization points by restricting the discretization of states in defined sampling intervals. Discrete control schemes such as discrete-PID or MPC/NMPC is out of the scope of this research. To allow the finite elements to move, it becomes necessary to estimate the collocation error via the implementation of a *monitor function* [121]. These functions can be constructed in different ways: i) estimate error using correlations to determine the arclength or curvature of the functions; ii) estimate error such as solution residuals or the estimation of derivative jumps on the element boundaries; and iii) error estimation based on the *physics* of the problem [165]. Interested readers are encouraged to consult the work presented by Budd et al. [121] to know more about monitor functions in moving grids for discretization. In this study, the collocation error is estimated using the information embedded in the polynomials of the discretization strategy (a posteriori error estimation strategy), i.e., the residuals are evaluated at noncollocation points (τ_{nc}). This approach was selected because avoids

the use of additional correlations for the estimation of the collocation error compared with other strategies. The global collocation error ($e_c(t) = \mathbf{x}(t) - \mathbf{x}^p(t)$), in the discretization of the DAE-based formulation (Equation (6.5)), satisfies the following local equalities [120]:

$$\|e_{c_i}(t)\| \leqq \bar{C}_{nc}\bar{\alpha}_i\|\Lambda_i(t_{i,nc})\| + O(\bar{\alpha}^{k+1}) \tag{6.6}$$

where $\mathbf{x}^p(t)$ represents the approximated discrete solution of states ($\mathbf{x}(t)$). $\Lambda_i(t_{i,nc})$ is called a monitor function of i^{th} finite element evaluated at the nc^{th} noncollocation point, $\bar{C}_{nc}$ is a constant that depends on noncollocation points. In the open literature, there are multiple options to define Λ_i, a complete review on the selection of function Λ_i can be found elsewhere [120]. In this study, function Λ_i is directly evaluated from the residuals of the DAE model (Equations (6.5b)-(6.5e)) at noncollocation points $t_{i,nc}$ as follows:

$$\Lambda_i(t_{i,nc}) = \begin{bmatrix} \frac{dx_{i,nc}}{d\tau}(t_{i,nc}) - \bar{\alpha}_i f(\eta, x_{i,nc}, \bar{u}_i, y_{i,nc}, d_{p_{i,nc}}) \\ h(\eta, x_{i,nc}, \bar{u}_i, y_{i,nc}, d_{p_{i,nc}}) \\ g(\eta, x_{i,nc}, \bar{u}_i, y_{i,nc}, d_{p_{i,nc}}) \end{bmatrix} \quad i = \{1, \ldots, N_{FE}\}, \;\; nc = \{1, \ldots, NC\} \tag{6.7}$$

$$\bar{C}_{nc} = \frac{1}{\bar{A}_{nc}} \int_0^{\tau_{nc}} \prod_{k=1}^{K} (\iota - \tau_k) d\iota, \;\; \bar{A}_{nc} = \prod_{k=1}^{K} (\tau_{nc} - \tau_k) \tag{6.8}$$

where $t_{i,nc} = t_{i-1} + \bar{\alpha}_i\tau_{nc}$, $\tau_{nc} \in [0, 1]$. At collocation points, the function Λ_i will be zero; therefore, $\tau_{nc} \neq \tau_k$. Then, the approximation error is estimated to be $\|e_{ci}(t)\| \leq \bar{C}_{nc}\|\Lambda_i(t_{i,nc})\|$. If an error tolerance (ϵ_Λ) is assigned to the estimation of the collocation error, finite elements can be adjusted such that the following constraint is satisfied:

$$\bar{C}_{nc}\|\Lambda_i(t_{i,nc})\| \leq \epsilon_\Lambda \tag{6.9}$$

6.2 Algorithmic framework

This section describes the proposed methodology to address the refinement and selection of the number of finite elements for integration of design and control. The strategy consists in the iterative

solution of optimization problems to determine if the finite elements are moved, eliminated, or added to the formulation for simultaneous design and control. To do so, the present algorithm identifies those sections where the residual error of the collocation strategy or the constant profile over time of the Hamiltonian function are not achieved. Algorithm 2 and Figure 6.1 present the proposed algorithm for the refinement of the discretization mesh in the integration of design and control framework. As shown in Algorithm 2, a feasible distribution and number of finite elements is calculated in the first stage. This initial calculation is carried out by the recursive solution of the formulation for optimal design and control given an estimated control law ($\mathbf{u}(t)$), a process design, and constrained by the monitor function Λ_i. In a second stage, the problem of simultaneous design and control is solved using a fixed size and number of finite elements. In the third stage, the size of the finite elements is refined based on the criteria of function Λ_i and the Hamiltonian function $\mathbb{H}(t)$. If the criteria is not satisfied, the number of finite elements is recalculated, as shown in Algorithm 2. Finite elements can be bisected in those regions where the Hamiltonian function is not constant, whereas relatively small finite elements may be removed. The problem converges if the criteria of function Λ_i and $\mathbb{H}(t)$ is satisfied. The detailed description of each stage in the algorithm is presented next.

6.2.1 Stage 1: Initialization

The algorithm is initialized by setting the iteration index $r_e = 1$; the tolerance for the estimation of the collocation error in Stage 1 (ϵ_Λ^s); and the maximum number of iteration (N_r). Moreover, additional parameters are defined as follows: the tolerance for the Hamiltonian function profile (ϵ_H), which aims to determine if function is constant over time; the step-size for sensitivity calculations ($\Delta\bar{\alpha}$), which determines the gradients of the decision variables; the tolerance for the estimation of the collocation error in Stage 3 (ϵ_Λ) that aims to improve the refinement of finite elements from Stage 1; and the search space region for the finite elements (δ) in the refinement stage (Stage 3). In this first stage, a feasible initial discretization mesh is calculated by the solution of a sequence of NLPs. The initialization accounts for the residual DAEs at noncollocation points given the dicretized model of the process (Equation (6.5)). The aim is to maximize the length of each finite element such

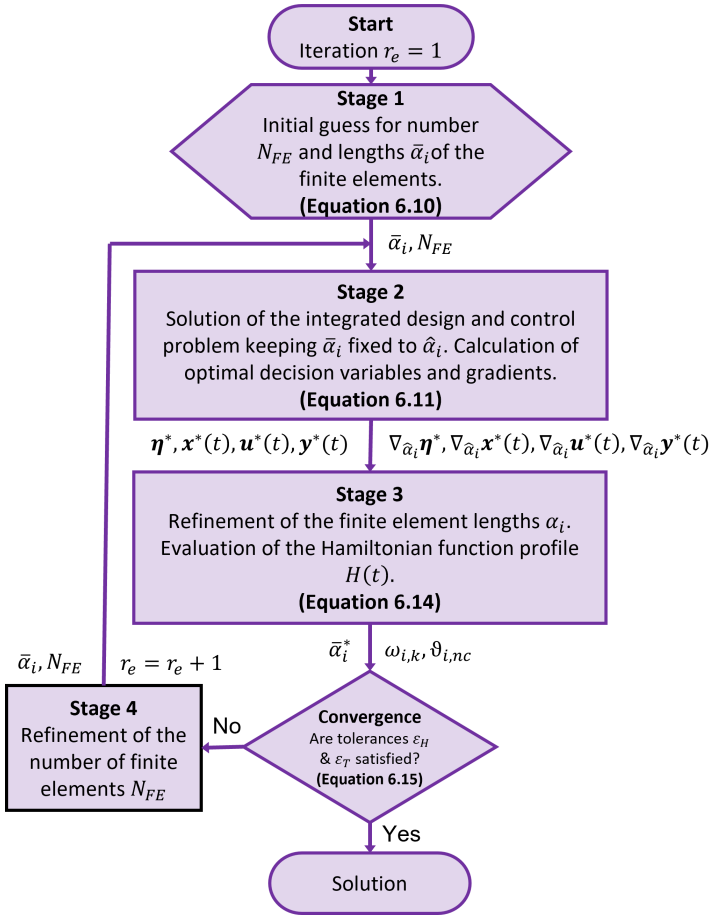

Figure 6.1: Algorithm for the refinement of the discretization mesh on the integration of design and control.

that the approximation error at noncollocation points remain below a user defined tolerance (ϵ_Λ^s); this reduces the number of finite elements required in the discretization. The initialization stage requires of an initial guess for the process design (η_{init}) and control actions ($\bar{\mathbf{u}}_{init}(t)$). The initial guess for η and $\bar{\mathbf{u}}(t)$ can be obtained by solving the problem in Equation (6.5) using equidistributed finite elements. This allows the algorithm to obtain feasible guesses for process design and control actions. The formulation of the optimization problems for the initialization stage is as follows:

$$\hat{\alpha}_i = \max \bar{\alpha}_i \tag{6.10a}$$

$$s.t. \sum_{j=0}^{K} \dot{\ell}_j(\tau_k) x_j - \bar{\alpha}_i f(\eta_{init}, x_k, \bar{\mathbf{u}}_{init}, y_k, d_{p_k}) = 0, \;\; x_0 = x_{i-1,K} \;\forall\, k = \{1, \ldots, K\} \tag{6.10b}$$

$$h(\eta_{init}, x_k, \bar{\mathbf{u}}_{init}, y_k, d_{p_k}) = 0, \;\forall\, k = \{1, \ldots, K\} \tag{6.10c}$$

$$-\epsilon_{\Lambda}^{s} \leq \bar{C}_{nc}\Lambda_i(t_{i,nc}) \leq \epsilon_{\Lambda}^{s} \tag{6.10d}$$

$$0 \leq \bar{\alpha}_i \leq \min\left(\bar{\alpha}_{max}, t_f - \sum_{i=1}^{i-1}\hat{\alpha}_i\right) \tag{6.10e}$$

This problem is solved piecewise to determine the size of i^{th} finite element ($\hat{\alpha}_i$), i.e., Equation (6.10) determines the size of a single finite element at a time. Note that initial values for ODEs are given by x_0. These values correspond to the last point of a previous iteration of Equation (6.10), i.e., $x_{i-1,K}$ (states at the last collocation point K in the $(i-1)^{th}$ finite element). The initialization problem (Equation(6.10)) is solved N_{FE} times until the summation of the length of finite elements is equal to the simulation time horizon, i.e., $\sum_{i=1}^{N}\bar{\alpha}_i = t_f$. Therefore, the initial number of finite elements corresponds to N_{FE}. In this stage, it is recommended to select relatively large tolerances, e.g., $\epsilon_{\Lambda}^{s} > 1 \times 10^{-3}$; this selection reduces the initial number of finite elements. Then, the algorithm can refine and increase the number of finite elements (if needed) in the following stages.

6.2.2 Stage 2: Integrated design and control problem

In this stage, the monitor function (residual function) Λ_i is appended to the integration of design and control problem shown in Equation (6.5). In the formulation for stage 2, the length and number of finite elements are fixed to the values determined in Stage 1, i.e., $\bar{\alpha}_i = \hat{\alpha}_i$ with N_{FE} finite elements. The problem formulation for stage 2 is as follows:

$$\min_{\eta, x_{i,j}, u_{i,j}, y_{i,j}} \Phi_d(\eta) + \psi_c(\eta, x_{N_{FE},K}, u_{N_{FE},K}, y_{N_{FE},K}, d_{p_{N_{FE},K}}) \tag{6.11a}$$

$$s.t. \sum_{j=0}^{K}\dot{\ell}_j(\tau_k)x_{i,j} - \hat{\alpha}_i f(\eta, x_{i,k}, u_{i,k}, y_{i,k}, d_{p_{i,k}}) = 0,\ \forall\, k = \{1,\ldots,K\},\ i = \{1,\ldots,N_{FE}\}, \tag{6.11b}$$

$$\sum_{j=0}^{K}\dot{\ell}_j(\tau_k)\psi_{c_{i,j}} - \hat{\alpha}_i \Phi_c(\eta, x_{i,k}, u_{i,k}, y_{i,k}, d_{p_{i,k}}) = 0,\ \forall\, k = \{1,\ldots,K\},\ i = \{1,\ldots,N_{FE}\} \tag{6.11c}$$

$$h(\eta, x_{i,k}, u_{i,k}, y_{i,k}, d_{p_{i,k}}) = 0,\ \forall\, k = \{1,\ldots,K\},\ i = \{1,\ldots,N_{FE}\}, \tag{6.11d}$$

$$g(\eta, x_{i,k}, u_{i,k}, y_{i,k}, d_{p_{i,k}}) \leq 0,\ \forall\, k = \{1,\ldots,K\},\ i = \{1,\ldots,N_{FE}\}, \tag{6.11e}$$

$$x_{i+1,0} = \sum_{k=0}^{K} \ell_k(1) x_{i,k}, \;\; \psi_{c_{i+1,0}} = \sum_{k=0}^{K} \ell_k(1) \psi_{c_{i,k}}, \; i = \{1, \ldots, N_{FE} - 1\}, \tag{6.11f}$$

$$x_f = \sum_{k=0}^{K} \ell_k(1) x_{I,k}, \;\; \psi_{c_f} = \sum_{k=0}^{K} \ell_k(1) \psi_{c_{N_{FE},k}} \;\; x_{1,0} = x(t_0) \tag{6.11g}$$

$$\Lambda_i(t_{i,nc}) = \begin{bmatrix} \frac{dx_{i,nc}}{d\tau}(t_{i,nc}) - \hat{\alpha}_i f(\eta, x_{i,nc}, u_{i,nc}, y_{i,nc}, d_{p_{i,nc}}) \\ h(\eta, x_{i,nc}, u_{i,nc}, y_{i,nc}, d_{p_{i,nc}}) \\ g(\eta, x_{i,nc}, u_{i,nc}, y_{i,nc}, d_{p_{i,nc}}) \end{bmatrix} \;\; i = \{1, \ldots, N_{FE}\}, \; nc = \{1, \ldots, NC\} \tag{6.11h}$$

Optimal solution for the decision variables $(\eta^*, \mathbf{x}^*(t), \mathbf{u}^*(t), \mathbf{y}^*(t))$ are obtained from the solution of Equation (6.11). Note that function Λ_i is not constrained, as shown in Equation (6.11h). Therefore, the solution of this optimization problem is straightforward since function Λ_i is being only evaluated. In this stage, it is necessary to calculate the gradients of the decision variables with respect to the size of each finite element, i.e., $\nabla_{\hat{\alpha}_i}\eta, \nabla_{\hat{\alpha}_i} x(t), \nabla_{\hat{\alpha}_i} u(t), \nabla_{\hat{\alpha}_i} y(t)$. To evaluate these gradients, forward $(\hat{\alpha}^+)$ and backward $(\hat{\alpha}^-)$ point evaluations of the finite elements are enforced around the nominal sizes of the finite elements $(\hat{\alpha})$. Then, the optimization problem (6.11) is systematically solved where each of the finite elements is set to $\hat{\alpha}_i^+$ and $\hat{\alpha}_i^-$ at a time, respectively, i.e., the optimization problem is solved assigning the i^{th} finite element $\bar{\alpha}_i = \hat{\alpha}_i^+$ or $\bar{\alpha}_i = \hat{\alpha}_i^-$ while keeping the rest of the finite elements constant and equal to their nominal values $(\hat{\alpha}_i)$. Therefore, the optimization problem in Equation (6.11) is solved $2N_{FE}$ times to determine the sensitivity of the decision variables with respect to the size of each finite element, i.e., first order gradients can thus be calculated using finite differences as follows:

$$\frac{\partial \mathbf{x}^*}{\partial \bar{\alpha}} \mid_{\hat{\alpha}} = \frac{\left(\mathbf{x}^*\left(\bar{\alpha}^+\right) \mid_{\hat{\alpha}} - \mathbf{x}^*\left(\bar{\alpha}^-\right) \mid_{\hat{\alpha}}\right)}{\Delta \bar{\alpha}} \tag{6.12}$$

where $\Delta\bar{\alpha}$ represents the difference between the forward step $(\hat{\alpha}_i^+)$ and the backward step $(\hat{\alpha}_i^-)$ for the i^{th} finite element. The gradients for the remaining decision variables are calculated in

a similar fashion. Note that these gradients are only valid around the nominal point $\bar{\alpha}_i = \hat{\alpha}_i$. Higher order gradients can be calculated but additional forward and backward evaluations around the nominal points are needed thus increasing the computational costs. Recommended values for $\Delta\bar{\alpha}$ can be $0.001\hat{\alpha}_i \leq \Delta\bar{\alpha} \leq 0.1\hat{\alpha}_i$. Further details on the calculation of sensitivity gradients and the selection of parameter $\Delta\bar{\alpha}$ can be found elsewhere [127]. Alternative options such as the implementation of analytic derivatives together with optimization solvers such as sIPOPT may reduce the computational burden [166]. Numerical alternatives such as automatic differentiation arise as a promising alternative for the determination of sensitivity gradients [167]. The potential of this numerical technique is out of the scope of this work; however, it will be considered as part of the future work.

6.2.3 Stage 3: Refinement of finite element sizes

As explained above, the Hamiltonian function must be continuous and constant over time for autonomous systems with optimized control actions ($\mathbf{u}^*(t)$) in the context of the simultaneous design and control tuning problems considered in this study and an accurate discretization mesh. Calculation of the Hamiltonian function depends on the solution of Equation (6.3), these optimality conditions provide information about adjoint variables ($\lambda(t)$, $\nu(t)$, $\mu(t)$, $\gamma_u^L(t)$, $\gamma_u^U(t)$, $\gamma_x^L(t)$ and $\gamma_x^U(t)$). Kameswaran and Biegler [168] showed that the KKT multipliers from the solution of Equation (6.11) provide an $O(\bar{\alpha}^K)$ approximation to the adjoint variables calculated in Equation (6.3). In this stage, the decision variables and the adjoint variables can be evaluated in terms of the size of the finite elements depending on the order of the gradients determined in the previous stage, i.e.,

$$\mathbf{x}(\bar{\alpha}) \mid_{\hat{\alpha}} = \mathbf{x}^*(\hat{\alpha}) + \sum_{k_l=1}^{\infty} \frac{1}{k_l!} \nabla^{k_l}\mathbf{x}(\bar{\alpha}) \mid_{\hat{\alpha}} (\bar{\alpha} - \hat{\alpha})^{k_l} \tag{6.13}$$

where $\nabla^{k_l}\mathbf{x}(\bar{\alpha})$ is the k_l^{th}-order gradient for the states ($\mathbf{x}$). Gradients are calculated with respect to the length of the finite elements ($\bar{\alpha}$) and evaluated at the nominal mesh distribution (i.e., $\hat{\alpha}$). $\mathbf{x}^*$ corresponds to the optimal values of the states obtained from the solution of Equation (6.11) (see Algorithm 2). The rest of the decision variables and adjoint variables are evaluated in terms of the

size of the finite elements in the same fashion. Consequently, the Hamiltonian function in Equation (6.2) can be stated as a function of the size of the finite elements, i.e., $\mathbb{H}(\bar{\alpha})$. The Hamiltonian function can then be implemented as a physical criterion of the refinement of the length of the finite elements by enforcing the condition that this function must be constant over time [169]. Thus, the size of the finite elements can be refined in terms of the criteria given by functions $\Lambda_i(\bar{\alpha})$ and $\mathbb{H}(\bar{\alpha})$. To do so, the economic objective function (Equation (6.11a)) is optimized and constrained by the criteria given by functions $\Lambda_i(\bar{\alpha})$ and $\mathbb{H}(\bar{\alpha})$ whereas the decision variables are the lengths of the finite elements ($\bar{\alpha}$). Therefore, the optimization problem for the refinement of the length of the finite elements is as follows:

$$\min_{\bar{\alpha}_i,\omega_{i,k},\vartheta_{i,nc},\bar{\mathbb{H}}} \Phi_d(\eta(\bar{\alpha}_i)) + \psi_c(x_{I,K}(\bar{\alpha}_i), u_{I,K}(\bar{\alpha}_i), y_{I,K}(\bar{\alpha}_i), d_{p_{I,K}}) + \bar{M}\left(\sum_{i=1}^{I}\sum_{k=1}^{K}\omega_{i,k} + \sum_{i=1}^{I}\sum_{nc=1}^{NC}\vartheta_{i,nc}\right) \quad (6.14a)$$

$$-(\vartheta_{i,nc}+\epsilon_\Lambda) \leq \bar{C}_{nc}\Lambda_i(\bar{\alpha}_i) \leq (\vartheta_{i,nc}+\epsilon_\Lambda),\ \ \vartheta_{i,nc} \geq 0,\ \ i=\{1,\ldots,N_{FE}\},\ nc=\{1,\ldots,NC\} \quad (6.14b)$$

$$-(\omega_{i,k}+\epsilon_H) \leq \mathbb{H}(\bar{\alpha}_i) - \bar{\mathbb{H}} \leq (\omega_{i,k}+\epsilon_H),\ \ \omega_{i,k} \geq 0,\ \ i=\{1,\ldots,N_{FE}\},\ k=\{1,\ldots,K\} \quad (6.14c)$$

$$\max(0, \hat{\alpha}_i(1-\delta)) \leq \bar{\alpha}_i \leq \hat{\alpha}_i(1+\delta) \quad (6.14d)$$

$$\sum_{i=1}^{I}\bar{\alpha}_i = t_f \quad (6.14e)$$

where $\omega_{i,k} \in \mathbb{R}^1_+$ and $\vartheta_{i,nc} \in \mathbb{R}^1_+$ are dummy variables that are necessary to ensure feasibility in the solution of the formulation in Equation (6.14). ϵ_Λ and ϵ_H are error tolerances for the approximation in the OCFE strategy and the Hamiltonian profile, respectively. The variable $\bar{\mathbb{H}}$ aims to enforce the Hamiltonian function profile to be constant over time. If the Hamiltonian function profile ($\mathbb{H}(\bar{\alpha}_i)$) is not constant over time, the artificial variable $\omega_{i,k}$ will take values different from zero, i.e., $\omega_{i,k} > 0$; likewise, if the approximation error accounted by the residual function Λ_i is greater than the tolerance (ϵ_Λ), the artificial variable $\vartheta_{i,nc}$ will be greater than zero ($\vartheta_{i,nc} > 0$). Since stage 3 aims to improve the sizing of finite elements across the iterations of the algorithm, the tolerance for the estimation of the collocation error must be improved with respect to the collocation tolerance in Stage 1, i.e., $\epsilon_\Lambda < \epsilon^s_\Lambda$. Note that the dummy variables are added to the cost function

as a term penalized by $\bar{M} > 0$. The magnitude of this penalty parameter ($\bar{M}$) is not know *a priori*. A strategy for the selection of this penalty term is to consider the magnitude of the adjoint variables, i.e., $\bar{M} \geq \|\boldsymbol{\Xi}\|_\infty$, where $\boldsymbol{\Xi} = [\lambda(t), \nu(t), \mu(t), \gamma_u^L(t), \gamma_u^U(t), \gamma_x^L(t), \gamma_x^U(t)]$. From Equation (6.14d), it can be observed that the bounds for the search space in the optimization formulation are given by the parameter δ. This parameter serves as an indicator of the region of feasibility of the approximation for the design and control variables, and the adjoint variables (Equation (6.13)). The approximation expressions stated in Equation (6.13) are only valid around the nominal length of the finite elements and the optimal solution of the optimization problem in Equation (6.11).

6.2.4 Stage 4: Refinement of the number of finite elements

The methodology adds finite elements in sections where the Hamiltonian function profile $\mathbb{H}(t)$ is not constant over time or the collocation error criterion is not satisfied, i.e., sections where the dummy variables in Stage 3 are $\omega_{i,k} > 0$ and $\vartheta_{i,nc} > 0$, respectively. The strategy proposed in this work consists of the bisection of the finite elements where the dummy variables $\omega_{i,k} \neq 0$ and $\vartheta_{i,nc} \neq 0$. Similarly, it is accounted for the standard deviation (σ) of the lengths of the finite element to determine if a finite element should be removed or not, i.e., relatively small finite elements are removed from the formulation. Thus, the heuristics for the the refinement of the number of finite elements (addition/elimination) are as follows:

- If the artificial variable $\omega_{i,k} > 0$ or $\vartheta_{i,nc} > 0$, then the i^{th} finite element is bisected.

- If i^{th} finite element has a length $\bar{\alpha}_i < \bar{a}\sigma$, then this finite element is merged to the $i^{th} + 1$ finite element. Where $\bar{a} \in \mathbb{R}_+$ is a multiplier to determine the confidence interval for finite element merging. The selection of this parameter determines the sensitivity of the algorithm to remove finite elements. A suggested selection for this parameter is $\bar{a} \geq 1$. Note that setting $\bar{a} < 1$ may merge relatively large finite elements, which may be difficult to accomplish with the collocation error criterion. Moreover, increasing the magnitude of $\bar{a}$ (e.g., $\bar{a} >> 1$) may

also increase the number of finite elements thereby increasing the computational burden in the algorithm.

The implementation of these heuristics returns a refined number of finite elements N_{FE}^{*} with corresponding lengths $\bar{\alpha}_i^{*}$.

6.2.5 Convergence criteria

As shown in Algorithm 2, the values obtained from Stage 3 for $\omega_{i,k}$ and $\vartheta_{i,nc}$ are used to determine if a suitable number of elements, and their sizes, have been found. If $\omega_{i,k}$ and $\vartheta_{i,nc}$ are equal to zero in all the discretization points and the noncollocation points, then stop, an optimal solution has been found, i.e., the criteria for the residual function Λ_i and the Hamiltonian function profile $\mathbb{H}(t)$ comply with the tolerances for the approximation in the OCFE strategy:

$$-\epsilon_H \leq \mathbb{H}(\bar{\alpha}) - \bar{\mathbb{H}} \leq \epsilon_H, \;\; -\epsilon_\Lambda \leq \bar{C}_{nc}\Lambda_i(\bar{\alpha}) \leq \epsilon_\Lambda \tag{6.15}$$

Otherwise, if the convergence criteria stated in Equation (6.15) is not satisfied, the number of finite elements is refined as described above in Stage 4. The refined finite elements in Stage 4 are set as the new estimation, i.e., N_{FE} and $\bar{\alpha}_i$ for the next iteration $r_e = r_e + 1$, respectively. Then, return to Step 2. This procedure continues until the convergence criteria is met or the maximum number of iterations (N_r) is reached. As mentioned in section 6.2.1, it is recommended to select a relatively large tolerance ϵ_Λ in the initialization stage. This aims to estimate a small initial number of finite elements. Then, the algorithm can increase and refine the finite elements until the convergence criteria is satisfied. If a unnecessary large number of finite elements is given at the initialization stage, there is the possibility that the convergence criteria is satisfied but a minimum of finite elements is not guaranteed, e.g., assume a refined solution retrieved from the refinement algorithm with N_{FE}^{*} and $\bar{\alpha}_i^{*}$, if all the finite elements are bisected (i.e., $2N_{FE}^{*}$ and $\bar{\alpha}_i^{*}/2$) the criteria of functions Λ_i and $\mathbb{H}(t)$ is still satisfied, but the number of finite elements was increased to $2N_{FE}^{*}$. If the algorithm converges in the first iteration, it is recommended to increase ϵ_Λ for Stage 1. The

algorithm presented in this chapter assumes that there are no integer decisions in the optimal design and control formulation.

As described above, convergence of the algorithm depends on minimization of the collocation error and the reduction of fluctuations in the Hamiltonian function profile to acceptable tolerances, i.e., tolerances ϵ_Λ and ϵ_H must be satisfied. Convergence of the algorithm may not be guaranteed due to relatively small tolerances for the collocation error (ϵ_Λ) may not be achieved with a finite number finite elements, i.e., the collocation error is not indefinitely improved if the number of finite elements are increased indefinitely. Wright [119] compared five adaptive methods for discretization refinement. They found that increasing the number of discretization points may not improve the estimation of the collocation error. Thus, the selection of tolerance ϵ_Λ plays a relevant role in the convergence of the proposed algorithm. Therefore, relatively small values on ϵ_Λ may not be possible to achieve by increasing indefinitely the number of finite elements. Wright [119] also found that the discretization of differential equations has an asymptotical behavior in the approximation error; thus, increasing the number of discretization points does not improve the approximation indefinitely. The selection of ϵ_Λ may depend on the scale of the process, the smoothness and stiffness of the differential equations, etc.; for example, processes with small time constants that experience large sudden changes to small variations in the process conditions may demand the implementation of relatively small finite elements to accurately describe the process dynamics; these scenarios are observed in most of the chemical processes. Further analysis on the estimation of the collocation error and selection of tolerance ϵ_Λ can be found elsewhere [116]. The later convergence criterion requires that the discretization mesh guarantees the accurate approximation of the control trajectories that satisfy the tolerance ϵ_H for the Hamiltonian function profile. However, there is not rigorous proof that the discretization of problem (6.1) (i.e., a Mayer problem) with a finite number of finite elements will always return a continuous over time Hamiltonian function profile. Nevertheless, some guidelines are provided for the termination of the iterative procedure. These guidelines ensure the convergence to a solution that satisfies the user-defined tolerances (ϵ_Λ and ϵ_H) or increases the magnitude of the tolerances such that they can be satisfied. These guidelines are as follows:

- If after NR consecutive iterations of the algorithm there are no changes in $\vartheta_{i,nc}$ (i.e., if $GRD_{\Lambda} = (\vartheta_{i,nc})_{r_e} - (\vartheta_{i,nc})_{r_e-1} = 0$ after NR consecutive iterations), then increase ϵ_{Λ} by an order of magnitude (i.e., $\epsilon_{\Lambda} = 10\,(\epsilon_{\Lambda})$).

- If after NR consecutive iterations of the algorithm there are no changes in $\omega_{i,k}$ (i.e., if $GRD_H = (\omega_{i,k})_{r_e} - (\omega_{i,k})_{r_e-1} = 0$ after NR consecutive iterations), then increase ϵ_H by an order of magnitude (i.e., $\epsilon_H = 10\,(\epsilon_H)$).

- If after NR consecutive iterations of the algorithm the magnitude of $\omega_{i,k}$ or $\vartheta_{i,nc}$ increases (i.e., if $GRD_{\Lambda} = (\vartheta_{i,nc})_{r_e} - (\vartheta_{i,nc})_{r_e-1} > 0$ or $GRD_H = (\omega_{i,k})_{r_e} - (\omega_{i,k})_{r_e-1} > 0$ after NR consecutive iterations), then take the last number and lengths of finite elements in which $GRD_{\Lambda}/GRD_H < 0$ and increase $\epsilon_{\Lambda}/\epsilon_H$ by an order of magnitude according.

- If after NR consecutive iterations of the algorithm the net number of finite elements does not vary (i.e., $GRD_{N_{FE}} = (N_{FE})_{r_e} - (N_{FE})_{r_e-1} = 0$) and there are no changes in $\omega_{i,k}$ or $\vartheta_{i,nc}$, then bisect the largest finite element in Stage 4, i.e., $max\,(\bar{\alpha}_i) = max\,(\bar{\alpha}_i)\,/2$. This increases the number of finite elements by 1 thus allowing the algorithm to conduct a new search.

For simplicity, only the first two items in the guidelines are indicated in the Algorithm (2) as part of the convergence criteria; the rest of the items follow the same structure.

6.3 Case studies

The methodology described in the previous section is illustrated using two case studies. All the numerical implementations were performed in GAMS 37.1 and IPOPT was used as the NLP solver. Operating system (OS) and hardware specifications are as follows: 64-bit Windows Server 2019, 2 Intel(R) Xeon(R) E5-2620 v4 CPU, 2.10GHz, and 96GB RAM.

6.3.1 Two CSTRs in series

The first case study presents a reaction system with 2 continuous stirred tank reactors (CSTRs) connected in series (see the process' diagram Figure 6.2). This case study is based on the system

Algorithm 2 Pseudocode for the algorithm for the refinement of the discretization mesh on the integration of design and control

Input: ϵ_{Λ}^{s}, ϵ_H, ϵ_{Λ}, $\Delta\bar{\alpha}, \delta$, $\bar{a}$, $\bar{\eta}$, $\bar{\mathbf{u}}(t)$, N_r, NR
Output: $\mathbf{x}^*(t)$, $\mathbf{u}^*(t)$, $\mathbf{y}^*(t)$, η^*, $\bar{\alpha}$, $\bar{\mathbb{H}}$
Stage 1: $\hat{\alpha}_i$, $N_{FE} \leftarrow$ Equation (6.10) $(\epsilon_{\Lambda}, \bar{\eta}, \bar{\mathbf{u}}(t))$
while $r_e \leq N_r$ **do**
  Stage 2: $\eta^*, \mathbf{x}^*(t), \mathbf{u}^*(t), \mathbf{y}^*(t), \nabla_{\hat{\alpha}_i}\eta^*, \nabla_{\hat{\alpha}_i}\mathbf{x}^*(t), \nabla_{\hat{\alpha}_i}\mathbf{u}^*(t), \nabla_{\hat{\alpha}_i}\mathbf{y}^*(t) \leftarrow$ Equation (6.11) $(\hat{\alpha}_i, N_{FE})$
  Stage 3: $\bar{\alpha}_i^*, \omega_{i,j}, \upsilon_{i,nc} \leftarrow$ Equation (6.14) $(\eta^*, \mathbf{x}^*(t), \mathbf{u}^*(t), \mathbf{y}^*(t), \nabla_{\hat{\alpha}_i}\eta^*, \nabla_{\hat{\alpha}_i}\mathbf{x}^*(t), \nabla_{\hat{\alpha}_i}\mathbf{u}^*(t), \nabla_{\hat{\alpha}_i}\mathbf{y}^*(t))$
  if $\omega_{i,j} = 0$ and $\upsilon_{i,nc} = 0$ **then return** $\mathbf{x}^*(t), \mathbf{u}^*(t), \mathbf{y}^*(t), \eta^*, \bar{\alpha}, \bar{H}$
    Algorithm has converged
  else if $GRD_T = (\upsilon_{i,nc})_{r_e} - (\upsilon_{i,nc})_{r_e-1} = 0$ (NR consecutive iterations) **then return** $\varepsilon_T = 10(\varepsilon_T)$
    $r_e = r_e + 1$, go to Stage 2
  else if $GRD_H = (\omega_{i,j})_{r_e} - (\omega_{i,j})_{r_e-1} = 0$ (NR consecutive iterations) **then return** $\varepsilon_H = 10(\varepsilon_H)$
    $r_e = r_e + 1$, go to Stage 2
  else
    $r_e = r_e + 1$, go to Stage 4
  end if
  Stage 4: Refine number of finite elements (I)
  if $\omega_{i,j} > 0$ or $\upsilon_{i,nc} > 0$ **then**
    Bisect i^{th} finite element
  else if $\bar{\alpha}_i < \bar{a}\sigma$ **then**
    i^{th} finite element is merged to the $i^{th} + 1$ finite element
  end if
end while

presented by Schweiger and Floudas [170], where an irreversible liquid phase exothermic reaction $\mathcal{A} \rightarrow \mathcal{B}$ takes place. The temperature in each reactor is controlled using water cooling flow rates passing through the cooling jackets. Reactant $\mathcal{A}$ is fed to the system by the flow rate $\bar{F}_{in}$ $[lbmol/min]$ at a concentration C_{A0} $[lbmol/ft^3]$ and an inlet temperature T_{in} $[^\circ F]$. Concentration of $\mathcal{A}$ leaving the first reactor is given by C_{A1}, whereas the concentration at the outlet stream of the second reactor is given by C_{A2}. The liquid holdup in both reactors is given by h_T (i.e., both reactors are assumed to have the same size), whereas the temperatures of the reaction media are T_1 and T_2, respectively. Likewise, the design decision variables are given by the diameter (D_e $[ft]$) of the CSTRs. The aspect ratio (h_T/D_e) is set to 2 [147]. The cooling jackets volume (Vj $[ft^3]$) and heat-transfer area (A_e $[ft^2]$) are functions of h_T and D_e, i.e., $Vj = h_{Vj}(h_T, D_e)$ and $A_e = h_{A_e}(h_T, D_e)$. The

fresh water introduced to the jackets as cooling media ($\bar{F}_{w1}$ and $\bar{F}_{w2}$, respectively) has an initial temperature T_c^0 [$^\circ F$]; thus, the temperatures for the cooling jackets are T_{c1} and T_{c2}, respectively. Boundaries for the temperatures of the cooling jackets are $80^\circ F \leq T_c \leq 212^\circ F$. The system aims to maintain the concentration of component $\mathcal{A}$ at the outlet flow rate (i.e., C_{A2}) at an specific concentration of 0.05 [$lbmol/ft^3$]. To enforce process dynamics, it is considered the implementation of a disturbance in the input parameters C_{A0} and T_{in}. This disturbance consists on the following step changes $C_{A0} = [1, 0.85]$ and $T_{in} = [600, 575]$. The step change is enforced in both variables at $t = 5h$. The dynamic model is shown in Equation (4.10), the controller models are given by Equation (6.16), whereas the corresponding model parameters are presented in Table 6.1.

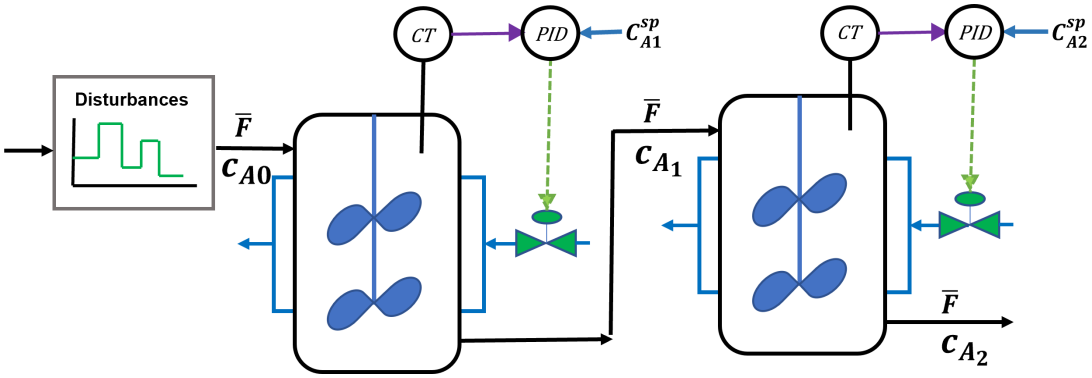

Figure 6.2: Reaction system with 2 CSTRs in series.

$$\bar{F}_{w1} = \bar{F}_{w1}^0 + K_{C1}\bar{e}_1(t) + K_{I1}\int_{t_0}^{t_f} \bar{e}_1(t)\,dt + K_{D1}\frac{d\bar{e}_1(t)}{dt} \tag{6.16a}$$

$$\bar{F}_{w2} = \bar{F}_{w2}^0 + K_{C2}\bar{e}_2(t) + K_{I2}\int_{t_0}^{t_f} \bar{e}_2(t)\,dt + K_{D2}\frac{d\bar{e}_2(t)}{dt} \tag{6.16b}$$

where the manipulated variables are denoted by $\bar{F}_{w1}$ and $\bar{F}_{w2}$, respectively; $\bar{F}_{w1}^0$ and $\bar{F}_{w2}^0$ are bias steady-state values of cooling water; K_C, K_I, and K_D are the controller's proportional, integral, and derivative gains, respectively. Error signal in the PID controller ($\bar{e}(t)$) is defined as the difference between the controller variables and the reference set-point, i.e., $\bar{e}(t) = \mathbf{x}(t) - \mathbf{x}^{sp}$.

The cost function consists of an annualized capital cost (CC_a), an operating cost (OC_a), and a variability cost (VC_a). The CC_a is related to the size of the required equipment. The OC_a depends

Table 6.1: Model parameters for the CSTRs case study.

Parameter	Value
C_p $[BTU/(ft^3\,R)]$	37.5
ΔH_{rx} $[BTU/lbmole]$	-3,000
E $[BTU/lbmole]$	30,000
k_{re} $[hr^{-1}]$	4.08×10^{10}
ρ $[lb/ft^3]$	50
MW $[lb/lbmole]$	50
C_p^w $[BTU/(ft^3\,R)]$	62.38
U_h $[BTU/(hr\,ft^2\,R)]$	300
T_{ref} $[R]$	600
T_1^L, T_2^L $[R]$	542.8
T_1^U, T_2^U $[R]$	670.0
T_{c1}^L, T_{j2}^L $[R]$	532.0
T_{c1}^U, T_{j2}^U $[R]$	668.0

on the cost of the availability, conditioning and transportation of the cooling water to cool down the reactors. In the VC_a, the deviations of C_{A1} and C_{A2} with respect to the corresponding set-points are penalized, i.e.,

$$CC_a = 2(1917(D_e^{1.066} + h_T^{0.802})) \tag{6.17}$$

$$OC_a = 32.77 \int_{t_0}^{t_f} \bar{F}_{w1}(t) + \bar{F}_{w2}(t)\ dt \tag{6.18}$$

$$VC_a = 1.0 \times 10^9 \left(\int_{t_0}^{t_f} (C_{A1}(t) - C_{A1}^{sp})^2\ dt + \int_{t_0}^{t_f} (C_{A2}(t) - C_{A2}^{sp})^2\ dt \right) \tag{6.19}$$

where the OC_a depends on the cost of the availability, conditioning and transportation of the cooling water to cool down the reactors; in the VC_a, the deviations of C_{A1} and C_{A2} with respect to the corresponding set-points are penalized; C_{A1}^{sp} and C_{A2}^{sp} correspond to the set-points of C_{A1} and C_{A2}, respectively.

In this study, decentralized PID controllers are considered to maintain the concentration of each reactor for component A at the set-points. Manipulated variables correspond to the flow rates of cooling water in each reactor $\bar{F}_{w1}$ and $\bar{F}_{w2}$, respectively. Boundaries for the manipulated variables are $0 \leq \bar{F}_w \leq 100 ft^3/h$. Therefore, the control pairing was selected from a RGA analysis and is as follows: $\bar{F}_{w1}$ is manipulated to control the concentration of A in the first reactor (C_{A1}) whereas $\bar{F}_{w2}$

is manipulated to control the concentration of A in the second reactor (C_{A2}). Controller's gains (K_{C1}, K_{I1}, K_{D1}, K_{C2}, K_{I2}, and K_{D2}) are part of the decision variables. The set-point for CSTR 1 (C_{A1}^{sp}) is included as part of the decision variables in the optimization formulation, where as the set-point for CSTR 2 is set to $C_{A2}^{sp} = 0.05$ $[lbmol/ft^3]$. In this case study, three Radau collocation points were selected ($K = 3$). Also, three noncollocation points per finite element are implemented ($\tau_{nc} = [0.77525, 0.399999, 0.822474]$); these were selected to be the middle point between each collocation point (i.e., $\tau_{nc} = (\tau_k - \tau_{k+1})/2$). The rest of the parameters for the algorithm are as follows: $\epsilon_\Lambda^s = 1 \times 10^{-3}$, $\Delta\bar{\alpha} = 0.01$, $\epsilon_H = 1 \times 10^{-9}$, $\epsilon_\Lambda = 1 \times 10^{-6}$, $\bar{M} = 1 \times 10^9$, $\delta = 0.15$, and $\bar{a} = 1.5$.

The initial estimation of finite elements in the first stage of the algorithm determined 26 nonequidistant finite elements, as shown in Table 6.2 (Scenario 1-Instance A). The refinement methodology returned a solution with 43 refined finite elements (Scenario 1-Instance B). As shown in Table 6.2, it is observed a difference of 60% in the size of the reactor's volume (V_R) between the solutions with 26 and 43 finite elements, that is, the solution with the refined finite elements shows a reduction in the equipment size. Moreover, the set-point for the first reactor is 58% larger in the solution with the refined finite elements (43 refined finite elements) with respect to the solution with the initial estimation of finite elements (26 finite elements). These differences between the initial estimation (Instance A) and the refined number of finite elements (Instance B) are also extended to the objective function. The total cost with the refined number of finite elements (2.37×10^5 $[\$/yr]$) is 39% lower than the total cost obtained with the initial estimation of finite elements (3.92×10^5 $[\$/yr]$). Moreover, from Table 6.2 it can be noted a differences in the steady-state cooling water flow rates ($\bar{F}_{w1}^0$ and $\bar{F}_{w2}^0$). The solution with 26 finite elements (Instance A) demands higher flow rates of cooling water at steady-state, i.e., 48% and 359% higher cooling flow rates in the reactors 1 and 2, respectively, compared to the solution with 43 refined finite elements.

The formulation for the integration of design and control in this case study was also solved with a conventional equidistributed finite elements strategy (Scenario 2). The optimization problem was solved using 26 (Instance C) and 43 (Instance D) equidistributed finite elements, i.e., the initial estimation and final solution of finite elements in Scenario 1, respectively. The results for Scenario

Table 6.2: Results for the two CSTRs in series case study.

Optimization variable	**Refined Elements (Scenario 1)**		**Equidistributed Elements (Scenario 2)**		**Augmented Model (Scenario 3)**
	Instance A	**Instance B**	**Instance C**	**Instance D**	
N_{FE}	26	43	26	43	86
D_e $[ft]$	7.36	5.53	7.34	6.73	6.06
V_R $[ft^3]$	626.7	266.7	622.9	480.3	350.6
C_{A1}^{sp} $[lbmole/ft^3]$	0.1487	0.235	0.239	0.248	0.250
$\bar{F}_{w1}^{0}$ $[ft^3/h]$	37.5	25.3	51.6	43.4	33.8
K_{C1}	4442.8	1472.4	4531.2	3692.4	3958.5
K_{I1}	2744.3	527.85	2863.6	3774.5	4284.3
K_{D1}	2110.8	794.96	3161.8	3028.3	2271.1
$\bar{F}_{w2}^{0}$ $[ft^3/h]$	34.1	7.21	8.68	6.72	5.75
K_{C2}	3226.6	1607.4	3230.3	2392.1	1987.9
K_{I2}	804.04	684.89	1143.4	1338.3	1584.3
K_{D2}	0.0	936.41	2767.8	2409.2	1965.1
Equations	1785	2941	1785	2941	5865
Variables	1787	2943	1787	2943	5867
Capital cost $[\$/yr]$	2.78×10^5	1.64×10^5	2.77×10^5	2.36×10^5	1.94×10^5
Operating cost $[\$/yr]$	5.53×10^4	2.43×10^4	3.99×10^4	3.02×10^4	2.03×10^4
Variability cost $[\$/yr]$	5.86×10^4	4.96×10^4	7.93×10^4	5.83×10^4	3.85×10^4
Total cost $[\$/yr]$	3.92×10^5	2.37×10^5	3.96×10^5	3.25×10^5	2.53×10^5
CPU $[s]$	98.2	7.1×10^3	17.6	31.2	238.4
Iterations	1	3	-	-	-

2 in Table 6.2 show that an increase in the number of equidistributed finite elements from 26 (Instance C) to 43 (Instance D) improves the economics since the objective function improved 18% from Instance C to Instance D. This improvement was similar to that observed for Scenario 1. From the design's point of view, reactor's volume (V_R) for Instance D is 22% smaller compared to that obtained for Instance C. This represents a reduction of 14% in the equipment size. Moreover, it can be observed reductions of 15% and 22% in the steady-state cooling water flow rates ($\bar{F}_{w1}^{0}$ and $\bar{F}_{w2}^{0}$, respectively) from Instance C to Instance D, respectively. Furthermore, the results in Table 6.2 show that the solution on Instance B returns a more economically attractive process design compared to the solution from Instance D (Scenario 2), i.e., the total cost with the refined finite elements (43 finite elements) is 27% lower than the solution with an equidistributed finite elements strategy. Also, it is noted that the controller gains are larger for the solution in Instance D (Scenario 2) with respect to the solution obtained on Instance B. Thus, the controller's gains K_I and K_D are larger for the solution with equidistributed finite elements. This may lead to a controller with a faster response. From Figure 6.3, it can be confirmed that the amplitude of the changes in

the controlled variables due to changes in the process disturbances, is smaller in the solution on Instance D (Scenario 2). Furthermore, it is distinguished that the reactors are larger in the solution on Instance D (Scenario 2) compared with the equipment size computed in Scenario 1, i.e., reactor's volume in Scenario 1 is 44% smaller than the solution on Instance D (Scenario 2). A comparison of the operating costs for the solutions with 43 finite elements (Scenarios 1 and 2) shows that the solution with refinement finite elements returned a 20% more economic process operation. Figure 6.4 displays the manipulated variables profiles, note that CSTR 1 demands the largest amount of cooling water to operate. Also, Figure 6.4 shows that the flow rate of cooling water on Instance D (Scenario 2) is 70% larger compared to the solution in Scenario 1, which further explains the difference in the operating costs. Therefore, the refinement algorithm returned a more economically attractive solution compared with the naive implementation with equidistributed finite elements. The solution in Instance B is more attractive because the equipment (reactor's volume) is smaller at expense of larger close-loop variability in the controlled and manipulated variables (see Figures 6.3 and 6.4). Moreover, Figure 6.5 shows the length distribution of finite elements. From this figure, it can be noted that most of the shortest finite elements are concentrated in the process transient time.

To provide further insight, it can be compared the solutions in this case study to another scenario where the number of equidistributed finite elements is increased (Augmented model (Scenario 3)). In Scenario 3, the number of finite element is duplicated such that the optimization problem was discretized with 86 equidistributed finite elements. A comparison of total costs for Instance D (Scenario 2) and Scenario 3 shows that by increasing the number of finite elements the cost improved by 22%. The augmented model returned a solution with a cost that is 7% higher than the solution in Scenario 1-Instance B. The size of the equipment in Scenario 3 is still 22% larger than the reported in the solution for Scenario 1-Instance B. From Figure 6.3, it is noted that the amplitude of the changes in the controlled variables for Scenario 3 is smaller compared to the profiles observed for the solution in Scenario 1-Instance B (43 refined finite elements). Moreover, from the manipulated variables profiles depicted in Figure 6.4, it is observed that the controller is more conservative in Scenario 3 compared to the solution in Scenario 1-Instance B, i.e., the magnitude of the control

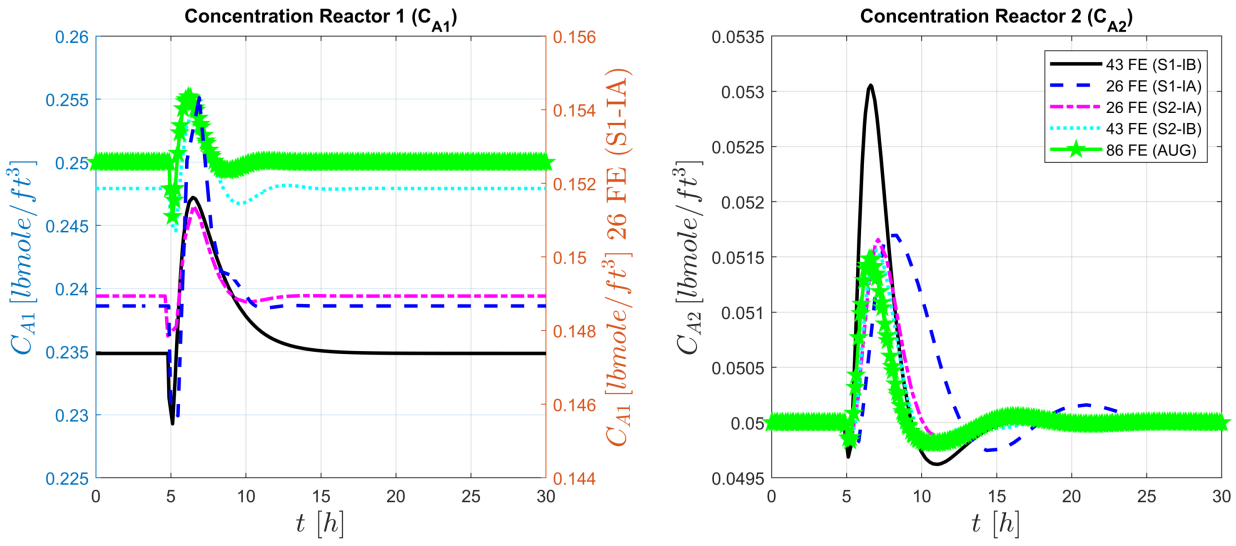

Figure 6.3: Dynamic profiles for the controlled variables (i.e., C_{A1} and C_{A2}) for different selections of finite elements (FE) (two CSTRs case study): 43 FE Scenario 1-Instance B (S1-IB), 26 FE Scenario 1-Instance A (S1-IA), 26 FE Scenario 2-Instance C (S2-IC), 43 FE Scenario 2-Instance D (S2-ID), and 86 FE Augmented model (AUG).

actions are smaller in Scenario 3 compared with the solution for Scenario 1-Instance B. To evaluate the accuracy of the selection of finite elements in Scenarios 2 and 3, the Hamiltonian function profiles for these scenarios was computed. As shown in Figure 6.6, the solutions in Scenario 1 and 3 returned a Hamiltonian function profile that is close to be constant over time. On the other hand, an estimation of the collocation error (i.e., evaluation of the monitor function Λ_i in Equation (6.7)) for the solutions in Scenario 2 (Instance D) and Scenario 3 averaged collocation errors of 1.1 and 0.5, respectively, i.e., the collocation errors in Scenarios 2 and 3 are orders of magnitude larger than the tolerance of $\epsilon_\Lambda = 1.0 \times 10^{-6}$. This suggests that the solutions in Scenarios 2 and 3 may not guarantee an adequate accuracy in the approximation to the functions in the optimization formulation. On the other hand, it is observed that the algorithm (Scenario 1) required relatively large computational time to converge; nevertheless, this allowed to determine an optimal design and control with an adequate discretization mesh that resulted in an economically attractive and dynamically feasible solution. In Scenario 2, it was implemented a naive approach with equidistributed finite elements using the same number of finite elements obtained in Scenario 1. For all scenarios, the initialization

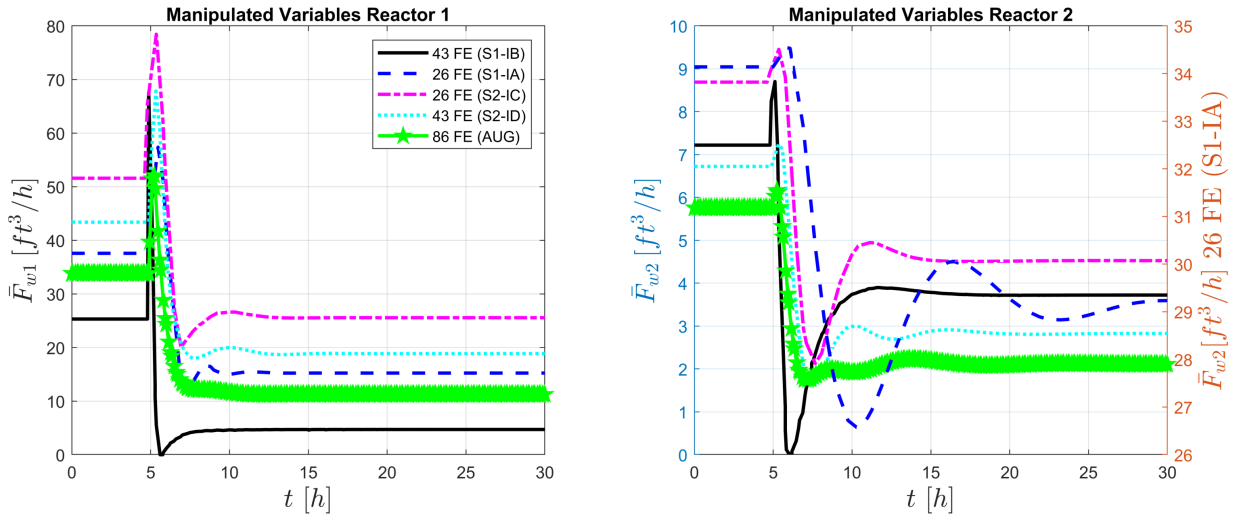

Figure 6.4: Dynamic profiles for the manipulated variables (i.e., $\bar{F}_{w1}$ and $\bar{F}_{w2}$) for different selections of finite elements (FE) (two CSTRs case study): 43 FE Scenario 1-Instance B (S1-IB), 26 FE Scenario 1-Instance A (S1-IA), 26 FE Scenario 2-Instance C (S2-IC), 43 FE Scenario 2-Instance D (S2-ID), and 86 FE Augmented model (AUG).

of the decision variables in the optimization problem for simultaneous design and control was the same. This avoids the determination of different local optimums for each scenario. The CPU costs in these scenarios were expected to be small since a refinement strategy was not implemented, i.e., those scenarios are the result of a simulation using insights gained from Scenario 1. However, from a comparison of the CPU costs for Scenarios 2 and 3, it is noted that CPU cost in Scenario 3 is one order of magnitude larger than that obtained for Scenario 2.

Moreover, the number of collocation points was increased from 3 to 4 to analyze their effect; accordingly, $K = 4$ using the proposed methodology for the selection and refinement of finite elements. The rest of the parameters considered in the algorithm remained the same. The results for Scenario 1 with $K = 4$ collocation points returned almost similar results to those obtained with $K = 3$, i.e., $V_R = 266.1\ [ft^3]$, $C_{A1}^{sp} = 0.234\ [lbmole/ft^3]$. This represents a reactor's volume 0.2% smaller and the same operation set-point for reactor 1 compared to the results with $K = 3$. In Stage 1, the algorithm initialized the methodology with 22 refined finite elements and converged to 39 finite elements. Total cost of Scenario 1 with $K = 4$ is $2.37 \times 10^5\ \$/yr$, which is similar to $K = 3$. On the other hand, the solution for Scenario 1 (i.e., 39 refined finite elements) with $K = 4$ returned

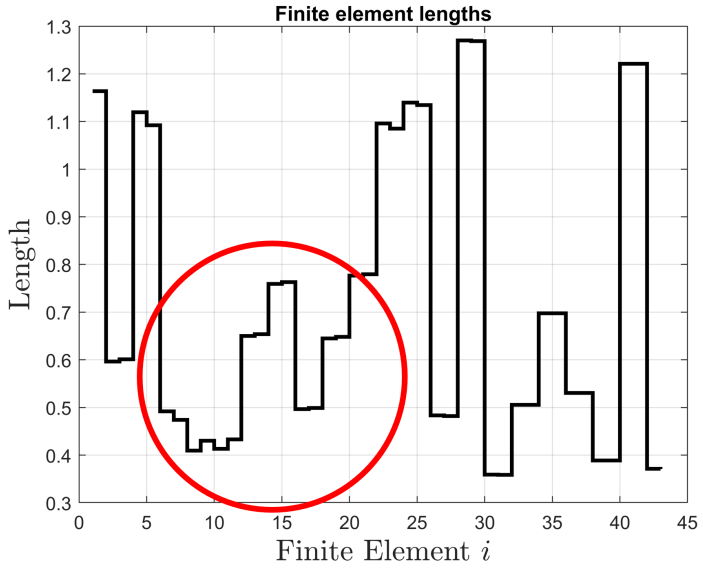

Figure 6.5: Distribution of finite element lengths for the CSTRs case study. Process transient time is shown in the red circle.

a model with 3915 equations and 3919 variables; this represents an increase of 33% in the model size with respect to the solution of Scenario 1 with $K = 3$. Dynamic profiles for the controlled and manipulated variables for Scenario 1 with 4 collocation points were the similar to those obtained for $K = 3$ (not shown for brevity). Thus, increasing the number of collocation points did not improve the solution. Moreover, the CPU time required to converge with 4 collocation points was $1.15 \times 10^4 s$; this is an increase of one order of magnitude of CPU time compared to the implementation with 3 collocation points (7.1×10^3).

6.3.2 Williams-Otto reactor

In the second case study, it is proposed the integration of design and optimal control of the Williams-Otto CSTR (WO-CSTR) [171]. This nonisothermal CSTR is fed by two pure inlet streams of components $\mathcal{A}$ and $\mathcal{B}$ with mass flow rates $\bar{F}_A$ and $\bar{F}_B$ [kg/s], respectively. The outlet streams contains the six components involved in the following three parallel reactions: $\mathcal{A}+\mathcal{B} \xrightarrow{k_1} \mathcal{C}$; $\mathcal{B}+\mathcal{C} \xrightarrow{k_2} \mathcal{D}+\mathcal{M}$; and $\mathcal{C}+\mathcal{D} \xrightarrow{k_3} \mathcal{Q}$. This process aims to control the transition between two different market concentrations of products, i.e., a set-point tracking control problem. In a simulation horizon of

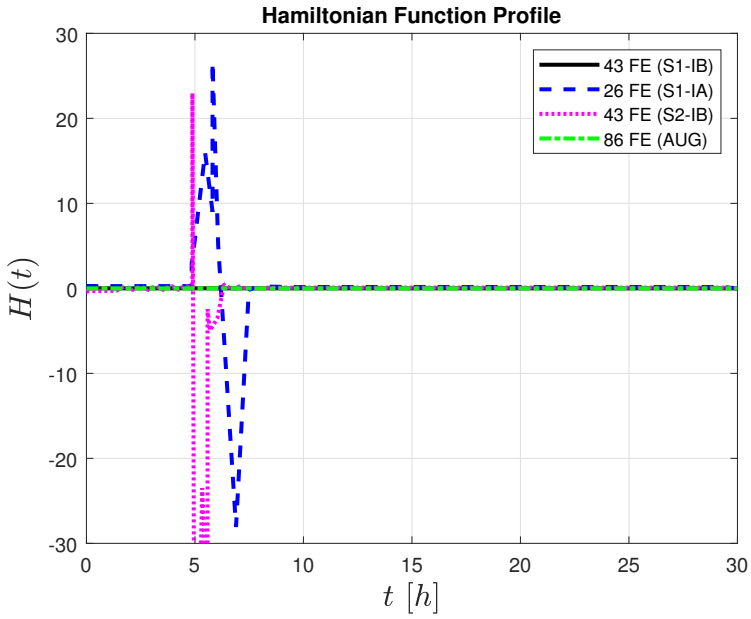

Figure 6.6: Comparison of the Hamiltonian function profiles for different selections of finite elements (FE) (two CSTRs case study): 43 FE Scenario 1-Instance B (S1-IB), 26 FE Scenario 1-Instance A (S1-IA), 43 FE Scenario 2-Instance D (S2-ID), and 86 FE Augmented model (AUG).

$5h$, the process transitions from initial set-points $x_M^{sp} = 0.2951$ and $x_D^{sp} = 0.1103$ (called normal operation condition) to a second operating condition $x_M^{sp} = 0.2265$ and $x_D^{sp} = 0.0909$ at $t = 1h$. Then, at $t = 3h$ the process operation return to the initial operation condition mentioned above. The process can manipulate the flow rate of component $\mathcal{B}$ ($\bar{F}_B$) and the reactor's temperature (T) to reach the control targets for components $\mathcal{M}$ and $\mathcal{D}$ (i.e., x_M and x_D). Inlet flow rate of component $\mathcal{A}$ (i.e., $\bar{F}_A$) is fixed to $1.8\,[kg/s]$. The mass holdup in the reactor is given by h_T $[kg]$. The dynamic model of the WO-CSTR is as follow:

$$\frac{dx_A}{dt} = \frac{\bar{F}_A}{h_T} - \frac{\left(\bar{F}_A + \bar{F}_B\right)}{h_T} x_A - \frac{r_1}{h_T} \tag{6.20a}$$

$$\frac{dx_B}{dt} = \frac{\bar{F}_B}{h_T} - \frac{\left(\bar{F}_A + \bar{F}_B\right)}{h_T} x_B - \frac{r_1}{h_T} - \frac{r_2}{h_T} \tag{6.20b}$$

$$\frac{dx_C}{dt} = -\frac{\left(\bar{F}_A + \bar{F}_B\right)}{h_T} x_C + 2\frac{r_1}{h_T} - 2\frac{r_2}{h_T} - \frac{r_3}{h_T} \tag{6.20c}$$

$$\frac{dx_M}{dt} = -\frac{\left(\bar{F}_A + \bar{F}_B\right)}{h_T} x_E + 2\frac{r_2}{h_T} \tag{6.20d}$$

$$\frac{dx_Q}{dt} = -\frac{\left(\bar{F}_A + \bar{F}_B\right)}{h_T} x_G + 1.5\frac{r_3}{h_T} \tag{6.20e}$$

$$\frac{dx_D}{dt} = -\frac{\left(\bar{F}_A + \bar{F}_B\right)}{h_T} x_P + \frac{r_2}{h_T} - 0.5\frac{r_3}{h_T} \tag{6.20f}$$

$$r_1 = k_1 x_A x_B h_T \tag{6.20g}$$

$$r_2 = k_2 x_B x_C h_T \tag{6.20h}$$

$$r_3 = k_3 x_C x_D h_T \tag{6.20i}$$

$$k_1 = 1.6599 \times 10^6 exp(-6666.77/(T(^\circ C) + 273.15)) \tag{6.20j}$$

$$k_2 = 7.2117 \times 10^8 exp(-8333.33/(T(^\circ C) + 273.15)) \tag{6.20k}$$

$$k_3 = 2.6745 \times 10^{12} exp(-11111/(T(^\circ C) + 273.15)) \tag{6.20l}$$

$$2 \leq \bar{F}_B(t) \leq 10, \;\; 50 \leq T(t) \leq 150 \tag{6.20m}$$

where x_A, x_B, x_C, x_M, x_Q, x_D are the mass fraction of each component in the reactions taking place in the reactor; reactions rates are given by r_1, r_2, r_3 $[s^{-1}]$; whereas the reaction constants given by k_1, k_2, k_3 $[s^{-1}]$ are functions of the rector's temperature (T $[^\circ C]$).

In this case study, the objective function consists of the maximization of the economic profit (i.e., $\max CC_a - VC_a$) where CC_a (gross profit) depends on the equipment sizing (i.e., the reactor's mass holdup (h_T) and the production of the process; VC_a quantifies the effect of the process dynamics (Variability cost) relating the deviations of the concentration of main products E and P in the outlet flow rate with respect to their corresponding target set-points. The process economics are obtained from empirical correlations and considers the annualized cost of raw materials and products for a determined plant lifetime [171]. Therefore, the economic terms in the objective function are described as follows:

$$CC_a = 100\frac{t_{op}MG - t_{op}SARE - t_{op}UF - FCP}{PIN} \tag{6.21}$$

where t_{op} is the operation time per year. In this study, $t_{op} = 8400$ $[h/yr]$. MG is the gross return per hour defined as the difference between the revenue and cost of raw materials, $SARE$ is

defined as the cost related to sales, administration, research, and engineering expenses. Associated costs to utilities and process flows are given by UF. FCP stands for the depreciation and labor taxes, i.e., fixed cost. The total initial investment of the plant is given by PIN. Expressions for each of these terms are as follows:

$$MG = P_M \bar{F}_M + P_D \bar{F}_D - P_A \bar{F}_A - P_B \bar{F}_B \tag{6.22}$$

$$SARE = 0.124 \left(P_M \bar{F}_M + P_D \bar{F}_D \right) \tag{6.23}$$

$$UF = 0.001 \left(\bar{F}_A + \bar{F}_B \right)^{1.5} \tag{6.24}$$

$$FCP = 60 h_T, \;\; PIN = 600 h_T \tag{6.25}$$

where $P_M = 125.91$ [\$/kg], $P_D = 5554.1$ [\$/kg], $P_A = 370.3$ [\$/kg], and $P_B = 555.42$ [\$/kg] are the market prices of products $mathcalM$ and $\mathcal{D}$, and reactants $\mathcal{A}$ and $\mathcal{B}$, respectively. On the other hand, the variability cost is stated as follows:

$$VC_a = 1.0 \times 10^5 \int_{t_0}^{t_f} \left(x_M^{sp} - x_M(t) \right)^2 + 1.0 \times 10^6 \int_{t_0}^{t_f} \left(x_D^{sp} - x_D(t) \right)^2 \tag{6.26}$$

where the dynamic decision variables include the vector of states $\mathbf{x}(t)$ and the control laws for $\bar{F}_B(t)$ and $T(t)$, whereas a static decision variable (design variable) is given by h_T. For discretization, three collocation points ($K = 3$) were selected. As in the previous case study (Section 6.3.1), a discretization using three noncollocation points per finite element is implemented ($\tau_{nc} = [0.77525, 0.399999, 0.822474]$). The set of parameters for the algorithm of selection and refinement of finite elements are as follows: $\epsilon_\Lambda^s = 1 \times 10^{-3}$, $\Delta\bar{\alpha} = 0.05$, $\epsilon_H = 1 \times 10^{-7}$, $\epsilon_\Lambda = 1 \times 10^{-6}$, $\bar{M} = 1 \times 10^7$, $\delta = 0.10$, and $\bar{a} = 1.5$.

As shown in Table 6.3, the initial estimation of finite elements in stage 1 determined 32 finite elements (Scenario 1-Instance A) whereas the refinement methodology resulted in a solution with 66 finite elements (Scenario 1-Instance B). Table 6.3 shows slight differences between the solutions for the initial estimation of finite elements (Instance A) and the final solution with the selection strategy (Instance B). The reactor's volume presents a variation of 0.02%, and the gross profit increased 1.1% for Instance B with respect to the solution on Instance A (Scenario 1). However,

Table 6.3: Results for the Williams-Otto case study.

Optimization variable	**Refined Elements (Scenario 1)**		**Equidistributed Elements (Scenario 2)**	
	Instance A	**Instance B**	**Instance C**	**Instance D**
N_{FE}	32	66	32	66
h_T $[Kg]$	2080.1	2079.6	2079.9	2079.7
Equations	2479	5193	2479	5193
Variables	2570	5290	2570	5290
Gross Profit (CC_a) [$/$yr$]	6.22×10^5	6.29×10^5	6.16×10^5	6.28×10^5
Variability cost (VC_a) [$/$yr$]	4.85×10^4	4.10×10^4	5.09×10^4	1.4×10^5
Net Profit [$/$yr$]	5.73×10^5	5.88×10^5	5.66×10^5	3.5×10^5
CPU $[s]$	1.73×10^3	6.84×10^3	18	153
t_{2N} $[s]$	6.92×10^2	9.6×10^2	-	-
Iterations	1	11	-	-

Instance B showed a reduction of 18% in the variability cost with respect to the initial solution on Instance A. Therefore, the refinement strategy improved the annualized profit by 2.56% with respect to the initial estimation of finite elements i.e., this represents an additional income of $14,697.6 per year.

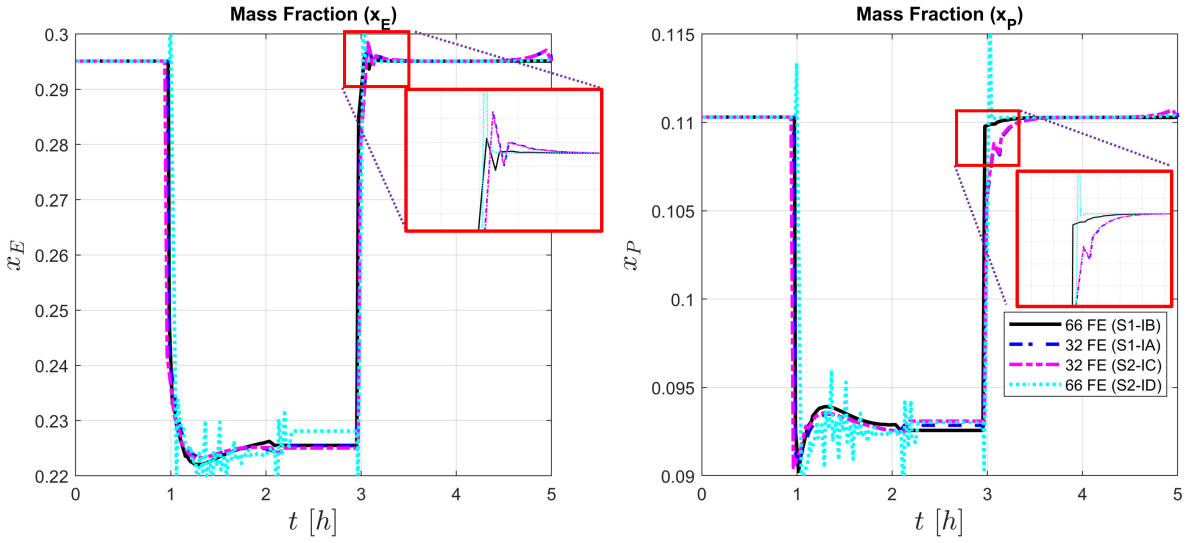

Figure 6.7: Dynamic profiles for the controlled variables (i.e., $x_E(t)$ and $x_P(t)$) with refined (FE-RF) and equidistributed (FE-EQ) finite elements for the Williams-Otto case study.

To provide further insight, the solutions of the selection and refinement strategy were compared with a conventional equidistributed finite elements strategy (Scenario 2). The optimization problem was solved using 32 (Scenario 2-Instance C) and 66 (Scenario 2-Instance D) equidistributed finite

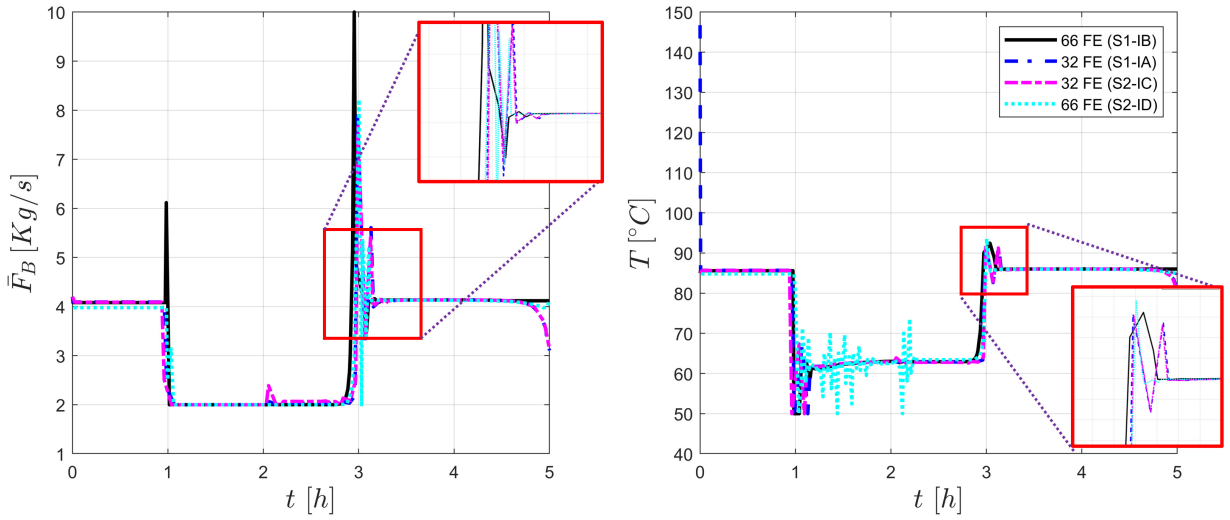

Figure 6.8: Dynamic profiles for the manipulated variables (i.e., $\bar{F}_B(t)$ and $T(t)$) with refined (FE-RF) and equidistributed (FE-EQ) finite elements for the Williams-Otto case study.

elements, the initial estimation and final solution of finite elements in Scenario 1, respectively. The results for Scenario 2 (Table 6.3) show slight differences between the Instances C and D for the reactor's volume, i.e., Instance D returned a reactor's volume 0.01% smaller compared to Instance C. The same relationship was observed for a comparison between Instance B (refined finite elements) and Instance D, the refinement strategy led to a reactor's volume 0.01% smaller compared to the equidistribution strategy (Instance D). Moreover, economic aspects follow the same tendency. In Scenario 2, the gross profit improved 2% by in creasing the number of equidistributed finite elements from 32 to 66. In addition, the solutions from Scenarios 1 and 2 showed that the refinement strategy returned a slight improvement in the gross profit, i.e., gross profit in Instance B (Scenario 1) is 0.15% higher compared to Instance D (Scenario 2).

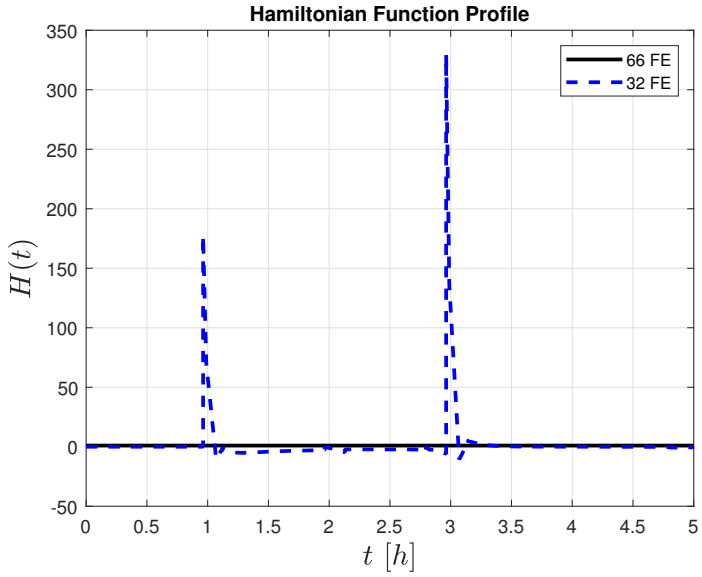

Figure 6.9: Comparison of the Hamiltonian function profiles for the initial estimation of refined finite elements (32 FE) and the final discretization mesh (66 FE) for the Williams-Otto case study.

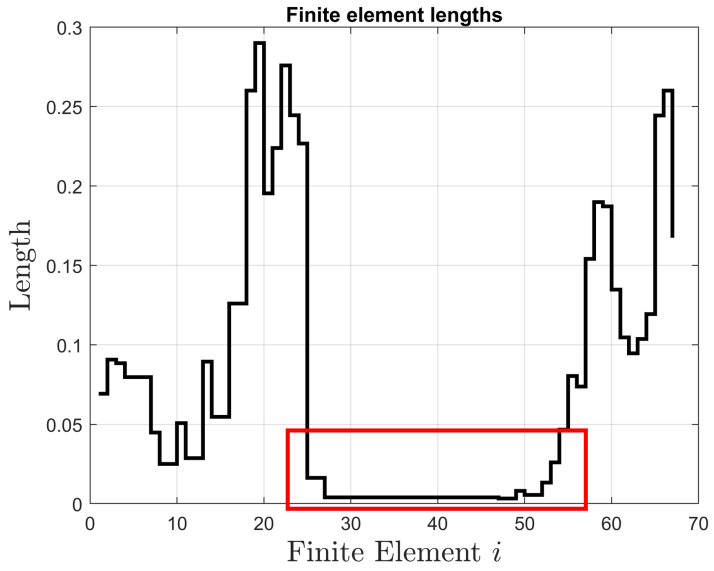

Figure 6.10: Distribution of finite element lengths for the Williams-Otto case study. Process transient time is shown in the red square.

As shown in Figure 6.7, similarities in the dynamic control profiles between Instances A and B can be noticed. Component x_D seems to reach faster the set-point after the second step change (i.e., at $t = 3h$). Figure 6.8 shows that additional control actions are executed in the solution of

Instance A. Nevertheless, a larger control action on $\bar{F}_B$ was observed at $t = 3h$ for Instance B. This may explain the slight faster response of x_D to the set-point change at $t = 3h$. Furthermore, the discretization for Instance A does not lead to a constant Hamiltonian function profile (see Figure 6.9). Moreover, the averaged estimated collocation error for instance A was $\bar{e}_c(t) = 1.68 \times 10^{-2}$. This estimated collocation error is 4 orders of magnitude larger than the desired tolerance $\epsilon_\Lambda = 1 \times 10^{-6}$. Therefore, the accuracy of the solution on Instance A is not guaranteed. Despite the slight differences in the solutions in Scenario 1 (i.e., Instances A and B in Table 6.3), it is observed an improvement in the process profits. On the other hand, from an inspection of the process dynamics in Figures 6.7 and 6.8 for the solutions in Scenario 2 (Instances C and D), it is noted that Instance D returns noisy dynamic profiles. Therefore, the discretization with 66 equidistributed finite elements is not able to properly capture the process dynamics. This explains the large variability cost observed for this instance in Table 6.3. Variability cost has a high impact in the net profit for the solution in Instance D compared to the solution with refined finite elements in Instance B, i.e., the solution with refined finite elements returned a net profit 68% larger than the solution with equidistributed finite elements. Similarly as in the CSTRs case study, the length distribution for finite elements shows that the smallest finite elements are concentrated in the process transient time (Figure 6.10). On the other hand, the largest contribution to the CPU time reported in Table 6.3 for Scenario 1 is associated to the determination of the sensitivity gradients. By increasing the number of finite elements, the estimation of gradients requires longer CPU times. To provide further insight in Scenario 1, the CPU time required to compute the sensitivity gradients ($\nabla_{\bar{\alpha}_i}\eta$, $\nabla_{\bar{\alpha}_i}x(t)$, $\nabla_{\bar{\alpha}_i}u(t)$, $\nabla_{\bar{\alpha}_i}y(t)$) in the first and the last iterations of the algorithm (t_{2N}) was compared. An increase of 38% was observed in the CPU time required to calculate such gradients in the last iteration with respect to the first iteration for the preset case study. The ratios between t_{2N} and the CPU time per iteration for the first and the last iterations of the algorithm, i.e., t_{2N}/CPU, it was found that 40% of the CPU time in the first iteration is dedicated to the calculation of the sensitivity gradients whereas the last iteration spent 97% of the CPU time in the same calculation. From these results, it was observed a linear relationship between the computational costs required to estimate the sensitivity gradients and the number of finite elements. Note that this linear dependency may not

always hold and is only provided here as a general guideline on the expected CPU costs associated with the sensitivity estimation.

From a comparison of process dynamics in both case studies, it is observed that the process in the CSTRs case study (Section 6.3.1) is subject to longer-period changes compared to Williams-Otto case study (Section 6.3.2), i.e., the process in the CSTRs case study takes longer to reach a steady-state; moreover, the magnitude of variations of the controlled and manipulated variables (Figures 6.3 and 6.4, respectively) in former case study are larger compared to the variations of process dynamics in the last case study (Figures 6.7 and 6.8). Therefore, the optimization model in the CSTRs case study needs a more accurate discretization to correctly capture the process dynamics. Also, note that changes of process dynamics at short time scales may not be captured with an equidistributed discretization strategy if no sufficient finite elements are selected.

6.4 Summary

A methodology for the selection and refinement of finite elements for the discretization of the optimization formulation for integrated design and control was presented in this chapter. This methodology considers two criteria for the refinement of the discretization mesh. The first criterion is based on the implementation of the PMP to calculate the Hamiltonian function associated with the optimization formulation. In comparison, the second criterion accounts for the estimation of the collocation error at noncollocation points. The performance of the proposed methodology is evaluated in two illustrative case studies. Results show that the transient time and the magnitude of the process dynamics affect the selection of the discretization mesh. The refined discretization model returned more economically attractive solutions and an improved control performance using fewer finite elements compared to the naive approach involving equidistributed finite elements. Similarly, as in the back-off method in Chapter 3, the selection/refinement method presented in this chapter required most of the CPU time for the computation of sensitivity parameters for model approximation.

Chapter 7

Conclusions and Future Work

Integration of design and control aims to optimize economic, environmental, and operational aspects that result in sustainable processes. This can lead to improved product quality, reduced variability, environmental friendly operation, increased throughput, safer operation, and reduced operating costs. An integrated approach allows for greater flexibility and adaptability in the face of changing market conditions or process requirements. The ability to quickly adjust process parameters or operating conditions can be critical in today's rapidly changing business environment. Just recently, early implementations regarding the integration of design and control with NMPC are unveiling the economic and operational benefits of this framework.

In this PhD thesis, novel methodologies addressing the integration of design and NMPC-based control were proposed. The implementation of NMPC schemes represents a challenging task due to the complexity of the bilevel formulation. Most of the studies reported in the open literature regarding the integration of design and control using MPC has focused on the implementation of linear control schemes. The implementation of nonlinear control schemes introduces a new level of complexity by increasing the nonconvexity of the formulation. The lack of practical methodologies for the implementation of NMPC for integrated design and control has motivated this PhD research.

A systematic back-off approach for the integration of design and NMPC-based control was initially proposed. This methodology allows the systematic identification of dynamically feasible operating conditions and process designs by the determination of the back-off from an optimal stead-state design that it is dynamically infeasible. The proposed methodology has the attractive feature of reducing the resulting bilevel formulation that emerge when NMPC is used for design and control. The bilevel formulation is transformed into a single-level optimization problem that is represented by power series expansions (PSE) formulated as explicit functions of the decision variables and uncertain parameters. This PSE-based optimization problem reduces the computational burden and determines the feasible search direction in the optimization framework. The formulation was successfully adapted for optimization formulations involving LMPC and classical PI controllers. The

results show that the use of an NMPC-based framework leads to improved control performance and reduced of plant costs, compared to implementations involving decentralized PI control or LMPC schemes. The presence of uncertainties in some of the model parameters leaded to important differences in the solutions computed using the proposed back-off approach. The CPU cost for the implementation of NMPC-based frameworks acts as one of the main limitations for the application of this methodology for larger scale applications. Most of the CPU time required by the back-off algorithm is dedicated to the identification step for the sensitivity parameters required for the computation of the PSE-based approximation model. On the other hand, the optimality of the solutions computed with the proposed back-off approach may not be guaranteed.

The implementation of the back-off approach resulted in economically attractive solutions; however, the optimality of the solutions obtained with this methodology are still not rigorously proved. On the other hand, a direct solution strategy using NLP solvers may provide optimality guarantees to the solutions for integrated design and NMPC-based control problems. In this research, a transformation strategy was proposed for the solution of the bilvel problem for integrated design and NMPC-based control under uncertainty as a single-level problem referred to as a mathematical program with complementarity constraints (MPCC). In this transformation strategy, the optimization problem for the NMPC is stated in terms of its KKT conditions for optimality. Then, the corresponding set of nonlinear algebraic equations for the KKT-based controller are embedded in the design problem (upper-level) as part of the constraints. The introduction of complementarity constraint assumes the solution of a degenerate highly nonlinear formulation, which violates multiple CQs at every feasible point. Potential reformulation strategies for complementarity constraints are necessary to overcome this issue. Although the solutions for the MPCCs may not represent a solution to the original bilevel formulation, the solutions for the reformulations with MPCCs resulted in economically attractive process design and NMPC-based control schemes. On the other hand, when a proper initialization is available, the formulation with MPCCs showed an improvement of orders of magnitude in the CPU times compared with the benchmark (the back-off approach). Since the MPCC formulation is a single-level problem, the use of systematic solution algorithms is not required. Therefore, the full problem for the integration of design and NMPC-based control can be

solved with state-of-the-art optimization solvers as a conventional NLP formulation.

Formulations involving continuous decision variables have multiple applications in chemical engineering; nevertheless, integer decisions such as the location of equipment or selection of number of process units are described with discrete variables. The formulation for integrated design and NMPC-based control under uncertainty and structural decisions requires the solution of a MIBLP. Likewise to the continuous bilevel problem, the MIBLP is hard to solve using conventional MINLP solvers. In this PhD study, a proposed D-SDA approach addresses the simultaneous design and NMPC-based control of process under uncertainty and naturally ordered structural decisions. This method determines the optimal location of processing units or streams over a naturally ordered discrete set, e.g., a sequence of liquid-liquid separators, the number of trays in a distillation column, or the order of reactions units. This methodology requires the transformation of the associated MIBLP into a single-level MINLP by the implementation of a classical KKT transformation strategy. The binary variables within the formulation can be expressed as a function of reduced variable sets called external variables. A decomposition of the single-level MINLP into a master (IPLC) and a set of FNLPs primal problems. The master problem contains all the logical constraints for the selection of the superstructure. This master IPLC is solved with a D-SDA approach, whereas the primal FNLPs are solver as traditional NLPs. The D-SDA enables the exploration of neighborhoods described by the external variables, in which the primal FNLPs are solved in concordance with superstructure provided by the master problem in terms of the external variables. A search direction that provides the steepest descent in the objective function is calculated through the comparison of the neighborhood solution from the primal FNLPs. The proposed algorithmic framework is based on the definition of integral convexity. Consequently, a steepest-descent direction strategy can be implemented to explore the discrete search space. This allows the computation of local solutions that cannot be efficiently identified using conventional MINLP solvers. Note that the decomposition strategy reduces the complexity of the formulation because all logical constraints are solved in the master problem; consequently, the primal sub-problems are simpler NLPs compared to the original MINLP. A comparison of the performance of the proposed D-SDA approach and the DSTO method shows that the DSTO method is more sensitive to the initialization of the superstructure than the

D-SDA approach. Moreover, the DSTO method converged to local solutions that were closer to the initialization point. On the other hand, the D-SDA approach allowed to skip sub-optimal solution regions because the framework does not demand the relaxation of the discrete variables.

The methodology for the selection and refinement of finite elements for the discretization of the optimization formulation for the integration of design and control accounts for two criteria for the refinement of the discretization mesh. The results indicate that the selection of the discretization mesh may severely affect the solution for the integrated design and control framework, i.e., the number and quality of the finite elements returned solutions with significant differences in the process design and process dynamics. For those cases with process dynamics variations in long term periods, the discretization strategy demands higher accuracy to describe the changes in the process dynamics. On the contrary, short term variations in the process dynamics (i.e., a process with long term periods operating at steady-state) does not require high accuracy in the discretization. Furthermore, the proposed refinement strategy returned more economically attractive solutions with improved control performance using fewer finite elements compared to the naive approach involving equidistributed finite elements. Similarly, as in the back-off method, the methodology for selection/refinement of finite elements required most of the CPU time for the computation of sensitivity parameters for model approximation.

7.1 Recommendations for future work

The insights gained through this thesis have demonstrated an important number of applications for the proposed methodologies; however, several potential improvements can be considered as part of future work. The mayor recommendations derived from this research are as follows:

- The high computational demand of the proposed methodologies in this PhD study limits their application for larger scale problems. In Chapters 3 and 6, the computation of sensitivity terms demands the higher CPU times; thus, alternative techniques such as automatic differentiation can be explored in the future to enable faster computation of model sensitivities. On the other hand, in Chapter 4, the classical KKT transformation strategy returns higher dimension

NLP formulations compared with the original bilevel problems. Moreover, the substitution of the NMPC by its KKT conditions introduces new decision variables that are not physically meaningful for the system, this complicates the search for a solution. Therefore, the implementation of decomposition strategies for the solution of large-scale formulations, e.g., the decomposition of the optimization model and parallel solution can be explored in the future to improve the computational time required to converge to a solution [172]. In Chapter 5, the D-SDA approach expended most of the CPU time in the solution of the primal sub-problem during the neighborhood explorations. A strategy involving linear approximations of the primal sub-problems for the neighborhood exploration may reduce the computational burden. A validation strategy for the solutions obtained in every neighbor involving linear model approximations may consists in the evaluation of such linear solutions in the nonlinear formulation. Therefore, the solution of nonlinear primal sub-problems is enforced only for those neighbors in which the linear and nonlinear formulations have clear differences given a tolerance.

- The back-off approach presented in Chapter 3 addresses the solution of formulations for integrated design and NMPC control under uncertainty involving continuous decision variables. However, decisions associated with the topology of the process and control schemes represent discrete decisions, e.g., number and location of units. The introduction of discrete decisions increases the flexibility of the formulation for improving economic and performance aspects of the processes. Future work could focus on an enhanced version of the back-off approach that can handle formulations with both discrete and continuous decision variables, i.e., MINLP formulations for integrated design and NMPC-based control.

- The methodologies proposed in Chapters 4 and 5 implement a classical KKT transformation strategy to restate the bilevel problem for integrated design and NMPC-based control. For a convex optimization formulation for the MPC, the KKT conditions may be necessary and sufficient conditions for optimality. However, for chemical processes, a control scheme with NMPC requires the implementation of nonconvex control formulations. Under these conditions, the KKT conditions for the NMPC problem may not be sufficient conditions for optimality. Therefore, depending on the quality of the solution (i.e., a the stationarity point)

for the corresponding single-level MPCC, this solution may not be a solution to the original bilevel problem. Future work may consider the implementation of the first and second order conditions for optimality for the NMPC problem in order to determine optimal solutions for the single-level MPCC that guarantee optimal solutions for the original bilevel problem. The implementation of second order conditions for optimality drastically increases the complexity of the corresponding MPCC, thus the search for a solution to this formulation may be a challenging task.

- The D-SDA approach presented in Chapter 5 requires the initialization of the algorithm from an educated guess for the discrete decisions; otherwise, the algorithm may not converge. Moreover, the proposed D-SDA approach performs neighborhood explorations near the initialization of external variables, i.e., the algorithm does not evaluate distant neighbors from the initialization point. Thus, the algorithm may explore a large number of neighbors before it can find an optimal solution if such solution is relatively far from the initial guess. Future work may consider the application of LD-BD algorithm, in which the algorithm generates cuts that approximate the convex envelope of the objective function based on the neighborhood of potential solution candidates [173]. Moreover, the LD-BD algorithm allows the exploration of neighbors that are far from the initial guess and does not require a feasible initialization point.

- In Chapter 6, the proposed algorithm for the selection and refinement of finite elements does not consider uncertainties and discrete decisions in the integrated design and control framework. The outcome of the implementations addressed in this PhD thesis point out the close interactions of the process design and its corresponding dynamic behavior. Therefore, a future work can address the accurate selection of the discretization mesh for applications involving structural decisions for integrated design and MPC-based control problems under uncertainty.

- The methodologies proposed in this PhD thesis assume the measurement of the complete set of process states, i.e., full access to the states. In real world applications, it is not always

possible to have access to the measurements for all process states. Moreover, previous studies have shown the need to consider process noise and uncertainty within state estimation schemes to avoid infeasible operating scenarios [174, 175, 176]. Future studies can incorporate state estimation techniques to investigate more realistic scenarios under measurement noises and uncertainties for the integration of design and NMPC-based control. These studies aim to improve the process design and control performance for real world applications.

- The proposed methodologies can be extended for the intensification of process systems, e.g., reactive distillation columns [149, 177]. These systems aim to improve efficiency, reduce costs, and minimize environmental impact by increasing the effectiveness of process equipment and operations management. Integrated implementations using NMPC-based control approaches may enhance process performance, reduce energy consumption and waste generation, improve product quality and yield.

- Modern approaches with machine learning are rapidly gaining popularity in the process system engineering community [178, 179, 180]. Application with machine learning for the integration design and control have pointed out the benefits in terms of computational times, in particular for stochastic formulations that may lead to large scale problems [181]. Future work could explore the use of machine learning techniques, such as RL, to evaluate discrete decisions in integrated design and NMPC-based control formulations that involve structural decisions.

Letters of Copyright Permissions

Simultaneous design and nonlinear model predictive control under uncertainty: A back-off approach

Author: Oscar Palma-Flores,Luis A. Ricardez-Sandoval
Publication: Journal of Process Control
Publisher: Elsevier
Date: February 2022

JOHN WILEY AND SONS LICENSE
TERMS AND CONDITIONS

Apr 24, 2023

This Agreement between Mr. Oscar Palma-Flores ("You") and John Wiley and Sons ("John Wiley and Sons") consists of your license details and the terms and conditions provided by John Wiley and Sons and Copyright Clearance Center.

License Number	5535251303427
License date	Apr 24, 2023
Licensed Content Publisher	John Wiley and Sons
Licensed Content Publication	AIChE Journal
Licensed Content Title	Selection and refinement of finite elements for optimal design and control: A Hamiltonian function approach
Licensed Content Author	Luis A. Ricardez-Sandoval, Oscar Palma-Flores
Licensed Content Date	Jan 12, 2023
Licensed Content Volume	69
Licensed Content Issue	5
Licensed Content Pages	16
Type of use	Dissertation/Thesis

Requestor type	Author of this Wiley article
Format	Electronic
Portion	Full article
Will you be translating?	No
Title	Graduate Student
Institution name	University of Waterloo
Expected presentation date	Jun 2023
Order reference number	2
Requestor Location	Mr. Oscar Palma-Flores 66 Albert St, Waterloo, ON N2L 3S5 Canada Attn: Mr. Oscar Palma-Flores
Publisher Tax ID	EU826007151
Total	0.00 USD

Terms and Conditions

TERMS AND CONDITIONS

This copyrighted material is owned by or exclusively licensed to John Wiley & Sons, Inc. or one of its group companies (each a"Wiley Company") or handled on behalf of a society with which a Wiley Company has exclusive publishing rights in relation to a particular work (collectively "WILEY"). By clicking "accept" in connection with completing this licensing transaction, you agree that the following terms and conditions apply to this transaction (along with the billing and payment terms and conditions established by the Copyright Clearance Center Inc., ("CCC's Billing and Payment terms and conditions"), at the time that

you opened your RightsLink account (these are available at any time at http://myaccount.copyright.com).

Terms and Conditions

- The materials you have requested permission to reproduce or reuse (the "Wiley Materials") are protected by copyright.

- You are hereby granted a personal, non-exclusive, non-sub licensable (on a stand-alone basis), non-transferable, worldwide, limited license to reproduce the Wiley Materials for the purpose specified in the licensing process. This license, **and any CONTENT (PDF or image file) purchased as part of your order,** is for a one-time use only and limited to any maximum distribution number specified in the license. The first instance of republication or reuse granted by this license must be completed within two years of the date of the grant of this license (although copies prepared before the end date may be distributed thereafter). The Wiley Materials shall not be used in any other manner or for any other purpose, beyond what is granted in the license. Permission is granted subject to an appropriate acknowledgement given to the author, title of the material/book/journal and the publisher. You shall also duplicate the copyright notice that appears in the Wiley publication in your use of the Wiley Material. Permission is also granted on the understanding that nowhere in the text is a previously published source acknowledged for all or part of this Wiley Material. Any third party content is expressly excluded from this permission.

- With respect to the Wiley Materials, all rights are reserved. Except as expressly granted by the terms of the license, no part of the Wiley Materials may be copied, modified, adapted (except for minor reformatting required by the new Publication), translated, reproduced, transferred or distributed, in any form or by any means, and no derivative works may be made based on the Wiley Materials without the prior permission of the respective copyright owner.**For STM Signatory Publishers clearing permission under the terms of the STM Permissions Guidelines only, the terms of the license are extended to include subsequent editions and for editions in other languages, provided such editions are for the work as a whole in situ and does not involve the separate exploitation of the permitted figures or extracts,** You may not alter, remove or suppress in any manner any copyright, trademark or other notices displayed by the Wiley Materials. You may not license, rent, sell, loan, lease, pledge, offer as security, transfer or assign the Wiley Materials on a stand-alone basis, or any of the rights granted to you hereunder to any other person.

- The Wiley Materials and all of the intellectual property rights therein shall at all times remain the exclusive property of John Wiley & Sons Inc, the Wiley Companies, or their respective licensors, and your interest therein is only that of having possession of and the right to reproduce the Wiley Materials pursuant to Section 2 herein during the continuance of this Agreement. You agree that you own no right, title or interest in or to the Wiley Materials or any of the intellectual property rights therein. You shall have no rights hereunder other than the license as provided for above in Section 2. No right, license or interest to any trademark, trade name, service mark or other branding ("Marks") of WILEY or its licensors is granted hereunder, and you agree that you shall not assert any such right, license or interest with respect thereto

- NEITHER WILEY NOR ITS LICENSORS MAKES ANY WARRANTY OR REPRESENTATION OF ANY KIND TO YOU OR ANY THIRD PARTY, EXPRESS, IMPLIED OR STATUTORY, WITH RESPECT TO THE MATERIALS OR THE

ACCURACY OF ANY INFORMATION CONTAINED IN THE MATERIALS, INCLUDING, WITHOUT LIMITATION, ANY IMPLIED WARRANTY OF MERCHANTABILITY, ACCURACY, SATISFACTORY QUALITY, FITNESS FOR A PARTICULAR PURPOSE, USABILITY, INTEGRATION OR NON-INFRINGEMENT AND ALL SUCH WARRANTIES ARE HEREBY EXCLUDED BY WILEY AND ITS LICENSORS AND WAIVED BY YOU.

- WILEY shall have the right to terminate this Agreement immediately upon breach of this Agreement by you.
- You shall indemnify, defend and hold harmless WILEY, its Licensors and their respective directors, officers, agents and employees, from and against any actual or threatened claims, demands, causes of action or proceedings arising from any breach of this Agreement by you.
- IN NO EVENT SHALL WILEY OR ITS LICENSORS BE LIABLE TO YOU OR ANY OTHER PARTY OR ANY OTHER PERSON OR ENTITY FOR ANY SPECIAL, CONSEQUENTIAL, INCIDENTAL, INDIRECT, EXEMPLARY OR PUNITIVE DAMAGES, HOWEVER CAUSED, ARISING OUT OF OR IN CONNECTION WITH THE DOWNLOADING, PROVISIONING, VIEWING OR USE OF THE MATERIALS REGARDLESS OF THE FORM OF ACTION, WHETHER FOR BREACH OF CONTRACT, BREACH OF WARRANTY, TORT, NEGLIGENCE, INFRINGEMENT OR OTHERWISE (INCLUDING, WITHOUT LIMITATION, DAMAGES BASED ON LOSS OF PROFITS, DATA, FILES, USE, BUSINESS OPPORTUNITY OR CLAIMS OF THIRD PARTIES), AND WHETHER OR NOT THE PARTY HAS BEEN ADVISED OF THE POSSIBILITY OF SUCH DAMAGES. THIS LIMITATION SHALL APPLY NOTWITHSTANDING ANY FAILURE OF ESSENTIAL PURPOSE OF ANY LIMITED REMEDY PROVIDED HEREIN.
- Should any provision of this Agreement be held by a court of competent jurisdiction to be illegal, invalid, or unenforceable, that provision shall be deemed amended to achieve as nearly as possible the same economic effect as the original provision, and the legality, validity and enforceability of the remaining provisions of this Agreement shall not be affected or impaired thereby.
- The failure of either party to enforce any term or condition of this Agreement shall not constitute a waiver of either party's right to enforce each and every term and condition of this Agreement. No breach under this agreement shall be deemed waived or excused by either party unless such waiver or consent is in writing signed by the party granting such waiver or consent. The waiver by or consent of a party to a breach of any provision of this Agreement shall not operate or be construed as a waiver of or consent to any other or subsequent breach by such other party.
- This Agreement may not be assigned (including by operation of law or otherwise) by you without WILEY's prior written consent.
- Any fee required for this permission shall be non-refundable after thirty (30) days from receipt by the CCC.
- These terms and conditions together with CCC's Billing and Payment terms and conditions (which are incorporated herein) form the entire agreement between you and WILEY concerning this licensing transaction and (in the absence of fraud) supersedes all prior agreements and representations of the parties, oral or written. This Agreement

may not be amended except in writing signed by both parties. This Agreement shall be binding upon and inure to the benefit of the parties' successors, legal representatives, and authorized assigns.

- In the event of any conflict between your obligations established by these terms and conditions and those established by CCC's Billing and Payment terms and conditions, these terms and conditions shall prevail.
- WILEY expressly reserves all rights not specifically granted in the combination of (i) the license details provided by you and accepted in the course of this licensing transaction, (ii) these terms and conditions and (iii) CCC's Billing and Payment terms and conditions.
- This Agreement will be void if the Type of Use, Format, Circulation, or Requestor Type was misrepresented during the licensing process.
- This Agreement shall be governed by and construed in accordance with the laws of the State of New York, USA, without regards to such state's conflict of law rules. Any legal action, suit or proceeding arising out of or relating to these Terms and Conditions or the breach thereof shall be instituted in a court of competent jurisdiction in New York County in the State of New York in the United States of America and each party hereby consents and submits to the personal jurisdiction of such court, waives any objection to venue in such court and consents to service of process by registered or certified mail, return receipt requested, at the last known address of such party.

WILEY OPEN ACCESS TERMS AND CONDITIONS

Wiley Publishes Open Access Articles in fully Open Access Journals and in Subscription journals offering Online Open. Although most of the fully Open Access journals publish open access articles under the terms of the Creative Commons Attribution (CC BY) License only, the subscription journals and a few of the Open Access Journals offer a choice of Creative Commons Licenses. The license type is clearly identified on the article.

The Creative Commons Attribution License

The Creative Commons Attribution License (CC-BY) allows users to copy, distribute and transmit an article, adapt the article and make commercial use of the article. The CC-BY license permits commercial and non-

Creative Commons Attribution Non-Commercial License

The Creative Commons Attribution Non-Commercial (CC-BY-NC)License permits use, distribution and reproduction in any medium, provided the original work is properly cited and is not used for commercial purposes.(see below)

Creative Commons Attribution-Non-Commercial-NoDerivs License

The Creative Commons Attribution Non-Commercial-NoDerivs License (CC-BY-NC-ND) permits use, distribution and reproduction in any medium, provided the original work is properly cited, is not used for commercial purposes and no modifications or adaptations are made. (see below)

Use by commercial "for-profit" organizations

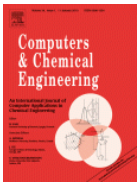

Integration of design and NMPC-based control for chemical processes under uncertainty: An MPCC-based framework

Author: Oscar Palma-Flores,Luis A. Ricardez-Sandoval

Publication: Computers & Chemical Engineering

Publisher: Elsevier

Date: June 2022

JOHN WILEY AND SONS LICENSE
TERMS AND CONDITIONS

Apr 24, 2023

This Agreement between Mr. Oscar Palma-Flores ("You") and John Wiley and Sons ("John Wiley and Sons") consists of your license details and the terms and conditions provided by John Wiley and Sons and Copyright Clearance Center.

License Number	5535250739994
License date	Apr 24, 2023
Licensed Content Publisher	John Wiley and Sons
Licensed Content Publication	AIChE Journal
Licensed Content Title	Optimal control and the Pontryagin's principle in chemical engineering: History, theory, and challenges
Licensed Content Author	Luis A. Ricardez-Sandoval, Oscar Palma-Flores, Oswaldo Andrés-Martínez
Licensed Content Date	Jun 8, 2022
Licensed Content Volume	68
Licensed Content Issue	8
Licensed Content Pages	22
Type of use	Dissertation/Thesis

Requestor type	Author of this Wiley article
Format	Electronic
Portion	Full article
Will you be translating?	No
Title	Graduate Student
Institution name	University of Waterloo
Expected presentation date	Jun 2023
Order reference number	1
Requestor Location	Mr. Oscar Palma-Flores 66 Albert St, Waterloo, ON N2L 3S5 Canada Attn: Mr. Oscar Palma-Flores
Publisher Tax ID	EU826007151
Total	0.00 CAD

Terms and Conditions

TERMS AND CONDITIONS

This copyrighted material is owned by or exclusively licensed to John Wiley & Sons, Inc. or one of its group companies (each a"Wiley Company") or handled on behalf of a society with which a Wiley Company has exclusive publishing rights in relation to a particular work (collectively "WILEY"). By clicking "accept" in connection with completing this licensing transaction, you agree that the following terms and conditions apply to this transaction (along with the billing and payment terms and conditions established by the Copyright Clearance Center Inc., ("CCC's Billing and Payment terms and conditions"), at the time that

you opened your RightsLink account (these are available at any time at http://myaccount.copyright.com).

Terms and Conditions

- The materials you have requested permission to reproduce or reuse (the "Wiley Materials") are protected by copyright.

- You are hereby granted a personal, non-exclusive, non-sub licensable (on a stand-alone basis), non-transferable, worldwide, limited license to reproduce the Wiley Materials for the purpose specified in the licensing process. This license, **and any CONTENT (PDF or image file) purchased as part of your order,** is for a one-time use only and limited to any maximum distribution number specified in the license. The first instance of republication or reuse granted by this license must be completed within two years of the date of the grant of this license (although copies prepared before the end date may be distributed thereafter). The Wiley Materials shall not be used in any other manner or for any other purpose, beyond what is granted in the license. Permission is granted subject to an appropriate acknowledgement given to the author, title of the material/book/journal and the publisher. You shall also duplicate the copyright notice that appears in the Wiley publication in your use of the Wiley Material. Permission is also granted on the understanding that nowhere in the text is a previously published source acknowledged for all or part of this Wiley Material. Any third party content is expressly excluded from this permission.

- With respect to the Wiley Materials, all rights are reserved. Except as expressly granted by the terms of the license, no part of the Wiley Materials may be copied, modified, adapted (except for minor reformatting required by the new Publication), translated, reproduced, transferred or distributed, in any form or by any means, and no derivative works may be made based on the Wiley Materials without the prior permission of the respective copyright owner.**For STM Signatory Publishers clearing permission under the terms of the STM Permissions Guidelines only, the terms of the license are extended to include subsequent editions and for editions in other languages, provided such editions are for the work as a whole in situ and does not involve the separate exploitation of the permitted figures or extracts,** You may not alter, remove or suppress in any manner any copyright, trademark or other notices displayed by the Wiley Materials. You may not license, rent, sell, loan, lease, pledge, offer as security, transfer or assign the Wiley Materials on a stand-alone basis, or any of the rights granted to you hereunder to any other person.

- The Wiley Materials and all of the intellectual property rights therein shall at all times remain the exclusive property of John Wiley & Sons Inc, the Wiley Companies, or their respective licensors, and your interest therein is only that of having possession of and the right to reproduce the Wiley Materials pursuant to Section 2 herein during the continuance of this Agreement. You agree that you own no right, title or interest in or to the Wiley Materials or any of the intellectual property rights therein. You shall have no rights hereunder other than the license as provided for above in Section 2. No right, license or interest to any trademark, trade name, service mark or other branding ("Marks") of WILEY or its licensors is granted hereunder, and you agree that you shall not assert any such right, license or interest with respect thereto

- NEITHER WILEY NOR ITS LICENSORS MAKES ANY WARRANTY OR REPRESENTATION OF ANY KIND TO YOU OR ANY THIRD PARTY, EXPRESS, IMPLIED OR STATUTORY, WITH RESPECT TO THE MATERIALS OR THE

ACCURACY OF ANY INFORMATION CONTAINED IN THE MATERIALS, INCLUDING, WITHOUT LIMITATION, ANY IMPLIED WARRANTY OF MERCHANTABILITY, ACCURACY, SATISFACTORY QUALITY, FITNESS FOR A PARTICULAR PURPOSE, USABILITY, INTEGRATION OR NON-INFRINGEMENT AND ALL SUCH WARRANTIES ARE HEREBY EXCLUDED BY WILEY AND ITS LICENSORS AND WAIVED BY YOU.

- WILEY shall have the right to terminate this Agreement immediately upon breach of this Agreement by you.
- You shall indemnify, defend and hold harmless WILEY, its Licensors and their respective directors, officers, agents and employees, from and against any actual or threatened claims, demands, causes of action or proceedings arising from any breach of this Agreement by you.
- IN NO EVENT SHALL WILEY OR ITS LICENSORS BE LIABLE TO YOU OR ANY OTHER PARTY OR ANY OTHER PERSON OR ENTITY FOR ANY SPECIAL, CONSEQUENTIAL, INCIDENTAL, INDIRECT, EXEMPLARY OR PUNITIVE DAMAGES, HOWEVER CAUSED, ARISING OUT OF OR IN CONNECTION WITH THE DOWNLOADING, PROVISIONING, VIEWING OR USE OF THE MATERIALS REGARDLESS OF THE FORM OF ACTION, WHETHER FOR BREACH OF CONTRACT, BREACH OF WARRANTY, TORT, NEGLIGENCE, INFRINGEMENT OR OTHERWISE (INCLUDING, WITHOUT LIMITATION, DAMAGES BASED ON LOSS OF PROFITS, DATA, FILES, USE, BUSINESS OPPORTUNITY OR CLAIMS OF THIRD PARTIES), AND WHETHER OR NOT THE PARTY HAS BEEN ADVISED OF THE POSSIBILITY OF SUCH DAMAGES. THIS LIMITATION SHALL APPLY NOTWITHSTANDING ANY FAILURE OF ESSENTIAL PURPOSE OF ANY LIMITED REMEDY PROVIDED HEREIN.
- Should any provision of this Agreement be held by a court of competent jurisdiction to be illegal, invalid, or unenforceable, that provision shall be deemed amended to achieve as nearly as possible the same economic effect as the original provision, and the legality, validity and enforceability of the remaining provisions of this Agreement shall not be affected or impaired thereby.
- The failure of either party to enforce any term or condition of this Agreement shall not constitute a waiver of either party's right to enforce each and every term and condition of this Agreement. No breach under this agreement shall be deemed waived or excused by either party unless such waiver or consent is in writing signed by the party granting such waiver or consent. The waiver by or consent of a party to a breach of any provision of this Agreement shall not operate or be construed as a waiver of or consent to any other or subsequent breach by such other party.
- This Agreement may not be assigned (including by operation of law or otherwise) by you without WILEY's prior written consent.
- Any fee required for this permission shall be non-refundable after thirty (30) days from receipt by the CCC.
- These terms and conditions together with CCC's Billing and Payment terms and conditions (which are incorporated herein) form the entire agreement between you and WILEY concerning this licensing transaction and (in the absence of fraud) supersedes all prior agreements and representations of the parties, oral or written. This Agreement

may not be amended except in writing signed by both parties. This Agreement shall be binding upon and inure to the benefit of the parties' successors, legal representatives, and authorized assigns.

- In the event of any conflict between your obligations established by these terms and conditions and those established by CCC's Billing and Payment terms and conditions, these terms and conditions shall prevail.
- WILEY expressly reserves all rights not specifically granted in the combination of (i) the license details provided by you and accepted in the course of this licensing transaction, (ii) these terms and conditions and (iii) CCC's Billing and Payment terms and conditions.
- This Agreement will be void if the Type of Use, Format, Circulation, or Requestor Type was misrepresented during the licensing process.
- This Agreement shall be governed by and construed in accordance with the laws of the State of New York, USA, without regards to such state's conflict of law rules. Any legal action, suit or proceeding arising out of or relating to these Terms and Conditions or the breach thereof shall be instituted in a court of competent jurisdiction in New York County in the State of New York in the United States of America and each party hereby consents and submits to the personal jurisdiction of such court, waives any objection to venue in such court and consents to service of process by registered or certified mail, return receipt requested, at the last known address of such party.

WILEY OPEN ACCESS TERMS AND CONDITIONS

Wiley Publishes Open Access Articles in fully Open Access Journals and in Subscription journals offering Online Open. Although most of the fully Open Access journals publish open access articles under the terms of the Creative Commons Attribution (CC BY) License only, the subscription journals and a few of the Open Access Journals offer a choice of Creative Commons Licenses. The license type is clearly identified on the article.

The Creative Commons Attribution License

The Creative Commons Attribution License (CC-BY) allows users to copy, distribute and transmit an article, adapt the article and make commercial use of the article. The CC-BY license permits commercial and non-

Creative Commons Attribution Non-Commercial License

The Creative Commons Attribution Non-Commercial (CC-BY-NC)License permits use, distribution and reproduction in any medium, provided the original work is properly cited and is not used for commercial purposes.(see below)

Creative Commons Attribution-Non-Commercial-NoDerivs License

The Creative Commons Attribution Non-Commercial-NoDerivs License (CC-BY-NC-ND) permits use, distribution and reproduction in any medium, provided the original work is properly cited, is not used for commercial purposes and no modifications or adaptations are made. (see below)

Use by commercial "for-profit" organizations

References

[1] Mina Rafiei and Luis A Ricardez-Sandoval. New frontiers, challenges, and opportunities in integration of design and control for enterprise-wide sustainability. *Computers & Chemical Engineering*, 132:106610, 2020.

[2] Sami S Bahakim and Luis A Ricardez-Sandoval. Simultaneous design and mpc-based control for dynamic systems under uncertainty: A stochastic approach. *Computers & Chemical Engineering*, 63:66–81, 2014.

[3] Gloria Gutierrez, Luis A Ricardez-Sandoval, H Budman, and C Prada. An mpc-based control structure selection approach for simultaneous process and control design. *Computers & chemical engineering*, 70:11–21, 2014.

[4] Vassilis Sakizlis, John D Perkins, and Efstratios N Pistikopoulos. Parametric controllers in simultaneous process and control design optimization. *Industrial & Engineering Chemistry Research*, 42(20):4545–4563, 2003.

[5] Jakob Kjøbsted Huusom. Challenges and opportunities in integration of design and control. *Computers & Chemical Engineering*, 81:138–146, 2015.

[6] Mario Francisco, Silvana Revollar, Pastora Vega, and Rosalba Lamanna. Simultaneous synthesis, design and control of processes using model predictive control. *IFAC Proceedings Volumes*, 42(11):863–868, 2009.

[7] Jeonghwa Moon, Seon Kim, and Andreas A Linninger. Integrated design and control under uncertainty: Embedded control optimization for plantwide processes. *Computers & chemical engineering*, 35(9):1718–1724, 2011.

[8] Vassilis Sakizlis, John D Perkins, and Efstratios N Pistikopoulos. Recent advances in optimization-based simultaneous process and control design. *Computers & Chemical Engineering*, 28(10):2069–2086, 2004.

[9] Pastora Vega, R Lamanna, Silvana Revollar, and Mario Francisco. Integrated design and control of chemical processes–part ii: An illustrative example. *Computers & chemical engineering*, 71:618–635, 2014.

[10] DD Brengel and WD Seider. Coordinated design and control optimization of nonlinear processes. *Computers & Chemical Engineering*, 16(9):861–886, 1992.

[11] N Chawankul, LA Ricardez Sandoval, H Budman, and PL Douglas. Integration of design and control: A robust control approach using mpc. *The Canadian Journal of Chemical Engineering*, 85(4):433–446, 2007.

[12] Frank Allgower, Rolf Findeisen, Zoltan K Nagy, et al. Nonlinear model predictive control: From theory to application. *Journal-Chinese Institute Of Chemical Engineers*, 35(3):299–316, 2004.

[13] Michael Baldea, Prodromos Daoutidis, and Zoltan K Nagy. Nonlinear model predictive control of integrated process systems. *IFAC Proceedings Volumes*, 43(14):1040–1045, 2010.

[14] Christian Hoffmann, Joris Weigert, Erik Esche, and Jens-Uwe Repke. Integration of design and operation using dynamic perturbation and chance constraints with unscented transform. In *Computer Aided Chemical Engineering*, volume 48, pages 751–756. Elsevier, 2020.

[15] Stephan Dempe. Bilevel optimization: theory, algorithms, applications and a bibliography. *Bilevel Optimization: Advances and Next Challenges*, pages 581–672, 2020.

[16] H Eliasi, MB Menhaj, and H Davilu. Robust nonlinear model predictive control for a pwr nuclear power plant. *Progress in Nuclear Energy*, 54(1):177–185, 2012.

[17] Bruce A Finlayson. Orthogonal collocation on finite elements—progress and potential. *Mathematics and Computers in simulation*, 22(1):11–17, 1980.

[18] Lorenz T Biegler. *Nonlinear programming: concepts, algorithms, and applications to chemical processes*. SIAM, 2010.

[19] Uri M Ascher, Robert MM Mattheij, and Robert D Russell. *Numerical solution of boundary value problems for ordinary differential equations*. SIAM, 1995.

[20] Oswaldo Andrés-Martínez, Oscar Palma-Flores, and Luis A Ricardez-Sandoval. Optimal control and the pontryagin's principle in chemical engineering: History, theory, and challenges. *AIChE Journal*, 68(8):e17777, 2022.

[21] Oscar Palma-Flores, Mina Rafiei, and Luis A Ricardez-Sandoval. On the implementation of nonlinear model predictive control for simultaneous designand control using a back-off approach. *IFAC-PapersOnLine*, 53(2):11551–11556, 2020.

[22] Oscar Palma-Flores and Luis A Ricardez-Sandoval. Simultaneous design and nonlinear model predictive control under uncertainty: A back-off approach. *Journal of Process Control*, 110:45–58, 2022.

[23] Oscar Palma-Flores and Luis A Ricardez-Sandoval. Integration of design and nmpc-based control for chemical processes under uncertainty: An mpcc-based framework. *Computers & Chemical Engineering*, 162:107815, 2022.

[24] Oscar Palma-Flores and Luis A. Ricardez-Sandoval. Integration of design and nmpc-based control under uncertainty and structural decisions: An mpcc-based approach. *IFAC-PapersOnLine*, ACCEPTED, 2023.

[25] Oscar Palma-Flores, Luis A. Ricardez-Sandoval, and Lorentz T. Biegler. Integrated design and nmpc-based control under uncertainty and structural decisions: A discrete-steepest descent algorithm approach. *AIChE Journal*, SUBMITTED, 2023.

[26] Oscar Palma-Flores and Luis A Ricardez-Sandoval. Selection and refinement of finite elements for optimal design and control: A hamiltonian function approach. *AIChE Journal*, page e18009, 2023.

[27] Mina Rafiei and Luis A Ricardez-Sandoval. A trust-region framework for integration of design and control. *AIChE Journal*, 66(5):e16922, 2020.

[28] Mina Rafiei and Luis A Ricardez-Sandoval. Integration of design and control for industrial-scale applications under uncertainty: A trust region approach. *Computers & Chemical Engineering*, 141:107006, 2020.

[29] B Wayne Bequette. Nonlinear control of chemical processes: A review. *Industrial & Engineering Chemistry Research*, 30(7):1391–1413, 1991.

[30] Zhihong Yuan, Bingzhen Chen, Gürkan Sin, and Rafiqul Gani. State-of-the-art and progress in the optimization-based simultaneous design and control for chemical processes. *AIChE Journal*, 58(6):1640–1659, 2012.

[31] Luis A Ricardez-Sandoval, HM Budman, and PL Douglas. Integration of design and control for chemical processes: A review of the literature and some recent results. *Annual reviews in Control*, 33(2):158–171, 2009.

[32] Edgar Bristol. On a new measure of interaction for multivariable process control. *IEEE transactions on automatic control*, 11(1):133–134, 1966.

[33] T Chanh Nguyen, Geoffrey W Barton, John D Perkins, and Richard D Johnston. A condition number scaling policy for stability robustness analysis. *AIChE journal*, 34(7):1200–1206, 1988.

[34] Sigurd Skogestad and Manfred Morari. Effect of disturbance directions on closed-loop performance. *Industrial & engineering chemistry research*, 26(10):2029–2035, 1987.

[35] Dale E Seborg, Duncan A Mellichamp, Thomas F Edgar, and Francis J Doyle III. *Process dynamics and control*. John Wiley & Sons, 2010.

[36] Lorenz T. Biegler. A perspective on nonlinear model predictive control. *Korean Journal of Chemical Engineering*, 38(7):1317–1332, 2021.

[37] Emad Ali and Evanghelos Zafiriou. On the tuning of nonlinear model predictive control algorithms. In *1993 American Control Conference*, pages 786–790. IEEE, 1993.

[38] Manfred Morari and Jay H Lee. Model predictive control: past, present and future. *Computers & Chemical Engineering*, 23(4-5):667–682, 1999.

[39] Alberto Bemporad and Manfred Morari. Robust model predictive control: A survey. In *Robustness in identification and control*, pages 207–226. Springer, 2007.

[40] Jan Marian Maciejowski. *Predictive control: with constraints*. Pearson education, 2002.

[41] Zoltan K Nagy and Richard D Braatz. Robust nonlinear model predictive control of batch processes. *AIChE Journal*, 49(7):1776–1786, 2003.

[42] Rui Huang and Lorenz T Biegler. Robust nonlinear model predictive controller design based on multi-scenario formulation. In *2009 American Control Conference*, pages 2341–2342. IEEE, 2009.

[43] L Magni, G De Nicolao, RICCARDO Scattolini, and F Allgöwer. Robust receding horizon control for nonlinear discrete-time systems. *IFAC Proceedings Volumes*, 35(1):403–408, 2002.

[44] John Darlington, Constantinos C Pantelides, Berç Rustem, and BA Tanyi. Decreasing the sensitivity of open-loop optimal solutions in decision making under uncertainty. *European Journal of Operational Research*, 121(2):343–362, 2000.

[45] Stephan Dempe. *Foundations of bilevel programming*. Springer Science & Business Media, 2002.

[46] Stephan Dempe, Vyacheslav Kalashnikov, Gerardo A Pérez-Valdés, and Nataliya Kalashnykova. Bilevel programming problems. *Energy Systems. Springer, Berlin*, 2015.

[47] Styliani Avraamidou and Efstratios N Pistikopoulos. A bi-level formulation and solution method for the integration of process design and scheduling. In *Computer Aided Chemical Engineering*, volume 47, pages 17–22. Elsevier, 2019.

[48] Xuning Guo, Tiesong Hu, Tao Zhang, and Yibing Lv. Bilevel model for multi-reservoir operating policy in inter-basin water transfer-supply project. *Journal of Hydrology*, 424:252–263, 2012.

[49] Burcu Beykal, Styliani Avraamidou, and Efstratios N Pistikopoulos. Bi-level mixed-integer data-driven optimization of integrated planning and scheduling problems. In *Computer Aided Chemical Engineering*, volume 50, pages 1707–1713. Elsevier, 2021.

[50] Burcu Beykal, Styliani Avraamidou, and Efstratios N Pistikopoulos. Data-driven optimization of mixed-integer bi-level multi-follower integrated planning and scheduling problems under demand uncertainty. *Computers & chemical engineering*, 156:107551, 2022.

[51] Noriyuki Yoshio and Lorenz T Biegler. A nested schur decomposition approach for multiperiod optimization of chemical processes. *Computers & Chemical Engineering*, 155:107509, 2021.

[52] Mohsen Saffarian, Sobhan Mostafayi, Seyed Mahmood Kazemi, and Malihe Niksirat. A two-level pricing-inventory-routing problem in green closed-loop supply chain: Bi-level programming and heuristic method. *Journal of Industrial and Systems Engineering*, 13(4):62–80, 2021.

[53] Lorenz T Biegler. Nonlinear optimization strategies for process separations and process intensification. *Chemie Ingenieur Technik*, 92(7):867–878, 2020.

[54] Stephan Dempe, Vyacheslav Kalashnikov, and Roger Z Rıos-Mercado. Discrete bilevel programming: Application to a natural gas cash-out problem. *European Journal of Operational Research*, 166(2):469–488, 2005.

[55] Stephan Dempe and Alain B Zemkoho. The bilevel programming problem: reformulations, constraint qualifications and optimality conditions. *Mathematical Programming*, 138(1):447–473, 2013.

[56] Stephen Wright, Jorge Nocedal, et al. Numerical optimization. *Springer Science*, 35(67-68):7, 1999.

[57] Olvi L Mangasarian. *Nonlinear programming*. SIAM, 1994.

[58] Li Zhou, Zuwei Liao, Jingdai Wang, Binbo Jiang, Yongrong Yang, and Huanjun Yu. Simultaneous optimization of heat-integrated water allocation networks using the mathematical model with equilibrium constraints strategy. *Industrial & Engineering Chemistry Research*, 54(13):3355–3366, 2015.

[59] Manuel A Ramos, Jorge M Gómez, and Jean-Michel Reneaume. Simultaneous optimal design and control of an extractive distillation system for the production of fuel grade ethanol using a mathematical program with complementarity constraints. *Industrial & Engineering Chemistry Research*, 53(2):752–764, 2014.

[60] Jodie M Simkoff and Michael Baldea. Production scheduling and linear mpc: Complete integration via complementarity conditions. *Computers & Chemical Engineering*, 125:287–305, 2019.

[61] BT Baumrucker, Jeffrey G Renfro, and Lorenz T Biegler. Mpec problem formulations and solution strategies with chemical engineering applications. *Computers & Chemical Engineering*, 32(12):2903–2913, 2008.

[62] Jean-Pierre Dussault, Mounir Haddou, Abdeslam Kadrani, and Tangi Migot. How to compute a m-stationary point of the mpcc. *Available from: Optimization-Online.org*, 2017.

[63] Stephan Dempe and Alain B Zemkoho. On the karush–kuhn–tucker reformulation of the bilevel optimization problem. *Nonlinear Analysis: Theory, Methods & Applications*, 75(3):1202–1218, 2012.

[64] XM Hu and Daniel Ralph. Convergence of a penalty method for mathematical programming with complementarity constraints. *Journal of Optimization Theory and Applications*, 123(2):365–390, 2004.

[65] Jie Lu, Jialin Han, Yaoguang Hu, and Guangquan Zhang. Multilevel decision-making: A survey. *Information Sciences*, 346:463–487, 2016.

[66] Thomas A Edmunds and Jonathan F Bard. An algorithm for the mixed-integer nonlinear bilevel programming problem. *Annals of Operations Research*, 34(1):149–162, 1992.

[67] Luis F Domínguez and Efstratios N Pistikopoulos. Multiparametric programming based algorithms for pure integer and mixed-integer bilevel programming problems. *Computers & Chemical Engineering*, 34(12):2097–2106, 2010.

[68] Nuno P Faísca, Vivek Dua, Berç Rustem, Pedro M Saraiva, and Efstratios N Pistikopoulos. Parametric global optimisation for bilevel programming. *Journal of Global Optimization*, 38(4):609–623, 2007.

[69] Nuno P Faísca, Pedro M Saraiva, Berç Rustem, and Efstratios N Pistikopoulos. A multiparametric programming approach for multilevel hierarchical and decentralised optimisation problems. *Computational management science*, 6(4):377–397, 2009.

[70] Alexander Mitsos. Global solution of nonlinear mixed-integer bilevel programs. *Journal of Global Optimization*, 47(4):557–582, 2010.

[71] PA Clark. Bilevel programming for steady-state chemical process design—ii. performance study for nondegenerate problems. *Computers & Chemical Engineering*, 14(1):99–109, 1990.

[72] William Robert Smith. Chemical reaction equilibrium analysis. *Theory and Algorithms*, 1982.

[73] Georges K Saharidis and Marianthi G Ierapetritou. Resolution method for mixed integer bi-level linear problems based on decomposition technique. *Journal of Global Optimization*, 44:29–51, 2009.

[74] Ue-Pyng Wen and YH Yang. Algorithms for solving the mixed integer two-level linear programming problem. *Computers & Operations Research*, 17(2):133–142, 1990.

[75] Kailash Lachhwani and Abhishek Dwivedi. Bi-level and multi-level programming problems: taxonomy of literature review and research issues. *Archives of Computational Methods in Engineering*, 25:847–877, 2018.

[76] James T Moore and Jonathan F Bard. The mixed integer linear bilevel programming problem. *Operations research*, 38(5):911–921, 1990.

[77] Bo Zeng and Yu An. Solving bilevel mixed integer program by reformulations and decomposition. *Optimization online*, pages 1–34, 2014.

[78] Christopher LE Swartz and Yoshiaki Kawajiri. Design for dynamic operation-a review and new perspectives for an increasingly dynamic plant operating environment. *Computers & Chemical Engineering*, 128:329–339, 2019.

[79] Thomas E Marlin. *Process control: designing processes and control systems for dynamic performance*. McGraw-Hill Science, Engineering & Mathematics, 2000.

[80] Lorenz T Biegler, Arturo M Cervantes, and Andreas Wächter. Advances in simultaneous strategies for dynamic process optimization. *Chemical engineering science*, 57(4):575–593, 2002.

[81] Lev Semenovich Pontrjagin, RV Gamkrelidze, and Vladimir Grigor'evic Boltjanskij. *The mathematical theory of optimal processes*. Macmillan Company, 1964.

[82] Shivakumar Kameswaran and Lorenz T Biegler. Simultaneous dynamic optimization strategies: Recent advances and challenges. *Computers & Chemical Engineering*, 30(10-12):1560–1575, 2006.

[83] Piernicola Bettiol and Richard B Vinter. Sensitivity interpretations of the costate variable for optimal control problems with state constraints. *SIAM journal on control and optimization*, 48(5):3297–3317, 2010.

[84] Sunil Kumar Agrawal and Brian C Fabien. *Optimization of dynamic systems*, volume 70. Springer Science & Business Media, 2013.

[85] Weifeng Chen, Zhijiang Shao, and Lorenz T Biegler. A bilevel nlp sensitivity-based decomposition for dynamic optimization with moving finite elements. *AIChE Journal*, 60(3):966–979, 2014.

[86] Fady Assassa and Wolfgang Marquardt. Optimality-based grid adaptation for input-affine optimal control problems. *Computers & Chemical Engineering*, 92:189–203, 2016.

[87] Mahdi Sharifzadeh. Integration of process design and control: A review. *Chemical Engineering Research and Design*, 91(12):2515–2549, 2013.

[88] Pastora Vega, R Lamanna De Rocco, Silvana Revollar, and Mario Francisco. Integrated design and control of chemical processes–part i: Revision and classification. *Computers & chemical engineering*, 71:602–617, 2014.

[89] Baris Burnak, Nikolaos A Diangelakis, and Efstratios N Pistikopoulos. Towards the grand unification of process design, scheduling, and control—utopia or reality? *Processes*, 7(7):461, 2019.

[90] C Loeblein and JD Perkins. Structural design for on-line process optimization: I. dynamic economics of mpc. *AIChE Journal*, 45(5):1018–1029, 1999.

[91] Vassilis Sakizlis, John D Perkins, and Efstratios N Pistikopoulos. Simultaneous process and control design using mixed integer dynamic optimization and parametric programming. *Computer Aided Chemical Engineering*, 17:187–215, 2004.

[92] Rhoda Baker and Christopher Swartz. Interior point solution of integrated plant and control designproblems with embedded mpc. *AIChE annual meeting*, pages 12–7, 2006.

[93] Luis A Ricardez-Sandoval, Hector M Budman, and Peter L Douglas. Application of robust control tools to the simultaneous design and control of dynamic systems. *Industrial & Engineering Chemistry Research*, 48(2):801–813, 2009.

[94] Luis A Ricardez-Sandoval, Hector M Budman, and Peter L Douglas. Simultaneous design and control: A new approach and comparisons with existing methodologies. *Industrial & Engineering Chemistry Research*, 49(6):2822–2833, 2010.

[95] Luis A Ricardez-Sandoval, PL Douglas, and HM Budman. A methodology for the simultaneous design and control of large-scale systems under process parameter uncertainty. *Computers & chemical engineering*, 35(2):307–318, 2011.

[96] Mario Francisco, Pastora Vega, and Omar Pérez. Process integrated design within a model predictive control framework. *IFAC Proceedings Volumes*, 38(1):409–414, 2005.

[97] Mario Francisco and Pastora Vega. Multi-model approaches for integrated design of wastewater treatment plants with model predictive control. *IFAC Proceedings Volumes*, 41(2):9380–9385, 2008.

[98] M Francisco, P Vega, and H Alvarez. Robust integrated design of processes with terminal penalty model predictive controllers. *Chemical Engineering Research and Design*, 89(7):1011–1024, 2011.

[99] Gloria Gutierrez, LA Ricardez, H Budman, and C Prada. Integration of design and control using an mpc-based superstructure for control structure selection. *IFAC Proceedings Volumes*, 44(1):7648–7653, 2011.

[100] Kelvyn B Sanchez-Sanchez and Luis A Ricardez-Sandoval. Simultaneous design and control under uncertainty using model predictive control. *Industrial & Engineering Chemistry Research*, 52(13):4815–4833, 2013.

[101] Baris Burnak and Efstratios N Pistikopoulos. Integrated process design, scheduling, and model predictive control of batch processes with closed-loop implementation. *AIChE Journal*, 66(10):e16981, 2020.

[102] Romero F de Carvalho and Luz A Alvarez. Simultaneous process design and control of the williams–otto reactor using infinite horizon model predictive control. *Industrial & Engineering Chemistry Research*, 59(36):15979–15989, 2020.

[103] Henrique Oyama and Helen Durand. Interactions between control and process design under economic model predictive control. *Journal of Process Control*, 92:1–18, 2020.

[104] Yuhe Tian, Iosif Pappas, Baris Burnak, Justin Katz, and Efstratios N Pistikopoulos. Simultaneous design & control of a reactive distillation system–a parametric optimization & control approach. *Chemical Engineering Science*, 230:116232, 2021.

[105] Haitao Huang and James B Riggs. Comparison of pi and mpc for control of a gas recovery unit. *Journal of Process Control*, 12(1):163–173, 2002.

[106] Nikolaos A Diangelakis, Baris Burnak, Justin Katz, and Efstratios N Pistikopoulos. Process design and control optimization: A simultaneous approach by multi-parametric programming. *AIChE Journal*, 63(11):4827–4846, 2017.

[107] Efstratios N Pistikopoulos, Nikolaos A Diangelakis, Richard Oberdieck, Maria M Papathanasiou, Ioana Nascu, and Muxin Sun. Paroc—an integrated framework and software platform for the optimisation and advanced model-based control of process systems. *Chemical Engineering Science*, 136:115–138, 2015.

[108] Wei Shyy. An adaptive grid method for navier-stokes flow computation. *Applied mathematics and computation*, 21(3):201–219, 1987.

[109] Wei Shyy. An adaptive grid method for navier-stokes flow computation ii: Grid addition. *Applied numerical mathematics*, 2(1):9–19, 1986.

[110] Panagiotis Seferlis and Andrew N Hrymak. Adaptive collocation on finite elements models for the optimization of multistage distillation units. *Chemical engineering science*, 49(9):1369–1382, 1994.

[111] Evgeny Lazutkin, Abebe Geletu, and Pu Li. An approach to determining the number of time intervals for solving dynamic optimization problems. *Industrial & Engineering Chemistry Research*, 57(12):4340–4350, 2018.

[112] Thomas Budiarto, Joris Weigert, Christian Hoffmann, Erik Esche, and JensUwe Repke. Evaluation of discretization methods for modeling the chloralkali membrane process. In *Computer Aided Chemical Engineering*, volume 46, pages 589–594. Elsevier, 2019.

[113] Hao Jie, Meichen Yuan, and Weirong Hong. A quasi-sequential algorithm for pde-constrained optimization based on space–time orthogonal collocation on finite elements. *Journal of Process Control*, 98:1–9, 2021.

[114] James E Cuthrell and Lorenz T Biegler. On the optimization of differential-algebraic process systems. *AIChE Journal*, 33(8):1257–1270, 1987.

[115] Stephen F Davis and Joseph E Flaherty. An adaptive finite element method for initial-boundary value problems for partial differential equations. *SIAM Journal on Scientific and Statistical Computing*, 3(1):6–27, 1982.

[116] Weizhang Huang and Robert D Russell. *Adaptive moving mesh methods*, volume 174. Springer Science & Business Media, 2010.

[117] Fengjin Liu, William W Hager, and Anil V Rao. Adaptive mesh refinement method for optimal control using nonsmoothness detection and mesh size reduction. *Journal of the Franklin Institute*, 352(10):4081–4106, 2015.

[118] Yiming Zhao and Panagiotis Tsiotras. Density functions for mesh refinement in numerical optimal control. *Journal of guidance, control, and dynamics*, 34(1):271–277, 2011.

[119] K Wright. Adaptive methods for piecewise polynomial collocation for ordinary differential equations. *BIT Numerical Mathematics*, 47(1):197–212, 2007.

[120] RD Russell and J Christiansen. Adaptive mesh selection strategies for solving boundary value problems. *SIAM Journal on Numerical Analysis*, 15(1):59–80, 1978.

[121] Chris J Budd, Weizhang Huang, and Robert D Russell. Adaptivity with moving grids. *Acta Numerica*, 18:111–241, 2009.

[122] JD Perkins. Interactions between process design and process control. *IFAC Proceedings Volumes*, 22(8):195–203, 1989.

[123] Lawrence T Narraway and John D Perkins. Selection of process control structure based on linear dynamic economics. *Industrial & Engineering Chemistry Research*, 32(11):2681–2692, 1993.

[124] Ioannis K Kookos and John D Perkins. An algorithm for simultaneous process design and control. *Industrial & engineering chemistry research*, 40(19):4079–4088, 2001.

[125] IK Kookos and JD Perkins. The back-off approach to simultaneous design control. In *Computer Aided Chemical Engineering*, volume 17, pages 216–238. Elsevier, 2004.

[126] Siddharth Mehta and Luis A Ricardez-Sandoval. Integration of design and control of dynamic systems under uncertainty: A new back-off approach. *Industrial & Engineering Chemistry Research*, 55(2):485–498, 2016.

[127] Mina Rafiei-Shishavan, Siddharth Mehta, and Luis A Ricardez-Sandoval. Simultaneous design and control under uncertainty: A back-off approach using power series expansions. *Computers & Chemical Engineering*, 99:66–81, 2017.

[128] Mina Rafiei and Luis A Ricardez-Sandoval. Stochastic back-off approach for integration of design and control under uncertainty. *Industrial & Engineering Chemistry Research*, 57(12):4351–4365, 2018.

[129] Seyedehmina Rafieishishavan. Integration of design and control for large-scale applications: a back-off approach. 2020.

[130] Erik Visser, Bala Srinivasan, Srinivas Palanki, and Dominique Bonvin. A feedback-based implementation scheme for batch process optimization. *Journal of Process Control*, 10(5):399–410, 2000.

[131] Balasubramaniam Srinivasan, Dominique Bonvin, Erik Visser, and Srinivas Palanki. Dynamic optimization of batch processes: Ii. role of measurements in handling uncertainty. *Computers & chemical engineering*, 27(1):27–44, 2003.

[132] Jun Shi, Lorenz T Biegler, and Intan Hamdan. Optimization of grade transitions in polyethylene solution polymerization processes. *AIChE Journal*, 62(4):1126–1142, 2016.

[133] Carmen G Moles, G Gutierrez, Antonio A Alonso, and Julio R Banga. Integrated process design and control via global optimization: a wastewater treatment plant case study. *Chemical Engineering Research and Design*, 81(5):507–517, 2003.

[134] NL Ricker. Optimal steady-state operation of the tennessee eastman challenge process. *Computers & chemical engineering*, 19(9):949–959, 1995.

[135] James J Downs and Ernest F Vogel. A plant-wide industrial process control problem. *Computers & chemical engineering*, 17(3):245–255, 1993.

[136] Linlin Liu, Haodong Song, Lei Zhang, and Jian Du. Heat-integrated water allocation network synthesis for industrial parks with sequential and simultaneous design. *Computers & Chemical Engineering*, 108:408–424, 2018.

[137] Nikolaos A Diangelakis, Styliani Avraamidou, and Efstratios N Pistikopoulos. Decentralized multiparametric model predictive control for domestic combined heat and power systems. *Industrial & Engineering Chemistry Research*, 55(12):3313–3326, 2016.

[138] Manuel Tejeda-Iglesias, Nikolaos H Lappas, Chrysanthos E Gounaris, and Luis Ricardez-Sandoval. Explicit model predictive controller under uncertainty: An adjustable robust optimization approach. *Journal of Process Control*, 84:115–132, 2019.

[139] Stephan Dempe and Joydeep Dutta. Is bilevel programming a special case of a mathematical program with complementarity constraints? *Mathematical programming*, 131(1):37–48, 2012.

[140] Vipin Gopal and Lorenz T Biegler. Smoothing methods for complementarity problems in process engineering. *AIChE journal*, 45(7):1535–1547, 1999.

[141] Daniel Ralph and Stephen J Wright. Some properties of regularization and penalization schemes for mpecs. *Optimization Methods and Software*, 19(5):527–556, 2004.

[142] Xiaojun Chen and Masao Fukushima. A smoothing method for a mathematical program with p-matrix linear complementarity constraints. *Computational Optimization and Applications*, 27(3):223–246, 2004.

[143] Tim Hoheisel, Christian Kanzow, and Alexandra Schwartz. Theoretical and numerical comparison of relaxation methods for mathematical programs with complementarity constraints. *Mathematical Programming*, 137(1):257–288, 2013.

[144] Aurél Galántai. Properties and construction of ncp functions. *Computational Optimization and Applications*, 52(3):805–824, 2012.

[145] Larry C Young. Orthogonal collocation revisited. *Computer Methods in Applied Mechanics and Engineering*, 345:1033–1076, 2019.

[146] Bruce A Finlayson. *The method of weighted residuals and variational principles*. SIAM, 2013.

[147] P Seferlis and M Georgiadis. The need for simultaneous design education. *The integration of process design and control*, 17(10), 2004.

[148] James Merrill Douglas. *Conceptual design of chemical processes*, volume 1110. McGraw-Hill New York, 1988.

[149] David A Linán, David E Bernal, Luis A Ricardez-Sandoval, and Jorge M Gómez. Optimal design of superstructures for placing units and streams with multiple and ordered available locations. part i: A new mathematical framework. *Computers & Chemical Engineering*, 137:106794, 2020.

[150] EN Pistikopoulos. Uncertainty in process design and operations. *Computers & Chemical Engineering*, 19:553–563, 1995.

[151] Jan Kronqvist, David E Bernal, Andreas Lundell, and Ignacio E Grossmann. A review and comparison of solvers for convex minlp. *Optimization and Engineering*, 20:397–455, 2019.

[152] Pierre Bonami, Mustafa Kilinç, and Jeff Linderoth. Algorithms and software for convex mixed integer nonlinear programs. In *Mixed integer nonlinear programming*, pages 1–39. Springer, 2011.

[153] Amy R Ciric and Deyao Gu. Synthesis of nonequilibrium reactive distillation processes by minlp optimization. *AIChE Journal*, 40(9):1479–1487, 1994.

[154] Andreas Wächter and Lorenz T Biegler. On the implementation of an interior-point filter line-search algorithm for large-scale nonlinear programming. *Mathematical programming*, 106:25–57, 2006.

[155] Kazuo Murota and Akihisa Tamura. Application of m-convex submodular flow problem to mathematical economics. *Japan Journal of Industrial and Applied Mathematics*, 20(3):257, 2003.

[156] Laurence A Wolsey and George L Nemhauser. *Integer and combinatorial optimization*, volume 55. John Wiley & Sons, 1999.

[157] Kazuo Murota. On steepest descent algorithms for discrete convex functions. *SIAM Journal on Optimization*, 14(3):699–707, 2004.

[158] Metin Türkay and Ignacio E Grossmann. Logic-based minlp algorithms for the optimal synthesis of process networks. *Computers & Chemical Engineering*, 20(8):959–978, 1996.

[159] David A Liñán and Luis A Ricardez-Sandoval. Optimal design and dynamic transitions of multitask catalytic distillation columns: A discrete-steepest descend framework. *Chemical Engineering and Processing-Process Intensification*, 180:108655, 2022.

[160] William W Hager and Panos M Pardalos. *Optimal Control: Theory, Algorithms, and Applications*, volume 15. Springer Science & Business Media, 2013.

[161] Y-D Lang and LT Biegler. Distributed stream method for tray optimization. *AIChE Journal*, 48(3):582–595, 2002.

[162] V Bansal, JD Perkins, EN Pistikopoulos, R Ross, and JMG Van Schijndel. Simultaneous design and control optimisation under uncertainty. *Computers & Chemical Engineering*, 24(2-7):261–266, 2000.

[163] Minliang Gong, Aipeng Jiang, Quannan Zhang, Haokun Wang, Junjie Hu, and Yinghui Lin. An improved finite element meshing strategy for dynamic optimization problems. *Mathematical Problems in Engineering*, 2017, 2017.

[164] Bruce A Finlayson. Orthogonal collocation in chemical reaction engineering. *Catalysis Reviews Science and Engineering*, 10(1):69–138, 1974.

[165] Philippe G Ciarlet, F Cucker, and Jacques-Louis Lions. *Handbook of numerical analysis*, volume 11. Gulf Professional Publishing, 1990.

[166] Weifeng Chen and Lorenz T Biegler. Nested direct transcription optimization for singular optimal control problems. *AIChE Journal*, 62(10):3611–3627, 2016.

[167] Charles C Margossian. A review of automatic differentiation and its efficient implementation. *Wiley interdisciplinary reviews: data mining and knowledge discovery*, 9(4):e1305, 2019.

[168] Shivakumar Kameswaran and Lorenz T Biegler. Convergence rates for direct transcription of optimal control problems using collocation at radau points. *Computational Optimization and Applications*, 41(1):81–126, 2008.

[169] Lev Semenovich Pontryagin. *Mathematical theory of optimal processes*. CRC press, 1987.

[170] Carl A Schweiger and Christodoulos A Floudas. Interaction of design and control: Optimization with dynamic models. In *Optimal control*, pages 388–435. Springer, 1998.

[171] Theodore J Williams and Robert E Otto. A generalized chemical processing model for the investigation of computer control. *Transactions of the American Institute of Electrical Engineers, Part I: Communication and Electronics*, 79(5):458–473, 1960.

[172] Victor M Zavala, Carl D Laird, and Lorenz T Biegler. Interior-point decomposition approaches for parallel solution of large-scale nonlinear parameter estimation problems. *Chemical Engineering Science*, 63(19):4834–4845, 2008.

[173] David A Liñán and Luis A Ricardez-Sandoval. A benders decomposition framework for the optimization of disjunctive superstructures with ordered discrete decisions. *AIChE Journal*, page e18008.

[174] Mahshad Valipour and Luis A Ricardez-Sandoval. Extended moving horizon estimation for chemical processes under non-gaussian noises. *AIChE Journal*, 68(3):e17545, 2022.

[175] Mahshad Valipour and Luis A Ricardez-Sandoval. A robust moving horizon estimation under unknown distributions of process or measurement noises. *Computers & Chemical Engineering*, 157:107620, 2022.

[176] Mahshad Valipour and Luis A Ricardez-Sandoval. Constrained abridged gaussian sum extended kalman filter: constrained nonlinear systems with non-gaussian noises and uncertainties. *Industrial & Engineering Chemistry Research*, 60(47):17110–17127, 2021.

[177] David A Linán, David E Bernal, Luis A Ricardez-Sandoval, and Jorge M Gómez. Optimal design of superstructures for placing units and streams with multiple and ordered available locations. part ii: Rigorous design of catalytic distillation columns. *Computers & Chemical Engineering*, 139:106845, 2020.

[178] Panagiotis Petsagkourakis, Ilya Orson Sandoval, Eric Bradford, Dongda Zhang, and Ehecatl Antonio del Rio-Chanona. Reinforcement learning for batch bioprocess optimization. *Computers & Chemical Engineering*, 133:106649, 2020.

[179] Haochen Hua, Yuchao Qin, Chuantong Hao, and Junwei Cao. Optimal energy management strategies for energy internet via deep reinforcement learning approach. *Applied energy*, 239:598–609, 2019.

[180] Kody M Powell, Derek Machalek, and Titus Quah. Real-time optimization using reinforcement learning. *Computers & Chemical Engineering*, 143:107077, 2020.

[181] Tannia A Mendiola-Rodriguez and Luis A Ricardez-Sandoval. Integration of design and control for renewable energy systems with an application to anaerobic digestion: A deep deterministic policy gradient framework. *Energy*, 274:127212, 2023.

APPENDICES

Appendix A

MPCC-based formulation for two CSTRs in series

This appendix provides the complete discretized MPCC-based formulation for the integration of design and NMPC-based control under uncertainty of the two CSTRs in series. This problem corresponds to the case study 2 in Chapter 4.

$$\min_{D_e,h_T,\mathbf{x}_{i,k},\mathbf{u}_{i,k},C_{A1}^{sp},\mathbf{Q_{out}}} \Phi = 3834(D_e^{1.066}+h_T^{0.802}) + 37\sum_{i=1}^{N_{FE}} \bar{F}_{w1_i}(t)+\bar{F}_{w2_i}(t)dt + 1.0\times 10^6 \sum_{i,j=1}^{N_{FE}K} (C_{A2_{i,k}}-C_{A2}^{sp})^2 \quad \text{(A.1)}$$

$$\text{s.t. } \sum_{j=1}^{K} \dot{\ell}_{j,k} C_{A1_{i,j}} = \frac{\bar{F}}{V_R}(C_{A0}-C_{A1_{i,k}}) - k_{re} e^{\frac{-E}{RT_{1_{i,k}}}} C_{A1_{i,k}},\ i=\{1,\dots,N_{FE}\}\ k=\{1,\dots,K\}$$

$$\sum_{j=1}^{K} \dot{\ell}_{j,k} T_{1_{i,j}} = \frac{\bar{F}}{V_R}(T_{in}-T_{1_{i,k}}) + \frac{(-\Delta H_{rx})}{Cp^l} k_{re} e^{\frac{-E}{RT_{1_{i,k}}}} C_{A1_{i,k}} - \frac{U_h A_e (T_{1_{i,k}}-T_{c1_{i,k}})}{V_R Cp^l},$$
$$i=\{1,\dots,N_{FE}\},\ k=\{1,\dots,K\}$$

$$\sum_{j=1}^{K} \dot{\ell}_{j,k} T_{c1_{i,j}} = \frac{\bar{F}_{w1}}{Vj}(T_c^0-T_{c1_{i,k}}) + \frac{U_h A_e (T_{1_{i,k}}-T_{c1_{i,k}})}{Vj C_p^w},\ i=\{1,\dots,N_{FE}\},\ k=\{1,\dots,K\}$$

$$\sum_{j=1}^{K} \dot{\ell}_{j,k} C_{A2_{i,j}} = \frac{\bar{F}}{V_R}(C_{A1_{i,k}}-C_{A2_{i,k}}) - k_{re} e^{\frac{-E}{RT_{2_{i,k}}}} C_{A2_{i,k}},\ i=\{1,\dots,N_{FE}\},\ k=\{1,\dots,K\}$$

$$\sum_{j=1}^{K} \dot{\ell}_{j,k} T_{2_{i,j}} = \frac{\bar{F}}{V_R}(T_{1_{i,k}}-T_{2_{i,k}}) + \frac{(-\Delta H_{rx})}{C_p^l} k_{re} e^{\frac{-E}{RT_{2_{i,k}}}} C_{A2_{i,k}} - \frac{U_h A_e (T_{2_{i,k}}-T_{c2_{i,k}})}{V_R C_p^l},$$
$$i=\{1,\dots,N_{FE}\},\ k=\{1,\dots,K\}$$

$$\sum_{j=1}^{K} \dot{\ell}_{j,k} T_{c2_{i,j}} = \frac{\bar{F}_{w2}}{Vj}(T_c^0-T_{c2_{i,k}}) + \frac{U_h A_e (T_{2_{i,k}}-T_{c2_{i,k}})}{Vj C_p^w},\ i=\{1,\dots,N_{FE}\},\ k=\{1,\dots,K\}$$

$$C_{A1_{1,1}} = C_{A0},\ T_{1_{1,1}} = T_1^0,\ T_{c1_{1,1}} = T_{c1}^0,\ C_{A2_{1,1}} = C_{A1}^0,\ T_{2_{1,1}} = T_2^0,\ T_{c2_{1,1}} = T_{c2}^0$$

$$h_T/D_e = 2,\ V_R = \pi\frac{D_e^2 h_T}{4},\ A_d = \pi D_e h_T,\ Vj = \pi\frac{D_e h_T}{3}$$

$$\nabla_{C_{A1_{i,1}}}\mathcal{L} = \frac{d\Phi}{dC_{A1_{i,1}}} + \sum_{j=1}^{K} \dot{\ell}_{1,j}\lambda_{1_{i,j}} - \ell_{1,K}\nu_{1_{i+1}} + \nu_{1_i} - \mu_{9_{i,1}} + \mu_{10_{i,1}} = 0,$$

$$i = \{1, \ldots, N_{FE} - 1\}$$

$$\nabla_{T_{1_{i,1}}}\mathcal{L} = \sum_{j=1}^{K} \dot{\ell}_{1,j}\lambda_{2_{i,j}} - \ell_{1,K}\nu_{2_{i+1}} + \nu_{2_i} - \mu_{1_{i,1}} + \mu_{2_{i,1}} = 0, \;\; i = \{1, \ldots, N_{FE} - 1\}$$

$$\nabla_{T_{c1_{i,1}}}\mathcal{L} = \sum_{j=1}^{K} \dot{\ell}_{1,j}\lambda_{3_{i,j}} - \ell_{1,K}\nu_{3_{i+1}} + \nu_{3_i} - \mu_{3_{i,1}} + \mu_{4_{i,1}} = 0, \;\; i = \{1, \ldots, N_{FE} - 1\}$$

$$\nabla_{C_{A2_{i,1}}}\mathcal{L} = \frac{d\Phi}{dC_{A2_{i,1}}} + \sum_{j=1}^{K} \dot{\ell}_{1,j}\lambda_{4_{i,j}} - \ell_{1,K}\nu_{4_{i+1}} + \nu_{4_i} - \mu_{11_{i,1}} + \mu_{12_{i,1}} = 0,$$

$$i = \{1, \ldots, N_{FE} - 1\}$$

$$\nabla_{T_{2_{i,1}}}\mathcal{L} = \sum_{j=1}^{K} \dot{\ell}_{1,j}\lambda_{5_{i,j}} - \ell_{1,K}\nu_{5_{i+1}} + \nu_{5_i} - \mu_{5_{i,1}} + \mu_{6_{i,1}} = 0, \;\; i = \{1, \ldots, N_{FE} - 1\}$$

$$\nabla_{T_{c2_{i,1}}}\mathcal{L} = \sum_{j=1}^{K} \dot{\ell}_{1,j}\lambda_{6_{i,j}} - \ell_{1,K}\nu_{6_{i+1}} + \nu_{6_i} - \mu_{7_{i,1}} + \mu_{8_{i,1}} = 0, \;\; i = \{1, \ldots, N_{FE} - 1\}$$

$$\nabla_{C_{A1_{N_{FE},1}}}\mathcal{L} = \frac{d\Phi}{dC_{A1_{N_{FE},1}}} + \sum_{j=1}^{K} \dot{\ell}_{1,j}\lambda_{1_{N_{FE},j}} + \nu_{1_{N_{FE}}} - \mu_{9_{N_{FE},1}} + \mu_{10_{N_{FE},1}} = 0,$$

$$\nabla_{T_{1_{N_{FE},1}}}\mathcal{L} = \sum_{j=1}^{K} \dot{\ell}_{1,k}\lambda_{2_{N_{FE},k}} + \nu_{2_{N_{FE}}} - \mu_{1_{N_{FE},1}} + \mu_{2_{N_{FE},1}} = 0,$$

$$\nabla_{T_{c1_{N_{FE},1}}}\mathcal{L} = \sum_{j=1}^{K} \dot{\ell}_{1,j}\lambda_{3_{N_{FE},j}} + \nu_{3_{N_{FE}}} - \mu_{3_{N_{FE},1}} + \mu_{4_{N_{FE},1}} = 0,$$

$$\nabla_{C_{A2_{N_{FE},1}}}\mathcal{L} = \frac{d\Phi}{dC_{A2_{N_{FE},1}}} + \sum_{j=1}^{K} \dot{\ell}_{1,j}\lambda_{4_{N_{FE},j}} + \nu_{4_{N_{FE}}} - \mu_{11_{N_{FE},1}} + \mu_{12_{N_{FE},1}} = 0,$$

$$\nabla_{T_{2_{N_{FE},1}}}\mathcal{L} = \sum_{j=1}^{K} \dot{\ell}_{1,j}\lambda_{5_{N_{FE},j}} + \nu_{5_{N_{FE}}} - \mu_{5_{N_{FE},1}} + \mu_{6_{N_{FE},1}} = 0,$$

$$\nabla_{T_{c2_{N_{FE},1}}}\mathcal{L} = \sum_{j=1}^{K} \dot{\ell}_{1,j}\lambda_{6_{N_{FE},j}} + \nu_{6_{N_{FE}}} - \mu_{7_{N_{FE},1}} + \mu_{8_{N_{FE},1}} = 0$$

$$\nabla_{C_{A1_{i,k}}}\mathcal{L} = \frac{d\Phi}{dC_{A1_{i,k}}} + \sum_{j=2}^{K} \dot{\ell}_{j,k}\lambda_{1_{i,k}} - \bar{\alpha}_i\lambda_{1_{i,k}}\frac{df_1(\cdot)}{dC_{A1_{i,k}}} - \bar{\alpha}_i\lambda_{2_{i,k}}\frac{df_2(\cdot)}{dC_{A1_{i,k}}} - \bar{\alpha}_i\lambda_{4_{i,k}}\frac{df_4(\cdot)}{dC_{A1_{i,k}}}$$
$$- \ell_{k,K}\nu_{1_{i+1}} - \mu_{9_{i,k}} + \mu_{10_{i,k}} = 0,\ i = \{1,\ldots,N_{FE}-1\},\ k = \{1,\ldots,K-1\}$$

$$\nabla_{T_{1_{i,k}}}\mathcal{L} = \sum_{j=1}^{K} \dot{\ell}_{j,k}\lambda_{2_{i,k}} - \bar{\alpha}_i\lambda_{1_{i,k}}\frac{df_1(\cdot)}{dT_{1_{i,k}}} - \bar{\alpha}_i\lambda_{2_{i,k}}\frac{df_2(\cdot)}{dT_{1_{i,k}}} - \bar{\alpha}_i\lambda_{3_{i,k}}\frac{df_3(\cdot)}{dT_{1_{i,k}}} - \bar{\alpha}_i\lambda_{5_{i,k}}\frac{df_5(\cdot)}{dT_{1_{i,k}}}$$
$$- l_{k,K}\nu_{2_{i+1}} - \mu_{1_{i,k}} + \mu_{2_{i,k}} = 0,\ i = \{1,\ldots,N_{FE}-1\},\ k = \{1,\ldots,K-1\}$$

$$\nabla_{T_{c1_{i,k}}}\mathcal{L} = \sum_{j=1}^{K} \dot{\ell}_{j,k}\lambda_{3_{i,k}} - \bar{\alpha}_i\lambda_{2_{i,k}}\frac{df_2(\cdot)}{dT_{c1_{i,k}}} - \bar{\alpha}_i\lambda_{3_{i,k}}\frac{df_3(\cdot)}{dT_{c1_{i,k}}} - \ell_{k,K}\nu_{3_{i+1}} - \mu_{3_{i,k}} + \mu_{4_{i,k}} = 0,$$
$$i = \{1,\ldots,N_{FE}-1\},\ k = \{1,\ldots,K-1\}$$

$$\nabla_{C_{A2_{i,k}}}\mathcal{L} = \frac{d\Phi}{dC_{A2_{i,k}}} + \sum_{j=1}^{K} \dot{\ell}_{j,k}\lambda_{4_{i,k}} - \bar{\alpha}_i\lambda_{4_{i,k}}\frac{df_4(\cdot)}{dC_{A2_{i,k}}} - \bar{\alpha}_i\lambda_{5_{i,k}}\frac{df_5(\cdot)}{dC_{A2_{i,k}}} - \ell_{k,K}\nu_{4_{i+1}}$$
$$- \mu_{11_{i,k}} + \mu_{12_{i,k}} = 0,\ i = \{1,\ldots,N_{FE}-1\},\ k = \{1,\ldots,K-1\}$$

$$\nabla_{T_{2_{i,k}}}\mathcal{L} = \sum_{j=1}^{K} \dot{\ell}_{j,k}\lambda_{5_{i,k}} - \bar{\alpha}_i\lambda_{4_{i,k}}\frac{df_4(\cdot)}{dT_{2_{i,k}}} - \bar{\alpha}_i\lambda_{5_{i,k}}\frac{df_5(\cdot)}{dT_{2_{i,k}}} - \bar{\alpha}_i\lambda_{6_{i,k}}\frac{df_6(\cdot)}{dT_{2_{i,k}}} - \ell_{k,K}\eta_{5_{i+1}} - \mu_{5_{i,k}} + \mu_{6_{i,k}} = 0,$$
$$i = \{1,\ldots,N_{FE}-1\},\ k = \{1,\ldots,K-1\}$$

$$\nabla_{T_{c2_{i,k}}}\mathcal{L} = \sum_{j=2}^{K} \dot{\ell}_{j,k}\lambda_{6_{j,k}} - \bar{\alpha}_i\lambda_{5_{i,k}}\frac{df_5(\cdot)}{dT_{c2_{i,k}}} - \bar{\alpha}_i\lambda_{6_{i,k}}\frac{df_6(\cdot)}{dT_{c2_{i,k}}} - \ell_{k,K}\nu_{6_{i+1}} - \mu_{7_{i,k}} + \mu_{8_{i,k}} = 0,$$
$$i = \{1,\ldots,N_{FE}-1\},\ k = \{1,\ldots,K-1\}$$

$$\nabla_{C_{A1_{N_{FE},k}}}\mathcal{L} = \frac{d\Phi}{dC_{A1_{N_{FE},k}}} + \sum_{j=2}^{K} \dot{\ell}_{j,k}\lambda_{1_{N_{FE},k}} - \bar{\alpha}_{N_{FE}}\lambda_{1_{N_{FE},k}}\frac{df_1(\cdot)}{dC_{A1_{N_{FE},k}}} - \bar{\alpha}_{N_{FE}}\lambda_{2_{N_{FE},k}}\frac{df_2(\cdot)}{dC_{A1_{N_{FE},k}}}$$
$$- \bar{\alpha}_{N_{FE}}\lambda_{4_{N_{FE},k}}\frac{df_4(\cdot)}{dC_{A1_{N_{FE},k}}}$$
$$- \mu_{9_{N_{FE},k}} + \mu_{10_{N_{FE},k}} = 0,\ i = \{N_{FE}\},\ k = \{1,\ldots,K-1\}$$

$$\nabla_{T1_{N_{FE},k}}\mathcal{L} = \sum_{k=1}^{K} \dot{\ell}_{j,k}\lambda_{2_{N_{FE},k}} - \bar{\alpha}_{N_{FE}}\lambda_{1_{N_{FE},k}}\frac{df_1(\cdot)}{dT1_{N_{FE},k}} - \bar{\alpha}_{N_{FE}}\lambda_{2_{N_{FE},k}}\frac{df_2(\cdot)}{dT1_{N_{FE},k}}$$
$$- \bar{\alpha}_{N_{FE}}\lambda_{3_{N_{FE},k}}\frac{df_3(\cdot)}{dT1_{N_{FE},k}} - \bar{\alpha}_{N_{FE}}\lambda_{5_{N_{FE},k}}\frac{df_5(\cdot)}{dT1_{N_{FE},k}}$$
$$- \mu_{1_{N_{FE},k}} + \mu_{2_{N_{FE},k}} = 0,\ i = \{N_{FE}\},\ k = \{1,\ldots,K-1\}$$

$$\nabla_{Tc1_{N_{FE},k}}\mathcal{L} = \sum_{j=2}^{K} \dot{\ell}_{j,k}\lambda_{3_{N_{FE},k}} - \bar{\alpha}_{N_{FE}}\lambda_{2_{N_{FE},k}}\frac{df_2(\cdot)}{dTc1_{N_{FE},k}} - \bar{\alpha}_{N_{FE}}\lambda_{3_{N_{FE},k}}\frac{df_3(\cdot)}{dTc1_{N_{FE},k}} - \mu_{3_{N_{FE},k}}$$
$$+ \mu_{4_{N_{FE},k}} = 0,\ i = \{N_{FE}\},\ k = \{1,\ldots,K-1\}$$

$$\nabla_{CA2_{N_{FE},k}}\mathcal{L} = \frac{d\Phi}{dCA2_{N_{FE},k}} + \sum_{j=1}^{K} \dot{\ell}_{j,k}\lambda_{4_{N_{FE},k}} - \bar{\alpha}_{N_{FE}}\lambda_{4_{N_{FE},k}}\frac{df_4(\cdot)}{dCA2_{N_{FE},k}} - \bar{\alpha}_{N_{FE}}\lambda_{5_{N_{FE},k}}\frac{df_5(\cdot)}{dCA2_{N_{FE},k}}$$
$$- \mu_{11_{N_{FE},k}} + \mu_{12_{N_{FE},k}} = 0, i = \{N_{FE}\},\ k = \{1,\ldots,K-1\}$$

$$\nabla_{T2_{N_{FE},k}}\mathcal{L} = \sum_{j=2}^{K} \dot{\ell}_{j,k}\lambda_{5_{N_{FE},k}} - \bar{\alpha}_{N_{FE}}\lambda_{4_{N_{FE},k}}\frac{df_4(\cdot)}{dT2_{N_{FE},k}} - \bar{\alpha}_{N_{FE}}\lambda_{5_{N_{FE},k}}\frac{df_5(\cdot)}{dT2_{N_{FE},k}}$$
$$- \bar{\alpha}_{N_{FE}}\lambda_{6_{N_{FE},k}}\frac{df_6(\cdot)}{dT2_{N_{FE},k}} - \mu_{5_{N_{FE},k}} + \mu_{6_{N_{FE},k}} = 0,$$
$$i = \{N_{FE}\},\ k = \{1,\ldots,K-1\}$$

$$\nabla_{Tc2_{N_{FE},k}}\mathcal{L} = \sum_{j=2}^{K} \dot{\ell}_{j,k}\lambda_{6_{i,k}} - \bar{\alpha}_{N_{FE}}\lambda_{5_{N_{FE},k}}\frac{df_5(\cdot)}{dTc2_{N_{FE},k}} - \bar{\alpha}_{N_{FE}}\lambda_{6_{N_{FE},k}}\frac{df_6(\cdot)}{dTc2_{N_{FE},k}} - \mu_{7_{N_{FE},k}}$$
$$+ \mu_{8_{N_{FE},k}} = 0,\ i = \{N_{FE}\},\ k = \{1,\ldots,K-1\}$$

$$\nabla_{CA1_{i,K}}\mathcal{L} = \frac{d\Phi}{dCA1_{i,K}} + \sum_{j=1}^{K} \dot{\ell}_{K,k}\lambda_{1_{i,k}} - \bar{\alpha}_i\lambda_{1_{i,K}}\frac{df_1(\cdot)}{dCA1_{i,K}} - \bar{\alpha}_i\lambda_{2_{i,K}}\frac{df_2(\cdot)}{dCA1_{i,K}} - \bar{\alpha}_i\lambda_{4_{i,K}}\frac{df_4(\cdot)}{dCA1_{i,K}}$$
$$- \ell_{K,K}\nu_{1_{i+1}} - \mu_{9_{i,K}} + \mu_{10_{i,K}} = 0,\ i = \{1,\ldots,N_{FE}-1\}$$

$$\nabla_{T1_{i,K}}\mathcal{L} = \sum_{j=1}^{K} \dot{\ell}_{K,k}\lambda_{2_{i,k}} - \bar{\alpha}_i\lambda_{1_{i,K}}\frac{df_1(\cdot)}{dT1_{i,K}} - \bar{\alpha}_i\lambda_{2_{i,K}}\frac{df_2(\cdot)}{dT1_{i,K}} - \bar{\alpha}_i\lambda_{3_{i,K}}\frac{df_3(\cdot)}{dT1_{i,K}}$$
$$- \bar{\alpha}_i\lambda_{5_{i,K}}\frac{df_5(\cdot)}{dT1_{i,K}} - \ell_{K,K}\nu_{2_{i+1}} - \mu_{1_{i,K}} + \mu_{2_{i,K}} = 0,\ i = \{1,\ldots,N_{FE}-1\}$$

$$\nabla_{T_{c1_{i,K}}}\mathcal{L} = \sum_{j=1}^{K} \dot{\ell}_{K,k}\lambda_{3_{i,k}} - \bar{\alpha}_i\lambda_{2_{i,K}}\frac{df_2(\cdot)}{dT_{c1_{i,K}}} - \bar{\alpha}_i\lambda_{3_{i,K}}\frac{df_3(\cdot)}{dT_{c1_{i,K}}} - \ell_{K,K}\nu_{3_{i+1}}$$
$$- \mu_{3_{i,K}} + \mu_{4_{i,K}} = 0,\ i = \{1,\ldots,N_{FE}-1\}$$

$$\nabla_{C_{A2_{i,K}}}\mathcal{L} = \frac{d\Phi}{dC_{A2_{i,K}}} + \sum_{j=1}^{K} \dot{\ell}_{K,k}\lambda_{4_{i,k}} - \bar{\alpha}_i\lambda_{4_{i,K}}\frac{df_4(\cdot)}{dC_{A2_{i,K}}} - \bar{\alpha}_i\lambda_{5_{i,K}}\frac{df_5(\cdot)}{dC_{A2_{i,K}}}$$
$$- \ell_{K,K}\eta_{4_{i+1}} - \mu_{11_{i,K}} + \mu_{12_{i,K}} = 0,\ i = \{1,\ldots,N_{FE}-1\}$$

$$\nabla_{T_{2_{i,K}}}\mathcal{L} = \sum_{j=2}^{K} \dot{\ell}_{K,k}\lambda_{5_{i,k}} - \bar{\alpha}_i\lambda_{4_{i,K}}\frac{df_4(\cdot)}{dT_{2_{i,K}}} - \bar{\alpha}_i\lambda_{5_{i,K}}\frac{df_5(\cdot)}{dT_{2_{i,K}}} - \bar{\alpha}_i\lambda_{6_{i,K}}\frac{df_6(\cdot)}{dT_{2_{i,K}}} - \ell_{K,K}\nu_{5_{i+1}}$$
$$- \mu_{5_{i,K}} + \mu_{6_{i,K}} = 0,\ i = \{1,\ldots,N_{FE}-1\}$$

$$\nabla_{T_{c2_{i,K}}}\mathcal{L} = \sum_{j=1}^{K} \dot{\ell}_{K,k}\lambda_{6_{i,k}} - \bar{\alpha}_i\lambda_{5_{i,K}}\frac{df_5(\cdot)}{dT_{c2_{i,K}}} - \bar{\alpha}_i\lambda_{6_{i,K}}\frac{df_6(\cdot)}{dT_{c2_{i,K}}} - \ell_{K,K}\nu_{6_{i+1}}$$
$$- \mu_{7_{i,K}} + \mu_{8_{i,K}} = 0,\ i = \{1,\ldots,N_{FE}-1\}$$

$$\nabla_{C_{A1_{N_{FE},K}}}\mathcal{L} = \frac{d\Phi}{dC_{A1_{N_{FE},K}}} + \sum_{j=1}^{K} \dot{\ell}_{K,k}\lambda_{1_{N_{FE},k}} - \bar{\alpha}_i\lambda_{1_{N_{FE},K}}\frac{df_1(\cdot)}{dC_{A1_{N_{FE},K}}} - \bar{\alpha}_i\lambda_{2_{N_{FE},K}}\frac{df_2(\cdot)}{dC_{A1_{N_{FE},K}}}$$
$$- \bar{\alpha}_i\lambda_{4_{N_{FE},K}}\frac{df_4(\cdot)}{dC_{A1_{N_{FE},K}}} - \mu_{9_{N_{FE},K}} + \mu_{10_{N_{FE},K}} = 0$$

$$\nabla_{T_{1_{N_{FE},K}}}\mathcal{L} = \sum_{j=2}^{K} \dot{\ell}_{K,k}\lambda_{2_{N_{FE},k}} - \bar{\alpha}_i\lambda_{1_{N_{FE},K}}\frac{df_1(\cdot)}{dT_{1_{N_{FE},K}}} - \bar{\alpha}_i\lambda_{2_{N_{FE},K}}\frac{df_2(\cdot)}{dT_{1_{N_{FE},K}}} - \bar{\alpha}_i\lambda_{3_{N_{FE},K}}\frac{df_3(\cdot)}{dT_{1_{N_{FE},K}}}$$
$$- \bar{\alpha}_i\lambda_{5_{N_{FE},K}}\frac{df_5(\cdot)}{dT_{1_{N_{FE},K}}} - \mu_{1_{N_{FE},K}} + \mu_{2_{N_{FE},K}} = 0,$$

$$\nabla_{T_{c1_{N_{FE},K}}}\mathcal{L} = \sum_{j=1}^{K} \dot{\ell}_{K,k}\lambda_{3_{N_{FE},k}} - \bar{\alpha}_i\lambda_{2_{N_{FE},K}}\frac{df_2(\cdot)}{dT_{c1_{N_{FE},K}}} - \bar{\alpha}_i\lambda_{3_{N_{FE},K}}\frac{df_3(\cdot)}{dT_{c1_{N_{FE},K}}} - \mu_{3_{N_{FE},K}}$$
$$+ \mu_{4_{N_{FE},K}} = 0,$$

$$\nabla_{C_{A2_{N_{FE},K}}}\mathcal{L} = \frac{d\Phi}{dC_{A2_{N_{FE},K}}} + \sum_{j=2}^{K} \dot{\ell}_{K,k}\lambda_{4_{N_{FE},k}} - \bar{\alpha}_i\lambda_{4_{N_{FE},K}}\frac{df_4(\cdot)}{dC_{A2_{N_{FE},K}}} - \bar{\alpha}_i\lambda_{5_{N_{FE},K}}\frac{df_5(\cdot)}{dC_{A2_{N_{FE},K}}} - \mu_{11_{N_{FE},K}} + \mu_{12_{N_{FE},K}} = 0$$

$$\nabla_{T_{2_{N_{FE},K}}}\mathcal{L} = \sum_{j=2}^{K} \dot{\ell}_{K,k}\lambda_{5_{N_{FE},k}} - \bar{\alpha}_i\lambda_{4_{N_{FE},K}}\frac{df_4(\cdot)}{dT_{2_{N_{FE},K}}} - \bar{\alpha}_i\lambda_{5_{N_{FE},K}}\frac{df_5(\cdot)}{dT_{2_{N_{FE},K}}} - \bar{\alpha}_i\lambda_{6_{N_{FE},K}}\frac{df_6(\cdot)}{dT_{2_{N_{FE},K}}} - \mu_{5_{N_{FE},K}} + \mu_{6_{N_{FE},K}} = 0$$

$$\nabla_{T_{c2_{N_{FE},K}}}\mathcal{L} = \sum_{j=1}^{K} \dot{\ell}_{K,k}\lambda_{6_{N_{FE},k}} - \bar{\alpha}_i\lambda_{5_{N_{FE},K}}\frac{df_5(\cdot)}{dT_{c2_{N_{FE},K}}} - \bar{\alpha}_i\lambda_{6_{N_{FE},K}}\frac{df_6(\cdot)}{dT_{c2_{N_{FE},K}}} - \mu_{7_{N_{FE},K}} + \mu_{8_{N_{FE},K}} = 0$$

$$\nabla_{\bar{F}_{w1_i}}\mathcal{L} = -\frac{d\Phi}{dq_{w1_i}} + \nu_{7_i} + \mu_{13_i} + \mu_{15_i} - \mu_{16_i} - \bar{\alpha}_i\sum_{j=1}^{K}\lambda_{3_{i,j}}\frac{df_3(\cdot)}{d\bar{F}_{w1_i}} = 0, \;\; i = \{1\}$$

$$\nabla_{\bar{F}_{w2_i}}\mathcal{L} = -\frac{d\Phi}{dq_{w2_i}} + \nu_{8_i} + \mu_{14_i} + \mu_{17_i} - \mu_{18_i} - \bar{\alpha}_i\sum_{j=1}^{K}\lambda_{6_{i,j}}\frac{df_6(\cdot)}{d\bar{F}_{w2_i}} = 0, \;\; i = \{1\}$$

$$\nabla_{\bar{F}_{w1_i}}\mathcal{L} = \frac{d\Phi}{dq_{w1_{i-1}}} - \frac{d\Phi}{dq_{w1_{i+1}}} + \mu_{13_i} - \bar{\alpha}_i\sum_{j=1}^{K}\lambda_{3_{i,j}}\frac{df_3(\cdot)}{dq_{w1_i}} + \mu_{15_i} - \mu_{15_{i+1}} - \mu_{16_i} + \mu_{16_{i+1}} = 0, \quad i = \{2,\ldots,N_{FE}-1\}$$

$$\nabla_{\bar{F}_{w2_i}}\mathcal{L} = \frac{d\Phi}{dq_{w2_{i-1}}} - \frac{d\Phi}{d\bar{F}_{w2_{i+1}}} + \mu_{14_i} - \bar{\alpha}_i\sum_{j=1}^{K}\lambda_{6_{i,j}}\frac{df_6(\cdot)}{d\bar{F}_{w2_i}} + \mu_{17_i} - \mu_{17_{i+1}} - \mu_{18_i} + \mu_{18_{i+1}} = 0, \quad i = \{2,\ldots,N_{FE}-1\}$$

$$\nabla_{\bar{F}_{w1_i}}\mathcal{L} = \frac{d\Phi}{dq_{w1_i}} + \mu_{13_i} - \mu_{15_i} + \mu_{16_i} - \bar{\alpha}_i\sum_{j=1}^{K}\lambda_{3_{i,j}}\frac{df_3(\cdot)}{d\bar{F}_{w1_i}} = 0, \;\; i = \{N_{FE}\}$$

$$\nabla_{\bar{F}_{w2_i}}\mathcal{L} = \frac{d\Phi}{dq_{w2_i}} + \mu_{14_i} - \mu_{17_i} + \mu_{18_i} - \bar{\alpha}_i\sum_{j=1}^{K}\lambda_{6_{i,j}}\frac{df_6(\cdot)}{d\bar{F}_{w2_i}} = 0, \;\; i = \{N_{FE}\}$$

$$\sum_{j=1}^{K}\dot{\ell}_{j,k}C_{A1_{i,j}} - \bar{\alpha}_i f_1(D_e, h_T, C_{A1_{i,k}}, T_{1_{i,k}}) = 0, \;\; i = \{1,\ldots,N_{FE}\}, \;\; k = \{1,\ldots,K\}$$

$$\sum_{j=1}^{K} \dot{\ell}_{j,k} T_{1_{i,j}} - \bar{\alpha}_i f_2(D_e, h_T, C_{A1_{i,k}}, T_{1_{i,k}}, T_{c1_{i,k}}) = 0, \;\; i = \{1, \ldots, N_{FE}\}, \;\; k = \{1, \ldots, K\}$$

$$\sum_{j=1}^{K} \dot{\ell}_{j,k} T_{c1_{i,j}} - \bar{\alpha}_i f_3(D_e, h_T, C_{A1_{i,k}}, T_{1_{i,k}}, T_{c1_{i,k}}) = 0, \;\; i = \{1, \ldots, N_{FE}\}, \;\; k = \{1, \ldots, K\}$$

$$\sum_{j=1}^{K} \dot{\ell}_{j,k} C_{A2_{i,j}} - \bar{\alpha}_i f_4(D_e, h_T, C_{A2_{i,k}}, T_{2_{i,k}}) = 0, \;\; i = \{1, \ldots, N_{FE}\}, \;\; k = \{1, \ldots, K\}$$

$$\sum_{j=1}^{K} \dot{\ell}_{j,k} T_{2_{i,j}} - \bar{\alpha}_i f_5(D_e, h_T, C_{A2_{i,k}}, T_{2_{i,k}}, T_{c2_{i,k}}) = 0, \;\; i = \{1, \ldots, N_{FE}\}, \;\; k = \{1, \ldots, K\}$$

$$\sum_{j=1}^{K} \dot{\ell}_{jk} T_{c2_{i,j}} - \bar{\alpha}_i f_6(D_e, h_T, C_{A2_{i,k}}, T_{2_{i,k}}, T_{c2_{i,k}}) = 0, \;\; i = \{1, \ldots, N_{FE}\}, \;\; k = \{1, \ldots, K\}$$

$$g_1(C_{A1_{i,k}}) = C_{A1_{i+1,1}} - \sum_{j=1}^{K} \dot{\ell}_{j,K} C_{A1_{i,j}} = 0, \;\; i = \{1, \ldots, N_{FE} - 1\}, \;\; k = \{1, \ldots, K\}$$

$$g_2(T_{1_{i,k}}) = T_{1_{i+1,1}} - \sum_{j=1}^{K} \dot{\ell}_{j,K} T_{1_{i,j}} = 0, \;\; i = \{1, \ldots, N_{FE} - 1\}, \;\; k = \{1, \ldots, K\}$$

$$g_3(T_{c1_{i,k}}) = T_{c1_{i+1,1}} - \sum_{j=1}^{K} \dot{\ell}_{j,K} T_{c1_{i,j}} = 0, \;\; i = \{1, \ldots, N_{FE} - 1\}, \;\; k = \{1, \ldots, K\}$$

$$g_4(C_{A2_{i,j}}) = C_{A2_{i+1,1}} - \sum_{j=1}^{K} \dot{\ell}_{j,K} C_{A2_{i,j}} = 0, \;\; i = \{1, \ldots, N_{FE} - 1\}, \;\; k = \{1, \ldots, K\}$$

$$g_5(T_{2_{i,k}}) = T_{2_{i+1,1}} - \sum_{j=1}^{K} \dot{\ell}_{j,K} T_{2_{i,j}} = 0, \;\; i = \{1, \ldots, N_{FE} - 1\}, \;\; k = \{1, \ldots, K\}$$

$$g_6(T_{c2_{i,k}}) = T_{c2_{i+1,1}} - \sum_{j=1}^{K} \dot{\ell}_{j,K} T_{c2_{i,j}} = 0, \;\; i = \{1, \ldots, N_{FE} - 1\}, \;\; k = \{1, \ldots, K\}$$

$$g_1(C_{A1_{1,1}}) = C_{A1_{1,1}} - C^0_{A1} = 0, \;\; g_2(T_{1_{1,1}}) = T_{1_{1,1}} - T^0_1 = 0 \;\; g_3(T_{c1_{1,1}}) = T_{c1_{1,1}} - T^0_{c1} = 0,$$

$$g_4(C_{A2_{1,1}}) = C_{A2_{1,1}} - C^0_{A2} = 0, \;\; g_5(T_{2_{1,1}}) = T_{2_{1,1}} - T^0_2 = 0, \;\; g_6(T_{c2_{1,1}}) = T_{c2_{1,1}} - T^0_{c2} = 0,$$

$$T^{lb}_1 - T_{1_{i,j}} \leq 0, \;\; T_{1_{i,j}} - T^{ub}_1 \leq 0, \;\; T^{lb}_{c1} - T_{c1_{1,1}} \leq 0, \;\; T_{c1_{1,1}} - T^{ub}_{c1} \leq 0, \;\; i = \{1, \ldots, N_{FE}\}, \;\; j = \{1, \ldots, K\}$$

$$T^{lb}_2 - T_{2_{i,j}} \leq 0, \;\; T_{2_{i,j}} - T^{ub}_2 \leq 0, \;\; T^{lb}_{c2} - T_{c2_{1,1}} \leq 0, \;\; T_{c2_{1,1}} - T^{ub}_{c2} \leq 0, \;\; i = \{1, \ldots, N_{FE}\}, \;\; j = \{1, \ldots, K\}$$

$$\bar{F}_{w1_i} - \bar{F}_{w1}^{ub} \leq 0,\ \ \bar{F}_{w2_i} - \bar{F}_{w2}^{ub} \leq 0,\ i = \{1, \ldots, N_{FE}\}$$
$$\Delta\bar{F}_{w1} - \bar{F}_{w1_i} + \bar{F}_{w1_{i-1}} \leq 0,\ \ \bar{F}_{w1_i} - \bar{F}_{w1_{i-1}} + \Delta\bar{F}_{w1} \leq 0,\ i = \{2, \ldots, N_{FE}\}$$
$$\Delta\bar{F}_{w2} - \bar{F}_{w2_i} + \bar{F}_{w2_{i-1}} \leq 0,\ \ \bar{F}_{w2_i} - \bar{F}_{w2_{i-1}} + \Delta\bar{F}_{w2} \leq 0,\ i = \{2, \ldots, N_{FE}\}$$

where index i indicates the discretization finite elements in the upper-level problem, index i' indicates the discretization finite elements in the lower-level problem, index j and k indicate the internal collocation points. Discretization in Equation (A.1) is based on Lagrange polynomials using Radau points. Functions $f_1(\cdot)$ to $f_6(\cdot)$ are defined as follows:

$$f_1(C_{A1}, T_1) = \frac{\bar{F}_{in}}{V_R}(C_{A0} - C_{A1}) - k_{re}e^{\frac{-E}{RT_1}}C_{A1},$$

$$f_2(C_{A1}, T_1, T_{c1}) = \frac{\bar{F}}{V_R}(T_{in} - T_1) + \frac{(-\Delta H_{rx})}{C_p^l}k_{re}e^{\frac{-E}{RT_1}}C_{A1} - \frac{U_h A_e(T_1 - T_{c1})}{V_R C_p^l},$$

$$f_3(C_{A1}, T_1, T_{c1}) = \frac{\bar{F}_{w1}}{Vj}(T_c^0 - T_{c1}) + \frac{U_h A_e(T_1 - T_{c1})}{VjC_p^w},$$

$$f_4(C_{A2}, T_2) = \frac{\bar{F}}{V_R}(C_{A1} - C_{A2}) - k_{re}e^{\frac{-E}{RT_2}}C_{A2},$$

$$f_5(C_{A2}, T_2, T_{c2}) = \frac{\bar{F}}{V_R}(T_1 - T_2) + \frac{(-\Delta H_{rx})}{C_p^l}k_{re}e^{\frac{-E}{RT_2}}C_{A2} - \frac{U_h A_e(T_2 - T_{c2})}{V_R C_p^w},$$

$$f_6(C_{A2}, T_2, T_{c2}) = \frac{\bar{F}_{w2}}{Vj}(T_c^0 - T_{c2}) + \frac{U_h A_e(T_2 - T_{c2})}{VjC_p^w},$$

Appendix B

WWTP case study (Continuous MPCC formulation)

This appendix presents the complete discretized MPCC-based formulation for the integration of design and NMPC-based control under uncertainty of the Wastewater Treatment Plant (WWTP). This problem corresponds to the case study 3 in Chapter 4.

$$\min_{A_d,V_R,\mathbf{x}(t),f_k(t),q_p(t),s_w^{sp},c_w^{sp},\mathbf{Q_{in}},\mathbf{Q_{out}}} \quad 0.16(3500V_R + 2300A_d) + 870\sum_{i=1}^{N_{FE}}(f_{k_i} + q_{p_i}) + 1\times 10^5 \sum_{i,j=1}^{N_{FE}K}(100 - s_{w_{i,j}})^2 \quad \text{(A.2)}$$

s.t.

$$\sum_{j=1}^{K}\dot{\ell}_{j,k}x_{w_{i,j}} = y_w\bar{\mu}_w\frac{s_{w_{i,k}}x_{w_{i,k}}}{k_{sc}+s_{w_{i,j}}} - k_{ca}x_{w_{i,k}} - k_{dr}\frac{x_{w_{i,k}}^2}{s_{w_{i,k}}} + \frac{x_{in}q_{in}}{V_R} + \frac{x_{r_{i,k}}q_r}{V_R} - \frac{x_{w_{i,k}}q}{V_R}$$

$$\sum_{j=1}^{K}\dot{\ell}_{j,k}s_{w_{i,j}} = \frac{f_{kd}k_{dr}x_{w_{i,k}}^2}{s_{w_{i,k}}} - \frac{\bar{\mu}_w s_{w_{i,k}}x_{w_{i,k}}}{(k_{sc}+s_{w_{i,k}})} + f_{kd}k_{ca}x_{w_{i,k}} + \frac{s_{in}q_{in}}{V_R} + \frac{s_{w_{i,k}}q_r}{V_R} - \frac{x_{w_{i,k}}q}{V_R}$$

$$\sum_{j=1}^{K}\dot{\ell}_{j,k}x_{d_{i,j}} = \left(\frac{1}{A_d l_d}\right)\left(q_{out}(x_{b_{i,k}} - x_{d_{i,k}}) - A_d n_{nr}x_{d_{i,k}}e^{(a_{ar}x_{d_{i,k}})}\right)$$

$$\sum_{j=1}^{K}\dot{\ell}_{j,k}x_{b_{i,j}} = \left(\frac{1}{A_d l_b}\right)\left(qx_{w_{i,k}} - x_{b_{i,k}}(q_{out}+q_2) + A_d n_{nr}\left(x_{d_{i,k}}e^{(a_{ar}x_{d_{i,k}})} - x_{b_{i,k}}e^{(a_{ar}x_{b_{i,k}})}\right)\right)$$

$$\sum_{j=1}^{K}\dot{\ell}_{j,k}x_{r_{i,k}} = \left(\frac{1}{A_d l_r}\right)\left(q_2(x_{b_{i,k}} - x_{r_{i,k}}) + A_d n_{nr}x_{b_{i,k}}e^{(a_{ar}x_{b_{i,k}})}\right)$$

$$\sum_{j=1}^{K}\dot{\ell}_{j,k}c_{w_{i,k}} = k_{otw}f_k(c_s - c_{w_{i,k}}) - k_{od}\bar{\mu}_w\frac{x_{w_{i,k}}s_{w_{i,k}}}{(k_{sc}+s_{w_{i,k}})} - \frac{c_{w_{i,k}}q}{V_R}$$

$$q_r = q_2 - q_p,\;\; q = q_i + q_r,\;\; q_{out} = q + q_2$$

$$x_{w_{1,1}} = x_w^0,\;\; s_{w_{1,1}} = s_w^0,\;\; x_{d_{i,k}} = x_d^0,\;\; x_{b_{i,k}} = x_b^0,\;\; x_{r_{i,k}} = x_r^0,\;\; c_{w_{i,k}} = c_w^0,$$

$$\nabla_{x_{w_{i,1}}}\mathcal{L} = \sum_{j=2}^{K}\dot{\ell}_{1,j}\lambda_{1_{i,j}} - l_{1,K}\nu_{1_{i+1}} + \nu_{1_i} + \mu_{3_{i,1}}V_R - \mu_{4_{i,1}}V_R = 0,\;\; i = \{1,\ldots,N_{FE}-1\}$$

$$\nabla_{s_{w_{i,1}}}\mathcal{L} = \frac{d\Phi}{ds_{w_{i,1}}} + \sum_{j=2}^{K} \dot{\ell}_{1,j}\lambda_{2_{i,j}} - \ell_{1,K}\nu_{2_{i+1}} + \eta_{2_i} + \mu_{9_{i,1}} = 0, \;\; i = \{1, \ldots, N_{FE} - 1\}$$

$$\nabla_{x_{d_{i,1}}}\mathcal{L} = \sum_{j=2}^{K} \dot{\ell}_{1,j}\lambda_{3_{i,j}} - \ell_{1,K}\nu_{3_{i+1}} + \nu_{3_i} = 0, \;\; i = \{1, \ldots, N_{FE} - 1\}$$

$$\nabla_{x_{b_{i,1}}}\mathcal{L} = \sum_{j=2}^{K} \dot{\ell}_{1,j}\lambda_{4_{i,j}} - \ell_{1,K}\nu_{4_{i+1}} + \nu_{4_i} = 0, \;\; i = \{1, \ldots, N_{FE} - 1\}$$

$$\nabla_{x_{r_{i,1}}}\mathcal{L} = \sum_{j=2}^{K} \dot{\ell}_{1,j}\lambda_{5_{i,j}} - \ell_{1,K}\nu_{5_{i+1}} + \nu_{5_i} + \mu_{3_{i,1}}\frac{dg_3(\cdot)}{dx_{r_{i,1}}} + \mu_{4_{i,1}}\frac{dg_4(\cdot)}{dx_{r_{i,1}}} = 0, \;\; i = \{1, \ldots, N_{FE} - 1\}$$

$$\nabla_{c_{w_{i,1}}}\mathcal{L} = \frac{d\Phi}{dc_{w_{i,1}}} + \sum_{j=2}^{K} \dot{\ell}_{1,j}\lambda_{6_{i,j}} - \ell_{1,K}\nu_{6_{i+1}} + \nu_{6_i} = 0, \;\; i = \{1, \ldots, N_{FE} - 1\}$$

$$\nabla_{x_{w_{N_{FE},1}}}\mathcal{L} = \sum_{j=2}^{K} \dot{\ell}_{1,j}\lambda_{1_{N_{FE},j}} + \nu_{1_{N_{FE}}} + \mu_{3_{N_{FE},1}}V_R - \mu_{4_{N_{FE},1}}V_R = 0,$$

$$\nabla_{s_{w_{N_{FE},1}}}\mathcal{L} = \frac{d\Phi}{ds_{w_{N_{FE},1}}} + \sum_{j=2}^{K} \dot{\ell}_{1,j}\lambda_{2_{N_{FE},j}} + \nu_{2_{N_{FE}}} + \mu_{9_{N_{FE},1}} = 0,$$

$$\nabla_{x_{d_{N_{FE},1}}}\mathcal{L} = \sum_{j=2}^{K} \dot{\ell}_{1,j}\lambda_{3_{N_{FE},j}} + \nu_{3_{N_{FE}}} = 0,$$

$$\nabla_{x_{b_{N_{FE},1}}}\mathcal{L} = \sum_{j=2}^{K} \dot{\ell}_{1,j}\lambda_{4_{N_{FE},j}} + \nu_{4_{N_{FE}}} = 0,$$

$$\nabla_{x_{r_{N_{FE},1}}}\mathcal{L} = \sum_{j=2}^{K} \dot{\ell}_{1,j}\lambda_{5_{N_{FE},j}} + \nu_{5_{N_{FE}}} + \mu_{3_{N_{FE},1}}\frac{dg_3(\cdot)}{dx_{r_{N_{FE},1}}} + \mu_{4_{N_{FE},1}}\frac{dg_4(\cdot)}{dx_{r_{N_{FE},1}}} = 0,$$

$$\nabla_{c_{w_{N_{FE},1}}}\mathcal{L} = \frac{d\Phi}{dc_{w_{N_{FE},1}}} + \sum_{j=2}^{K} \dot{\ell}_{1,j}\lambda_{6_{N_{FE},j}} + \nu_{6_{N_{FE}}} = 0,$$

$$\begin{aligned}\nabla_{x_{w_{i,k}}}\mathcal{L} = &\sum_{k=2}^{K} \dot{\ell}_{j,k}\lambda_{1_{i,k}} - \bar{\alpha}_i\lambda_{1_{i,k}}\frac{df_1(\cdot)}{dx_{w_{i,k}}} - \bar{\alpha}_i\lambda_{2_{i,k}}\frac{df_2(\cdot)}{dx_{w_{i,k}}} - \bar{\alpha}_i\lambda_{4_{i,k}}\frac{df_4(\cdot)}{dx_{w_{i,j}}} - \bar{\alpha}_i\lambda_{6_{i,j}}\frac{df_6(\cdot)}{dx_{w_{i,k}}} \\ &- \ell_{j,K}\nu_{1_{i+1}} + \mu_{3_{i,k}}\frac{dg_3(\cdot)}{dx_{w_{i,k}}} - \mu_{4_{i,k}}\frac{dg_3(\cdot)}{dx_{w_{i,k}}} = 0, \; i = \{1, \ldots, N_{FE} - 1\}, \; k = \{1, \ldots, K - 1\}\end{aligned}$$

$$\nabla_{s_{w_{i,j}}}\mathcal{L} = \frac{d\Phi}{ds_{w_{i,k}}} + \sum_{k=2}^{K} \dot{\ell}_{j,k}\lambda_{2_{i,k}} - \bar{\alpha}_i\lambda_{1_{i,k}}\frac{df_1(\cdot)}{ds_{w_{i,k}}} - \bar{\alpha}_i\lambda_{2_{i,k}}\frac{df_2(\cdot)}{ds_{w_{i,k}}}$$
$$- \bar{\alpha}_i\lambda_{6_{i,k}}\frac{df_6(\cdot)}{ds_{w_{i,k}}} - \ell_{j,K}\nu_{2_{i+1}} + \mu_{9_{i,k}} = 0,\ i = \{1,\ldots,N_{FE}-1\},\ k = \{1,\ldots,K-1\}$$

$$\nabla_{x_{d_{i,k}}}\mathcal{L} = \sum_{k=2}^{K} \dot{\ell}_{j,k}\lambda_{3_{i,k}} - \bar{\alpha}_i\lambda_{3_{i,k}}\frac{df_3(\cdot)}{dx_{d_{i,k}}} - \bar{\alpha}_i\lambda_{4_{i,k}}\frac{df_4(\cdot)}{dx_{d_{i,k}}} - \ell_{j,K}\nu_{3_{i+1}} = 0,\ i = \{1,\ldots,N_{FE}-1\},$$
$$j = \{1,\ldots,K-1\}$$

$$\nabla_{x_{b_{i,k}}}\mathcal{L} = \sum_{k=2}^{K} \dot{\ell}_{jk}\lambda_{4_{i,k}} - \bar{\alpha}_i\lambda_{3_{i,j}}\frac{df_3(\cdot)}{dx_{b_{i,j}}} - \bar{\alpha}_i\lambda_{4_{i,j}}\frac{df_4(\cdot)}{dx_{b_{i,j}}} - \bar{\alpha}_i\lambda_{5_{i,j}}\frac{df_5(\cdot)}{dx_{b_{i,j}}} - \ell_{j,K}\nu_{4_{i+1}} = 0,$$
$$i = \{1,\ldots,N_{FE}-1\},\ j = \{1,\ldots,K-1\}$$

$$\nabla_{x_{r_{i,j}}}\mathcal{L} = \sum_{k=2}^{K} \dot{\ell}_{jk}\lambda_{5_{i,k}} - \bar{\alpha}_i\lambda_{1_{i,j}}\frac{df_1(\cdot)}{dx_{r_{i,j}}} - \bar{\alpha}_i\lambda_{5_{i,j}}\frac{df_5(\cdot)}{dx_{r_{i,j}}} - \ell_{j,K}\nu_{5_{i+1}} + \mu_{3_{i,j}}\frac{dg_3(\cdot)}{dx_{r_{i,j}}} + \mu_{4_{i,j}}\frac{dg_4(\cdot)}{dx_{r_{i,j}}} = 0,$$
$$i = \{1,\ldots,N_{FE}-1\},\ j = \{1,\ldots,K-1\}$$

$$\nabla_{c_{w_{i,j}}}\mathcal{L} = \frac{d\Phi}{dc_{w_{i,j}}} + \sum_{k=2}^{K} \dot{\ell}_{j,k}\lambda_{6_{j,k}} - \bar{\alpha}_i\lambda_{6_{i,j}}\frac{df_6(\cdot)}{dc_{w_{i,j}}} - \ell_{j,K}\eta_{6_{i+1}} = 0,\ i = \{1,\ldots,N_{FE}-1\},$$
$$j = \{1,\ldots,K-1\}$$

$$\nabla_{x_{w_{N_{FE},j}}}\mathcal{L} = \sum_{k=2}^{K} \dot{\ell}_{j,k}\lambda_{1_{N_{FE},k}} - \bar{\alpha}_{N_{FE}}\lambda_{1_{N_{FE},j}}\frac{df_1(\cdot)}{dx_{w_{N_{FE},j}}} - \bar{\alpha}_{N_{FE}}\lambda_{2_{N_{FE},j}}\frac{df_2(\cdot)}{dx_{w_{N_{FE},j}}}$$
$$- \bar{\alpha}_{N_{FE}}\lambda_{4_{N_{FE},j}}\frac{df_4(\cdot)}{dx_{w_{N_{FE},j}}} - \bar{\alpha}_{N_{FE}}\lambda_{6_{N_{FE},j}}\frac{df_6(\cdot)}{dx_{w_{N_{FE},j}}} + \mu_{3_{N_{FE},j}}\frac{dg_3(\cdot)}{dx_{r_{N_{FE},j}}} - \mu_{4_{N_{FE},j}}\frac{dg_3(\cdot)}{dx_{r_{N_{FE},j}}} = 0,$$
$$i = \{N_{FE}\},\ j = \{2,\ldots,K-1\}$$

$$\nabla_{s_{w_{N_{FE},j}}}\mathcal{L} = \frac{d\Phi}{ds_{w_{N_{FE},j}}} + \sum_{k=2}^{K} \dot{\ell}_{j,k}\lambda_{2_{N_{FE},k}} - \bar{\alpha}_{N_{FE}}\lambda_{1_{N_{FE},j}}\frac{df_1(\cdot)}{dx_{w_{N_{FE},j}}} - \bar{\alpha}_{N_{FE}}\lambda_{2_{N_{FE},j}}\frac{df_2(\cdot)}{dx_{w_{N_{FE},j}}}$$
$$- \bar{\alpha}_{N_{FE}}\lambda_{6_{N_{FE},j}}\frac{df_6(\cdot)}{dx_{w_{N_{FE},j}}} + \mu_{9_{N_{FE},j}} = 0,\ i = \{N_{FE}\},\ j = \{2,\ldots,K-1\}$$

$$\nabla_{x_{d_{N_{FE},j}}}\mathcal{L} = \sum_{k=2}^{K} \dot{\ell}_{j,k}\lambda_{3_{N_{FE},k}} - \bar{\alpha}_{N_{FE}}\lambda_{3_{N_{FE},j}}\frac{df_3(\cdot)}{dx_{d_{N_{FE},j}}} - \bar{\alpha}_{N_{FE}}\lambda_{4_{N_{FE},j}}\frac{df_4(\cdot)}{dx_{d_{N_{FE},j}}} = 0,$$
$$i = \{N_{FE}\},\ j = \{1,\ldots,K-1\}$$

$$\nabla_{x_{b_{N_{FE},j}}}\mathcal{L} = \sum_{k=2}^{K} \dot{\ell}_{jk}\lambda_{4_{N_{FE},k}} - \bar{\alpha}_{N_{FE}}\lambda_{3_{N_{FE},j}}\frac{df_3(\cdot)}{dx_{b_{N_{FE},j}}} - \bar{\alpha}_{N_{FE}}\lambda_{4_{N_{FE},j}}\frac{df_4(\cdot)}{dx_{b_{N_{FE},j}}}$$
$$- \bar{\alpha}_{N_{FE}}\lambda_{5_{N_{FE},j}}\frac{df_5(\cdot)}{dx_{b_{N_{FE},j}}} = 0, i = \{N_{FE}\},\ j = \{1,\ldots,K-1\}$$

$$\nabla_{x_{r_{N_{FE},j}}}\mathcal{L} = \sum_{k=2}^{K} \dot{\ell}_{jk}\lambda_{5_{N_{EF},k}} - \bar{\alpha}_{N_{FE}}\lambda_{1_{N_{FE},j}}\frac{df_1(\cdot)}{dx_{r_{N_{FE},j}}} - \bar{\alpha}_{N_{FE}}\lambda_{5_{N_{FE},j}}\frac{df_5(\cdot)}{dx_{r_{N_{FE},j}}} + \mu_{3_{N_{FE},j}}\frac{dg_3(\cdot)}{dx_{r_{N_{FE},j}}}$$
$$+ \mu_{4_{N_{FE},j}}\frac{dg_4(\cdot)}{dx_{r_{N_{FE},j}}} = 0,\ i = \{N_{FE}\},\ j = \{1,\ldots,K-1\}$$

$$\nabla_{c_{w_{N_{FE},j}}}\mathcal{L} = \frac{d\Phi}{dc_{w_{N_{FE},j}}} + \sum_{k=2}^{K} \dot{\ell}_{j,k}\lambda_{6_{i,k}} - \bar{\alpha}_{N_{FE}}\lambda_{6_{N_{FE},j}}\frac{df_6(\cdot)}{dc_{w_{N_{FE},j}}} = 0,\ i = \{N_{FE}\},$$
$$j = \{1,\ldots,K-1\}$$

$$\nabla_{x_{w_{i,K}}}\mathcal{L} = \sum_{k=2}^{K} \dot{\ell}_{K,k}\lambda_{1_{i,k}} - \bar{\alpha}_i\lambda_{1_{i,K}}\frac{df_1(\cdot)}{dx_{w_{i,K}}} - \bar{\alpha}_i\lambda_{2_{i,K}}\frac{df_2(\cdot)}{dx_{w_{i,K}}} - \bar{\alpha}_i\lambda_{4_{i,K}}\frac{df_4(\cdot)}{dx_{w_{i,K}}} - \bar{\alpha}_i\lambda_{6_{i,K}}\frac{df_6(\cdot)}{dx_{w_{i,K}}}$$
$$- \ell_{K,K}\nu_{1_{i+1}} + \mu_{3_{i,K}}\frac{dg_3(\cdot)}{dx_{w_{i,K}}} - \mu_{4_{i,K}}\frac{dg_3(\cdot)}{dx_{w_{i,K}}} = 0,\ i = \{1,\ldots,N_{FE}-1\}$$

$$\nabla_{s_{w_{i,K}}}\mathcal{L} = \frac{d\Phi}{ds_{w_{i,K}}} + \sum_{k=2}^{K} \dot{\ell}_{K,k}\lambda_{2_{i,k}} - \bar{\alpha}_i\lambda_{1_{i,K}}\frac{df_1(\cdot)}{dx_{w_{i,K}}} - \bar{\alpha}_i\lambda_{2_{i,K}}\frac{df_2(\cdot)}{dx_{w_{i,K}}} - \bar{\alpha}_i\lambda_{6_{i,K}}\frac{df_6(\cdot)}{dx_{w_{i,K}}}$$
$$- \ell_{K,K}\nu_{2_{i+1}} + \mu_{9_{i,K}} = 0,\ i = \{1,\ldots,N_{FE}-1\}$$

$$\nabla_{x_{d_{i,K}}}\mathcal{L} = \sum_{k=2}^{K} \dot{\ell}_{Kk}\lambda_{3_{i,k}} - \bar{\alpha}_i\lambda_{3_{i,K}}\frac{df_3(\cdot)}{dx_{d_{i,K}}} - \bar{\alpha}_i\lambda_{4_{i,K}}\frac{df_4(\cdot)}{dx_{d_{i,K}}} - \ell_{K,K}\nu_{3_{i+1}} = 0,\ i = \{1,\ldots,N_{FE}-1\}$$

$$\nabla_{x_{b_{i,K}}}\mathcal{L} = \sum_{k=2}^{K} \dot{\ell}_{K,k}\lambda_{4_{i,k}} - \bar{\alpha}_i\lambda_{3_{i,K}}\frac{df_3(\cdot)}{dx_{b_{i,K}}} - \bar{\alpha}_i\lambda_{4_{i,K}}\frac{df_4(\cdot)}{dx_{b_{i,K}}} - \bar{\alpha}_i\lambda_{5_{i,K}}\frac{df_5(\cdot)}{dx_{b_{i,K}}}$$
$$- \ell_{K,K}\nu_{4_{i+1}} = 0,\ i = \{1,\ldots,N_{FE}-1\}$$

$$\nabla_{x_{r_{i,K}}}\mathcal{L} = \sum_{k=2}^{K} \dot{\ell}_{K,k}\lambda_{5_{i,k}} - \bar{\alpha}_i\lambda_{1_{i,K}}\frac{df_1(\cdot)}{dx_{r_{i,K}}} - \bar{\alpha}_i\lambda_{5_{i,K}}\frac{df_5(\cdot)}{dx_{r_{i,K}}} - l_{K,K}\nu_{5_{i+1}} + \mu_{3_{i,K}}\frac{dg_3(\cdot)}{dx_{r_{i,K}}} + \mu_{4_{i,K}}\frac{dg_4(\cdot)}{dx_{r_{i,K}}} = 0,\ i = \{1,\ldots,N_{FE}-1\}$$

$$\nabla_{c_{w_{i,K}}}\mathcal{L} = \frac{d\Phi}{dc_{w_{i,K}}} + \sum_{k=2}^{K} \dot{\ell}_{K,k}\lambda_{6_{i,k}} - \bar{\alpha}_i\lambda_{6_{i,K}}\frac{df_6(\cdot)}{dc_{w_{i,K}}} - \ell_{K,K}\nu_{6_{i+1}} = 0,\ i = \{1,\ldots,N_{FE}-1\}$$

$$\nabla_{x_{w_{N_{FE},K}}}\mathcal{L} = \sum_{k=2}^{K} \dot{\ell}_{K,k}\lambda_{1_{N_{FE},k}} - \bar{\alpha}_{N_{FE}}\lambda_{1_{N_{FE},K}}\frac{df_1(\cdot)}{dx_{w_{N_{FE},K}}} - \bar{\alpha}_{N_{FE}}\lambda_{2_{N_{FE},K}}\frac{df_2(\cdot)}{dx_{w_{N_{FE},K}}} - \bar{\alpha}_{N_{FE}}\lambda_{4_{N_{FE},K}}\frac{df_4(\cdot)}{dx_{w_{N_{FE},K}}} - \bar{\alpha}_{N_{FE}}\lambda_{6_{N_{FE},K}}\frac{df_6(\cdot)}{dx_{w_{N_{FE},K}}} + \mu_{3_{N_{FE},K}}\frac{dg_3(\cdot)}{dx_{r_{N_{FE},K}}} - \mu_{4_{N_{FE},K}}\frac{dg_3(\cdot)}{dx_{r_{N_{FE},K}}} = 0,$$

$$\nabla_{s_{w_{N_{FE},K}}}\mathcal{L} = \frac{d\Phi}{ds_{w_{N_{FE},K}}} + \sum_{k=2}^{K} \dot{\ell}_{K,k}\lambda_{2_{N_{FE},k}} - \bar{\alpha}_{N_{FE}}\lambda_{1_{N_{FE},K}}\frac{df_1(\cdot)}{ds_{w_{N_{FE},K}}} - \bar{\alpha}_{N_{FE}}\lambda_{2_{N_{FE},K}}\frac{df_2(\cdot)}{ds_{w_{N_{FE},K}}} - \bar{\alpha}_{N_{FE}}\lambda_{6_{N_{FE},K}}\frac{df_6(\cdot)}{ds_{w_{N_{FE},K}}} + \mu_{9_{N_{FE},K}} = 0,$$

$$\nabla_{x_{d_{N_{FE},K}}}\mathcal{L} = \sum_{k=2}^{K} \dot{\ell}_{K,k}\lambda_{3_{N_{FE},k}} - \bar{\alpha}_{N_{FE}}\lambda_{3_{N_{FE},K}}\frac{df_3(\cdot)}{dx_{d_{N_{FE},K}}} - \bar{\alpha}_{N_{FE}}\lambda_{4_{N_{FE},K}}\frac{df_4(\cdot)}{dx_{d_{N_{FE},K}}} = 0,$$

$$\nabla_{x_{b_{N_{FE},K}}}\mathcal{L} = \sum_{k=2}^{K} \dot{\ell}_{Kk}\lambda_{4_{N_{FE},k}} - \bar{\alpha}_{N_{FE}}\lambda_{3_{N_{FE},K}}\frac{df_3(\cdot)}{dx_{b_{N_{FE},K}}} - \bar{\alpha}_{N_{FE}}\lambda_{4_{N_{FE},K}}\frac{df_4(\cdot)}{dx_{b_{N_{FE},K}}} - \bar{\alpha}_{N_{FE}}\lambda_{5_{N_{FE},K}}\frac{df_5(\cdot)}{dx_{b_{N_{FE},K}}} = 0,$$

$$\nabla_{x_{r_{N_{FE},K}}}\mathcal{L} = \sum_{k=2}^{K} \dot{\ell}_{K,k}\lambda_{5_{N_{FE},k}} - \bar{\alpha}_{N_{FE}}\lambda_{1_{N_{FE},K}}\frac{df_1(\cdot)}{dx_{r_{N_{FE},K}}} - \bar{\alpha}_{N_{FE}}\lambda_{5_{N_{FE},K}}\frac{df_5(\cdot)}{dx_{r_{N_{FE},K}}} + \mu_{3_{N_{FE},K}}\frac{dg_3(\cdot)}{dx_{r_{N_{FE},K}}} + \mu_{4_{N_{FE},K}}\frac{dg_4(\cdot)}{dx_{r_{N_{FE},K}}} = 0,$$

$$\nabla_{c_{w_{N_{FE},K}}}\mathcal{L} = \frac{d\Phi}{dc_{w_{N_{FE},K}}} + \sum_{k=2}^{K} \dot{\ell}_{K,k}\lambda_{6_{N_{FE},k}} - \bar{\alpha}_{N_{FE}}\lambda_{6_{N_{FE},K}}\frac{df_6(\cdot)}{dc_{w_{N_{FE},K}}} = 0,$$

$$\nabla_{q_{p_i}}\mathcal{L} = -\frac{d\Phi}{dq_{p_i}} + \nu_{7_i} + \nu_{9_i} + \mu_{1_i} - \mu_{2_i} - \sum_{j=1}^{K}\mu_{3_{i,j}}\frac{dg_3(\cdot)}{dq_{p_i}} + \sum_{j=1}^{K}\mu_{4_{i,j}}\frac{dg_4(\cdot)}{dq_{p_i}} - \mu_{5_{i+1}}\frac{dg_5(\cdot)}{dq_{p_{i+1}}} + \mu_{6_{i+1}}\frac{dg_6(\cdot)}{dq_{p_{i+1}}} = 0,\ i = \{1\}$$

$$\nabla_{f_{k_i}}\mathcal{L} = -\frac{d\Phi}{dq_{p_i}} + \nu_{8_i} - \mu_{7_{i+1}}\frac{dg_7(\cdot)}{df_{k_{i+1}}} + \mu_{8_{i+1}}\frac{dg_8(\cdot)}{df_{k_{i+1}}} = 0,\ i = \{1\}$$

$$\nabla_{q_{p_i}}\mathcal{L} = \frac{d\Phi}{dq_{p_{i-1}}} - \frac{d\Phi}{dq_{p_{i+1}}} + \nu_{9_i} + \mu_{1_i} - \mu_{2_i} - \sum_{j=1}^{K}\mu_{3_{i,j}}\frac{dg_3(\cdot)}{dq_{p_i}} + \sum_{j=1}^{K}\mu_{4_{i,j}}\frac{dg_4(\cdot)}{dq_{p_i}} + \mu_{5_i} = 0,$$
$$- \mu_{5_{i+1}}\frac{dg_5(\cdot)}{dq_{p_{i+1}}} - \mu_{6_i} + \mu_{6_{i+1}}\frac{dg_6(\cdot)}{dq_{p_{i+1}}},\ i = \{2,\dots,N_{FE}-1\}$$

$$\nabla_{f_{k_i}}\mathcal{L} = \frac{d\Phi}{dq_{p_i}} - \frac{d\Phi}{dq_{p_{i+1}}} + \mu_{7_i} - \mu_{7_{i+1}}\frac{dg_7(\cdot)}{df_{k_{i+1}}} - \mu_{8_i} + \mu_{8_{i+1}}\frac{dg_8(\cdot)}{df_{k_{i+1}}} = 0,\ i = \{2,\dots,N_{FE}-1\}$$

$$\nabla_{q_{p_i}}\mathcal{L} = \frac{d\Phi}{dq_{p_i}} + \nu_{9_i} + \mu_{1_i} - \mu_{2_i} - \sum_{j=1}^{K}\mu_{3_{i,j}}\frac{dg_3(\cdot)}{dq_{p_i}} + \sum_{j=1}^{K}\mu_{4_{i,j}}\frac{dg_4(\cdot)}{dq_{p_i}} + \mu_{5_i} - \mu_{6_i} = 0,$$
$$i = \{N_{FE}\}$$

$$\nabla_{f_{k_i}}\mathcal{L} = \frac{d\Phi}{dq_{p_i}} + \mu_{7_i} - \mu_{8_i} = 0,\ i = \{N_{FE}\}$$

$$\nabla_{q_{r_i}}\mathcal{L} = -\bar{\alpha}_i\sum_{j=2}^{K}\lambda_{1_{i,j}}\frac{df_1(\cdot)}{dq_{r_i}} - \bar{\alpha}_i\sum_{j=2}^{K}\lambda_{2_{i,j}}\frac{df_2(\cdot)}{dq_{r_i}} + \nu_{9_i} - \nu_{10_i} = 0,\ i = \{1,\dots,N_{FE}\}$$

$$\nabla_{q_i}\mathcal{L} = -\bar{\alpha}_i\sum_{j=2}^{K}\lambda_{1_{i,j}}\frac{df_1(\cdot)}{dq_i} - \bar{\alpha}_i\sum_{j=2}^{K}\lambda_{2_{i,j}}\frac{df_2(\cdot)}{dq_i} - \bar{\alpha}_i\sum_{j=2}^{K}\lambda_{4_{i,j}}\frac{df_4(\cdot)}{dq_i}$$
$$- \bar{\alpha}_i\sum_{j=2}^{K}\lambda_{6_{i,j}}\frac{df_6(\cdot)}{dq_i} + \nu_{10_i} - \nu_{11_i} = 0,\ i = \{1,\dots,N_{FE}\}$$

$$\nabla_{q_{out_i}}\mathcal{L} = -\bar{\alpha}_i\sum_{j=2}^{K}\lambda_{3_{i,j}}\frac{df_3(\cdot)}{dq_{out_i}} - \bar{\alpha}_i\sum_{j=2}^{K}\lambda_{4_{i,j}}\frac{df_4(\cdot)}{dq_{out_i}} + \nu_{11_i} = 0,\ i = \{1,\dots,N_{FE}\}$$

$$\sum_{j=1}^{K}\dot{\ell}_{j,k}x_{w_{i,j}} - \bar{\alpha}_i f_1(A_d, V_R, x_{w_{i,j}}, s_{w_{i,j}}, x_{r_{i,j}}) = 0,\ \ i = \{1,\dots,N_{FE}\},\ k = \{2,\dots,K\}$$

$$\sum_{j=1}^{K}\dot{\ell}_{j,k}s_{w_{i,j}} - \bar{\alpha}_i f_2(A_d, V_R, x_{w_{i,j}}, s_{w_{i,j}}) = 0,\ \ i = \{1,\dots,N_{FE}\},\ k = \{2,\dots,K\}$$

$$\sum_{j=1}^{K} \dot{\ell}_{j,k} x_{d_{i,j}} - \bar{\alpha}_i f_3(A_d, V_R, x_{d_{i,j}}, x_{b_{i,j}}) = 0, \;\; i = \{1, \ldots, N_{FE}\}, \;\; k = \{2, \ldots, K\}$$

$$\sum_{j=1}^{K} \dot{\ell}_{j,k} x_{b_{i,j}} - \bar{\alpha}_i f_4(A_d, V_R, x_{w_{i,j}}, x_{d_{i,j}}, x_{b_{i,j}}) = 0, \;\; i = \{1, \ldots, N_{FE}\}, \;\; k = \{2, \ldots, K\}$$

$$\sum_{j=1}^{K} \dot{\ell}_{j,k} x_{r_{i,j}} - \bar{\alpha}_i f_5(A_d, V_R, x_{b_{i,j}}, x_{r_{i,j}}) = 0, \;\; i = \{1, \ldots, N_{FE}\}, \;\; k = \{2, \ldots, K\}$$

$$\sum_{j=1}^{K} \dot{\ell}_{j,k} c_{w_{i,j}} - \bar{\alpha}_i f_6(A_d, V_R, x_{w_{i,j}}, s_{w_{i,j}}, c_{w_{i,j}}) = 0, \;\; i = \{1, \ldots, N_{FE}\}, \;\; k = \{2, \ldots, K\}$$

$$g_1(q) = -\frac{q_{p_i}}{q_{r_i} + q_{p_i}} \leq -0.01, \;\; i = \{1, \ldots, N_{FE} - 1\}$$

$$g_2(q) = \frac{q_{p_i}}{q_{r_i} + q_{p)i}} \leq 0.2, \;\; i = \{1, \ldots, N_{FE} - 1\}$$

$$g_3(x_{w_{ij}}) = -\frac{V_R x_{w_{i,j}}(t) + A_d \, l_r \, x_{r_{i,j}}(t)}{24 \, q_{p_{i,j}} \, x_{r_{i,j}}(t)} \leq -0.8, \;\; i = \{1, \ldots, N_{FE} - 1\}, \;\; j = \{1, \ldots, K\}$$

$$g_3(x_{w_{ij}}) = \frac{V_R x_{w_{i,j}}(t) + A_d \, l_r \, x_{r_{i,j}}(t)}{24 \, q_{p_i} \, x_{r_{i,j}}(t)} \leq 15, \;\; i = \{1, \ldots, N_{FE} - 1\}, \;\; j = \{1, \ldots, K\}$$

$$g_5(s_{w_{i,j}}) = s_{w_{i,j}}(t) \leq 100, \;\; i = \{1, \ldots, N_{FE} - 1\}, \;\; j = \{1, \ldots, K\}$$

$$g_6(x_{w_{i,j}}) = x_{w_{i+1,1}} - \sum_{j=1}^{K} \dot{\ell}_{j,K} x_{w_{i,j}} = 0, \;\; i = \{1, \ldots, N_{FE} - 1\}, \;\; j = \{1, \ldots, K\}$$

$$g_7(s_{w_{i,j}}) = s_{w_{i+1,1}} - \sum_{j=1}^{K} \dot{\ell}_{j,K} s_{w_{i,j}} = 0, \;\; i = \{1, \ldots, N_{FE} - 1\}, \;\; j = \{1, \ldots, K\}$$

$$g_8(x_{d_{i,j}}) = x_{d_{i+1,1}} - \sum_{j=1}^{K} \dot{\ell}_{j,K} x_{d_{i,j}} = 0, \;\; i = \{1, \ldots, N_{FE} - 1\}, \;\; j = \{1, \ldots, K\}$$

$$g_9(x_{b_{i,j}}) = x_{b_{i+1,1}} - \sum_{j=1}^{K} \dot{\ell}_{j,K} x_{b_{i,j}} = 0, \;\; i = \{1, \ldots, N_{FE} - 1\}, \;\; j = \{1, \ldots, K\}$$

$$g_{10}(x_{r_{i,j}}) = x_{r_{i+1,1}} - \sum_{j=1}^{K} \dot{\ell}_{j,K} x_{r_{i,j}} = 0, \;\; i = \{1, \ldots, N_{FE} - 1\}, \;\; j = \{1, \ldots, K\}$$

$$g_{11}(c_{w_{i,j}}) = c_{w_{i+1,1}} - \sum_{j=1}^{K} \dot{\ell}_{j,K} c_{w_{i,j}} = 0, \;\; i = \{1, \ldots, N_{FE} - 1\}$$

$$g_6(x_{w_{1,1}}) = x_{w_{1,1}} - x_w^0 = 0,\ \ g_7(s_{w_{1,1}}) = s_{w_{1,1}} - s_w^0 = 0\ \ g_8(x_{d_{1,1}}) = x_{d_{1,1}} - x_d^0 = 0,$$

$$g_9(x_{b_{1,1}}) = x_{b_{1,1}} - x_b^0 = 0,\ \ g_{10}(x_{r_{1,1}}) = x_{r_{1,1}} - x_r^0 = 0,\ \ g_{11}(c_{w_{1,1}}) = c_{w_{1,1}} - c_w^0 = 0,$$

$$q_p^{lb} - q_{p_i} \leq 0,\ \ f_k^{lb} - f_{k_i} \leq 0,\ i = \{1, \ldots, N_{FE}\},\ j = \{1, \ldots, K\}$$

$$q_{p_i} - q_p^{ub} \leq 0,\ \ f_{k_i} - f_k^{ub} \leq 0,\ i = \{1, \ldots, N_{FE}\}$$

where functions $f_1(\cdot)$ to $f_6(\cdot)$ are defined as follows:

$$f_1(x_w, s_w, x_r) = y_w \bar{\mu}_w \frac{s_w x_w}{k_{sc} + s_w} - k_{ca} x_w - k_{dr} \frac{x_w^2}{s_w} + \frac{x_{in} q_{in}}{V_R} + \frac{x_r q_r}{V_R} - \frac{x_w q}{V_R}$$

$$f_2(x_w, s_w) = \frac{f_{kd} k_{dr} x_w^2}{s_w} - \frac{\bar{\mu}_w s_w x_w}{(k_{sc} + s_w)} + f_{kd} k_{ca} x_w + \frac{s_{in} q_{in}}{V_R} + \frac{s_w q_r}{V_R} - \frac{x_w q}{V_R}$$

$$f_3(x_d, x_b) = \left(\frac{1}{A_d l_d}\right)\left(q_{out}(x_b - x_d) - A_d n_{nr} x_d e^{(a_{ar} x_d)}\right)$$

$$f_4(x_w, x_d, x_b) = \left(\frac{1}{A_d l_b}\right)\left(q x_w - x_b(q_{out} + q_2) + A_d n_{nr}\left(x_d e^{(a_{ar} x_d)} - x_b e^{(a_{ar} x_b)}\right)\right)$$

$$f_5(x_b, x_r) = \left(\frac{1}{A_d l_r}\right)\left(q_2(x_b - x_r) + A_d n_{nr} x_b e^{(a_{ar} x_b)}\right)$$

$$f_6(x_w, s_w, c_w) = k_{otw} f_k(c_s - c_w) - k_{od} \mu_w \frac{x_w s_w}{(k_{sc} + s_w)} - \frac{c_w q}{V_R}$$